THE TRANSITION FROM SEVERE TO MILD WEAR

IN LOW ALLOY STEEL

BY

SAMSUDI BIN SAKRANI, B.Sc., M.Tech.

A thesis submitted for the degree of

DOCTOR OF PHILOSOPHY

THE UNIVERSITY OF ASTON IN BIRMINGHAM

APRIL 1988

<u>THE UNIVERSITY OF ASTON IN BIRMINGHAM</u>

THE TRANSITION FROM SEVERE TO MILD WEAR IN LOW ALLOY STEEL

BY   SAMSUDI BIN SAKRANI

DOCTOR OF PHILOSOPHY

1988

SUMMARY

The wear rates of sliding surfaces are significantly reduced if mild oxidational wear can be encouraged. It is hence of prime importance in the interest of component life and material conservation to understand the factors necessary to promote mild oxidational wear. The present work investigates the fundamental mechanism of the running-in wear of BS EN 31/EN 8 steel couples, under various conditions of load, speed and test duration. Unidirectional sliding experiments were carried out on a pin-on-disc wear machine where frictional force, wear rate, temperature and contact resistance were continuously monitored during each test. Physical methods of analysis (x-ray, scanning electron microscopy etc.) were used to examine the wear debris and worn samples.

The wear rate versus load curves revealed mild wear transitions, which under long duration of running, categorized mild wear into four distinct regions. $\alpha-Fe_2O_3$, Fe_3O_4, FeO and an oxide mixture were the predominant oxides in four regions of oxidational wear which were identified above the Welsh T_2 transition. The wear curves were strongly effected by the speed and test duration. A surface model was used to calculate the surface parameters, and the results were found to be comparable with the experimentally observed parameters.

Oxidation was responsible for the transition from severe to mild wear at a load corresponding to the Welsh T_2 transition. In the running-in period sufficient energy input and surface hardness enabled oxide growth rate to increase and eventually exceeded the rate of removal, where mild wear ensued. A model was developed to predict the wear volume up to the transition. Remarkable agreement was found between the theoretical prediction and the experimentally-measured values.

The oxidational mechanism responsible for transition to mild wear under equilibrium conditions was related to the formation of thick homogenous oxide plateaux on subsurface hardened layers. FeO was the oxide formed initially at the onset of mild wear but oxide type changed during the total running period to give an equilibrium oxide whose nature depended on the loads applied.

Wear/ Friction/ Transition/ Oxidation/ Temperature

ACKNOWLEDGEMENTS

C O N T E N T S

LIST OF TABLES

LIST OF FIGURES

CHAPTER 1

INTRODUCTION

1.1 Background to the problem

Tribological phenomena were apparent during the stone age, when human beings first realised the importance of sliding and rolling for transportation purposes. The first recorded case was about 2400 BC in the time of ancient Egypt (1).

Nowadays, technology has become more advanced and sophisticated, but in spite of developements, problems still arise because component life in engineering situations is reduced by mechanical failure due to wear, even when lubrication is employed. There are many situations where lubrication is impossible or intolerable, for example, in the case of components (gears, bearing or slip-rings) in vacuum, space applications for aircraft and satellites or components in nuclear power plants (2,3). Although the present study is not aimed directly at any of these above fields, it is in the unlubricated aspects of tribology that the study is concentrated, in order to give a fundamental understanding of the factors governing the establishment of mild oxidational wear.

Studies into the behaviour of unlubricated or dry wear began in 1930 with the identification of oxide compounds in

wear debris produced from the sliding of a rail-way type steel (4). Some years later the magnitude of wear of steels was investigated by Rosenberg and Jordan (5) in different environments. Wear rates for experiments carried out in air were low, due to oxide formed on the surfaces, while wear rates were relatively high, about 50 times greater, for similar experiments carried out in oxygen-free nitrogen gas atmospheres. The change in magnitude and character of the wear of steels was studied by Kehl and Siebel (6) who in agreement with the observation of Mailander and Dies (7), showed that the wear rate was either load or speed dependent and was usually demonstrated either by high or low values over the range of loads or speeds employed. These are examples of the most notable early work in this field.

The early fifties marked a period where many outstanding results were produced by a number of workers. These covered both experimental and theoritical investigations. Archard's (8,9,10) work was noteable for the many contributions made to the establishment of the laws, description of mechanisms and production of theories of wear. The classification into severe and mild wear was the conclusion of some observation made by earlier workers. Bowden and Tabor's adhesion theory of friction (11) was widely accepted and was able, at least, to explain some mechanisms relating to wear. Investigations of wear behaviour were further studied by Lancaster (12), and later by Welsh (13,14,15) who described modes of wear on the

basis of the variation of wear rate with a wide range of loads. He established a wear pattern which now bears his name.

The classical Welsh curve describes a wear pattern which is universally accepted for most steels. The curves show clearly the distinction between various equilibrium wear modes at well-defined loads . For a given speed, and for plain carbon steels, a basic pattern consisting of three transitions is found (see figure 1.2). These are transitions indicated by T_1 where a change from mild to severe wear occurs at light loads, T_2, where a further change from severe to mild wear occurs at high loads and by T_3 where a small variation in mild wear occurs at loads above T_2. This enables the separation of two mild wear regimes below T_1 and above T_2 and severe wear regimes between T_1 and T_2. In general, however, a complete pattern is rarely observed as the transition loads are influenced by a number of factors such as hardness, speed and temperature.

Investigations have shown that mild wear below the T_1 is produced by a combination of low wear rate oxidation and material transfer (12,16). This region has been assumed by some workers to correspond to the antiwear regime of lubricated wear with the initial siezure load corresponding to the Welsh T_1 transition (17).

Mild wear above the T_2 transition is probably more important since most practical engineering situations will

fall in this region and hence a knowledge of the processes involved in this region will be of greater general benefit. Quinn, Sullivan and Rowson (18,19,20,21) have made extensive studies in the oxidational wear region above the T_2 transition. They were able to relate the varying oxide types produced with a predicted surface model. In fact, Quinn et al. were only interested in equilibrium wear for which the initial sliding conditions were never taken into consideration. There is, thus, a situation where there is a gap in the knowledge, in particular of the period preceding to the establishment of equilibrium mild wear conditions. Limited studies in this area have been made, for example, by Wilson et al. (22) and Stott et al. (23), but they studied quite different systems to the one described in this work. These latter studies were usually at high temperature with reciprocating motion on 12% chromium steel. In order to address the problems of transition to and establishment of mild wear it is necessary to re-examine the portion of the classical Welsh curve corresponding to the high load-speed mild wear, and an important aspect of the study must be on the effect of test duration.

1.2 Classification of wear

Wear may be defined as *severe* and *mild* (8). Severe wear is characterized by intermetallic contact, large scale damage

to the surface and the production of loose wear particles, while mild wear is by smooth oxide-covered surface, high contact resistance and fine wear debris. There are various mechanisms occurring within these classes. Burwell and Strang (24,25) classified wear into five basic mechanisms; adhesion, corrosion, abrasion, surface fatigue and minor types of wear. Quinn (26,27) suggested that adhesive wear and scuffing were responsible for severe wear and corrosive wear for mild wear, while all the other mechanisms were considered to be combinations of both severe and mild wear. In a very recent review, Ko (28) has indicated from the work of Peterson (29) that the classification of wear is related to the types of motion, for example, unidirection sliding can result in delamination, scoring, scuffing and erosive wear and reciprocating sliding responsible for delamination and fretting wear. Explained below are the most commonly and widely accepted categories of wear proposed by Burwell and Strang.

1.2.1 Adhesive wear

If a metallic surface is brought into contact with another surface under a certain load, adhesion due to cold welding can occur at the local contact areas where metal-metal junctions are formed (11,30). These minute welds increase in number and in strength under relative sliding

motion. However, subsequent shearing cause them to rupture and material fragments are formed and may transfer to one of the sliding member before eventually becoming detached from the surface as loose wear particles. For hard asperities sliding over soft asperities penetration into the bulk of the softer member occurs which then produces wear particle by ploughing action. Adhesive wear is related to the severe wear action categorised by Archard and Hirst (8) and Quinn (26).

1.2.2 Corrosive wear

This type of wear is caused by the interaction of corrosive agents (gas or liquid environments) with sliding surfaces, where corrosion takes place by chemical attack (24). The reaction product, usually in the form of a thin film is removed and reformed between subsequent periods of sliding. In air containing oxygen, the chemical attack is so mild that surface oxidation leads to the formation of wear protecting film and this results in the *mild* form of wear (8) or *mild oxidational wear* (31).

Halling (32) stated that in some cases of corrosive wear high contact stresses developed during metallic sliding may cause enhanced local corrosion, and thus lead to pitting. There is also stress-corrosion cracking induced by the internal stress which exists during the formation of a

material in corossive atmospheres. When such a situation is
combined with surface rubbing catastrophic wear can occur.

1.2.3 Abrasive wear

Abrasive wear occurs when a hard material slides against
the surface of softer material. An extreme example is the
rubbing of a file or emery paper on a piece of wood. This is
known as *two-body abrasive wear*.

It may also happen that abrasive particles detach from
the harder material or from the softer material containing
hard surface particles, and accumulate at the conjunction,
probably by entrapment, and thus contribute to the abrasion
action. This is *three-body abrasive wear* and is generally
about ten times less in wear rate than the two-body abrasive
wear (33).

1.2.4 Surface fatigue

Fatigue wear is a typical process occurring in most
mechanical components under rolling and sliding contacts.
The principle cause is a repeated cyclic loading which
changes the propagation of stresses below the surface,
followed by structural deformation at the point of contact
and eventually when a fracture or break is formed the surface
fails due to *fatigue*. Miki and Kobayashi (34) included the
fatigue process in their pit formation study for rolling

contacts. The sequence of mechanisms were as follows; wear, plastic flow, work hardening and finally fatigue.

In sliding contact there are cases where asperities are not subject to adhesive or abrasive contact similar to adhesive wear, but just pass each other, leaving one or both asperities plastically deformed. Such repeated contacts lead to failure due to fatigue with subsequent formation of fragment as wear particles. It is likely that such process is predominant in oxide-oxide contacts.

1.2.5 Fretting

Fretting occurs in a periodic or reciprocating tangential motion of small amplitude which is commonly found in some vibrating components of nuclear power plants (35). Halliday and Hirst (36) in their study using mild steel found fine reddish-brown particles of iron oxide as a corossion product. Halling (32) described fretting as a form of adhesive wear in which normal load caused adhesion between asperities and vibrations caused rupture of the adhearing contacts. In other situations fretting results in the formation of delaminated wear particles induced by small amplitude vibrations (37). This occurs when the surface is initially oxidized, and the combined effect of stresses produced by such motion leave subsurface layers cracked and eventually lead to delaminated.

1.3 Friction

1.3.1 Concept of real area of contact

No surface, whatsoever, can be regarded as completely
flat. A mirror finish of any engineering surface is, in
fact, made of irregular protuberances similar to hills and
valley-like structures. When two such surfaces are resting,
one over the other, they actually make contact at the peaks
or asperities. The total area of these tiny contacts is
called the *real area of contact*, and it is a concept of
fundamental importance in explaining the phenomena of
friction and wear. On the other hand, the apparent area of
contact fictitiously appears as if all the interfacial area
makes contact. For metal the latter plays no role in either
friction or wear.

Probably the most widely accepted derivation of the real
area of contact was due to a model proposed by Bowden and
Tabor (11,38) from their adhesive theory of friction. Some
of the important aspects of the theory are presented here.

Adhesion involves surface interactions where atoms from
one surface are bonded to atom of another member by weak
interatomic forces resulting in welded junctions. If a load
W is applied the high local pressures deform the contacting
asperities elastically until the yield point of the softer of
the two materials is exceeded. Once full plastic flow occurs
the final area of contact, A_r, is given by the actual

deformed area of contact which supports the load W, i.e.

$$A_r = \frac{W}{P_m} \qquad \dots \dots \dots \dots (1.1)$$

where P_m is the penetration hardness of the underlying surface. Equation (1.1) was obtained from the assumption of a single spherical asperity resting on a flat surface, but it applies to multiple asperities under similar conditions.

In realising the failure of certain aspect of the friction theory to be discussed later, Bowden and Tabor (38) introduced an alternative form of real area of contact for rubbing materials. It includes a tangential force, F in addition to the normal load, W which causes plastic flow deformation and expansion of the contacting asperities. The increased area is given by

$$A_r^2 = \left(\frac{W}{P_m}\right)^2 + \alpha \left(\frac{F}{P_m}\right)^2 \qquad \dots \dots \dots \dots (1.2)$$

where $\alpha = (P_m/S_o)^2$, S_o is the shear stress of the softer material. Equation (1.2) shows an increase of contact area by the second term due to frictional force. Without sliding motion F is negligible and equation (1.2) equals to equation (1.1). A value of $\alpha = 9$ was assumed to be valid for most metals.

There is a case where surface asperities are very small that elastic deformation takes place in the bulk of the solid

materials only. For a spherical asperity (e.g. highly polished ball bearing surface) pressed on a flat pollished surface by a load W, the elastically deformed area of contact is given by the Hertz equation (39,11) as

$$A_r = 2.3 \left[Wr \left(\frac{1}{E_1} + \frac{1}{E_2} \right) \right]^{2/3} \qquad \ldots \ldots \ldots \ldots (1.3)$$

where r is the radius of spherical asperity, and E_1 and E_2 are Young moduli of the sphere and flat surface respectively.

Equation (1.3) is valid for a single contact which has been deformed elastically. For multiple contacts under the same condition of deformation, Archard (40,41) found that the real area of contact was proportional to load to the power of n where $2/3 < n < 1$, and by making the surface completely flat his model showed a tendency close to linearity between A_r and W as n approached unity, i.e. n=44/45.

There is a condition of the contacting surface where the asperity deformed neither plastically nor elastically. Instead an intermediate between them or so-called elastoplastic contact is formed. Greenwood and Williamson (41) have indicated that the "plasticity index", a factor related to the physical properties of the material, was necessary in determining the conditions of the contact. This gives values less than one for elastic contact and greater

than one for plastic contact. Under the circumstances of their investigation the increase in load through the enlargement of existing contacts is always exactly balanced by the creation of new small areas of both plastic and elastic contacts. Thus the actual contact area is always directly proportional to the load, and this was supported by experimental evidence.

1.3.2 Mechanism and theories

Friction or sliding friction is, in general, the force that resists relative motion between sliding bodies whose opposing surfaces are clean and dry, i.e. unlubricated. Two types of force are required to overcome the initial resistance to motion: firstly the *static friction force* which is just large enough to cause the body to start to slide and secondly the *kinetic friction force* needed to keep the body moving at the same speed once sliding has begun. The two basic friction laws are;

1) The friction force between two solids is independent of the apparent area of contact. This is true for metals, but not for some other materials.

2) The friction force is proportional to the applied load. A dimensionless friction coefficient, μ, is expressed as the ratio between the frictional force, F and applied load, W, i.e.

$$\mu = \frac{F}{W} \qquad \dots \dots \dots \dots (1.4)$$

The above friction laws are, undoubtedly, applicable to the three types of deformation, since the relationship between load and real contact area is approximately a direct proportionality. Quinn (27,43) suggested that the plastic and elastic deformation hyphothesis was relevant to explaining the frictional behaviour under severe wear and mild wear respectively. It may, therefore, be reasonable to say that the elastoplastic hypothesis is suitable for the case of friction under the intermediate severe and mild wear due to metal-oxide contacts.

The basic friction law is, in fact, too oversimplified, since the friction force, F, may be a function of many variables such as speed, material and temperature. The adhesion theory of friction assumes that the friction force results from two major components: the force required to shear minute welded junctions formed at points of contact between two rubbing materials, and the force required to plough hard asperities through a softer surface. Thus under ideal conditions of elastic and plastic deformation the total friction force is the summation of these two forces, i.e.

$$F = A_r S + F_p \qquad \dots \dots \dots \dots (1.5)$$

where

S = mean tangential shearing stress needed to shear the
   welded junctions.

A_r = real area of contact.

F_p = Ploughing term.

For unlubricated metals the ploughing term is
insignificant because the surface at the asperity-asperity
contact is flat due to mutual shearing action of the
interacting bodies, hence less contribution to the ploughing
action. This term was derived by Bowden and Tabor (38) on
the assumption of conical asperity which penetrated into the
bulk of mating surface of softer materials, such as polymer.
By substitution from equations (1.1) and (1.5) into equation
(1.4) the expression for friction coefficient becomes

$$\mu = \frac{S}{P_m} \qquad \ldots\ldots\ldots\ldots(1.6)$$

In considering the effect of work-hardening Bowden and Tabor
replaced S with S_o, the critical stress of the softer
material. Equation (1.6) is, thus redefined as

$$\mu = \frac{S_o}{P_m}$$

$$= \frac{\text{critical shear stess of the softer material}}{\text{plastic yield pressure of the underlying metal}} (1.7)$$

Equation (1.7) gives a theoretical coefficient of friction of
0.2 because the ratio S_o/P_m for a large range of materials is

found to be around 1/5, whereas experimental evidence gives greater values to the friction coefficient, i.e. 0.3 to 0.6 in air (11,44) and 4.5 to 4.8 in vacuum (45). The increase in friction values in vacuum is due to the elimination of contaminating effect of air which reduce the adhesion component of the friction. Bowden and Tabor(38) further re-examined equation (1.7) by taking into account the presence of an interfacial film between sliding surfaces. Surface films such as oxide, boundary lubricant and even contaminants can give rise to the critical shear stress of the interface, S_f. The generalised form of equation (1.7) is obtained using S_f in place of S_o.

Rubenstein (46) who used a similar friction theory found that the contacting asperities of the rubbing surfaces deform according to the law in which stress varies proportional to strain to the power of n (where n is interger). He showed from his mathematical model that the friction force depends on the applied normal load, physical properties of the sliding materials, surface roughness and area of contact.

The aspect of friction which is relevent to the present research work is the friction change caused by oxide film formation. Wilson, Stott and Wood (22) proposed a theory to account for the change in the friction coefficient by the progressive change in the nature of sliding contacts preceding to the formation of compacted oxides. They showed that friction coefficients under this condition are basically

due to three types of interaction; metal to metal, metal to oxide or oxide to metal and oxide to oxide. Thus they proposed that:

$$\mu = \frac{S_m}{P_m}\left[\sigma_m(1-Q)^2 + 2\,\sigma_{mo}Q(1-Q) + \sigma_o\,i-\frac{Q^2}{K}\right] \quad \ldots\ldots(1.8)$$

where

Q = fraction of real contact area covered by compacted oxide.

σ_m = junction growth constant for metal/metal contact.

σ_{mo} = junction growth constant for metal/oxide contact.

σ_m = junction growth constant for oxide/oxide contact.

i,K = Interfacial constants.

Stott et al. indicated that the extent of the junction growth of metal-oxide asperities, at least for σ_{mo} between 1.0 and 3.0, was not very critical in determining the overall frictional behaviour, instead the oxide junction growth constant, σ_o was more important, particularly when Q = 0.8.

Based on the same principle Stott, Glascott and Wood (23) were also able to express the variation in coefficient of friction with the reciprocating sliding time. They suggested that a decrease in friction is associated with the increase of area growth rate of oxide as sliding progressed. The mathematical relationship is given by

$$\mu = A_\mu - B_\mu\left\{1 - \exp(-ct)\right\} + C_\mu\left\{1 - \exp(-ct)\right\}^2 \ldots(1.9)$$

where A_μ, B_μ and C_μ are defined in terms of material parameters; c is a constant and t is the sliding time. The model applies to temperature ranges of between 300 to 400°C and suggests that the transition to mild wear is due to progessive oxidation.

The initial break-in friction was studied in great detail by Suh and Sin (47) and Blau (48). The former were interested in the generation of friction from purely metallic contact using hardened steels carried out in air and argon. Blau (48) categorized from a compilation of the frictional break-in data, eight friction versus time curves for a wide range of materials collected from different workers. Figure 1.1 shows the three most common shapes of unlubricated wear curves for steels at room temperature. Curves (i) and (ii) show the frictional behaviour of sliding under condition of severe to mild wear transition at room and elevated temperature using a pin-on-disc system (49,50), while curve (iii) is observed from flat-on-flat reciprocating sliding during a transition from severe to mild wear (23,51). Blau discussed the possibility that each of the eight curves originated from the same family of curves might interchange one to another due to the following influence: load, speed, temperature, material and compositions, environment and contact geometry. For example, the variation of curve (i) is the result from flat copper sliding on flat steel under high

Aston University

Content has been removed due to copyright restrictions

Figure 1.1 Typical friction break-in curves
for sliding metals (ref. 48).

speed in air; this change to a curve which shows an initial
gradual increase in friction with time as the same materials
of different composition slide from flat on ring geometry at
high load and low speed in argon. The mechanism responsible
was the mechanical disruption of surface oxide film with
increasing metallic contact.

1.4 Severe-mild wear transition

Wear may be defined as the loss of material caused by
rubbing when two bodies are in sliding contact. The wear
process is somewhat unpredictable, if compared to the
friction. In explaining this Archard (10) emphasized the
importance of encounters during the rubbing of two surfaces
in which all asperity encounters contribute to the friction,
but only a small proportion contribute to wear. Friction is
therefore dominated by the behaviour of undamaged contacts
and is practically independent of what happens at the small
number of encounters contributing to the wear. He stated
that wear rate, w is proportional to the apparent area of
contact (10), i.e.

$$w = K A_r \qquad \ldots\ldots\ldots\ldots(1.10)$$

where K is the probablity of producing a wear particle
(assumed to be spherical in shape) per asperity encounter and
often called the Archard K-factor. If a particle takes a

shape other than that of a sphere (e.g. flake and sheet) then K must be adapted accordingly. Quinn (52) interpreted the inverse value of K (or 1/K) to be the number of asperity encounters required to produce a wear particle. By comparison the number of encounters required to produce wear on the sliding of polythene on steel is about 10^5 times greater than that of sliding of identical steels.

Most metals exhibit two types of wear under unlubricated conditions, i.e. severe wear and mild wear (8,16). Both are distinguished by their observable characteristics; severe wear is associated with extensive intermetallic contact, leaving a rough shiny surface and coarse metallic debris in the order 10^{-2} mm in diameter, whilst mild wear which is concerned with oxidation in air produces surfaces covered with a dark smooth film of oxide. The fine wear debris is about 10^{-4} mm in diameter.

The factors effecting the change in modes of wear have been studied elsewhere (5,6,7,8,9,12). Lancaster (12) observed two interesting features; one being the transition from mild to severe wear at low load, speed and temperature and another transition from severe to mild wear at high load, speed and temperature. These variations, he maintained, were determined by the two opposing processes; the mechanism of severe wear exposed clean metal surfaces and the exposure of the surfaces to the atmosphere which lead to the formation of oxide film, thus mild wear occurs when there was sufficient

time between contacts for stable oxide to grow. Under the condition of his experiments using brass pins and steel rings he was able to show, from his earlier result (53) that, no wear particle was produced during the initial stage of running. Instead a transferred film of brass built up on the steel surface. When a critical thickness was reached it became detached as wear particles. This happens because the brass particles became heavily work hardened at the first transfer and any further interaction resulted in fracture of softer brass. The initiation of back-transfer was believed to be due to an increase in the strength of the surface layer of the pin resulting from the adherence of an oxide layer. Archard and Hirst (16) in their study using two identical hard steels found sliding transfer to take place by the production of transferred lumps, aggregated and eventually appearing as large metallic debris. As sliding proceeded to transition to mild wear, however, little transfer occurred.

Welsh (14,15) was probably the first to make a comprehensive study of severe-mild wear transition on a wide range of steel material combinations. He was able to depict the general wear pattern from a series of wear rate versus load curves, the result of which showed large changes in wear modes with small changes in applied load at three transitions, i.e. T_1, T_2 and T_3. A generalised form of Welsh curve is shown in figure 1.1. It clearly shows two mild wear regimes below T_1 and above T_2 transition loads and severe

Figure 1.2   General wear pattern (reference 14).

wear regime between T_1 and T_2. All the transitions are found to be dependent on the sliding speed, the hardness of the steel specimens and the environment. An increase in speed lowers the values of T_1, T_2 and T_3 while decreasing the speed increases them accordingly. An increase in hardness increases T_1 and lowers T_2 and T_3 and at some critical value which varies with the carbon content, both T_1 and T_2 merge together, thus eliminating the range of severe wear. The general wear pattern is not effected by the moderate addition of the common alloying elements.

Welsh's explanation of the wear transitions was based on the variation of work hardening due to plastic deformation of the surface. Mild wear in the range below T_1 is maintained by the combined rates of oxidation and surface hardness provided by strain hardening, but these process were over-ruled by the increasing scale and vigour of the severe wear process when the load reach T_1. T_2 transition occurs at a load where intensive hardening and high frictional heating induced surface oxidation resulted in mild wear. During this transition it is expected that the austenite formation temperature was initially attained, but due to rapid cooling in air a hard phase-transformed martensite is produced. Microhardness measurement on the hardened layer showed approximate values of 800 VPN. The T_3 transition is considered to be the minimum load required to cause permanent surface hardening, and the variation above this point of load

was due to special effects associated with the thermal asymmetry of the rubbing system. The different magnitude of temperatures and wear rates of the pin and ring occurred as a result.

The presence of a hardened layer and oxide film is very important in maintaining mild wear above T_2 and Welsh found two conditions of critical hardness using a tempering and etching experiment, the first being that value falling within the limits 340 to 425 VPN required for supporting oxide film when the surface is initially oxidized. This apparently shows that this hardness value is a prerequisite for the transition from severe to mild wear at T_2. The other critical hardness lies between the limits 553 to 775 VPN, that is the limiting value of surface hardness above which severe wear cannot develope in any atmosphere, and hence mild wear rates exist without necessary contribution of a protective film. The formation of a hardened surface layer prior to the establishment of mild wear condition was also suggested by other workers. Eyre and Mynard (54) in confirming the earlier result of Eyre and Baxter (55) found white hardened layers formed during running-in periods before the attainment of equilibrium condition; for a 0.4% carbon steel a value between 800 and 1200 VPN was recorded.

There has been growing interests in a particular study of transition from severe to mild wear. Farrel and Eyre (56) studied the initiation of mild wear on and above the Welsh T_2

transition load and found that the sliding distance before the onset of mild wear decreases exponentially with the increasing loads according to an empirical equation. Similar investigations on reciprocating sliding were carried out by Stott et al. (23) at low temperatures and Sullivan and Granville (57) at elevated temperatures. At low temperatures up to 200°C the transition to mild wear is associated with a minimum in the friction coefficient time and contact resistance time traces, and the nature of wear debris changes from metallic to oxide. The transition time to mild wear decreases with increasing temperature. Sullivan and Granville working in an atmosphere of CO_2 noticed similar transition at a minimum disc temperature of 290°C essentially by the reaction of oxygen molecules dissociating from the high temperature carbon dioxide.

The general pattern of wear must also include the change in wear rate of the mild wear region. Much of the work in this area is reported by Quinn, Sullivan and Rowson (18,19,20,21) who were able to catogerize three distinct regions of wear rate dependent on the type of oxide produced (see Figure 1.3). Above the T_2 transition load the low wear rate is dominated by the presence of $\alpha-Fe_2O_3$ then lowered at T_3 transition load by Fe_xO_4 before the next higher wear rate of FeO. A similar pattern is obtained at elevated temperatures (50) where the change in the transition loads appeared to be more pronounced than that of room temperature.

Figure 1.3   General mild wear pattern above the
T_2 transition (reference 19, 81).

1.5 Oxidation, oxide growth and its removal

Oxidation of metal occurs when it gains oxygen, normally from the atmosphere or compounds, and this causes deterioration of engineering materials such as iron and steel. Prior to the formation of an oxide film, oxygen molecules are usually dissociated to a singly charged anion and the surface ions rearrange to accomodate chemisorption on adjacent cation sites in the form of metal-oxide bonding. Further oxidation takes place by a mechanism called *place-exchange* (58) and Smith and Crane (59) used this model to explain the oxidation of iron. Basically after the initial stage of iron-oxygen bonding a series of activated interchanges between the oxygen and the underlying atoms occurs, providing cation sites which are available for dissociative adsorption of the incoming oxygen molecules. This very early process is then followed by an oxide film growth described by Fromhold (60) as ionic migration into the film due to the potential difference build up between the negatively charged oxygen ions and positively charged surface iron ions.

In general, oxide film growth obeys one of the following growth of rate laws (61):

1) Logarithmic, $\Delta m = c \log (kt + 1)$ $\qquad \ldots\ldots\ldots\ldots$(1.11a)

2) Parabolic, $\Delta m^2 = kt$ $\qquad \ldots\ldots\ldots\ldots$(1.11b)

3) Linear, $\Delta m = kt$ $\qquad \ldots\ldots\ldots\ldots$(1.11c)

4) Inverse logarithmic,

$$\frac{1}{\Delta m} = c - k \log t \qquad \ldots\ldots\ldots\ldots (1.11d)$$

5) Cubic, $\Delta m^3 = kt$ $\ldots\ldots\ldots\ldots (1.11e)$

where Δm is the mass uptake of oxygen at time t; c and k are growth constants.

Temperature and oxygen partial pressure play important roles in determining the types of growth rate. Oxidation in the thin film range usually involve logarithmic or inverse logarithmic film growth at a temperature below the normal room temperature and even lower at the liquid-helium temperature. The process is due to electron tunnelling to the adsorbed and dissociated oxygen molecules followed by anion migration at constant electrical field (direct logarithmic) or by cation movement at constant potential drop across the film (inverse logarithmic). Another type of growth in this range is the linear rate law in which the oxide-gas interface reaction is the rate-controlling factor, and usually observed on porous or volatile oxidation layers. Parabolic and cubic rate laws are applicable to oxidation in the thick film range. The former takes place at high temperature and pressure at a film thickness greater then 500°A. Here the ions become so mobile that they can speed up diffusion and reaction within the oxide. The latter is found in a typical copper or nickel oxidation to form p-type semiconductor layer and usually very rare in occurrence.

The effect of heating on the oxidation of metal was studied by Paidassi (62) and Stanley (63) who found scalling layers of iron oxides when pure iron was heated at temperatures above 600°C. They were, in sequence order, comprised of FeO (Wùstite) adjacent to the metal, occupying about 95% of the thickness, Fe_3O_4 (haemetite) in the middle of about 4.5% and $\alpha-Fe_2O_3$, the uppermost and thinnest layer of about 0.5%. It was then suggested that high oxygen diffusivity took place in the interface between oxide and gas rather than diffusion in the bulk metal.

In contrast, increase in temperatures up to 600°C produce oxide types according to their limiting ranges. Davies et al. (64) and Caplan and Cohen (65) have shown that $\alpha-Fe_2O_3$ was formed below 200°C, Fe_3O_4 between 200 to 570°C and FeO above 570°C. In fact, static oxidation is a complicated process and the theories and mechanisms are described elsewhere (66,67).

Oxidation in a tribological situation is associated with surface disruption in which oxide film grows and increases in thickness under the influence of sliding motion and load bearing pressure. In such circumstances the most likely growth rate is a logarithmic law or a parabolic law depending on the conditions of sliding and the temperature governing the oxide growth. Cocks (68,69) study on the role of oxidation in unlubricated sliding indicated that high load frictional heating was responsible for the formation of the

protecting film. The oxide formed was then responsible for low tearing and low friction coefficient, although no direct explanation for the mechanism was proposed. Molgaard (70) while stressing the importance of mechanical characteristics of the oxide layer on both oxide thickness and attrition rate, also pointed out that oxidation took place at increased temperature due to frictional heating. The role of oxides in the protection of tribological surfaces was reported by Sullivan (71,72) in his very recent review.

Many workers have different views on the formation and removal of oxide films, but they principally agree with the establishment of a film of critical thickness. Quinn (73) proposed two mechanisms for the formation of wear particles on a unidirectional sliding system; firstly the bulk of the oxidation occurs at the instant the virgin metal is exposed, followed by further contacts which merely caused the oxide to shear at the metal interface, secondly an equal amount of oxidation occurs at each contact until a critical oxide thickness is reached, beyond which shearing occurs at the metal-oxide interface. On applying the in-contact oxidation (i.e. the second mechanism) to an oxidational wear theory (52,27) he suggested the formation of oxide plateaux which increase both in area laterally and in thickness before being broken up and swept away by wear. Other plateaux elsewhere on the surface immediately emerge as the new operating and protecting film, and the process was repeated.

The detachment of oxide plateaux from the surface was explained in terms of fatigue wear induced during the intermittent heat and stress cycle, a similar process described earlier by Aronov (74). When such a process occurs the plateaux, after attaining a critical thickness between 2 to 3 µm, cracked and fractured to form wear particles.

Quinn may not be alone in this respect because his proporsals are rather similar to that proposed by Tao (75) whose model assumed 1) the gradual growth and instanteneous removal of oxide and 2) the time for oxide growth is negligibly small in comparison with its removal. The second mechanism can be represented as a periodic form of sharp rise and constant fall in oxide film thickness. Earles and Powell (76) and Molgard and Srivastava (77) shared the idea of gradual growth of oxide to a critical thickness before becoming detached from the substrate as a wear particle.

Wilson et al. (22) and Stott et al. (23) in considering the low speed sliding on a reciprocating system described the importance of oxidation during the in-contact, out-of-contact and oxidation within the debris. They proposed two mechanisms, one in which the newly-formed oxide film (together with the pre-oxidized film) is not completely removed by the sliding action, instead it continuously grows at a constant rate of thickening and is removed completely during each wear traversal (22) and another model where they expected that metallic wear debris formed during the early

stage of sliding is accumulated and at the same time fractured and fragmented to become easily oxidized, even at room temperature producing a compacted form of oxide film (23). The former is known as total oxide mechanism while the latter as metal debris mechanism. A specially oxide glazed layer found earlier by Stott et al. (78) is included in the second mechanism. It is formed from the grinding down and smearing due to thermal softening of larger, compacted oxide particles, resulting from severe wear deformation and wear during the early stage of sliding. A conclusion which can be drawn is that compacted agglomerate film are formed only when wear debris is trapped at the interface; this is true for reciprocating sliding of vertical pin on horizontal flat. If the debris is removed from the interface diffusion controlled oxidation takes place and thick homogenous films are formed.

The oxide formed during unlubricated sliding varies in composition with temperature, essentially $\alpha-Fe_2O_3$ is formed at temperature below 200°C with growth of oxide film initiated by oxygen diffusion, Fe_3O_4 from 200°C to 570°C by both iron and oxygen diffusion and FeO above 570°C by iron diffusion (79,80). In the elevated temperature experiments carried out by Sullivan and Athwal (81) the types of oxide produced were found to be dependent on the range of loads at heated disc temperatures. Typically $\alpha-Fe_2O_3$ is predominant below the 30 N of load at temperatures up to 100°C; Fe_3O_4 is formed at all loads above the 400°C, but limited at loads up

to 80 N when the temperature is below 400°C; FeO is the
dominant oxide above 80 N load at temperatures up to 300°C.
In all the cases a mixture of oxides (except $\alpha-Fe_2O_3$) is
present in the debris probably formed by a rapid cooling of
the higher oxide to the lower one.   Most researchers agree
with Bisson et al.'s (82) view of Fe_3O_4 being the most stable
oxide which offers better protection against wear.   FeO is
unstable at temperatures below 570°C, giving rise to thin
oxide film and high wear rate although this was previously
misinterpreted by Cornelious and Roberts (83) as a protective
oxide.

The stability of oxide formed on the sliding surfaces
is determined by the ratio of unit cell volume in the oxide
to the volume of the unit cell in the metal known as the
Pilling Bedworth ratio (84).   This produces different
compressional stresses within the oxide film according to
the types of oxide when a load bearing pressure is applied
to the surface.   According to Birk and Miller (85) and
Sullivan (72) $\alpha-Fe_2O_3$ film is unstable because the Pilling
Bedworth ratio is high (≈ 2.14) that the large apparent
internal stess, coupled with expansion of the lattice due to
oxide growth by anion migration lead to the loss of
metal/oxide adhesion and brittle wear debris is finally
formed.   The situation is reversed in the case of FeO where
while the internal stress is low (≈ 1.68) cation migration
across the films results in the formation of cavities at the

metal/oxide interface which eventually reduce the adherence
of the oxide film to metal substrate. As a consequence
loose wear particles are produced. The most mechanically
stable oxide of Fe_3O_4 is not effected much by either of the
above mentioned factors, instead the balance diffusion of
both anion and cation into the film make the bulk of the
oxide more stable and adhesion with the metal substrate
becomes strengthened.

1.6 Theories of wear

There is no theory which is relevant to all conditions
of severe wear. Suh's (86,87) delamination theory is
concerned with purely metallic contact and is applicable to
sliding situations under light load and speed. It is based
on the nucleation and growth of subsurface cracks in the
base material. When two surfaces are in sliding contact a
relatively smooth surface is initially generated either by
deformation or removal of asperities. The surface traction
exerted by harder asperities at the contact points deforms
the subsurface layer, generating dislocation and vacancies.
Voids and cracks are formed when further plastic deformation
occurs, and this is enhanced by the presence of hard second
phase particles such as inclusions and large precipitate
particles. As the subsurface deformation continues the
voids coalesce either by growths or by shearing action of

the surrounding material around hard particles. These make up cracks which are extended parallel with the surface and after sufficient critical length is reached they shear off to the surface as sheet-like wear particles.

The delamination theory seems to be valid for most metals under the application of light load and low speed in non-reactive gases. The expression relating to wear is given by the simplified form (88) as

$$w = \left[\frac{B_1\,h_1}{d_{c1}} + \frac{B_2\,h_2}{d_{c2}} \right] A_r \qquad \dots\dots\dots\dots(1.12)$$

where

h_1, h_2 = the thickness of removed layer from the sliding
    sliding members.

d_{c1}, d_{c2} = critical sliding distance required for complete
    removal of layers on both surfaces.

c_1, c_2 = constants which depend mainly on the surface
    topography.

For mild wear the first theoretical consideration was given by Yoshimoto and Tsukizoe (89) in 1957. They proposed a model which assumed identical asperities on both sides of the sliding members and contact is made only after a constant slid distance equivalent to the distance between two neighbouring asperities. It is further assumed that oxide film growth takes place during the out-of-contact

periods after which film thickness is increased and removed
completely from the actual contact area. The same process
is repeated at each encounter. A simple expression for wear
rate relating the speed, load and hardness is obtained using
a model representing the profile of the metal surface and
assuming a growth rate obeying a logarithmic law of
oxidation. Unfortunately no experimental evidence has been
fowarded to justify the validification of the theory.

In another approach Tenwick and Earles (90) were able
to express wear rate in terms of Arrhenius equation for a
typical linear oxidation from the simple model of a single
asperity. They assumed that during sliding this asperity
remains continuously in contact with the flat underlying
surface until an oxide layer is generated, and when a
critical thickness is reached wear particles are detached
from the surface. Assumption of a parabolic growth rate law
failed to satisfy the theoretical prediction due to
difficulties in determining the critical oxide thickness.

The most advanced theory, in terms of their extensive
exeperimental verification is probably due to the work of
Quinn and his co-workers (52,18,19). Basically the model
assumed oxidation at the real area of contact, A_r, at mean
contact temperture, T_c, of the sliding asperities of mean
diameter, d. After 1/K (K is wear factor) encounters the
total time of contact required to establish a critical film
thickness, ζ_c, is equal to the ratio of d/UK(U is sliding

speed). Parabolic growth rates were assumed, and the derived K-factor is substituted into Archard wear law (equation 1.10) to give an expression for wear rate of

$$w = \frac{d \ A_p \ \exp \ -(Q_p/RT_c)}{\zeta_c^2 \ \rho_o^2 \ f \ U} \ A_r \qquad \dots\dots\dots\dots(1.13)$$

where

A_p = Arrhenius constant.

Q_p = Activation energy for parabolic oxidation.

R = gas constant.

ρ_o = oxide density.

f = fraction of oxide which is oxygen.

Equation (1.13) has been shown to be valid for unidirectional sliding of a pin-on-disc system using steels at ambient temperature and high sliding speeds above 0.5 ms^{-1}.

Recently Stott et al. (91) advanced a theoretical model to their current investigation of the generation of oxide preceding to mild wear under reciprocating sliding motion. They considered that oxidation occurs over the entire areas of contact with possibilities of oxidation by flash-temperature rises at the asperity junction similar to Quinn (52) and also by the fractured metal debris (23).

The model is based on the sliding of an upper pin surface, assuming it comprises of n asperities over an

underlying disc surface assumed to be covered with oxide
film. During the traversal (to and fro) it was further
assumed that each of the pin asperity which penetrates into
the oxide makes a load-bearing contact, abrading the
contacting asperities and removed the oxide completely from
the track. Also, the asperities remain in contact after a
mean sliding distance, and when an asperity of the pin
surface ceases to be load-bearing, it is replaced by a new
load-bearing asperity. By considering a single traversal of
the area fraction of oxide film removed from the pin and disc
surface and applying the parabolic growth rate then the ratio
of mass of oxide generated at the load-bearing asperities,
M^r, to the mass of oxide generated over the entire apparent
area, M^{aa}, in one trversal is given by (after simplification)

$$\frac{M^r}{M^{aa}} \approx K \, n^{1/4} \left(\frac{A_p}{A_p{}^{aa}} \right)^{3/4} \quad\quad \dots\dots\dots\dots(1.14)$$

where

K   = an exponential term relating to temperatures and
      equivalent to unity.

A_p = real area of contact (pin) per traversal.

$A_p{}^{aa}$ = apparent area of contact (pin) per traversal.

From the consideration of experimental results the ratio
given by equation (1.14) were about 0.07 and 0.8 for oxide
growth by metal debris mechanism and by total oxide mechanism

respectively. Stott et al., therefore suggested that, under low speed reciprocating sliding motion oxidation at the asperity contacts was negligible compared with the general surface oxidation.

1.7 Research programme

Numerous investigations have been devoted to the study of unlubricated wear of steels in which the experimental and theoretical work has provided the foundation for a better understanding of the various mechanism of wear. In view of the severe and mild aspects of wear on low alloy steels there has been a lack of information on the history behind the establishment of equilibrium wear which many workers may have neglected or forgotten.

The first aim in the present research study was to re-establish the general wear patterns similar to Welsh curves with consideration of two operational variables,i.e. the running durations and application of heavy loads. The former enabled the curves obtained under the long running periods to be distinguished from the short running periods whereas the latter case was essential in predicting several mild wear transitions, so that new set of curves could be expected from such tests. The behaviour of mild wear can, thus be explained in terms of various surface parameters predicted from the surface model.

Based on an understanding of mild wear, the second aim was to examine the initiation and the factors effecting the transition to mild wear in regions at and above the Welsh T_2 transition load. Test runs were carried out on a selected speed during which the friction, temperature, contact resistance and wear were recorded from the start of sliding to the end of transition time. A theoretical model was developed to account for the change in volume of the severe wear with sliding time up to the onset of mild wear.

Finally, research work was carried out to investigate the running-in behaviour on specific areas of the newly-established curve. Essentially they were the regions where oxide types (α-Fe_2O_3, Fe_3O_4, FeO and oxide mixtures) were dominant. Assesment of the friction, temperatures, contact resistance and wear were made from the recorded sliding parameters and samples were analysed in every succession of fixed running-time. Theoretical estimates of the surface parameters were based on available models.

Several physical method of analysis are used to analyse the samples. A selected number of pins were chosen for scanning electron microscopy, microhardness and macrohardness measurements and Auger depth profile whereas samples of wear debris collected during the test run were analysed using x-ray diffraction.

CHAPTER 2

EXPERIMENTAL DETAILS

2.1 The Wear Test Machine

Experiments were carried out in a specially designed unlubricated wear test rig in an environment of atmospheric air and at ambient temperature. The machine was originally developed by Dunckley (92) and consists essentially of a horizontal stationary pin pneumatically loaded against one face of a vertical motor driven disc in such a way that the two surfaces generated sliding contacts. The machine was constructed from the systems comprising of the drive, shafts specimen holders assemblies, and equipped with ancillary devices (friction and wear transducers, thermometer and contact resistance devices) for measuring the sliding parameters. A general view of the wear machine is shown in Figure 2.1 and its component parts are described in the proceeding sections.

The machine was driven by a 3 H.P. electric driven motor through a reduction gearbox and produced output speeds between 120 and 720 rpm. With an arrangement of V-belts and two external pulleys of different sizes, however, the range of speeds could be extended between 40 - 1440 rpm for a constant sliding radius of 50.9 mm. This was equivalent to 0.2 to 7.6 ms^{-1} linear track speed.
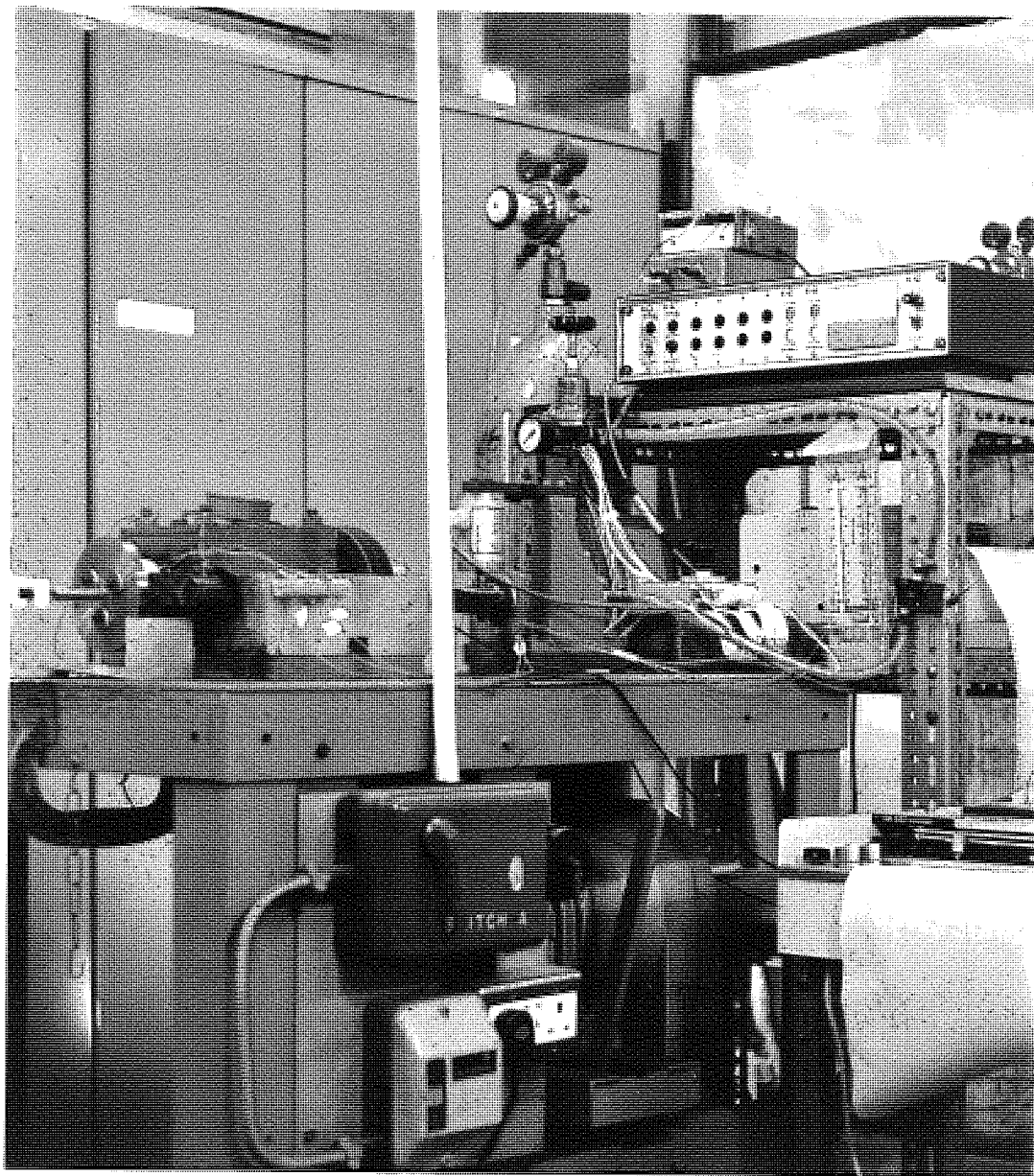
Figure 2.1 General view of the pin on disc wear test machine.
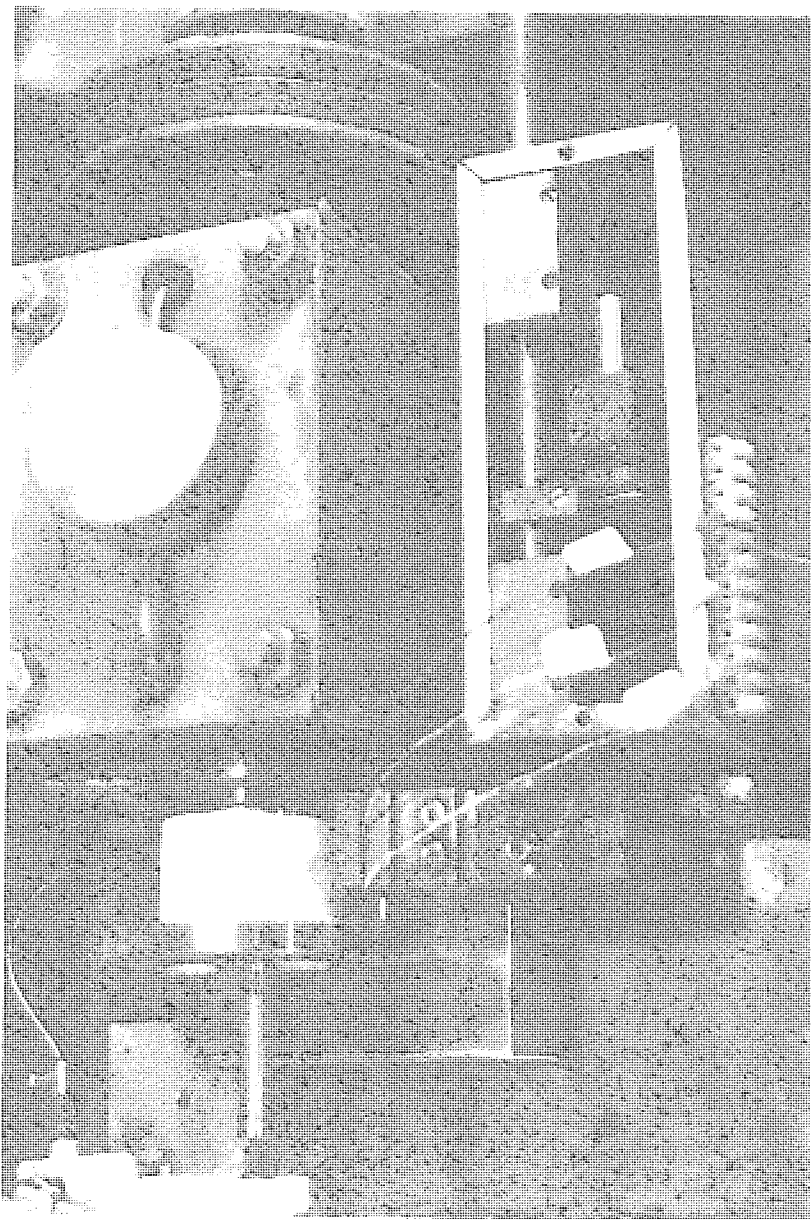
Figure 2.2 Details of the pin loading assembly and contact resistance facility.

A desired speed, say $w_1 = 1.2$ ms^{-1} (300 rpm) at the disc radius ($r_1 = 50.9$ mm) was normally fixed prior to an experiment, so that the speed (w_2) at a known radius of the pulley ($r_2 = 160$ mm) could be determined using the relationship $w_1 r_1 = w_2 r_2$. The measurement of such speed was accomplished using an optical digital tachometer in which a light beam was directed onto a reflecting tape attached to the pulley. The beam was reflected back consecutively and automatically sensed a digital readout in rpm. The reduction gearbox was altered until the computed $w_2 = 95.4$ rpm was attained.

The main shaft and loading shaft were mounted parallel one to each other in separate housings (see figure 2.2). The former rotated the disc through rotation of the pulleys which were fixed to its end. In some application of elevated temperature experiments a water cooling system was incoporated inside the shaft, in order to reduce overheating of the surrounding components. The latter was capable of rotation in its roller bearings, which enabled frictionless horizontal and vertical movements of ancillary components fixed to this shaft, such as wear transducer plate, friction arm and pin holder arm.

The specimens arrangement is as shown in Figure 2.3. The disc was mounted vertically onto the main shaft (opposite to the pulleys) while a horizontal pin was mounted facing the disc surface at a fixed radius from its centre. As the disc
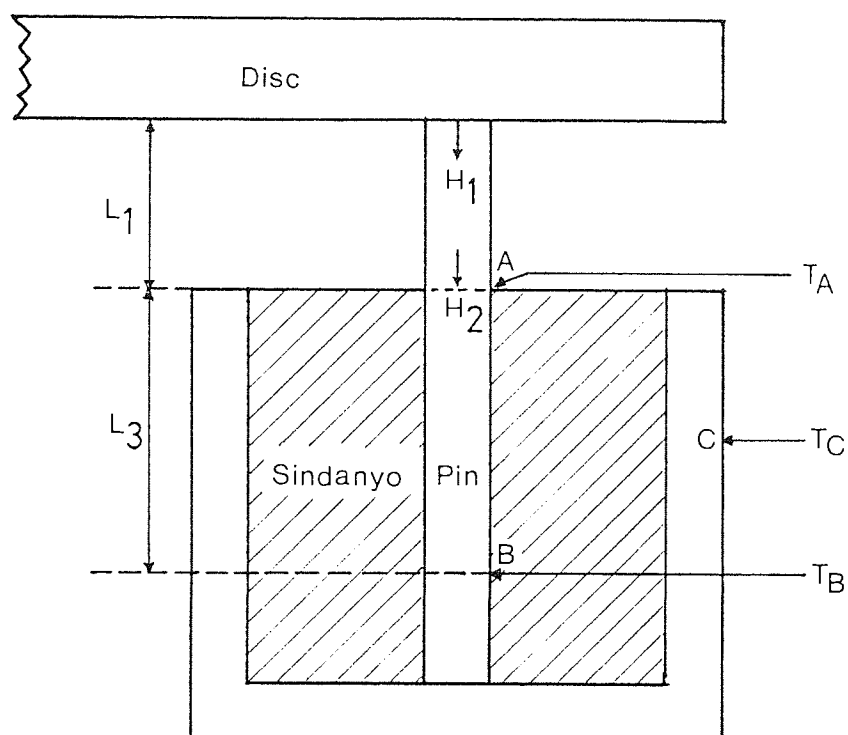
Figure 2.3 Cross-sectional diagram of the pin and
pin holder showing heat flow and
thermocouples positions.

rotated in an anticlockwise direction its surface was brought
into sliding contacts with the stationary pin by the
pneumatic application of load at any given speed (see figure
2.2). An advantage of using this pin-on-disc system was that
the debris, once detached from the surfaces, fell from the
sliding interface, enabling easy collection for analysis.
This further ensured that debris did not accumulate at the
conjunction.

The pin was held in a calorimeter-type holder fixed to
the loading arm in order that heat flow analysis into the pin
could be accomplished. Within the copper calorimeter (with
thermocouple leads) the pin was held between two hollow
cylindrical halves of sindanyo material. The assembly was
then pushed into the holder and clamped with two tightened
side screws.

2.2 Load Application

Loads were applied using a pneumatic system which
allowed compressed air, regulated through a pressure gauge to
a piston via a quick-release valve. This could only be used
for loads greater than 10 N. A simple dead weight system was
used for lighter loads up to 10 N since the regulator became
insensitive for small pressure variations. Both methods
provide a wide range of pressures between 0.1 - 1.6 bar or an
equivalent load range of 0.15 to 200 N.

The air pressure was calibrated using a friction force transducer, providing a direct conversion from mbar of pressure to Newton (N) of applied load. The transducer was placed in an upside down position and first loaded with a known normal weight, say 9.81 N, and the deflection measured on a chart recorder. An average of six such readings resulted in a 53.5 mm deflection per 9.81 N of load for 100 mV sensitivity (or 5.35 mm for 1V sensitivity), giving a calibration factor, $c_1 = 0.183$ N per mm displacement. The same transducer was then positioned axially to the pin in place of the disc, when the pressure was increased and the chart pen displacement noted. The displacement was multiplied by c_1 to convert to load in Newton (N). The resulting calibration curve is shown in Figure 2.4 where 1 bar = 11.1 N load.

2.3 Friction Measurement

Friction force was measured indirectly by means of a strain gauge transducer. It sensed the torque produced by the frictional drag of the rotating disc on the pin as an upward force exerted via the friction arm. The resulting output was fed to a strain gauge amplifier unit and onto a chart recorder.

The device was calibrated by placing known weights, on the pin holder exactly over the place where the centre of
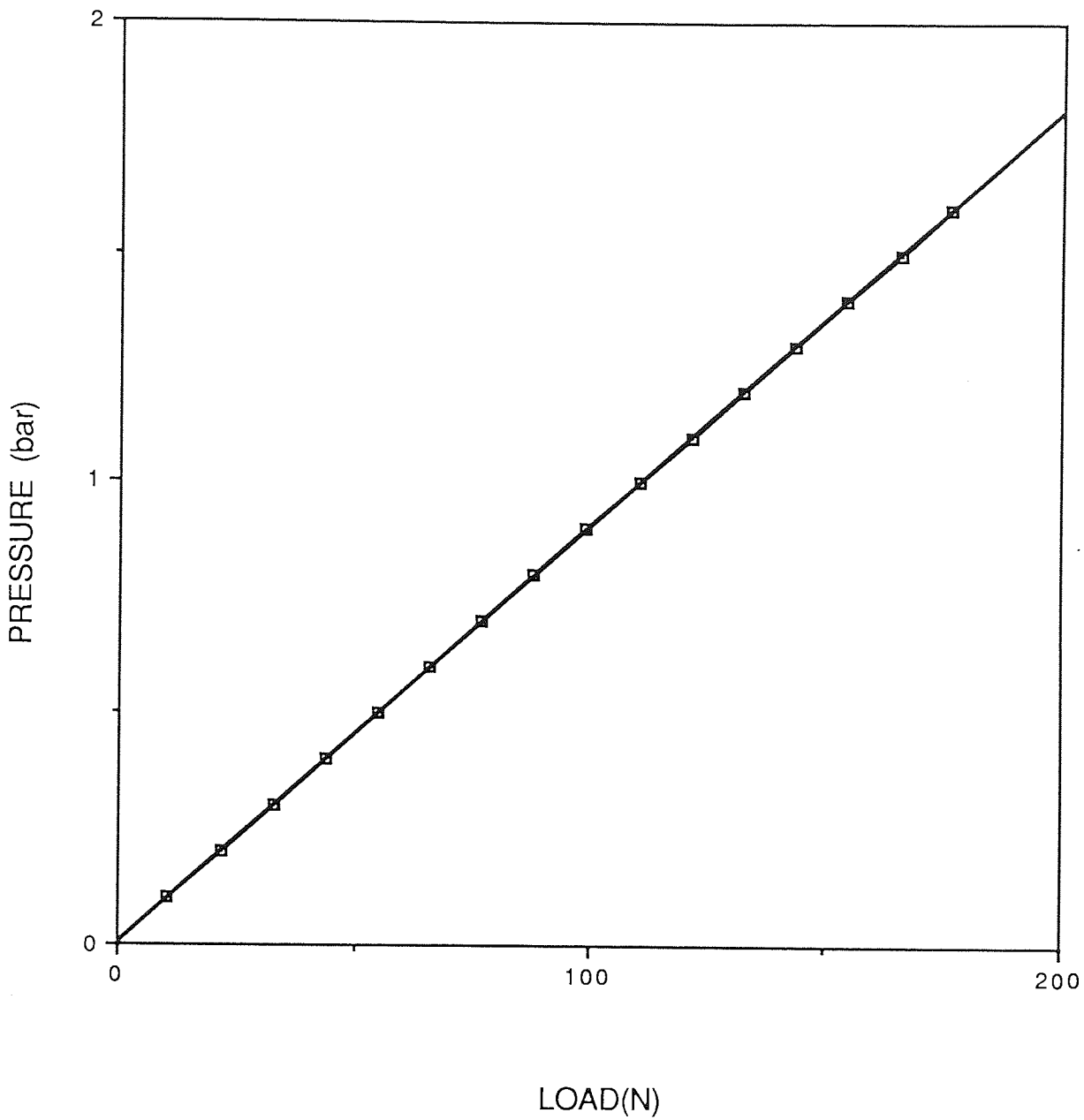
Figure 2.4 Graph of calibration showing pressure

variation with load.

gravity coincided with the pin axis. Examples of the five
load readings on both ranges of sensivity are given in the
following table.

Load at pin (N): 9.81   19.62   29.43   49.05   78.48

Displacement of: 51.0   102.8   153.2   25.7   40.6
chart pen (mm)

100 mV   1V

The average calibration factor, c_f was found to be 0.192 N
and 1.92 N per mm deflection for 100 mV and 1V sensitivities
respectively. The friction coefficient of sliding interface
caused by any h_f (mm) deflection of the chart pen is given by

$$\mu = \frac{h_f \, c_f}{W} \qquad\qquad \dots\dots\dots\dots (2.1)$$

where W is the applied load.

2.4 Wear Measurement

The pin wear was measured by means of linear voltage
differential transformer (LVDT) fixed alongside the loading
shaft. A constant D.C. voltage was supplied from the same
strain gauge unit as that described above. During operation
the LVDT sensed the forward movement of a wear plate caused
by the pin wear and converted the displacement into
electrical output signal. This output was fed directly to a

chart recorder for continuous monitoring. The sensitivity of the LVDT was 1.22 mm of pin wear per Volt.

The device was calibrated by means of a micrometer held in a hollow metal cylinder. Typically a 1.092 mm displacement at the pin gave 179 mm deflection of the chart pen when a 10 V range selector was chosen. Under the same range the average calibration factor, c_w for at least six readings was 0.0061 mm (pin wear) per mm (pen deflection). Using the basic defination of wear as volume removed per unit sliding distance the wear rate of the pin may be expressed as

$$w = \frac{r^2 \ c_w \ h_w}{DU}\left(\frac{}{t}\right) \qquad mm^3 mm^{-1} \qquad \dots\dots\dots\dots(2.2)$$

where

r = mean radius of the pin (mm).

h_w/t= slope of the wear trace (mm min.$^{-1}$).

D = mean diameter of the wear tracks (mm).

U = sliding speed (rpm).

A conversion to SI unit ($m^3 m^{-1}$) was made after each calculation.

2.5 Temperature Measurement

A chromel-alumel or K-type thermocouple junction was used for the measurement of temperature because of its wide range of linearity, i.e. between -200 to 1100°C.

Thermocouple outputs were detected by a chart recorder.

For the disc one thermocouple was placed on the wearing face at the radius of the sindanyo insulator ring holding the disc, coupled with two adjacent carbon slip-ring-brush combinations for external connection with a chart recorder. The dics temperature was designated as T_D. For the pin, three such thermocouples were spot welded at positions A and B along the pin and C on the copper calorimeter to determine the pin temperatures T_A, T_B and T_C respectively (see Figure 2.3). Other thermocouples included two blank junctions which were exposed to the ambient room air and in contact with a wet cloth respectively. This arrangement was aimed at measuring the relative humidity of the air from dry and wet room temperature readings.

An electronic digital thermometer with compensated automatic cold junction, was connected between the thermocouple junctions and the chart recorders via a multiway switch to provide direct temperature readings when the test run was in operation. The temperatures read from the meter were compared with chart pen deflections over six different readings, in order to obtain the average calibration factor, c_t expressed in degree celcius per mm deflection. Approximately $c_t = 12 \pm 3$ $^{\circ}C$ mm^{-1} at 10mV setting, but individual calibration was performed during each run for better accuracy. The sensitivity of the thermocouple was found to be 0.04 mV $^{\circ}C^{-1}$. The temperature for any value of

h_T (mm deflection) of a chart pen above the room temperature is given by

$$T = T_r + h_T c_T \quad {}^{\circ}C \qquad \qquad \dots\dots\dots\dots(2.3)$$

where T_r = room temperature (${}^{\circ}C$).

2.5.1 Heat Flow

The arrangement of pin calorimeter and thermocouples described in the earlier sections (see Figure 2.3) enabled heat flow along the pin to be measured continuously. Based on a theory given in reference (93) the general surface temperature, T_s, and heat flow per second at the interface, H_1, were calculated using the following expressions.

$$T_s = (T_A - T_B)\ \cosh\left(\frac{L_1}{zR_p}\right) + \frac{z\,H_2}{K_s R_p}\ \sinh\left(\frac{L_1}{zR_p}\right) + T_c \quad ..(2.4)$$

$$H_1 = \frac{K_s R_p}{z}\ (T_A - T_B)\ \sinh\left(\frac{L_1}{zR_p}\right) + H_2\ \cosh\left(\frac{L_1}{zR_p}\right) \quad ....(2.5)$$

where

$$z = \frac{K_s}{(2hR_t)^{1/2}} \qquad \text{and} \qquad M^2 = \frac{2K_1}{K_s R_t{}^2\ \ln(R_m/R_p)}$$

R_p, R_m = radius of the pin and insulator outer ring respectively.

K_s, K_i = thermal conductivity of the pin and insulator respectively.

h = heat transfer coefficient between the cylindrical exposed surface of the pin and the air.

2.6 Contact Resistance Measurement

Following the design by Stott, Glascott and Wood (94) a device was constructed for the measurement of contact resistance in the range between 1 to 10^4 Ω. The basic circuit diagram is shown in Figure 2.5. A +10 mV stabilized reference voltage is developed at point X to provide a potential difference across the sliding specimens. The resulting current flow through the contact is amplified and the output gives a measure of the change in contact resistance, R_c. The circuit design was such that the input current varied according to an exponential current-voltage characteristic. Obviously this characteristic was necessary because of the large current variations between metal/metal (minimum resistance) and oxide/oxide (maximum resistance) contacts, so that when converted to output signal detectable ranges of reading may be observed. The output obtained from the operational amplifier (amplifier 1) is given by

$$V = K \ln R_c - K \ln(V_r/C) \qquad \dots\dots\dots\dots(2.6)$$
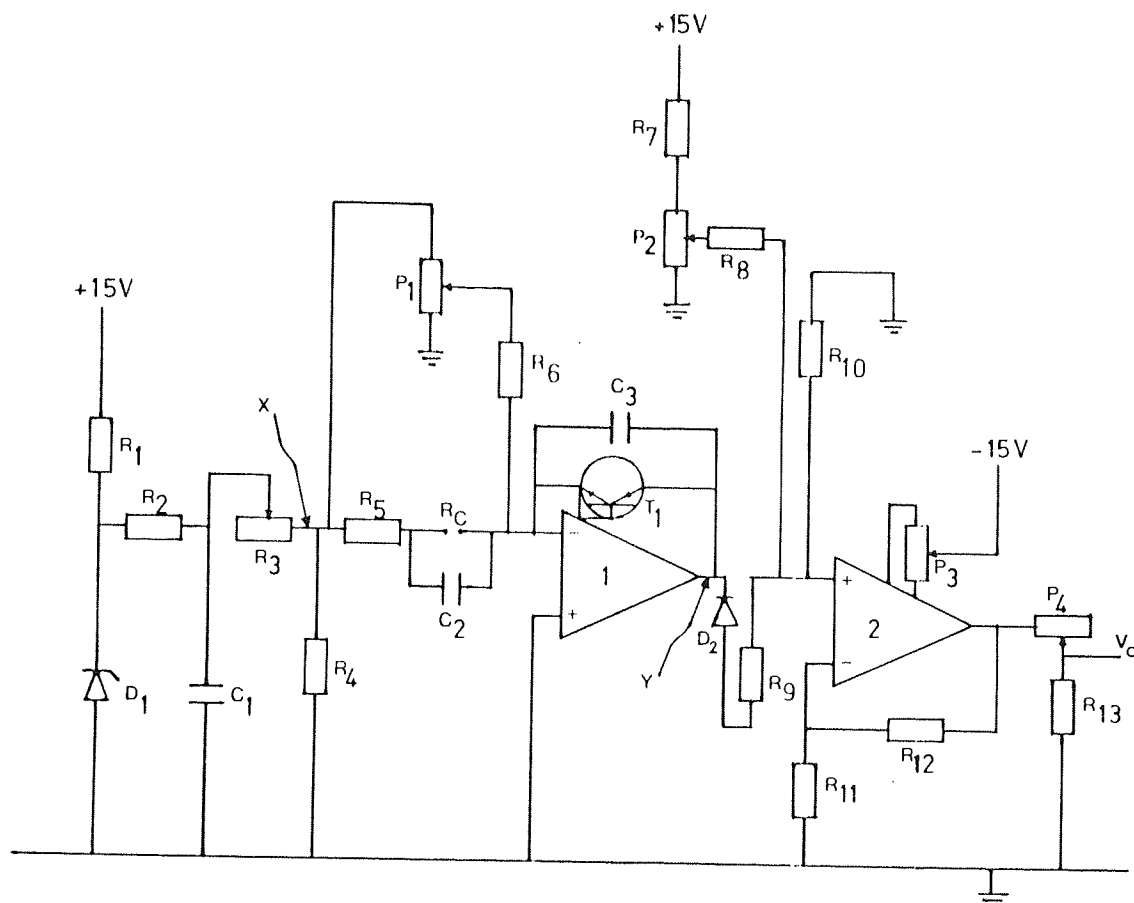
$R_1 = 330 \, \Omega$, $R_2 = 220 \, \Omega$, $R_3 = 390 \, \Omega$, $R_4 = 1 \, \Omega$, $R_5 = 10 \, \Omega$, $R_6 = 470 \, k\Omega$, $R_7 = R_8 = R_9 = R_{11} = 2.2 \, k\Omega$, $R_{10} = R_{12} = 22 \, k\Omega$, $R_{13} = 100 \, \Omega$. Amplifier 1, 308 A; amplifier 2, 741 A; transistor T_1, BC109; diode D_1, BYZ 88 (5.6V); diode D_2, signal diode; $C_1 = 100 \, \mu F$, $C_2 = 0.1 \, \mu F$; $P_1 = 100 \, \Omega$, $P_2 = 220 \, \Omega$, $P_3 = 10 \, k\Omega$, $P_4 = 1 \, k\Omega$, $C_3 = 0.1 \, \mu F$.

Figure 2.5   Schematic diagram of contact resistance

measurement device.

where

V_r = resistance voltage.

C = collective term relating to a number of transistor
parameter.

K = a ratio of fundamental constant and the transistor
junction temperature.

For a range of contact resistance between $1 - 10^6 \, \Omega$ the
corresponding output voltage at point Y increased from -660
to -330 mV.   The second stage amplifier produces an
output signal which can be fed to a chart recorder for
contact resistance monitoring.

Figure 2.6 shows the range of sensitivity of the device,
apparently slow respond at the beginning of $10^2 \, \Omega$, but
increasingly linear with log contact resistance up to 10^5
before eventually dying out at $10^6 \, \Omega$.   The device was
connected to the specimens via a contact resistance facility
(see figure 2.2) and calibrated using standard resistances.

2.7 Test Specimens

Two alloys of medium-carbon steels, BS EN 31 and BS EN 8
were used as a pin and a disc respectively.   Details of the
material compositions are as follows:
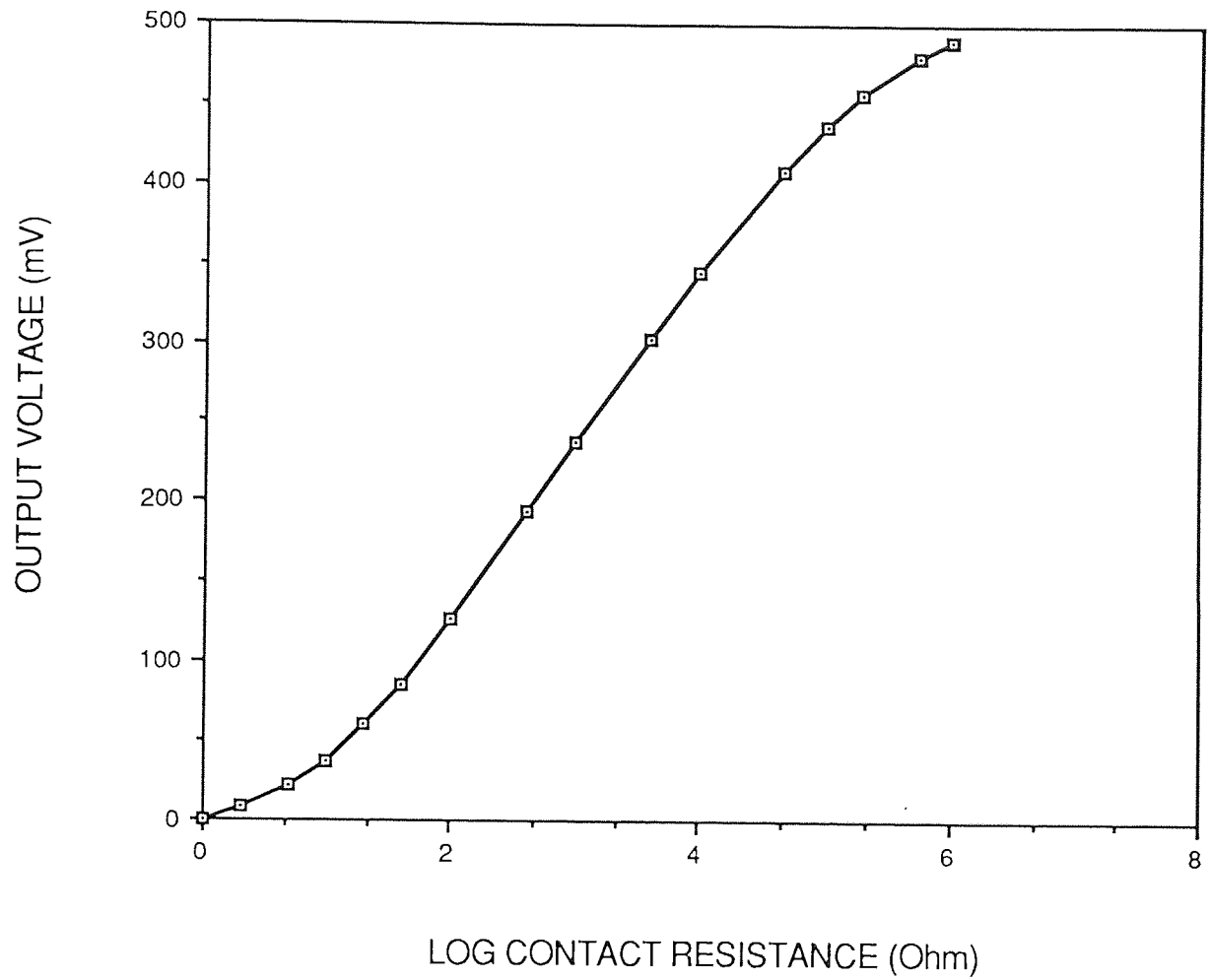
Figure 2.6   Variation of output voltage with log contact resistance.

COMPOSITION	C	Si	Mn	S	P	Cr	Fe
BS EN 8 DISC* (%)	0.35– 0.45	0.05– 0.35	0.6– 1.0	0.06 max.	0.06 max.	–	remin der
BS EN 31 PIN** (%)	0.9– 1.2	0.1– 0.35	0.3– 0.75	0.05 max.	0.05 max.	1.0– 1.6	remin der

These materials are now designated * EN 8   BS 080 M40
                                    ** EN 31   BS 535 A99

The discs were prepared from 135 mm diameter BS EN 8 black bar, sliced into 13 mm thick and turned to a surface finish of 8 um centre line average. Two removable plugs were inserted in each disc at diametrically opposite positions, centered about the middle of the wear track anulus (see Figure 2.7) to provide disc specimen for analysis after experimental investigation. The discs were reusable by repeated grinding.

The 6.3 mm diameter pins were machined from a cold-rolled bar into three different lengths of 32mm, 35mm and 38mm, the larger sizes were used for experiments under heavier loads, and they were ground to similar surface finish of the disc. The presence of chromium in BS EN 31 steel gave rise to a mean bulk hardness of 285 ± 10 VPN, obviously higher than that of BS EN 8 which measured 205 ± 12 VPN. Prior to each experiment the specimens were cleaned in an electrically heated vapour bath of petroleum ether for at least 30 minutes to remove contamination on the surface.
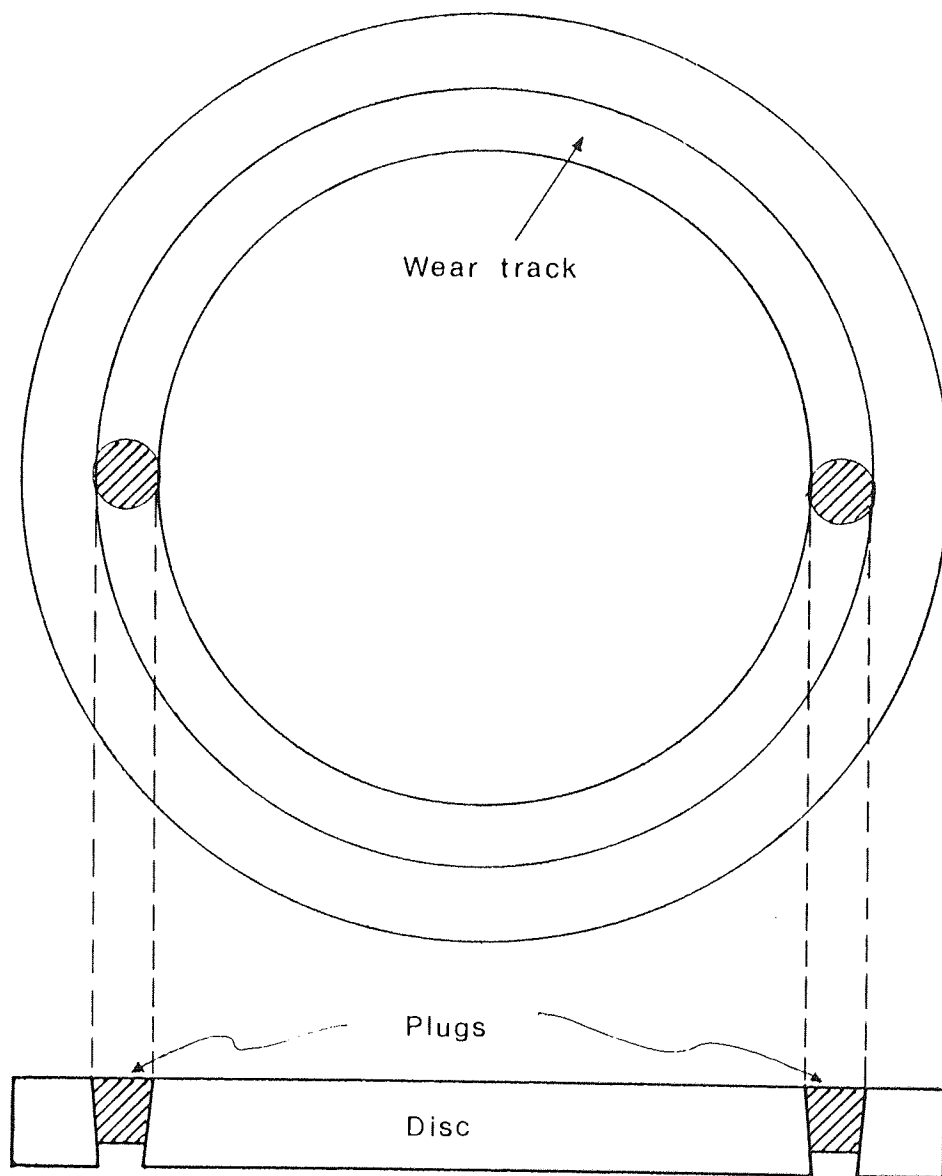
Figure 2.7 Plugs at diametrically opposite positions in wear track.

2.8 Wear Tests

2.8.1 Introduction

Wear tests have been carried out on each of the EN 31 pin/EN 8 disc couples for a combination of loads and sliding speeds at room temperature. Normally the machine was prerun for about one hour to establish a constant operating sliding speed, since there was normally a slight increase of 2 - 3 rpm during the initial stages of a run. The machine was then stopped to enable final preparation for the test run, such as specimen mounting and loading of air pressure as well as setting the initial readings of the ancillary devices. During each test run the frictional force, pin wear, temperatures and contact resistance were continuously recorded on separate chart recorders.

2.8.2 Establishment of Curves

A series of Welsh curves were generated to include the region of the T_2 transition region and above. Curves were generated by plotting wear rate versus load, over a load range from 2 to 155 N for sliding speeds of 0.6, 0.8, 1.0, 1.2 and 1.6 ms^{-1}. The experiments were repeated at least six times to obtain the mean quoted values.

The wear test runs were conducted under two series of conditions: one where the duration was for two hours (short

running periods) for each of the 0.8, 1.0 and 1.2 ms^{-1}

speeds, and secondly a longer duration (long running periods)

between four to seven hours at all speeds.

2.8.3 Progression of Test Run

In order to provide a history of the development of

oxides, experiments were conducted on selected areas of the

Welsh curve at a speed of 1.2 ms^{-1}. A series of progressive

test runs were made at the T_2 transition load around 11.0 N

($\pm$ 0.8 N), a value obtained from Welsh results, and such test

was usually indicated by the initial long periods of severe

wear after which mild wear persisted. All sliding parameters

were carefully monitored and debris collected successively

every ten minutes from the start of the run until just after

the transition to mild wear where the test run was

terminated. This provides specimen pins and discs for

analysis.

Another series of progressive test runs were conducted

at loads above the T_2 where the preliminary long durations of

mild wear was studied. Four different loads were chosen each

of which represented the different mild wear regimes and test

runs were stopped after 5 minutes, 20 minutes and so on every

further increment of 20 minutes until equilibrium condition

of mild wear was established. A new set of pins and discs

were used for every progression of such fixed runs, thus

enabling the collection of specimens and wear debris.

2.9 X-ray analysis

The wear debris was analysed using a cylindrical
Debye-Scherrer powder x-ray diffraction camera (114.6 mm in
diameter) (95). The sample was carefully prepared in a fine
non-crystalline glass capillary tube (0.5 mm in diameter) and
placed inside the camera at its centre. The x-ray tube was
set at a voltage of 40 KV and a filament current of 30 mA to
produce targetted cobalt x-ray. K_α radiation was obtained by
absorbing the unwanted components with an iron filter. The
sample was irradiated for 45 minutes of exposure time.
The interplanar spacings of a series of diffracted beams
(angle Θ) are determined by using Bragg equation, i.e. $d_{hkl} = n\lambda/\sin\Theta$. A direct comparison with ASTM standards (appendix
I) enables identification of any particular types of element
or compound in a given sample.

Some selected worn pin surfaces were analysed using a
glance angle x-ray diffraction technique. The specimen was
mounted at the centre of the powder camera and its position
was arranged so that x-ray beam impinges on an edge of the
surface at a glancing angle of 30°. Cobalt K_α x-rays were
used to irradiate the desired area of the specimen, at an
x-ray tube setting of 40 KV and 30 mA for 30 minutes.

A microdensitometer was used to obtain a line profile of

the x-ray diffraction patterns. It transformed the line pattern of each x-ray intensity into line density and this can be represented as peaks of different heights. The relative integrated intensities of the diffraction lines is equal to the product of these peak heights and the widths of the peak at half its height.

2.10 Scanning Electron Microscopy

Some selected specimens were examined using the Scanning Electron Microscopy (SEM) from which micrographs of the worn surfaces were produced for topographical study and for direct measurement of the oxide film thickness. The specimens (about 5mm in length) just needed a double sided adhesive tape to stick them onto the specimen holder and were made electrically conductive by applying silver paint. An aeorosol conducting film was also sprayed on top of the oxide which covered the worn surfaces to prevent specimen charging.

SEM uses a narrow beam of electrons scanning the surface in a T.V. type raster. The instrument operates by converting the secondary electrons produced into images of the desired area under investigation. Photographs of the resulting T.V. image enable interpretation of the surface features to be made.

An additional tilt correction facility on the instrument was used for the measurement of vertical thicknesses. The

tilt correction angle, normally fixed at 45° was set to the same tilt angle to unify the magnification over the area of the specimen, i.e. both lateral and vertical magnification became equal in magnitude. The horizontal bar at the bottom left of the micrograph (μm) was used as a reference scale.

Micrographs of the subsurface microstructure were obtained from the tapered microsection of the worn pins. Test samples were prepared by first moulding into a conducting bakelite, then grinding with different grit silicon carbide papers (180, 240, 400, 600 and 1200 grit) in running water. They were finally finished by polishing with 6 μm and 1 μm diamond wheels. A typical alcholic ferric chloride etchant was used for microstructure identification.

2.11 Macrohardness and Microhardness Measurement

2.11.1 Bulk Hardnness

The bulk hardness of the untreated specimens were measured using a Vickers Macrohardness Tester. It just needed measurements of two diagonals of the indented diamond like pyramid , then averaged and converted to Vicker Pyramid Number (VPN) using a conversion table provided. An alternative method was to employ a hardness expression, H as follows (96):

$$H = \frac{1.8544 \times P}{d^2} \qquad Nm^{-2} \qquad \ldots\ldots\ldots\ldots(2.7)$$

where

P = indentation load (N).

d = average diagonal length (m).

An indentation load of 20 Kg. was used throughout. If for example the average measured of d = 400 μ (4.0 x 10^{-4} m) then equation (2.7) gives H = 2.27 x 10^{9} Nm^{-2} which equivalent to H = 227 VPN from the conversion table. Thus 1 VPN = 10^{7} Nm^{-2}. The mean bulk hardness was taken from at least ten readings.

2.11.2 Microhardness

A Miniload Microhardness Tester was used to measure the microhardness of the specimens especially on small restricted area of indentation, such as rough worn surface and subsurface microsection. Loads of 50 grm, 100 grm and 200 grm were used depending on the degrees of the surface hardness. The microhardness, H" was determined using an expression (97) relating to the load, P" (grm) and the average indented diagonal length, d" (micron), i.e.

$$H" = \frac{1854.4 \times P"}{d"^2} \qquad \ldots\ldots\ldots\ldots(2.8)$$

or it may simply be readable from the table if d" is known. Prior to each measurement the worn surface was cleaned with

petroleum ether to remove contaminants and oxide films from the surface.

Microhardness depth profiles were determined for the tapered section of the worn pin surfaces. Initially the pins were moulded into conducting bakelite at a taper angle of 10° and ground with wetted silicon carbide grit papers (180 – 1200 grit). After polishing with 6 μm and 1 μm diamond wheels the specimens were applied with an etchant, preferably of 2% nital solution to reveal faint normal spotted microstructure and white hardening layers (if present). This identified areas of varying deformation where microhardness measurements were to be made.

2.12 Auger Electron Spectroscopy

Auger Electron Spectroscopy (AES) is a high sensitivity analytical tool for obtaining the chemical composition in the 5 – 20 °A region near the solid surface. The instrument used in this particular study was a KRATOS XSAM 800, a combination of high performance x-ray photoelectron spectroscopy and scanning Auger Microprobe.

In order to obtain elemental composition as a function of depth, the specimen was bombarded with Argon ions set at a beam voltage of 5 KV and emission current of 30 μA when the gas pressure was 5×10^{-7} torr. This enabled successive removal of oxide layer from the surface by a sputtering

process rated at 30 ± 5 $^{\circ}Amin^{-1}$. Composition profiles were

obtained from the plotted Auger spectra which then converted

to the relative concentration of the elements using an

expression given in reference (98).

CHAPTER 3

EXPERIMENTAL RESULTS

3.1 Introduction

The first three sections in this chapter deal with the
results obtained from the main body of experimental work.
The wear pattern experiments are presented first, followed by
the results of the severe to mild wear transition tests and
running-in mild wear tests. All results were obtained at
ambient room temperature of approximately $23 \pm 5^{\circ}C$ and
relative humidity 49 ± 7 % for all seasons and weather
conditions.

The analysis of the wear debris and worn specimens is
given separately in section 3.5 to section 3.9. These
include results from various physical techniques; x-ray
diffraction of wear debris (section 3.5), proportional
analysis of wear debris (section 3.6), microhardness
measurements (section 3.7), scanning electron microscopy
(section 3.8) and finally Auger electron spectroscopy
(section 3.9).

3.2 Wear pattern experiments

3.2.1 Introduction

The wear patterns are based on graphs plotted on

equilibrium wear rate versus load, known as a Welsh curve.
Each point on each curve was obtained from a series of
experiments carried out in a time period such that the change
in room temperature and relative humidity was no more than ±
2°C and ±3% respectively.

3.2.2 Short duration wear tests

Three Welsh curves were produced for the experiments
carried out at sliding speeds of 0.8, 1.0 and 1.2 ms^{-1} where
the test runs were of about two hours duration, and it was in
this period of time that equilibrium wear rates were
determined.

The results are presented in figures 3.2, 3.3 and 3.4
with long duration curves presented on the same graphs. The
curves (see figures 3.2 to 3.4 in broken lines) show a marked
change in wear rate at the Welsh T_2 transition with further
transition in the regime of mild wear. Wear rate was
proportional to load below and above the inflexion in the
mild wear region of the curves. The extent of the curves was
limited at the higher load, since the 32 mm pins used in the
experiments wore down very rapidly during the initial period
of sliding. In general, the short duration curves exhibit
trends similar to those curves obtained by Welsh and other
researchers whose works were described in section 1.4 of
chapter 1.

3.2.3 Long duration wear tests

A further series of tests was carried out for running
durations of between two to seven hours at five sliding, at
speeds of 0.6, 0.8, 1.0, 1.2 and 0.6 ms^{-1}. At the end of
each such period an extra time of between one to two hours
was allowed to enable the calculation of equilibrium wear
rates. All the five curves are shown separately in figures
3.1 to 3.5. In order to obtain a broad range of wear
patterns, longer specimen pins of 38 mm diameter were used,
in particular at the heavier loads.

At 0.6 ms^{-1} (figure 3.1) the Welsh T_2 transition
occurred at a load of 108 N; the transition load was reduced
to 40 N at 0.8 ms^{-1} and 15.2 N at 1.0 ms^{-1} (see figures 3.2
and 3.3). At loads greater than the T_2 transition, the mild
wear rate firstly showed an increase with load, then at a
further transition load T_3 a decrease to minimum wear rate,
followed by a third transition T_4 with a sharp rise back to
the previous level of wear rate with finally another linear
increase with load.

Figure 3.4 plotted for a speed of 1.2 ms^{-1} shows, in
addition to the variation described, a further transition T_5
and a sharp drop in wear rate at a load around 100 N. The
tests carried out at a load of 105 N and above only exhibited
this for runs of more than 2 hours duration and this further
may not have been noticed had the long running duration been
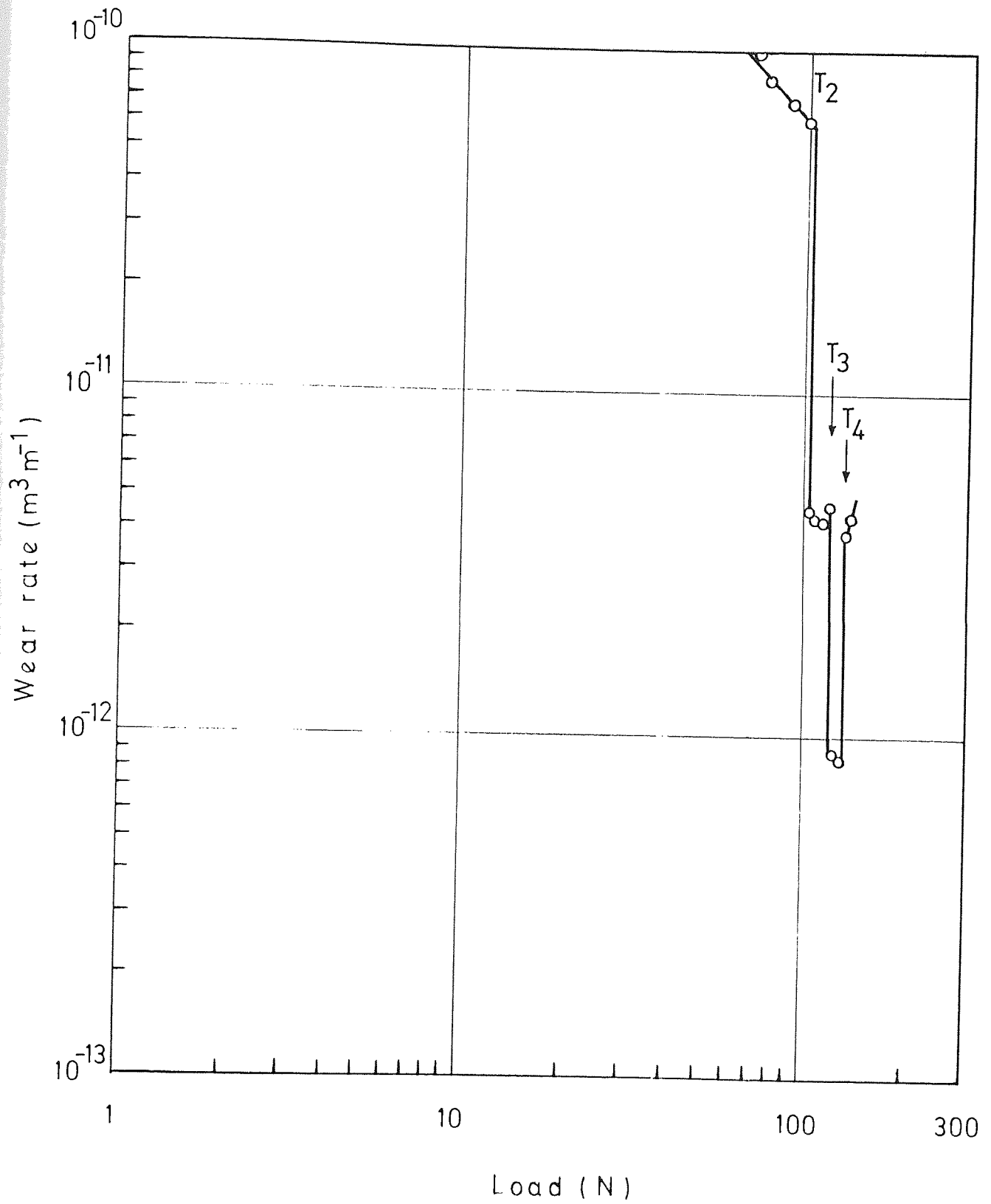
Figure 3.1   Wear rate versus load at 0.6 ms⁻¹.
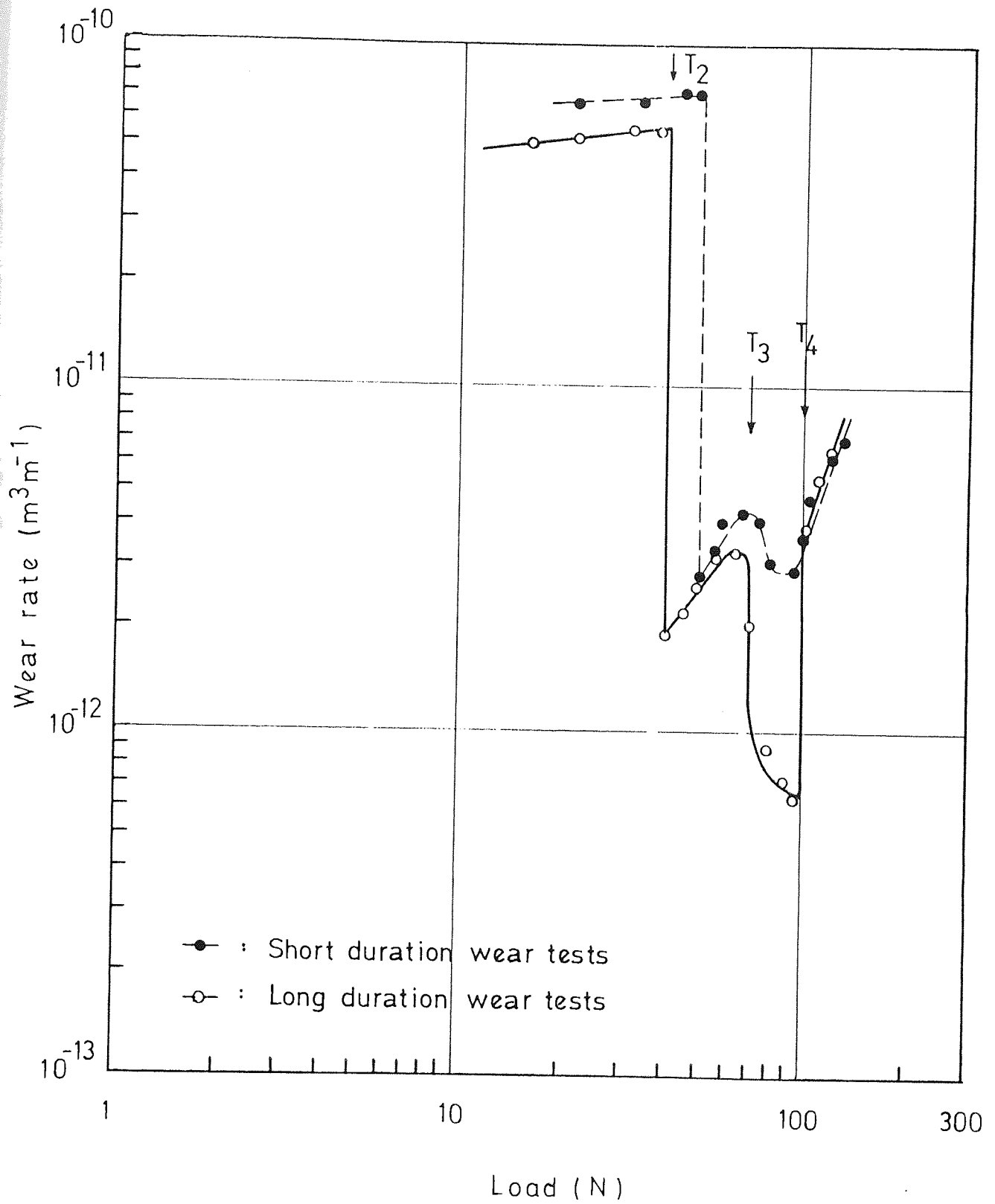
Figure 3.2 Wear rate versus load at 0.8 ms^{-1}, showing
the short and long running duration curves.
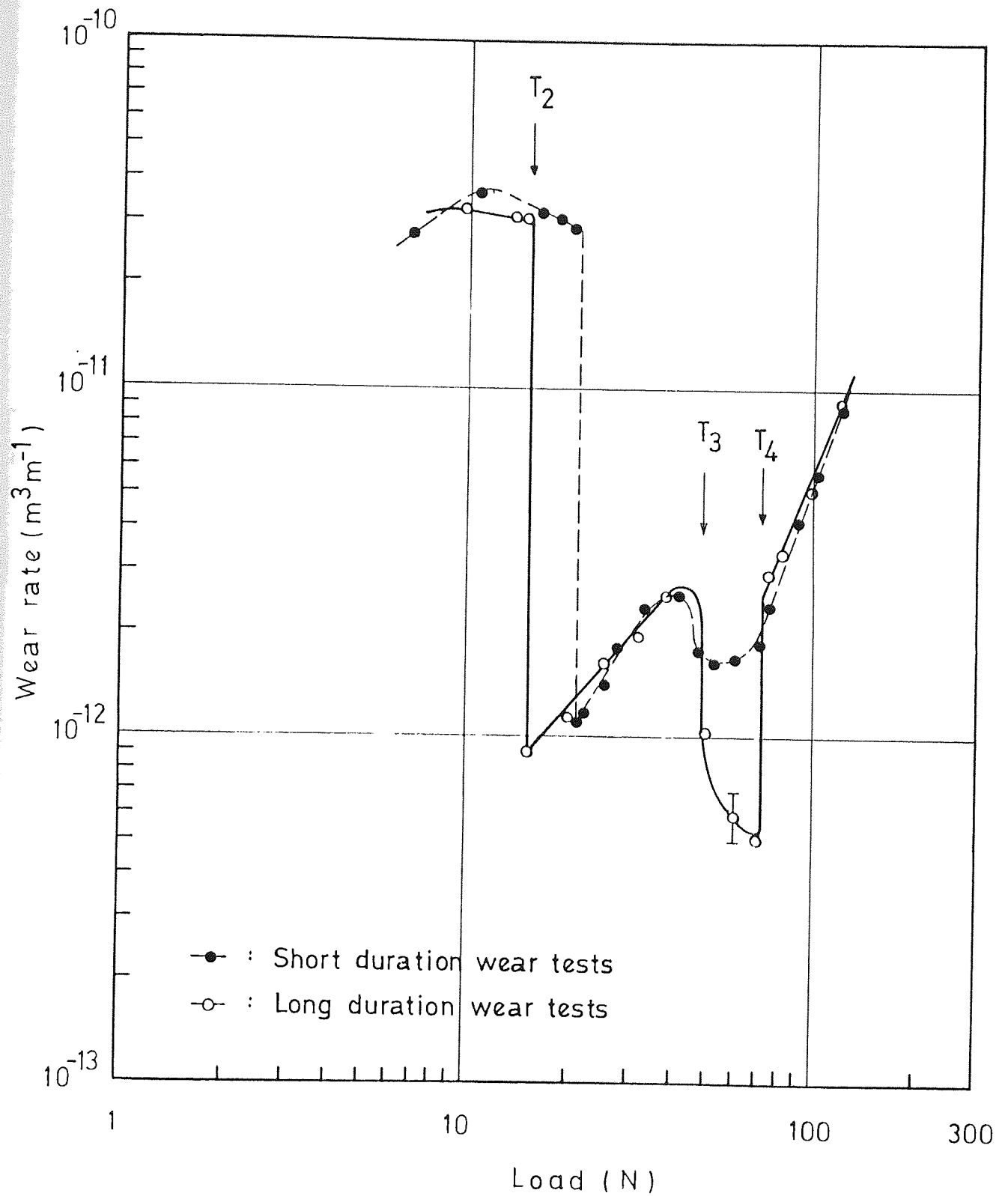
Figure 3.3 Wear rate versus load at 1.0 ms⁻¹, showing
the short and long running duration curves.
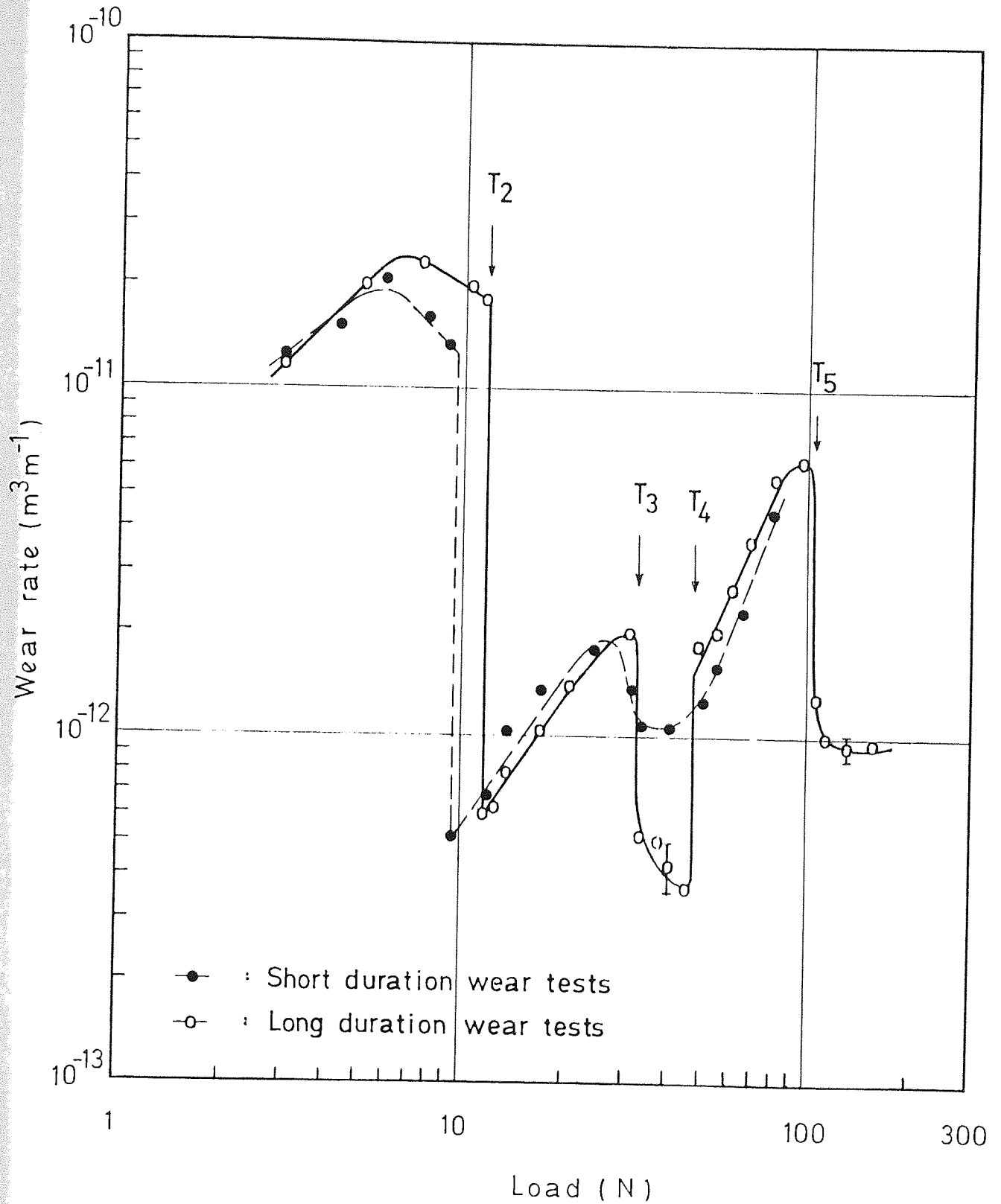
Figure 3.4   Wear rate versus load at 1.2 ms⁻¹, showing
the short and long running duration curves.

neglected. For running duration less than two hours the apparent equilibrium wear rate was high, and this gave a linear increase with load similar to that observed for curves obtained for the other short running duration tests.

The 1.6 ms^{-1} curve, shown in figure 3.5, represents the lowest detectable T_2 transition load of 2.4 N and the lowest range of wear rates. With the same trend of linear increase in wear rate a small inflexion occurred approximately between 21 to 35 N. During these tests running duration of seven hours were employed in order to establish whether any further drop in wear rate occurred. The resultant wear rate versus load curve was similar to that of figure 3.4 and also exhibited a second fall in wear rate, but at a lower load of 52 N. All the transitions T_2, T_3, T_4 and T_5 on the curves are summarized in table 3.1.

Table 3.1 Transition load data

Speed	Transition load (N)			
(ms^{-1})	T_2	T_3	T_4	T_5
0.6	102.0	110.0	120.0	No transition
0.8	40.0	70.0	100.0	No transition
1.0	15.2	48.0	72.0	No transition
1.2	11.8	32.0	47.0	105.0
1.6	2.4	21.0	35.0	52.0
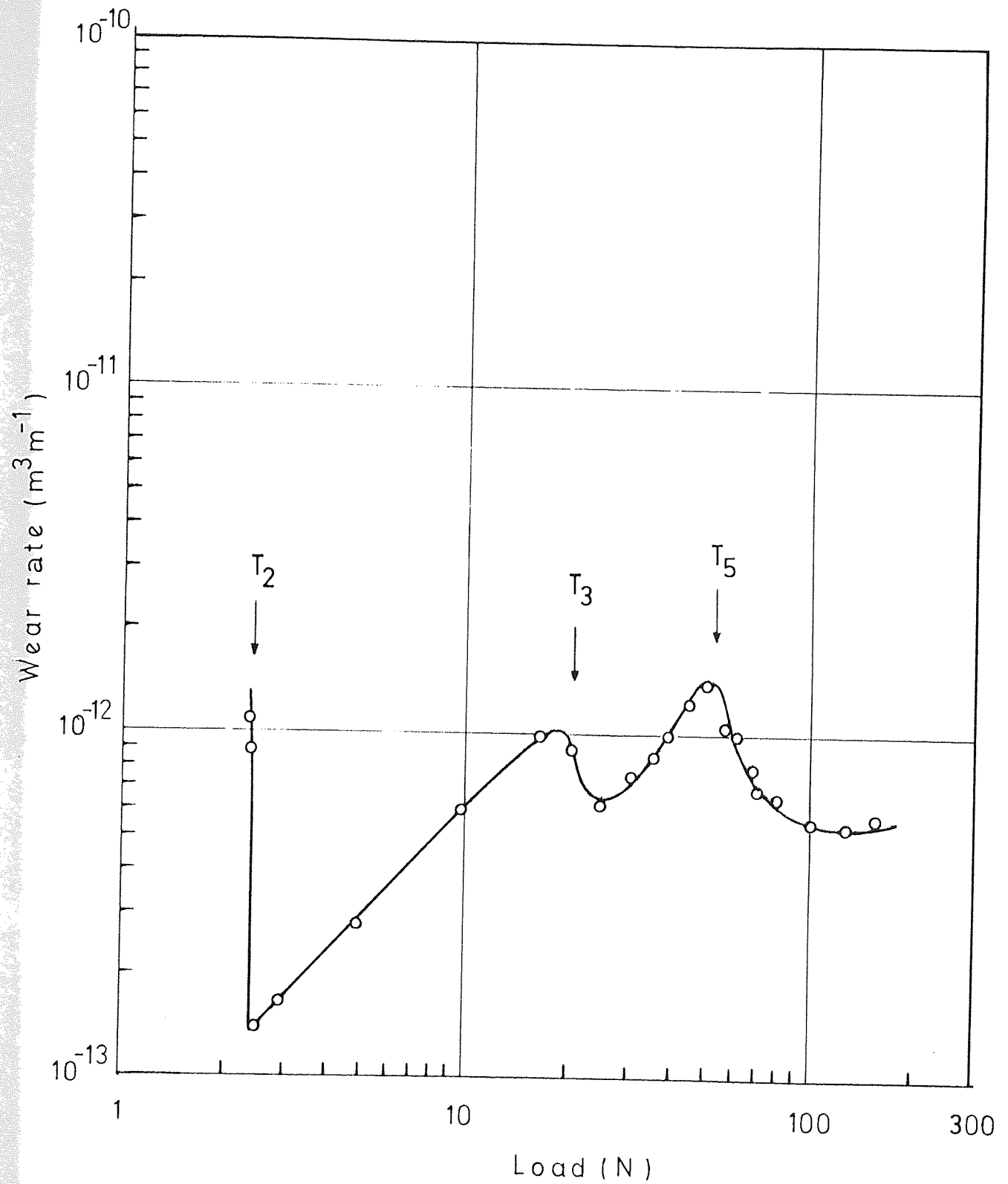
Figure 3.5 Wear rate versus load at 1.6 ms⁻¹.

3.2.4 Friction

The coefficient of friction results for tests at speeds of 0.8, 1.2 and 1.6 ms^{-1} were plotted against the load. The results, given in figure 3.6, show that, friction coefficient is a function of load and speed.

The initial friction coefficient at the T_2 transition was 1.3 for test with 1.6 ms^{-1}, fell to a minimum of 0.34 at 52 N and then gradual increased to 0.4 at 100 N (see figure 3.6(a)). For test carried out at 1.2 ms^{-1} the corresponding decreased was to 0.35 at 100 N, then friction coefficient increased slightly and maintained at a value of 0.46 (see figure 3.6(b)). The test with 0.8 ms^{-1} showed a decreased in friction coefficient from 0.7 to 0.31 (see figure 3.6(c)).

3.2.5 Heat flow

Heat flow analyses for various tests at speeds of 0.8, 1.2 and 1.6 ms^{-1} are given in tables 3.2, 3.3 and 3.4. These include temperature readings; T_A, T_B and T_C, the computed heat flow at the interface, H_1, total heat generated at pin, H_T, surface temperature, T_S, and the experimental division of heat, δ_{exp}, given by

$$\delta_{exp} = \frac{H_1}{H_T} \qquad \ldots\ldots\ldots\ldots(3.1)$$
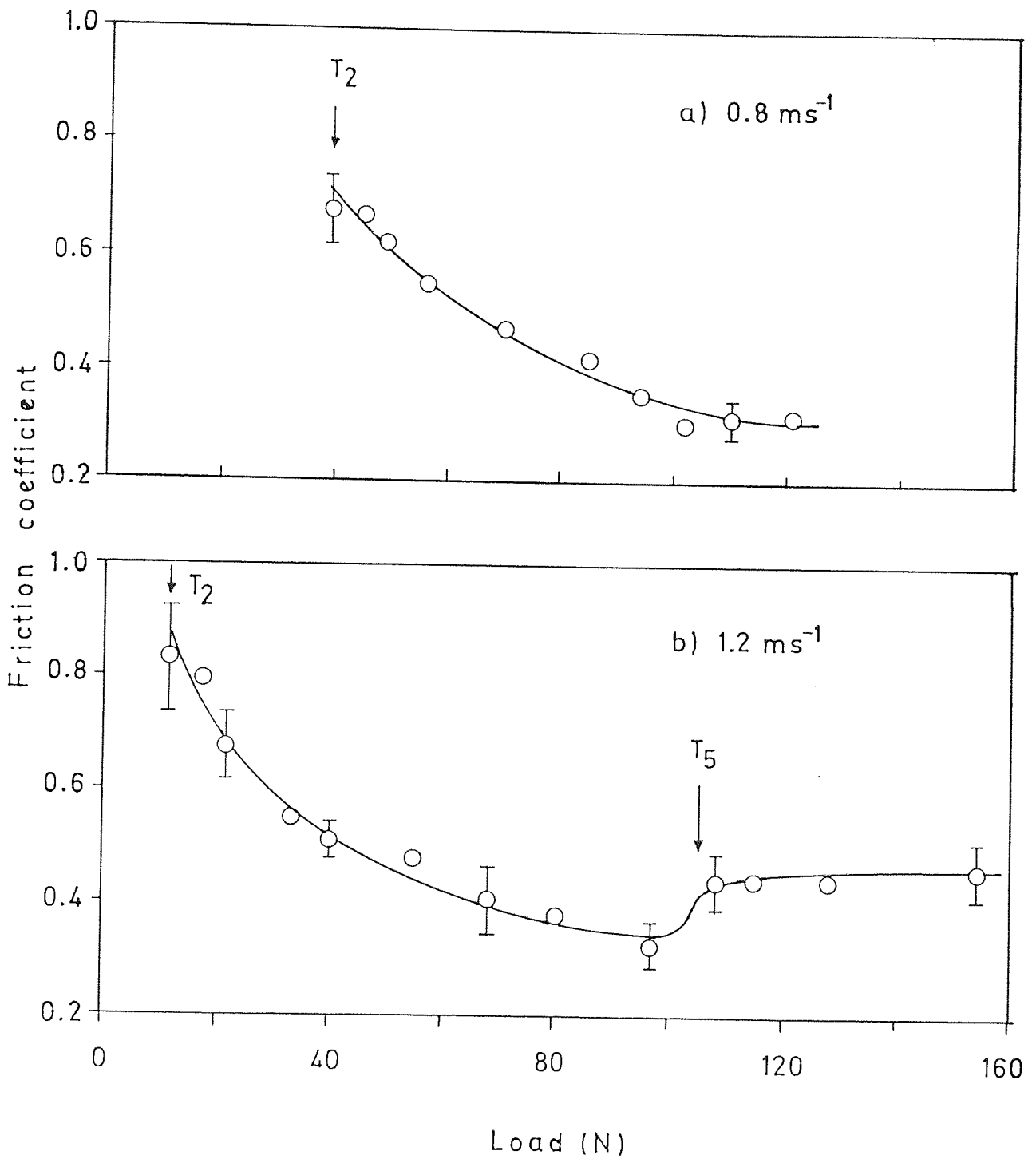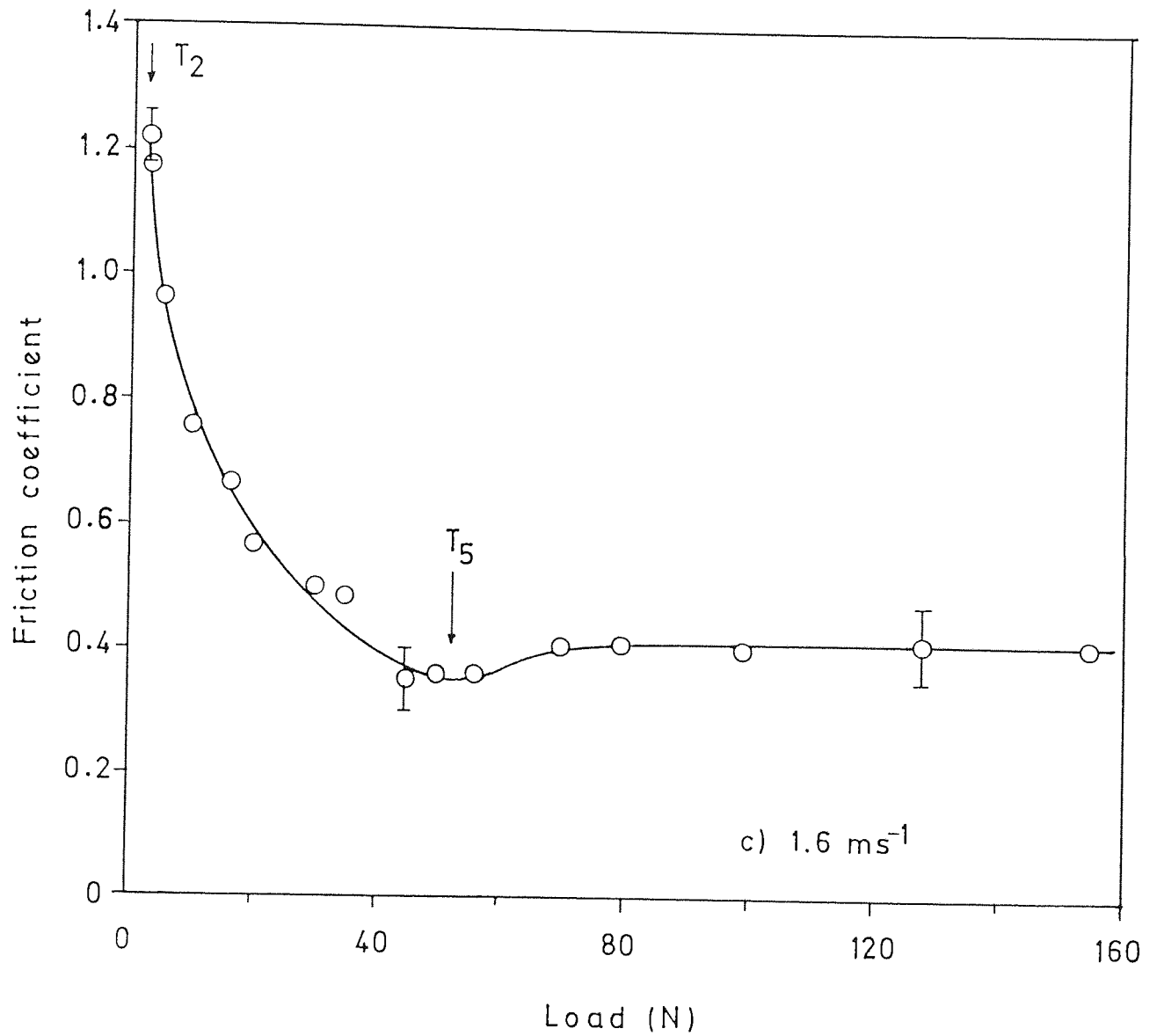
Figure 3.6 Friction coefficient versus load for tests
carried out at 0.8, 1.2 and 1.6 ms⁻¹.

Load (N)	T_A (°C)	T_B (°C)	T_C (°C)	H_1 (Js^{-1})	H_T (Js^{-1})	T_B (°C)	δ_{exp} (%)
40.0	99.5	65.3	49.0	2.9	19.6	111	14.8
49.0	118.1	76.4	56.7	3.5	22.2	131	15.4
54.9	125.8	73.2	54.0	4.7	22.8	152	20.4
62.7	128.3	81.7	59.8	4.4	24.1	153	18.1
70.2	124.4	80.6	55.9	4.3	27.2	152	15.5
76.9	115.0	70.3	56.4	4.4	25.4	145	17.4
85.1	116.6	72.8	56.1	4.1	30.1	142	13.6
94.1	117.4	78.4	58.5	3.5	26.9	132	12.9
102.5	166.3	95.3	72.6	6.8	23.0	213	29.6
110.0	188.5	116.6	76.5	7.5	27.5	238	27.5
121.2	195.1	117.5	82.2	7.2	29.4	236	24.8

Table 3.2   Heat flow analysis at 0.8 ms^{-1}.

Load	T_A	T_B	T_C	H_1	H_T	T_B	δ_{exp}
(N)	($^{\circ}$C)	($^{\circ}$C)	($^{\circ}$C)	(Js^{-1})	(Js^{-1})	($^{\circ}$C)	(%)
3.1	53.2	41.7	34.0	1.04	5.4	57	13.5
11.6	65.4	48.5	39.3	1.63	8.9	74	14.0
11.8	60.2	46.1	35.8	1.35	9.0	67	14.9
13.8	63.3	46.5	36.8	1.49	11.1	72	14.8
21.6	76.3	52.2	41.4	2.42	15.9	93	15.0
30.8	102.4	69.5	40.9	3.37	19.5	124	17.2
33.3	87.8	57.0	49.2	2.98	27.4	109	11.0
37.2	98.4	66.4	44.9	3.45	25.3	122	12.4
40.5	99.1	63.4	46.7	3.57	25.4	123	13.5
45.1	109.8	73.9	50.6	3.75	27.2	135	13.9
48.5	166.7	104.2	63.5	6.63	24.0	212	23.2
54.9	167.8	104.8	65.0	7.67	33.5	223	22.8
68.1	171.2	107.4	72.7	7.09	29.4	223	24.0
80.4	185.6	112.1	77.8	7.31	37.6	234	19.4
97.0	210.0	121.7	83.8	8.01	36.1	250	22.1
108.0	165.2	100.2	74.3	5.56	66.6	189	8.4
114.8	140.7	74.3	76.3	5.33	65.9	170	8.0
131.5	179.6	109.8	78.9	6.16	68.6	209	8.8
153.5	207.7	122.5	81.5	6.79	71.0	224	9.4

Table 3.3 Heat flow analysis at 1.2 ms^{-1}.

Load (N)	T_A (°C)	T_B (°C)	T_C (°C)	H_1 (Js⁻¹)	H_T (Js⁻¹)	T_B (°C)	δ_{exp} (%)
2.6	39.9	35.1	32.7	0.43	4.7	42	7.6
9.8	70.1	48.0	44.2	1.57	11.73	78	13.3
16.2	70.5	48.1	37.6	2.15	14.2	84	12.5
20.6	101.9	68.1	53.8	2.96	18.5	116	16.0
25.0	127.5	79.7	61.8	4.19	23.4	149	17.7
35.1	158.6	97.4	70.3	5.70	26.7	189	21.2
44.8	169.7	103.5	73.2	6.50	23.4	214	27.4
50.1	182.9	113.2	77.2	6.50	28.9	219	22.4
56.1	142.0	91.0	62.8	5.6	32.5	183	17.2
80.4	160.2	101.2	75.3	5.7	53.6	197	10.5
127.9	194.6	100.5	87.9	7.7	83.9	230	9.2
154.5	204.1	123.4	94.8	6.8	101.0	232	6.6

Table 3.4   Heat flow analysis at 1.6 ms⁻¹.

With reference to figure 3.7 surface temperature was found to vary linearly with the load, with transitions in temperature corresponding to the observed transitions in the mild wear region. At 0.8 ms^{-1} (figure 3.7(a)) there appeared to be an increase in surface temperature in three different stages, that is between T_2/T_3, T_3/T_4 and above T_4. The broad trends of temperature variations can be seen on the graph at 1.2 ms^{-1} (figure 3.7(b)) where all the transitions are clearly shown and for the graph at 1.6 ms^{-1} (figure 3.7(c)) these appear with the absent of temperature change at the T_4 transition.

3.3 Wear tests at the Welsh T_2 transition from severe to mild wear

3.3.1 Transition parameters

More than 30 wear tests were carried out to determine the T_2 transition load; at least six tests at each of the speeds 0.6, 0.8, 1.0, 1.2, 1.4 and 1.6 ms^{-1} and including single test at speeds of 0.7, 0.9, 1.1, 1.3 and 1.5 ms^{-1}. Tables 3.5 to 3.10 present the various wear parameters, comprising of the transition load, transition time, running-in severe wear rate, equilibrium wear rate and equilibrium friction coefficient, together with their mean values and standard deviations.

Each of the T_2 transition points were obtained by
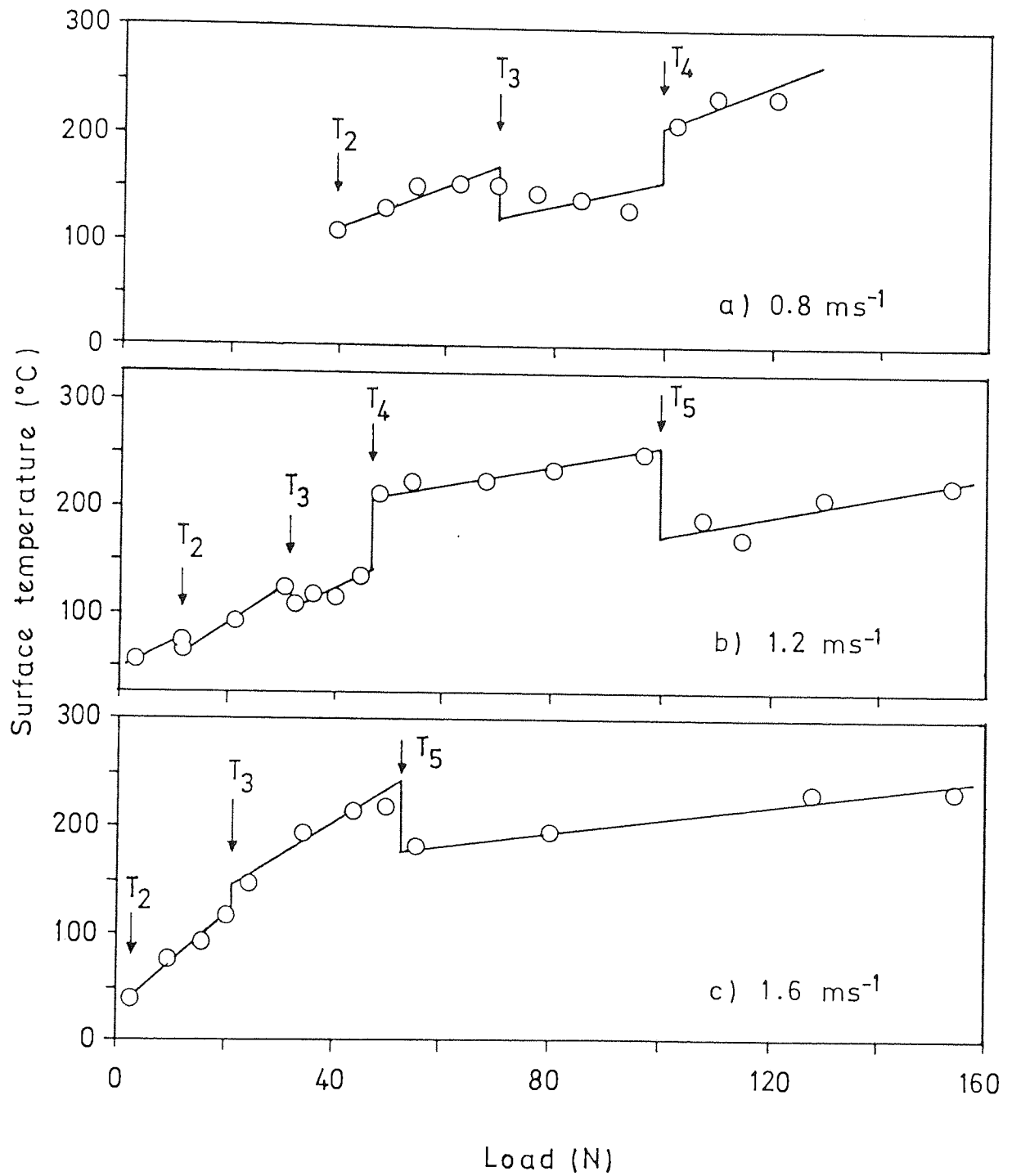
Figure 3.7   Surface temperature versus load for tests
carried out at 0.8, 1.2 and 1.6 ms^{-1}.

varying load and determining the load responsible for the transition to mild wear after long periods of severe wear. Any load slightly less than this leads to prolong equilibrium severe wear. The measured transition load varied from one test to another due to small variations in the bulk hardness of the materials. A plot of mean transition load versus speed is shown in figure 3.8. This shows a fall in transition load with increase in speed and follows the relationship

$$W_T = 1111 \exp(-3.9U) \qquad \qquad \ldots\ldots\ldots\ldots(3.2)$$

where W_T in N and U in ms^{-1}.

Transition time is the duration of the running-in time for severe wear before the onset of mild wear. For series of experiments carried out at T_2 transition load and at a particular fixed speeds the value varied considerably between tests. An example from table 3.9 shows that, the 150 minutes transition time for test 1 is about three times greater than transition time for test 2. The average transition time varied with the speed from about 23 minutes at 0.6 ms^{-1}, up to 150 minutes at 1.4 ms^{-1}. The mean transition time, t_T was found to be increased with the speed, as can be seen from the graph shown in figure 3.9; the relationship is

$$t_T = 816 \exp(1.42U) \qquad \qquad \ldots\ldots\ldots\ldots(3.3)$$
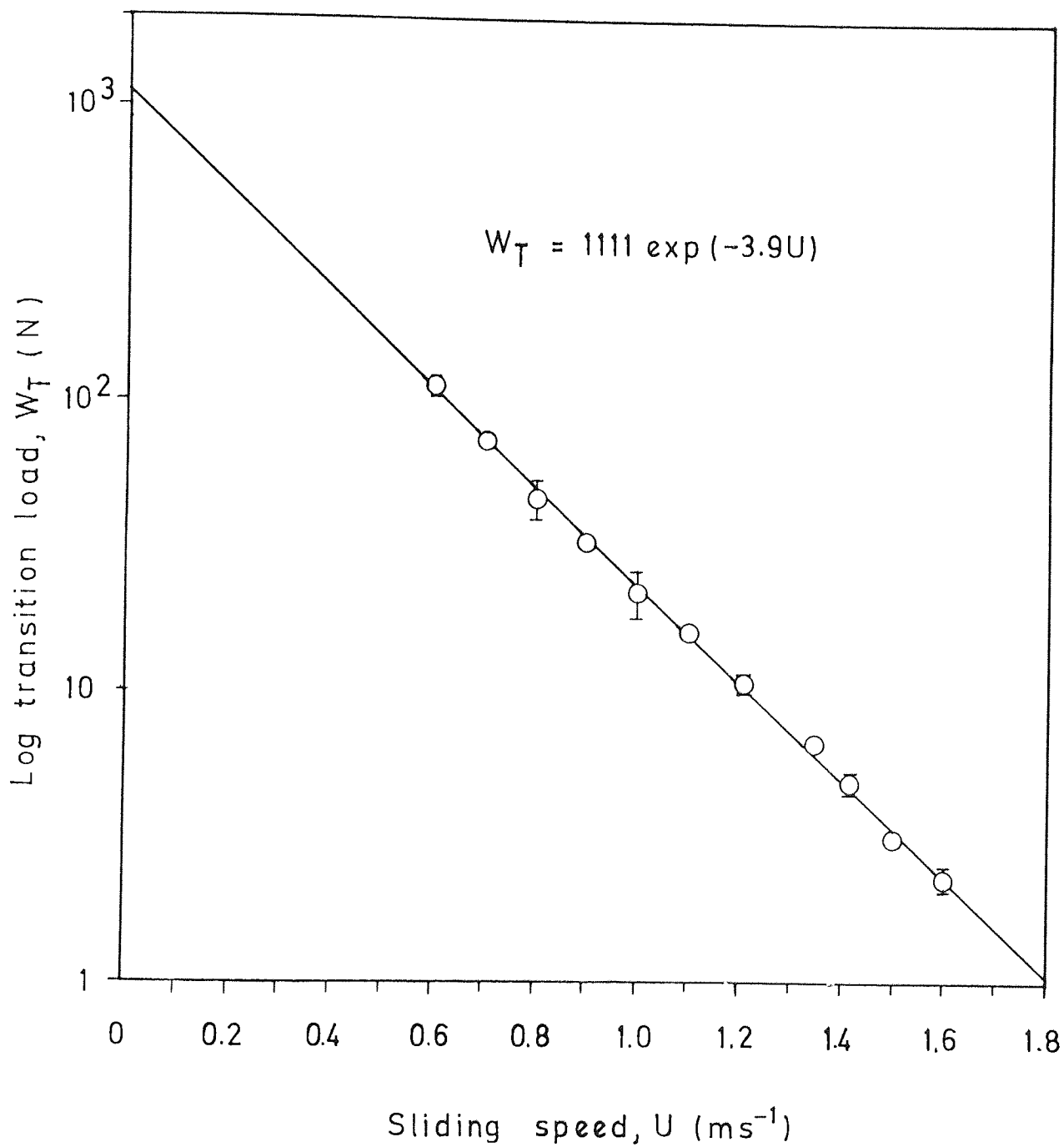
Figure 3.8   Log transition load versus sliding speed.
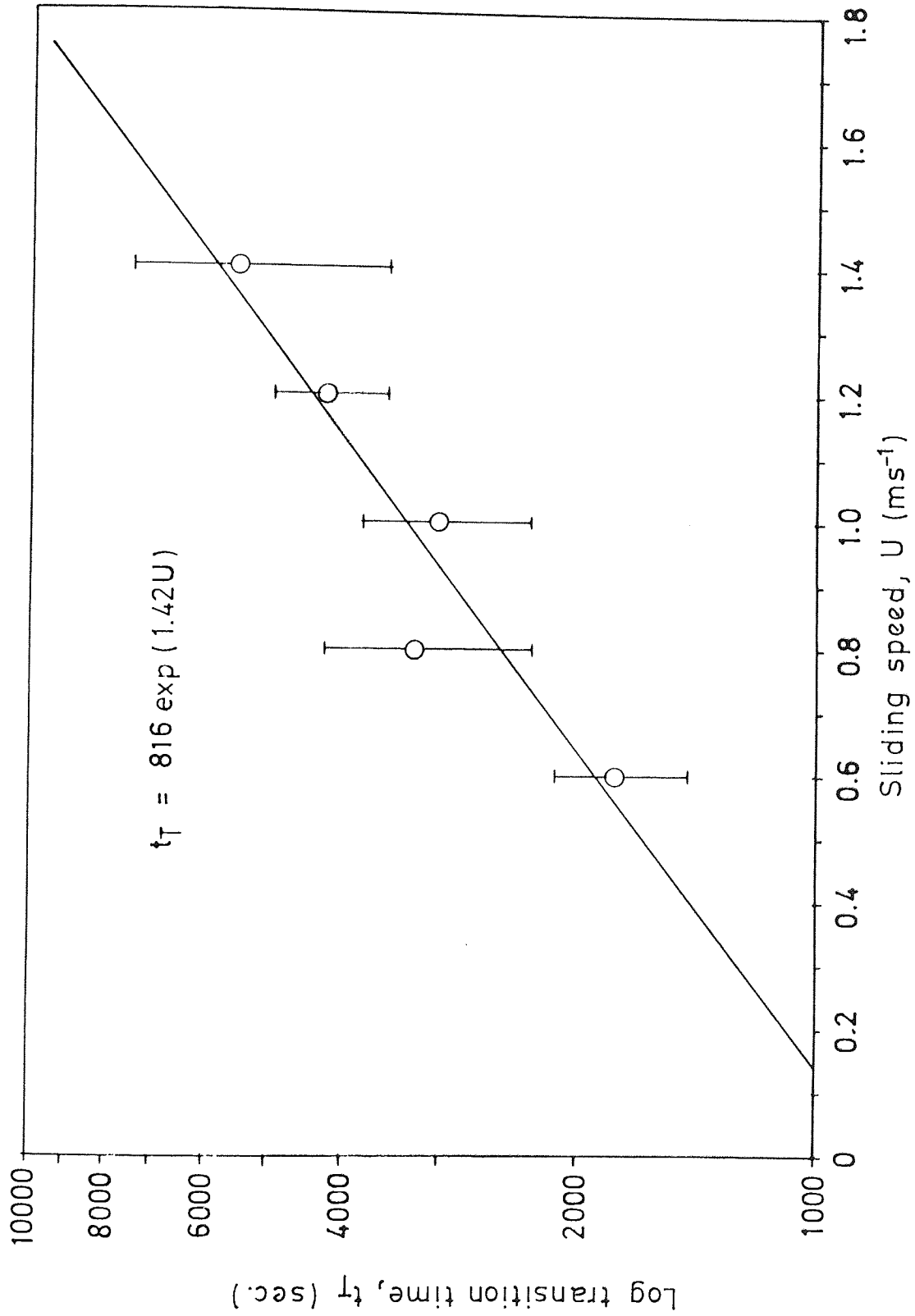
Figure 3.9 Log transition time versus sliding speed.

where t_T in second and U in ms^{-1}. Equations (3.2) and (3.3) are interrelated by an expression given by $W_T t_T = 9.06 \times 10^4$ $exp(-2.48U)$.

Both coefficient of friction and wear rates taken during equilibrium condition vary with the speed or transition load; these are shown separately in figures 3.10 and 3.11.

For a further investigation of the T_2 transition, tests at 0.8 and 1.2 ms^{-1} were used as standards. The results of friction, wear, contact resistance and heat flow are described in the following sections.

3.3.2 Friction

During the running-in severe wear mode the frictional force generated at the interface was normally high with a great deal of fluctuation, as can be observed from the friction trace in figure 3.12. The average friction force decreased slightly with sliding time up to the transition point where the vibration decreased and immediately fell to a new low value when mild wear was established. This point usually corresponded to a smooth friction trace.

Figure 3.13 shows that the coefficient of friction for test 2 at 0.8 ms^{-1} varied from 0.80 to 0.56, while the corresponding variation for test 6 at 1.2 ms^{-1} varied from 0.92 to 0.71. During transitions these values reduced slightly and then increase as mild wear progressed. For

$$\mu = 0.76U$$
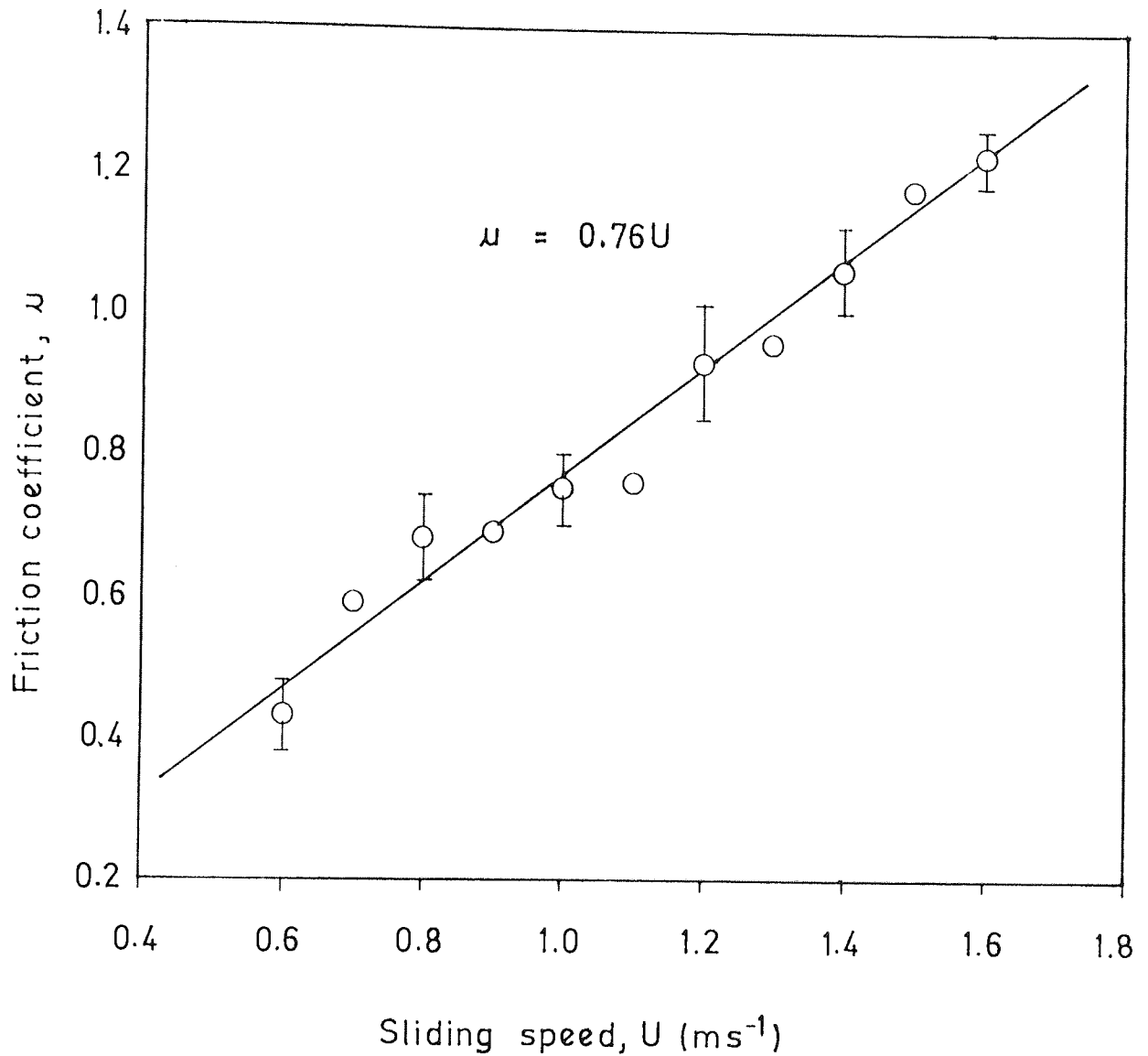
Figure 3.10 Friction coefficient versus sliding
speed for T_2 transition experiments in
equilibrium mild wear.
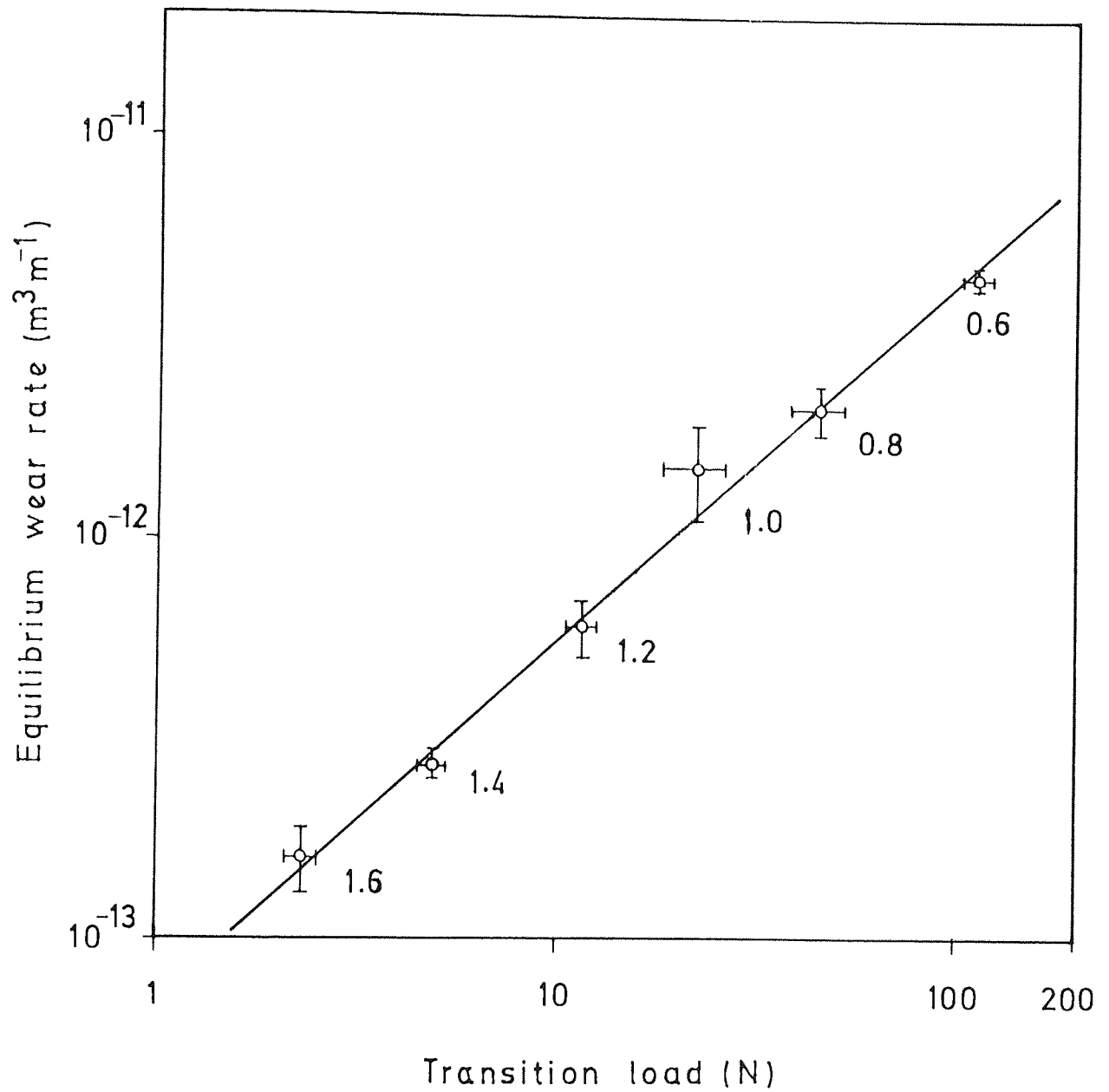
Figure 3.11   Wear rate versus transition load for T_2
transition experiments in equilibrium
mild wear.

Figure 3.12 Typical traces of friction, wear and temperature versus time during the running-in severe period at T_2.
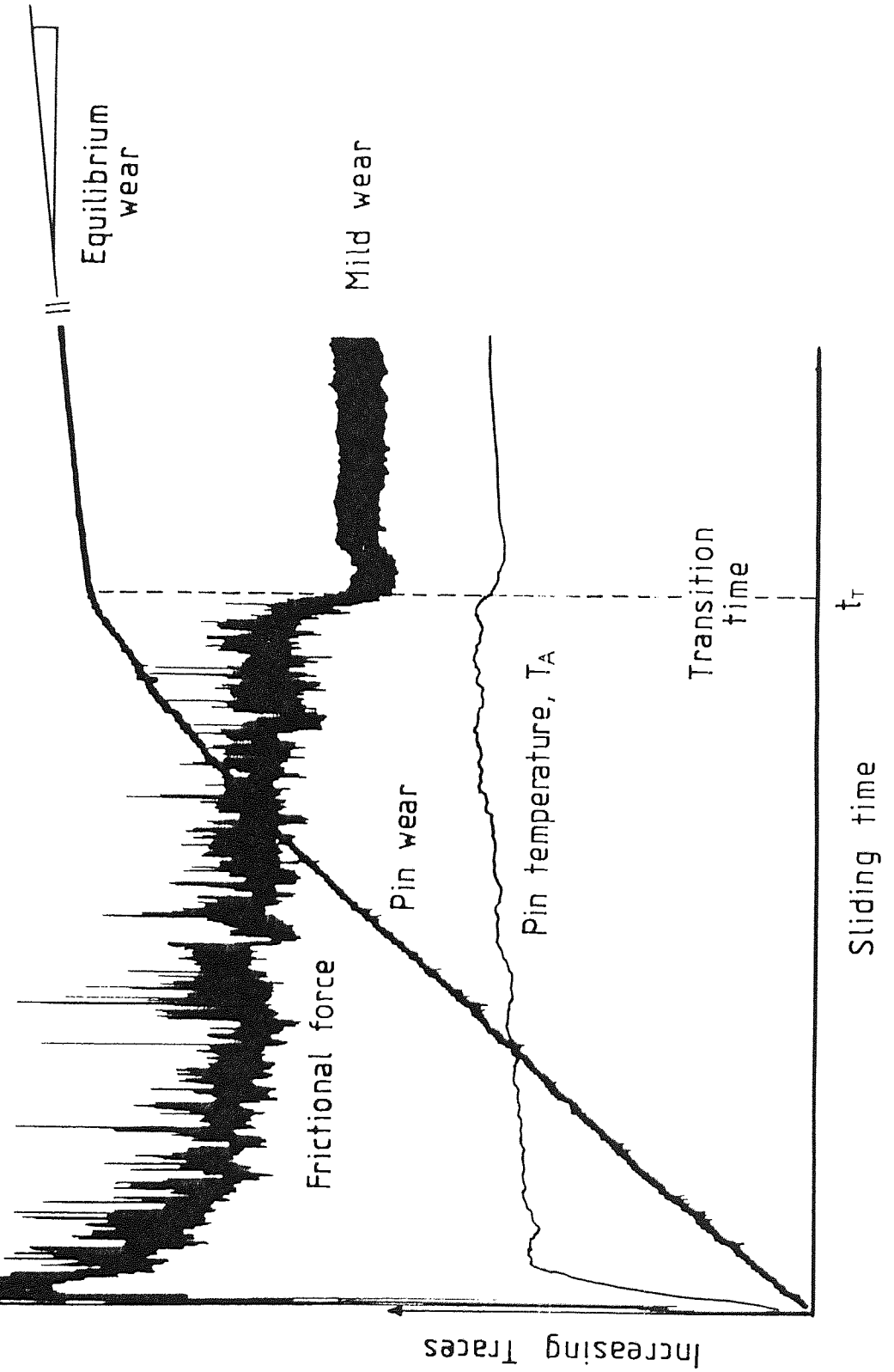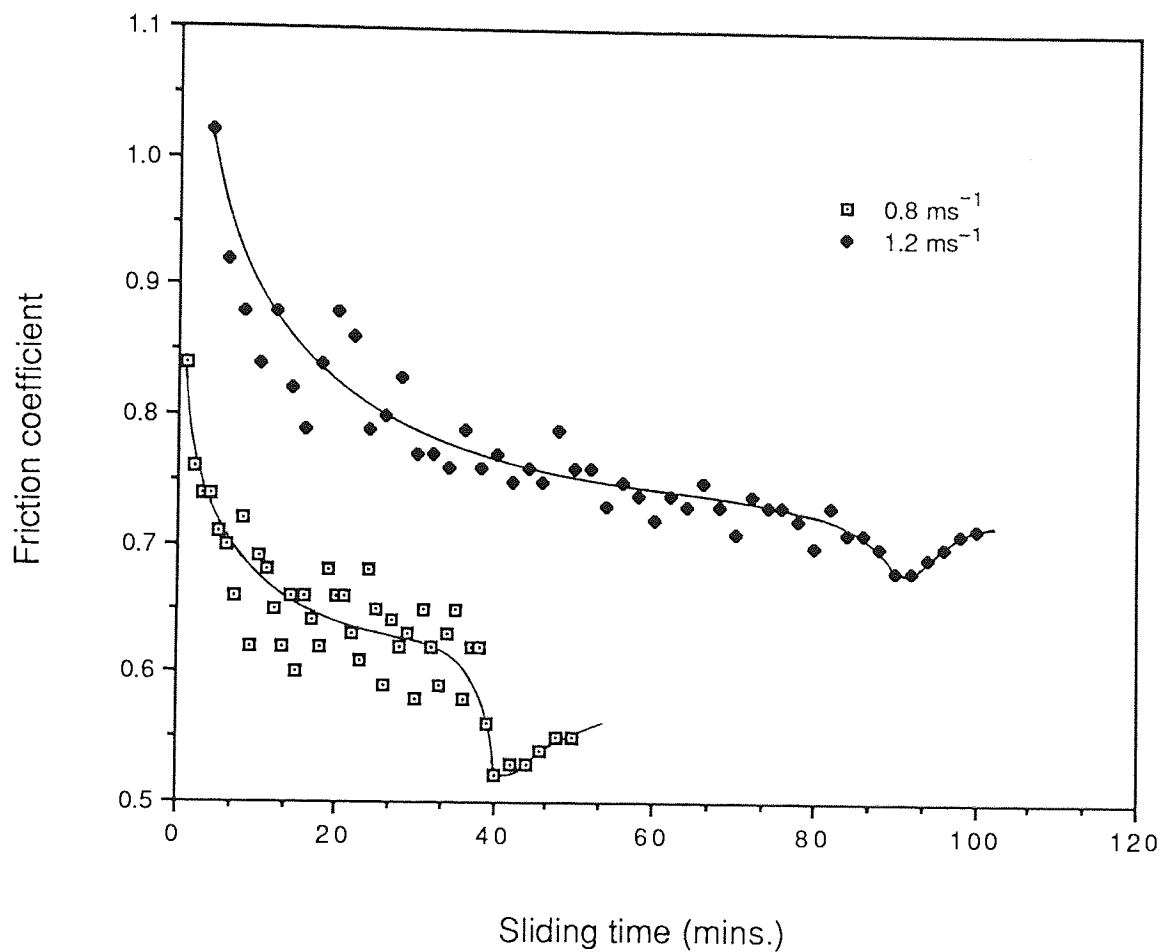
Figure 3.13   Variation of friction coefficient with
sliding time for T_2 transition experiments
at 0.8 and 1.2 ms^{-1}.

comparison the fiction coefficient obtained during the equilibrium mild wear for both speeds were 0.61 and 0.85 respectively (see tables 3.6 and 3.8).

3.3.3 Wear

The test runs carried out at the T_2 transition load exhibited running-in severe wear and mild wear traces similar to that shown in figure 3.12. In the former case the mean wear rate was calculated on each of the six tests made at a fixed speed, and the overall results are shown in tables 3.5 to 3.10. The mean wear running-in severe rate decreased from 6.6×10^{-11} to 8.3×10^{-12} m^3m^{-1} as the speed was increased from 0.6 to 1.4 ms^{-1}. The amount of pin removed during the running-in severe wear was also calculated, and the results (see figure 3.14) show that the rate of removal was greater for pins from experiments run at 0.8 ms^{-1}, but the total volume removed in the running-in periods was approximately equal to 1.1×10^{-8} m^3 in both 0.8 and 1.2 ms^{-1}.

The wear rate for equilibrium mild wear, included in tables 3.5 to 3.10 was generally much less than the wear rate for running-in severe wear, about 15 times less at 0.6 ms^{-1} speed and about 50 times less at higher speed of 1.4 ms^{-1}. The average equilibrium mild wear rate was found to decrease with the speed, that is from 4.4×10^{-12} to 1.5×10^{-13} m^3m^{-1} with increase in speed from 0.6 to 1.4 ms^{-1}.
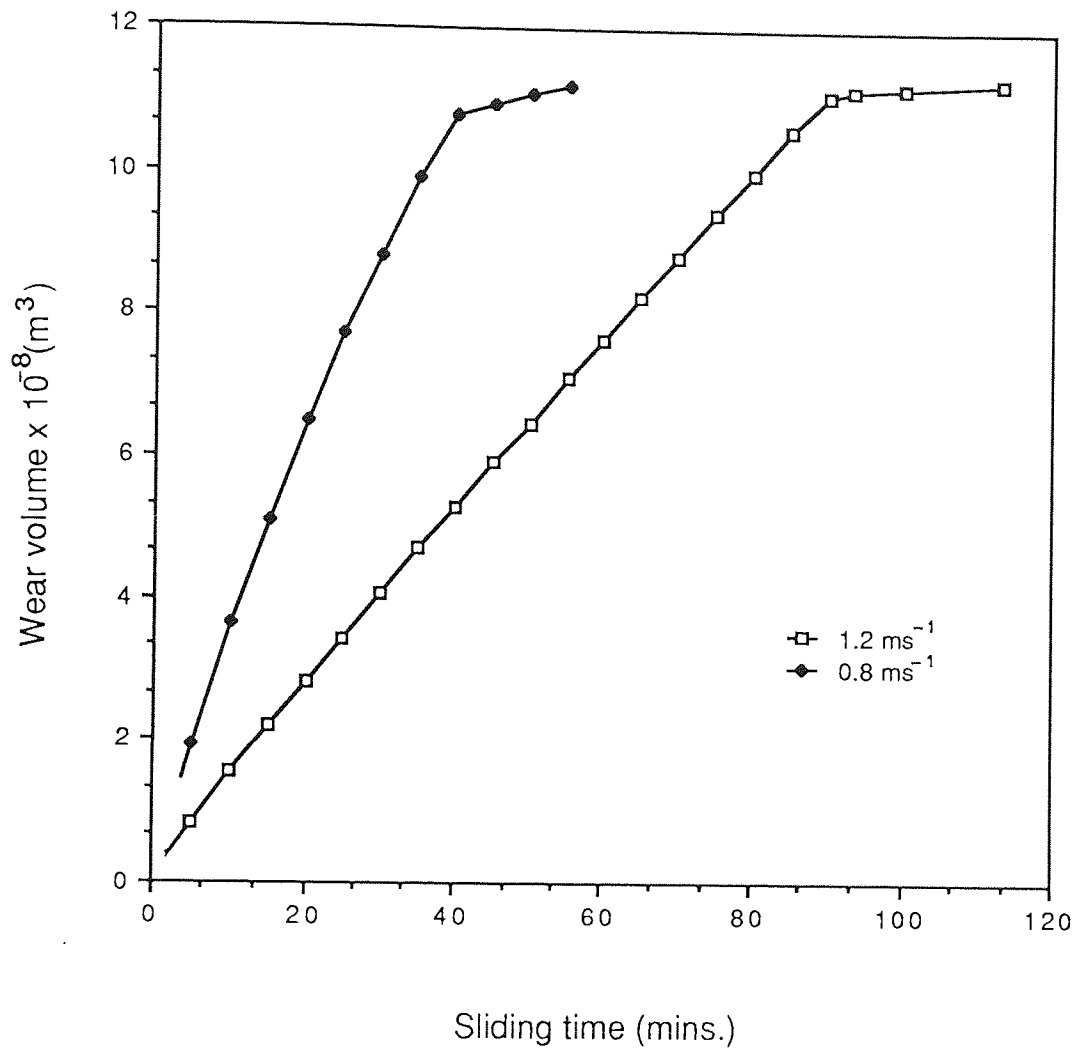
Figure 3.14   Increase in wear volume with sliding time
as the T_2 transition experiments at 0.8
and 1.2 ms^{-1} progressed.

Test number	Transition load, W_T (N)	Transition time, t_T (sec.)	Wear rate Severe wear $(m^3 m^{-1})$	Eq. mild wear $(m^3 m^{-1})$	Friction coeff.
1	126.6	1380	6.6×10^{-11}	4.5×10^{-12}	0.45
2	110.4	2040	6.5×10^{-11}	4.6×10^{-12}	0.51
3	107.6	2400	6.6×10^{-11}	4.3×10^{-12}	0.41
4	110.4	1680	6.0×10^{-11}	4.2×10^{-12}	0.37
5	113.8	1500	6.8×10^{-11}	4.6×10^{-12}	0.45
6	108.3	1800	6.9×10^{-11}	4.7×10^{-12}	0.39
7	110.4	stopped after 20 minutes run			
average	113 ± 6	1800 ± 341	$6.6 \times 10^{-11} \pm 0.3 \times 10^{-11}$	$4.4 \times 10^{-12} \pm 0.2 \times 10^{-12}$	0.43 ± 0.05

Table 3.5   Measured wear parameters for experiments

carried out at 0.6 ms^{-1}.

Test number	transition load, W_T (N)	transition time, t_T (sec.)	Wear rate Severe wear ($m^3 m^{-1}$)	Eq. mild wear ($m^3 m^{-1}$)	Friction coeff.
1	33.4	3480	4.8×10^{-11}	1.8×10^{-12}	0.76
2	49.1	3240	5.0×10^{-11}	2.3×10^{-12}	0.61
3	48.1	2400	5.2×10^{-11}	2.0×10^{-12}	0.67
4	45.1	5040	4.9×10^{-11}	1.9×10^{-12}	0.70
5	40.2	4080	4.7×10^{-11}	1.9×10^{-12}	0.73
6	57.4	1800	5.4×10^{-11}	2.6×10^{-12}	0.60
7	49.1	2940	5.0×10^{-11}	stopped at t_T	
8	49.1	stopped after 30 minutes run			
average	46 $\pm$ 7	3283 $\pm$ 990	5.0×10^{-11} $\pm$ 0.2×10^{-11}	2.2×10^{-12} $\pm$ 0.3×10^{-12}	0.67 $\pm$ 0.06

Table 3.6 Measured parameters for experiments carried out at 0.8 ms^{-1}.

Test number	Transition load, W_T (N)	Transition time, t_T (sec.)	Wear rate Severe wear $(m^3 m^{-1})$	Eq. mild wear $(m^3 m^{-1})$	Friction coeff.
1	22.3	3060	2.8×10^{-11}	1.1×10^{-12}	0.78
2	27.3	2700	3.3×10^{-11}	2.0×10^{-12}	0.69
3	15.2	4440	2.5×10^{-11}	9.0×10^{-13}	0.83
4	21.8	3420	2.9×10^{-11}	2.0×10^{-12}	0.72
5	26.1	2580	3.1×10^{-11}	1.4×10^{-12}	0.72
6	21.1	2040	3.1×10^{-11}	1.2×10^{-12}	0.76
7	21.8	stopped after 30 minutes run			
average	22 ± 4	3040 ± 13	3.0×10^{-11} ± 0.3×10^{-11}	1.5×10^{-12} ± 0.4×10^{-12}	0.75 ± 0.05

Table 3.7   Measured wear parameters for experiments carried out at 1.0 ms^{-1}.

| Test number | Transition load, W_T (N) | Transition time, t_T (sec.) | Wear rate | | Friction coeff. |
			Severe wear (m^3m^{-1})	Eq. mild wear (m^3m^{-1})	
1	10.8	4200	1.9×10^{-11}	8.5×10^{-13}	1.02
2	9.6	2820	1.4×10^{-11}	4.5×10^{-13}	0.93
3	10.3	4560	1.9×10^{-11}	7.5×10^{-13}	1.00
4	10.8	4320	1.9×10^{-11}	6.8×10^{-13}	0.78
5	11.4	3900	1.6×10^{-11}	5.0×10^{-13}	0.93
6	11.8	5400	1.7×10^{-11}	5.6×10^{-13}	0.92
7	10.0	3420	1.4×10^{-11}	5.5×10^{-13}	1.05
8	10.8	5100	1.6×10^{-11}	6.2×10^{-13}	0.95
9	11.3	4140	1.6×10^{-11}	7.4×10^{-13}	0.87
10	11.8	4020	1.8×10^{-11}	7.0×10^{-11}	0.85
11	11.8	4920	1.8×10^{-11}	stopped at t_T	
12	11.8	stopped after 10 minutes run			
13	11.8	stopped after 40 minutes run			
14	11.8	stopped after 60 minutes run			
average	10.9 ± 0.7	4255 ± 708	1.7×10^{-11} ± 0.2×10^{-11}	6×10^{-13} ± 1×10^{-13}	0.93 ± 0.08

Table 3.8 Measured wear parameters for experiments

carried out at 1.2 ms^{-1}.

Test number	Transition load, W_T (N)	Transition time, t_T (sec.)	Wear rate Severe wear ($m^3 m^{-1}$)	Eq. mild wear ($m^3 m^{-1}$)	Friction coeff.
1	5.5	9000	8.0×10^{-12}	2.9×10^{-13}	1.01
2	4.6	3240	9.1×10^{-12}	2.4×10^{-13}	1.02
3	4.9	3600	9.4×10^{-12}	2.7×10^{-13}	1.17
4	4.4	6060	7.0×10^{-12}	2.5×10^{-13}	1.07
5	4.6	4500	7.5×10^{-12}	2.8×10^{-12}	1.10
6	5.1	6540	8.5×10^{-12}	2.8×10^{-13}	0.98
7	4.6	stopped after 60 minutes run			
average	4.9 ± 0.4	5490 ± 1973	8.3×10^{-12} ± 0.8×10^{-12}	2.7×10^{-13} ± 0.2×10^{-13}	1.06 ± 0.06

Table 3.9 Measured wear parameters for experiments

carried out at 1.4 ms^{-1}.

Test number	Transition load, W_T (N)	Transition time, t_T (sec.)	Wear rate Eq. mild wear ($m^3 m^{-1}$)	Friction coeff.
1	2.0	3540	1.9×10^{-13}	1.27
2	2.0	2640	1.4×10^{-13}	1.28
3	2.4	2640	1.7×10^{-13}	1.17
4	2.4	3000	2.0×10^{-13}	1.18
5	2.6	2520	1.2×10^{-13}	1.25
6	2.2	3900	1.5×10^{-13}	1.20
average	2.3 ± 0.2	3040 ± 513	1.6×10^{-13} ± 0.3×10^{-13}	1.22 ± 0.04

Table 3.10   Measured wear parameters for experiments carried out at 1.6 ms^{-1}.

3.3.4 Heat flow

Heat flow analyses were conducted every minute during each wear test in order to gain information of the variation in the surface parameters as the experiment progressed. Due to very large number of results the analyses given in table 3.11 and table 3.12 are restricted to 10 selected running times. All the measured temperatures, i.e. T_A, T_B and T_C were found to increase with time, probably due to decreasing pin length, L_1. From figure 3.15, the resulting increase in surface temperature was from 142 to 157°C at 0.8 ms^{-1} and from 70 to 74°C at 1.2 ms^{-1} respectively. A small drop in these temperatures occurred at the establishment of mild wear.

3.3.5 Contact resistance

Figure 3.16 shows a typical contact resistance trace for a test at 1.2 ms^{-1}. There was an immediate slight increase in contact resistance ($\approx$150 Ω) associating with high friction at the start of the run, followed by a sharp drop and an associated low noise resistance trace. This low resistance, low noise condition remained for about 20 minutes before the trace gradually increased and rapidly fluctuated over the entire range of contact. The average contact resistance between 40 and 150 minutes was about 10^{-3} Ω, with an increase to 10^{-2} Ω at the onset of mild wear. The behaviour of contact

—115—

Test duration (mins.)	T_A (°C)	T_B (°C)	T_C (°C)	H_1 (Js^{-1})	H_T (Js^{-1})	T_S (°C)
1	88.5	41.1	21.2	4.87	32.3	124
5	106.5	49.7	30.5	5.62	27.4	146
10	110.6	54.6	36.3	5.44	26.6	147
15	113.4	58.3	38.7	5.31	23.1	147
20	119.0	60.8	42.1	5.47	25.5	152
25	120.4	63.2	44.5	5.32	25.1	152
30	124.5	65.7	46.8	5.39	22.5	155
35	127.3	68.1	48.2	5.38	24.8	156
40	120.4	65.7	48.0	4.91	20.2	146
SEVERE/MILD WEAR TRANSITION						
50	124.5	66.9	51.4	5.09	21.5	151

Table 3.11   Progressive heat flow analysis at 0.8 ms^{-1}.

Test duration (min.)	T_A (°C)	T_B (°C)	T_C (°C)	H_i (Js^{-1})	H_T (Js^{-1})	T_S (°C)
5	54.4	34.7	24.1	2.02	15.7	68.0
10	60.0	42.9	30.2	1.82	11.9	71.8
20	61.0	44.5	33.0	1.71	11.5	71.9
30	62.0	45.6	34.8	1.68	12.3	72.0
40	63.6	45.5	35.3	1.76	11.1	73.7
50	64.1	46.0	36.0	1.73	11.3	73.2
60	64.0	46.5	36.2	1.69	10.9	73.5
70	63.4	46.5	36.2	1.65	11.0	73.3
80	63.1	46.5	36.1	1.62	10.4	72.0
90	59.1	45.3	35.9	1.32	10.1	65.6
SEVERE/MILD WEAR TRANSITION						
100	58.3	44.8	35.6	1.29	11.5	64.6

Table 3.12   Progressive heat flow analysis at 1.2 ms^{-1}.
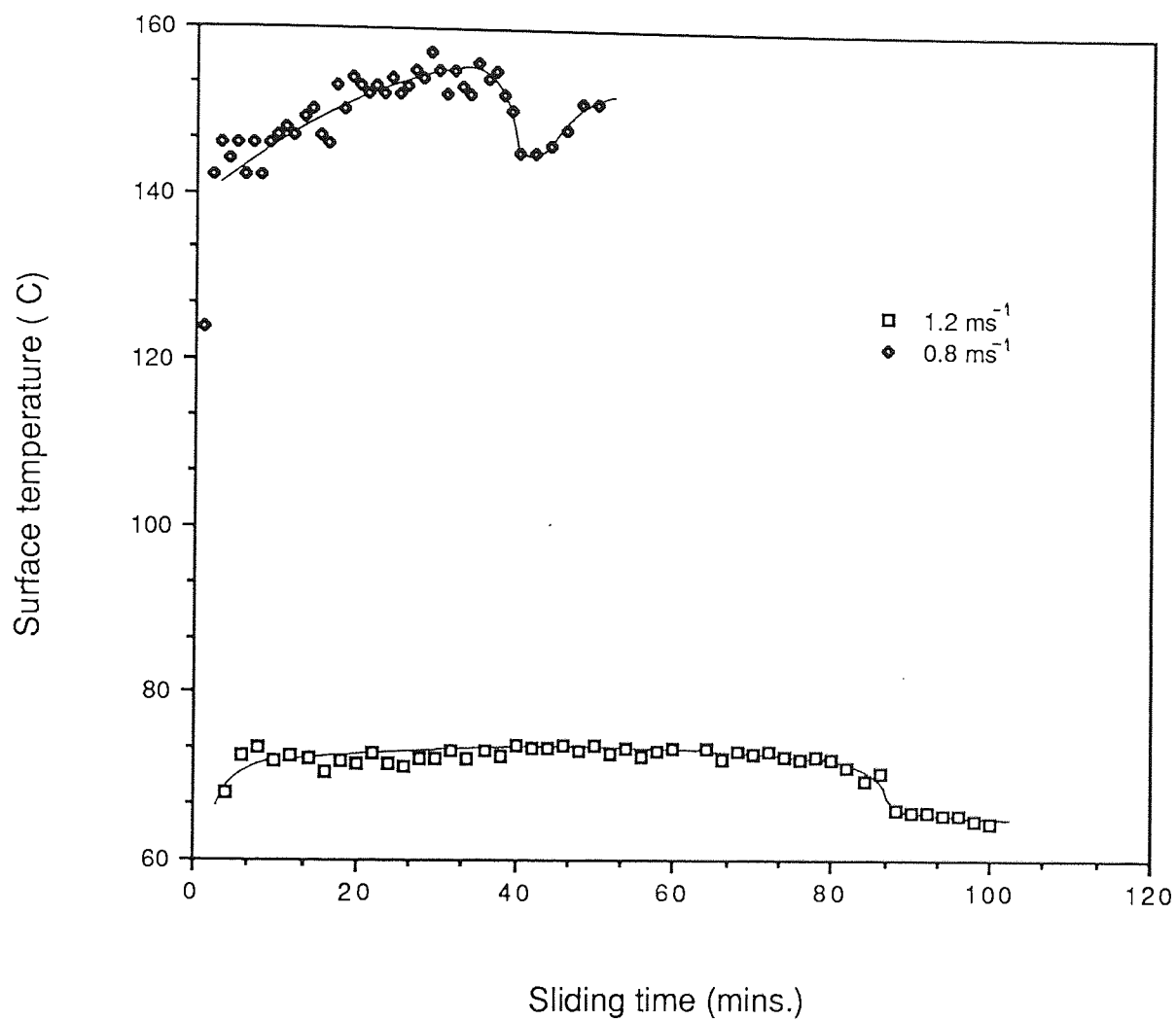
Figure 3.15 Variation of surface temperature with sliding time for T_2 transition experiments at 0.8 and 1.2 ms^{-1}.
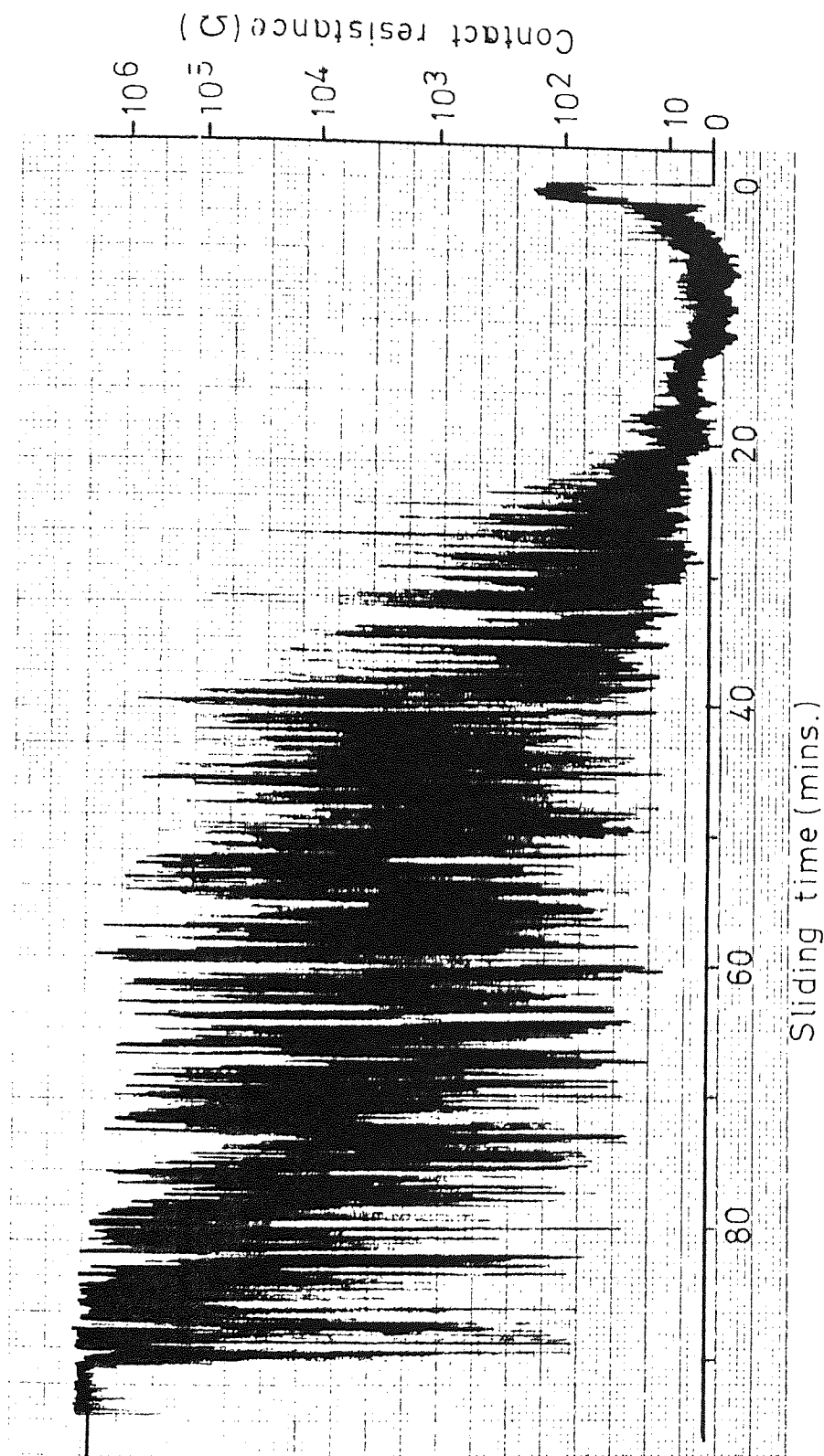
Figure 3.16 Variation of contact resistance with sliding time for T_2 transition experiments at 1.2 ms^{-1}.

resistance for the test at 0.8 ms^{-1} was found to be very similar.

3.4 Running-in mild wear test

3.4.1 Introduction

This section is concerned with the results obtained from four different mild wear experiments carried out at a speed of 1.2 ms^{-1}. Loads of 13.8 N, 40.5 N, 68.1 N and 131.5 N were used representing region 1 between T_2-T_3 transitions, region 2 between T_3-T_4 transitions, region 3 between T_4-T_5 transitions and region 4 above the T_5 transition. At least six long duration tests were made for each load with an additional ten to sixteen progressive running-in mild wear tests (including repeated tests), making a total of more than sixty tests. A summary of the results is given in table 3.13.

3.4.2 Friction

Figure 3.17 illustrates how the coefficient of friction varied with sliding time during the course of the mild wear experiments. All four curves had initial high friction for the first few minutes of each run (18 minutes for the 13.8 N load) due to severe wear and consequent metal/metal contact. After this friction coefficient fell and then rose again

1) Load: 13.8 N

<u>Test duration (minutes)</u>: 5, 20 and every 20 mins. up to 300.

<u>Frequency of test</u>: a) 2 tests for every 5, 20, 60, 120 mins.
b) 6 tests between 200 and 300 mins.

<u>Severe wear</u>: a) running-in period = 15 to 20 mins.
b) average wear rate = 1.3×10^{-11} $m^3 m^{-1}$.

<u>Mild wear</u>: a) wear rate = 1.5×10^{-12} to 1.3×10^{-12} $m^3 m^{-1}$
up to 200 mins. run.
b) average eq. wear rate = 1.2×10^{-12} $m^3 m^{-1}$.
c) average friction coefficient = 0.96.

2) Load: 40.5 N

<u>Test duration (minutes)</u>: 5, 20, and every 20 mins. up to 360.

<u>Frequency of test</u>: a) 2 tests for every 5, 20, 60 , 120 mins.
b) 6 tests between 240 and 360 mins.

<u>Severe wear</u>: running-in period = 4 to 5 minutes.

<u>Mild wear</u>: a) wear rate = 1.4×10^{-12} to 5.8×10^{-13} $m^3 m^{-1}$
up to 240 mins. run.
b) average eq. wear rate = 5.8×10^{-13} $m^3 m^{-1}$.
c) average friction coefficient = 0.52.

3) Load: 68.1 N

<u>Test duration (minutes)</u>: 5, 20, and every 20 mins. up to 300.

<u>Frequency of test</u>: a) 2 tests for every 5, 20, 60, 120 mins.
b) 6 tests between 200 and 300 mins.

<u>Severe wear</u>: running-in period = 1 to 2 minutes.

<u>Mild wear</u>: a) wear rate = 2.0×10^{-12} to 3.8×10^{-12} $m^3 m^{-1}$
up to 200 mins. run.
b) average wear rate = 3.9×10^{-12} $m^3 m^{-1}$.
c) average friction coefficient = 0.40

4) Load: 131.5 N

Test duration (minutes): 5, 20, and every 20 mins. up to 300.

Frequency of test: a) 2 tests for every 5, 20, 60, 120 mins.
                   b) 6 tests between 200 to 300 minutes.

Severe wear: a) running-in period = 2 to 3 minutes.
             b) average wear rate = 5.8×10^{-10} $m^3 m^{-1}$.

1st stage mild wear: average wear rate = 7.3×10^{-11} $m^3 m^{-1}$ between 3 to 60 minutes.

2nd stage mild wear: a) wear rate = 1.2×10^{-12} to 9.0×10^{-13} $m^3 m^{-1}$ up to 200 minutes.
                  b) average wear rate = 9.7×10^{-13} $m^3 m^{-1}$.
                  c) average friction coeff. = 0.46.

Table 3.13   Conditions and measured wear parameters for experiments carried out at 13.8 N, 40.5 N, 68.1 N and 131.5 N loads.

Figure 3.17 Variation of friction coefficient with sliding time for running-in mild wear experiments at 1.2 ms⁻¹.
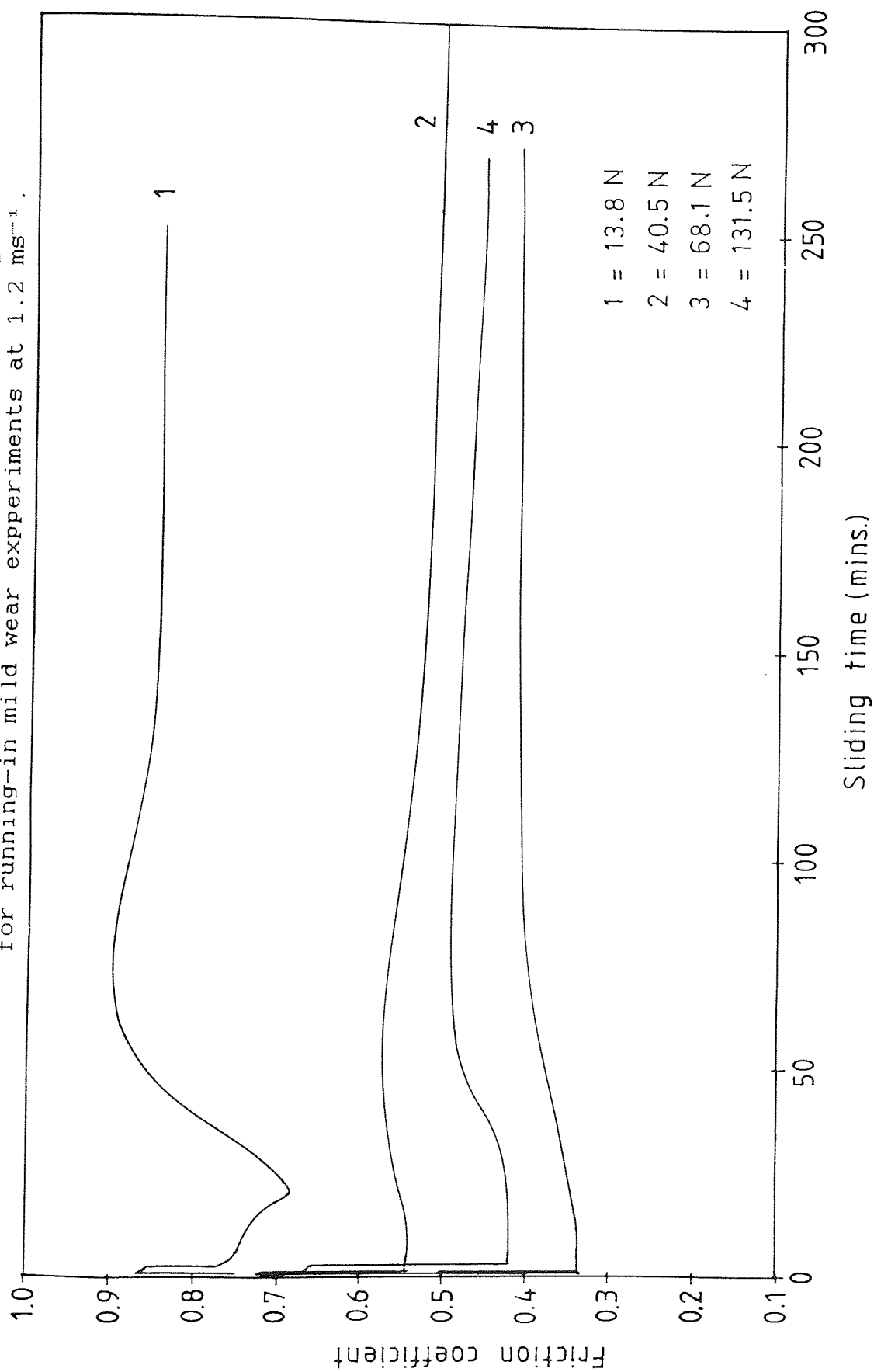
until a steady equilibrium value was attained.

Intermittent frictional force drops occurred during the course of the mild wear run at 131.5 N load. Figure 3.18 shows the two such friction force changes, with associated changes in contact resistance and surface and contact temperatures.

3.4.3 Wear

From the summary given in table 3.13 it may be seen that, the first 18 to 20 minutes run of the 13.8 N tests was dominated by the severe wear of average wear rate 1.3×10^{-11} m^3m^{-1}. After the transition to mild wear the wear rate decreased slightly from about 1.5×10^{-12} m^3m^{-1} to 1.3×10^{-12} m^3m^{-1} over a period of 200 minutes and then became constant at the lower value. The corresponding decrease in wear rate for tests with 40.5 N load was from 1.4×10^{-12} m^3m^{-1} to 5.8×10^{-13} m^3m^{-1} after 300 minutes. A different situation occurred for test with a 68.1 N load, where the mild wear rate increased from 2.0×10^{-12} to 3.8×10^{-12} m^3m^{-1} over almost 240 minutes of test run. In these cases the initial periods of severe wear were about 4 to 5 minutes and 1 to 2 minutes respectively.

For tests carried out with a 131.5 N load, a substantial amount of pin wear loss occurred during the first 2 to 3 minutes of the run, resulting an average severe

Figure 3.18   Typical traces of contact resistance,
               frictional force and temperatures, T_A
               and T_B at 1.2 ms^{-1} and 131.5 N.

Figure 3.18
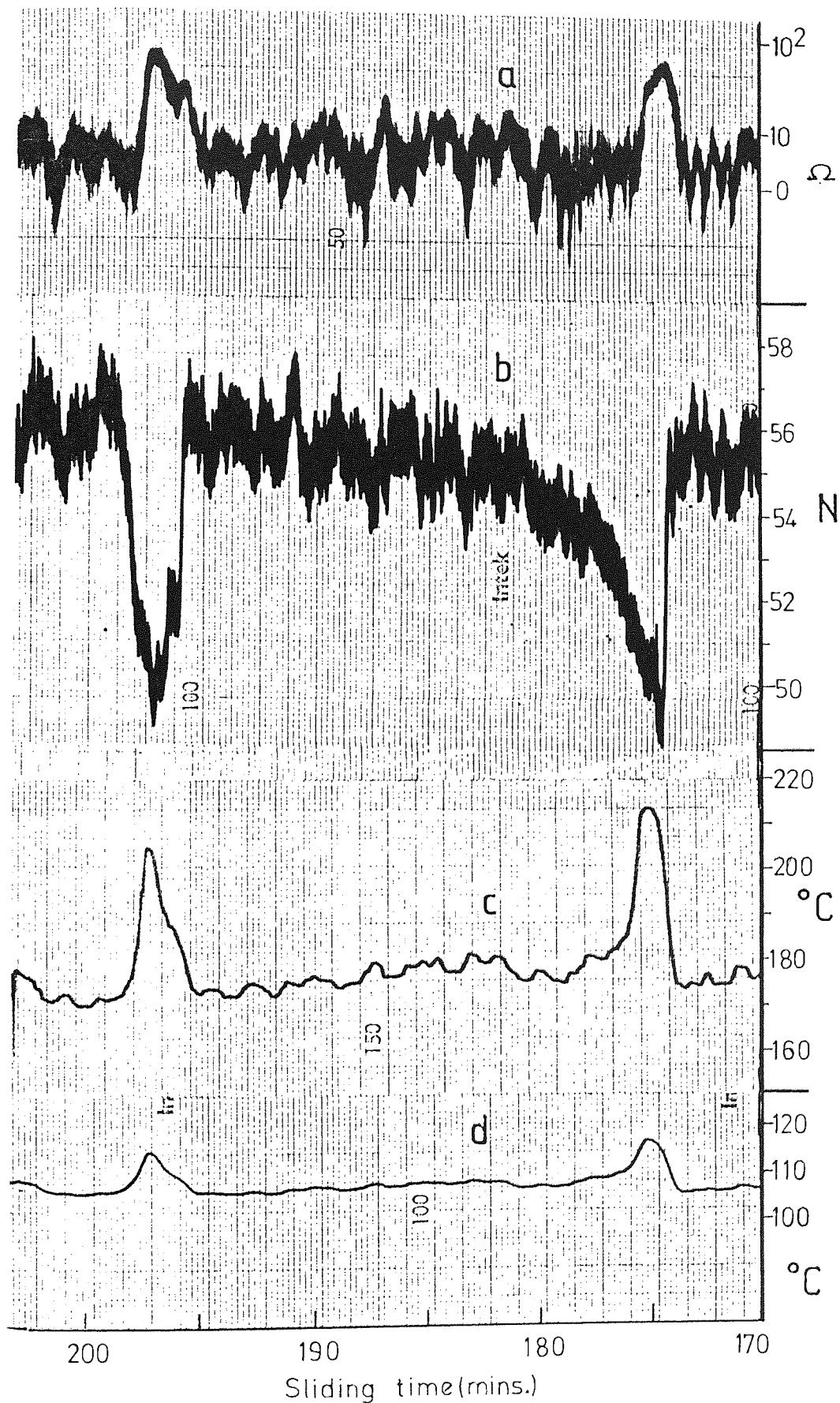
"running-in" wear rate of 5.8 x 10^{-10} m^3m^{-1}. The transition
to mild wear occurred in two stages; one in which the average
wear rate was about 7.3 x 10^{-12} m^3m^{-1} over a period of 40
minutes followed by a further period of low wear in which the
rate decreased from 1.2 x 10^{-12} to 9.0 x 10^{-13} m^3m^{-1} after
about 200 minutes. In the first stage of this investigation,
mild wear may be observed to occur after long periods (over 2
hours), if the load is greater than the T_m transition load
(see section 3.2.3).

The variation in wear volumes during the course of an
experiment is shown in figure 3.19.

3.4.4 Temperature

The variation in surface temperature, obtained from the
heat flow analysis, is shown in figure 3.20. These figures
showed that the initial surface temperature rise was very
rapid and increased with the load, that is 82°C, 150°C, 225°C
and 400°C for each of the 13.8 N, 40.5 N, 68.1 N and 131.5 N
load respectively. Temperature increase was then less rapid
and gradually fell with sliding time up to about 250 minutes,
when it became constant.

For the tests carried out with 131.5 N load, there was a
substantial increase in temperature followed by a rapid fall
(about 100°C) in the first few minutes of the run, and a
further rapid decrease as the test progressed (80°C). One
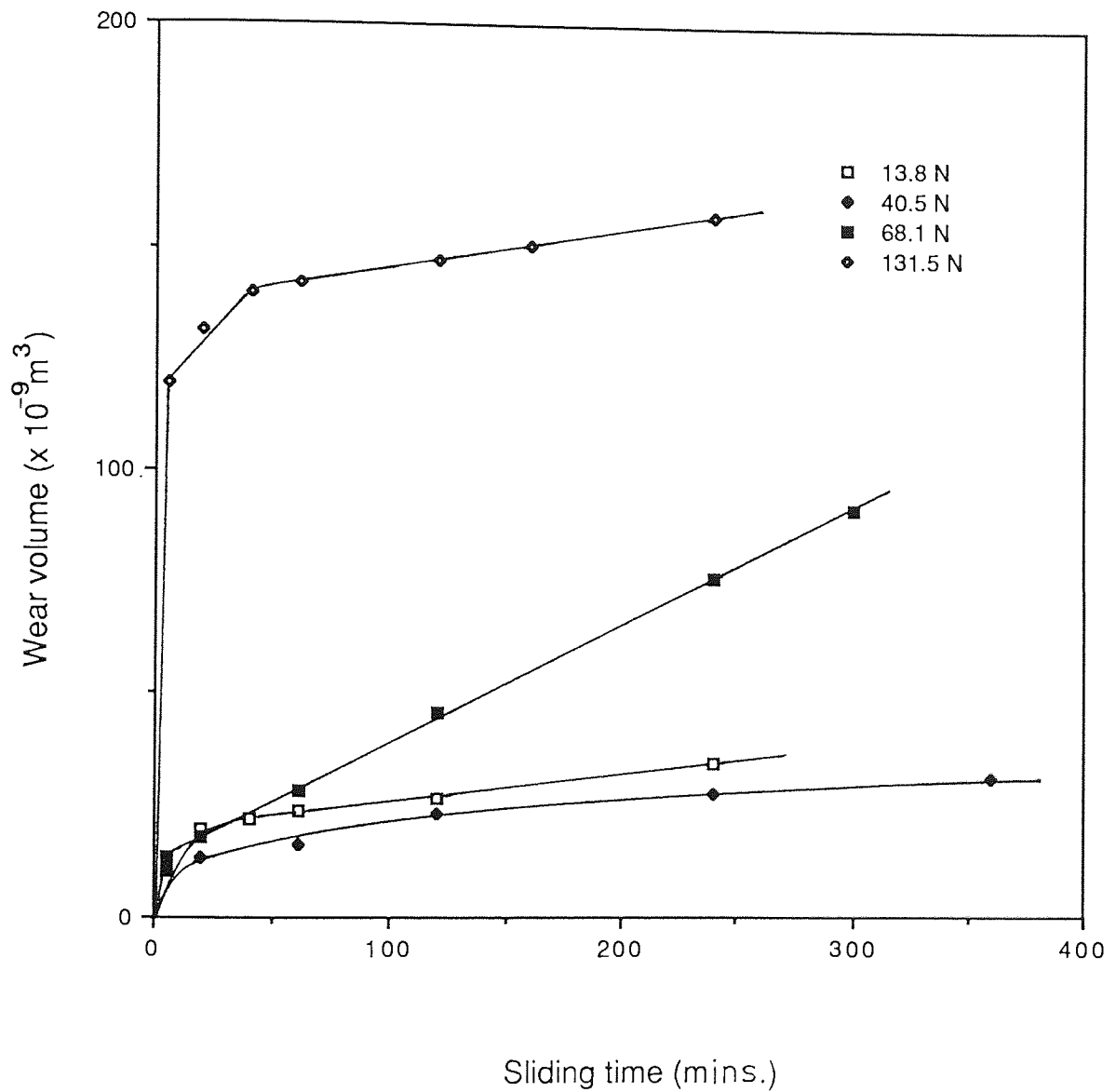
Figure 3.19   Increase in wear volume with sliding time
as the running-in mild wear experiments
at 1.2 ms^{-1} progressed.
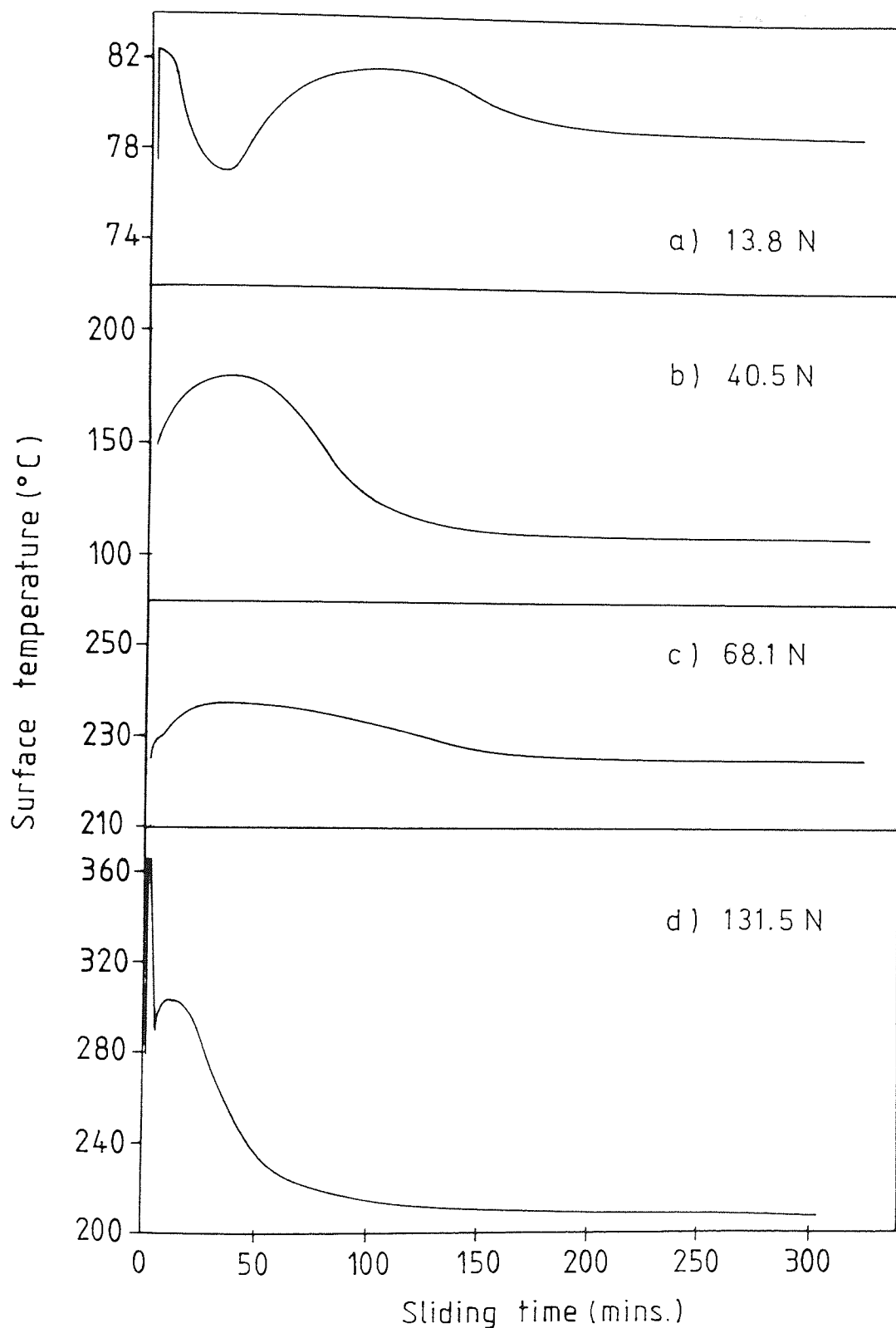
Figure 3.20   variation of surface temperature with
              sliding time for running-in mild wear
              experiments at 1.2 ms^{-1}.

interesting feature observed during the course of this run
was an intermittent increase of the pin temperatures, T_A and
T_B (see figure 3.18). Such temperature rise leads to a
similar effect in the computed surface temperature, but this
was excluded in the curves shown in figure 3.20(d).

3.4.5 Contact resistance

Figure 3.21 shows a contact resistance trace recorded
during the course of an experiment with a 40.5 N load. It
was found, from such a trace, that high initial contact
resistance dropped to virtually zero and then increased to an
average value of 10^3 Ω (approximately constant for 150
minutes run), it then further increased gradually to a mean
resistance of 10^5 Ω after more than 240 minutes of running
(this is not shown on the figure). The corresponding values
for the 68.1 N load test were 30 Ω and 95 Ω during the
running-in and equilibrium wear respectively. This latter
result indicating that there was little or no oxide present
in the region corresponding to 68.1 N load.

3.5 X-ray diffraction

3.5.1 Introduction

Wear debris was analysed by means of x-ray diffraction
from 1) selected wear pattern experiments where the debris

Figure 3.21   Variation of contact resistance with sliding
time for running-in mild wear experiment at 1.2
ms⁻¹ and 40.5 N.
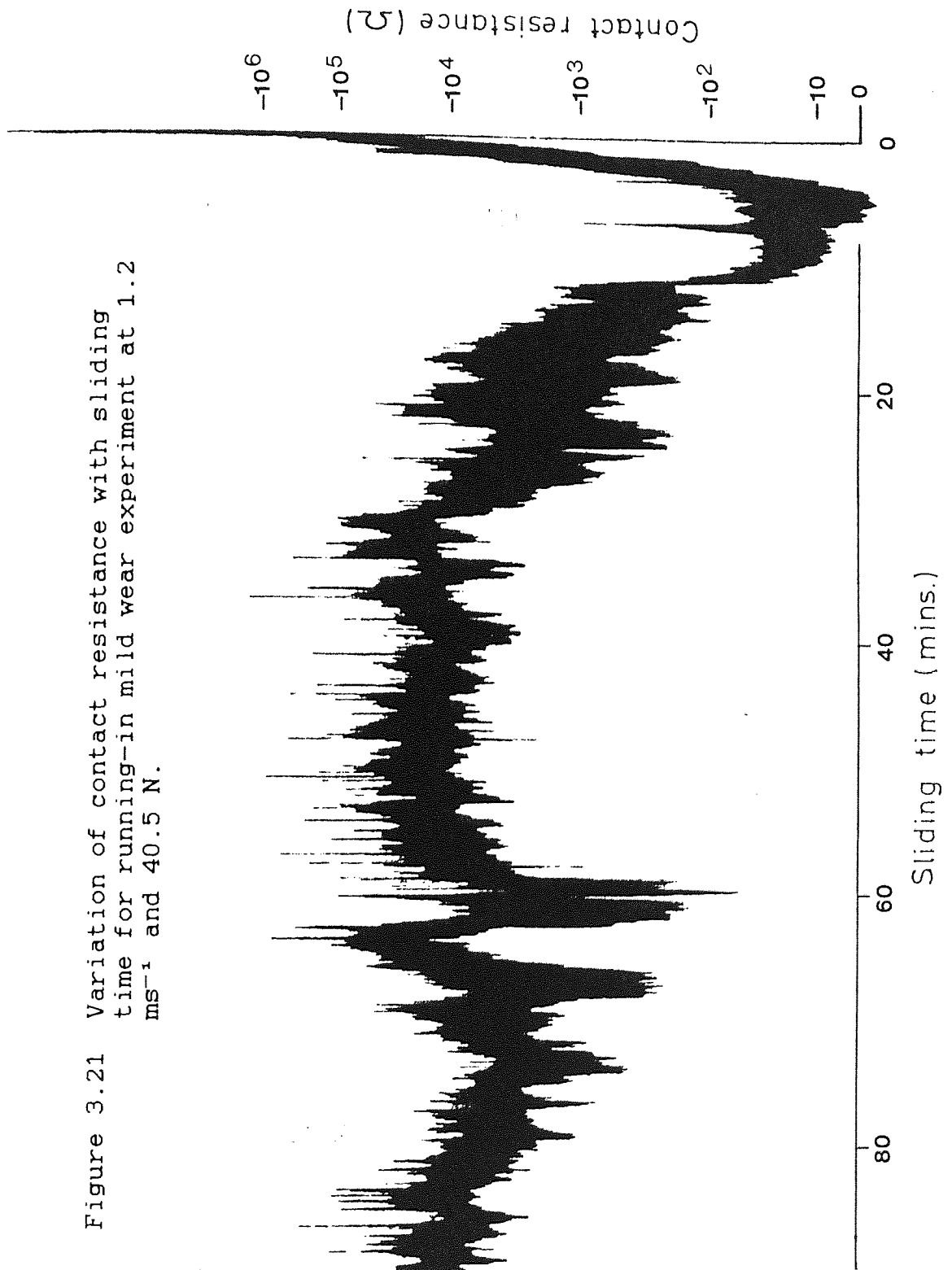
was mainly of oxide, 2) wear transition experiments where the debris was mostly metallic in form and 3) running-in mild wear experiments comprising of a mixture of both metallic and oxide debris.

The x-ray diffraction lines were identified using the ASTM index. The various constituents found in the wear debris were compared to the index given in appendix I.

3.5.2 Analysis of wear debris from wear pattern experiments

Analysis of selected samples of wear debris collected from experiments conducted at 0.6 to 1.6 ms-1 speeds are presented. The results, illustrated in figures 3.22 to 3.25, show microdensitometer traces obtained from the powder x-ray diffraction photographs of such wear debris. The experimentally measured d_{hkl} values and the detected constituents are tabulated in table 3.14. Analyses were carried out in regions 1 to 4 and typical traces are shown in figures 3.22 to 3.25.

a)   Wear debris in region 1

For this region the constituent of the wear debris at a speed of 1.6 ms^{-1} were found to be the rhombohedral oxide, $\alpha-Fe_2O_3$ and ferrite, $\alpha-Fe$ (see figure 3.22(b)). The proportion of $\alpha-Fe_2O_3$ in the debris decreased with load with small amounts of the spinel oxide, Fe_3O_4 appearing with
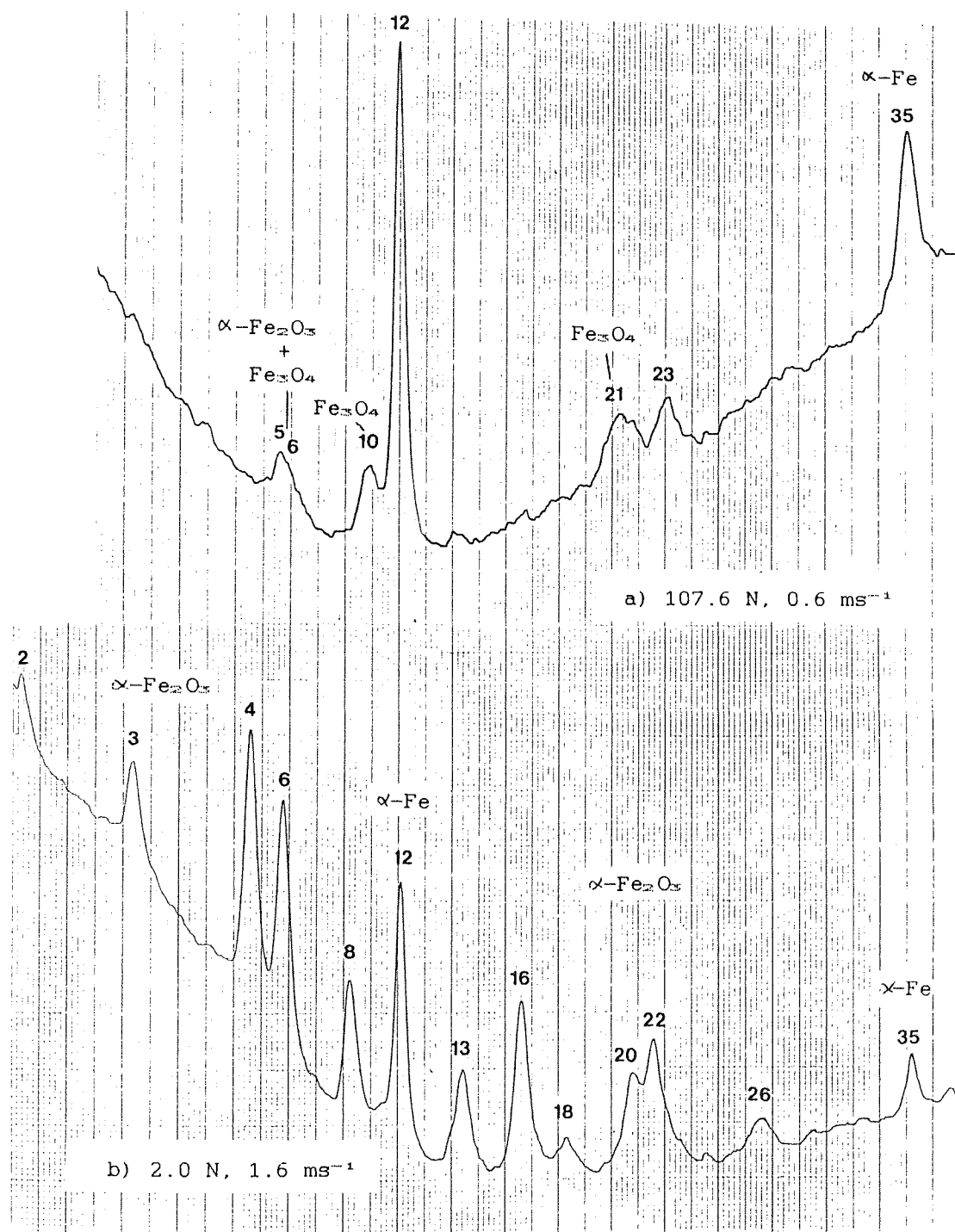
Figure 3.22 Typical microdensitometer traces of the
wear debris in region 1 (long duration).

increasing amounts of metallic iron. The results of other
analyses at speeds of 1.2, 1.0, and 0.8 ms^{-1} have shown both
types of oxide to be present as a mixture in the debris. An
example of this can be seen in the analysis at 0.6 ms^{-1} speed
where Fe_3O_4 and α-Fe were the dominant constituents of the
debris with α-Fe_2O_3 as a minor constituents (see figure
3.22(a)). Analysis of wear debris from both short and long
running duration test runs gave very similar results and were
difficult to distinguish.

b) Wear debris in region 2

The wear debris analysis at a speed of 1.6 ms^{-1} gave the
identification of Fe_3O_4, α-Fe and small amounts of FeO for
all durations up to seven hours. The oxides identified at
1.2 ms^{-1} were Fe_3O_4 for debris from long duration tests and a
mixture of Fe_3O_4 and wûstite (FeO) for debris from short
duration tests, with a reduced proportion of ferrite in the
former case. It was also observed that, for long test
duration, large increase in Fe_3O_4 occurred with increase in
load when the T_4 transition was approached.

At a speed of 1.0 ms^{-1} it was found that the
constituents of the wear debris were very similar to those of
the 1.2 ms^{-1} experiments for both short and long duration
test tuns, an example of which is shown in the
microdensitometer traces of figure 3.23. Wear debris
constituents at other speeds were also similar, but with
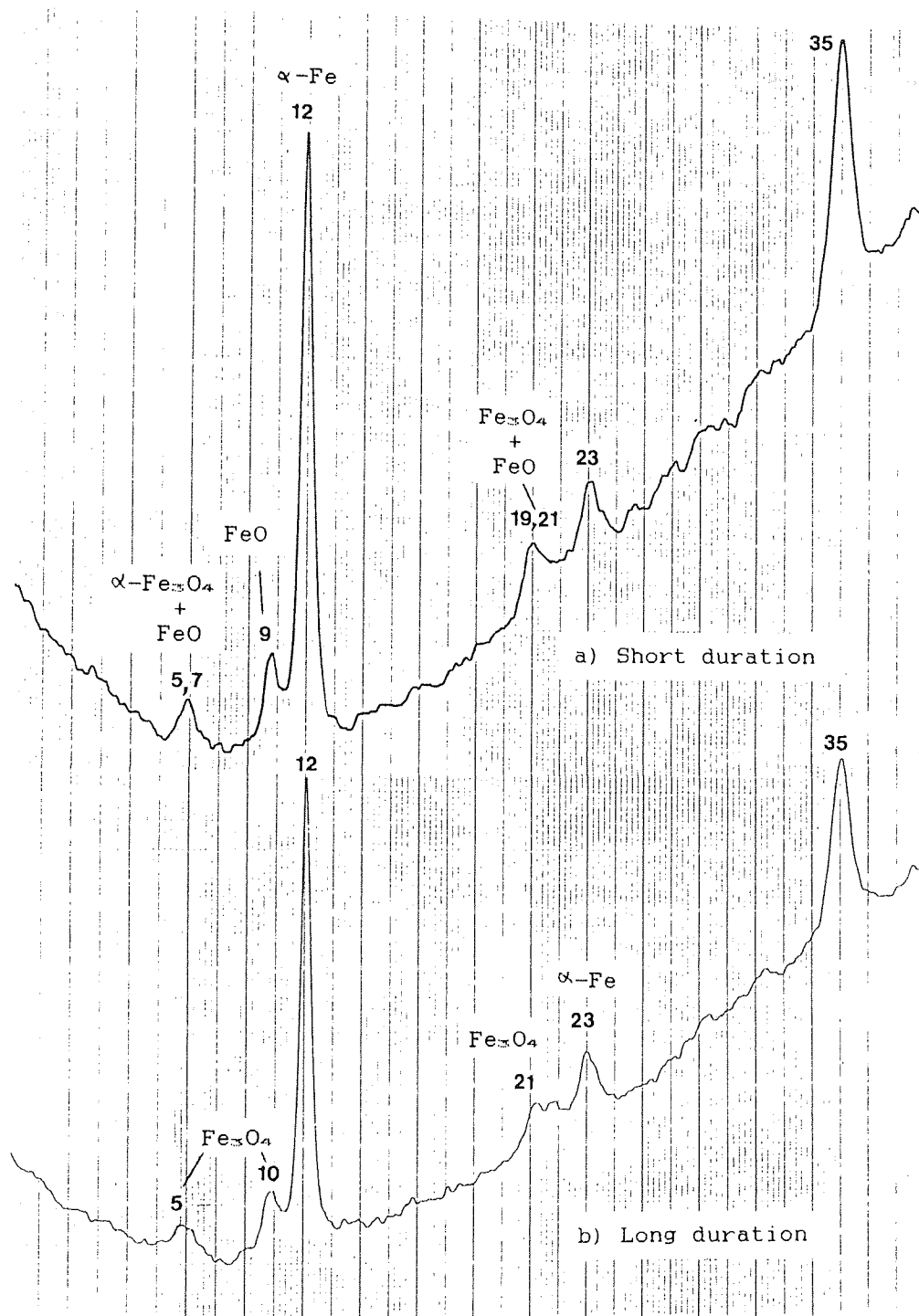
Figure 3.23 Typical microdensitometer traces of the wear debris in region 2 at 1.0 ms^{-1} and 57.2 N.

reduced proportions of Fe_3O_4 in the case of 0.8 and 0.6 ms^{-1}.

c) **Wear debris in region 3**

For the 1.6, 1.2 and 1.0 ms^{-1} speeds in region 3 the composition of wear debris as analysed by x-ray diffraction was, in relative order of proportion, a mixture of α-Fe, FeO and Fe_3O_4. Figure 3.24(b) shows typical microdensitometer traces of the x-ray diffraction patterns. It was observed that an increase in load through this region decreased the amount of Fe_3O_4 and increased the amount of α-Fe, with small reduction in the proportion of FeO. The analyses made at low speeds (0.8 and 0.6 ms^{-1}) produced α-Fe_2O_3, in addition to spinel, wùstite and ferrite. An example of this was observed on a typical microdensitometer trace of 0.8 ms-1 speed, shown in figure 3.24(a).

d) **Wear debris in region 4**

Figure 2.25 shows that for analysis made at 1.6 and 1.2 ms^{-1} speeds, the constituents of wear debris found in the forth region of mild wear were α-Fe_2O_3, Fe_3O_4, FeO and α-Fe. The proportion of FeO was reduced at loads less than 131.5N approaching the T_3 transition load. This was observed on the wear pattern analysis at 1.2 ms^{-1} speed.
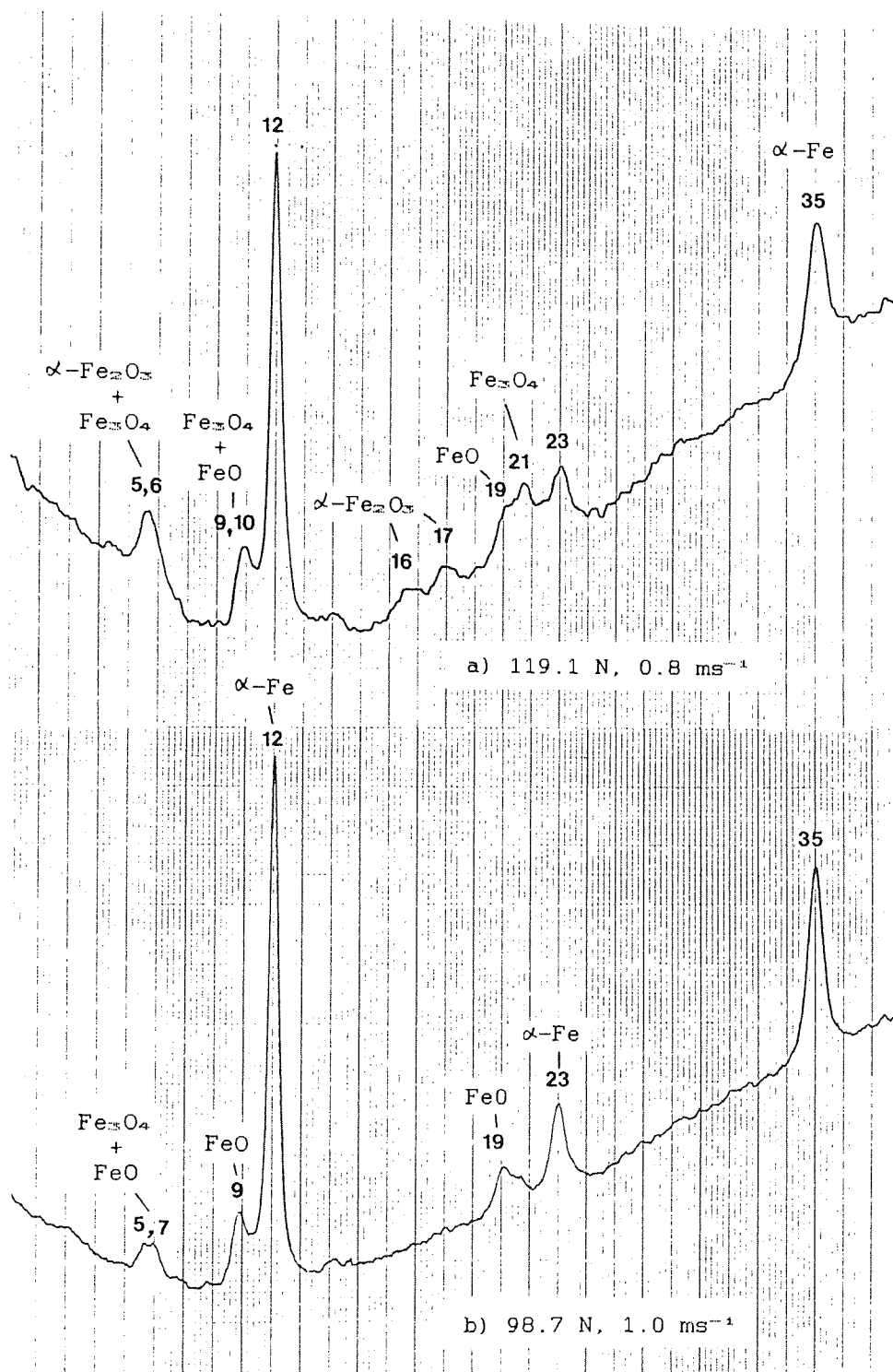
Figure 3.24 Typical microdensitometer traces of the

wear debris in region 3 (long duration).
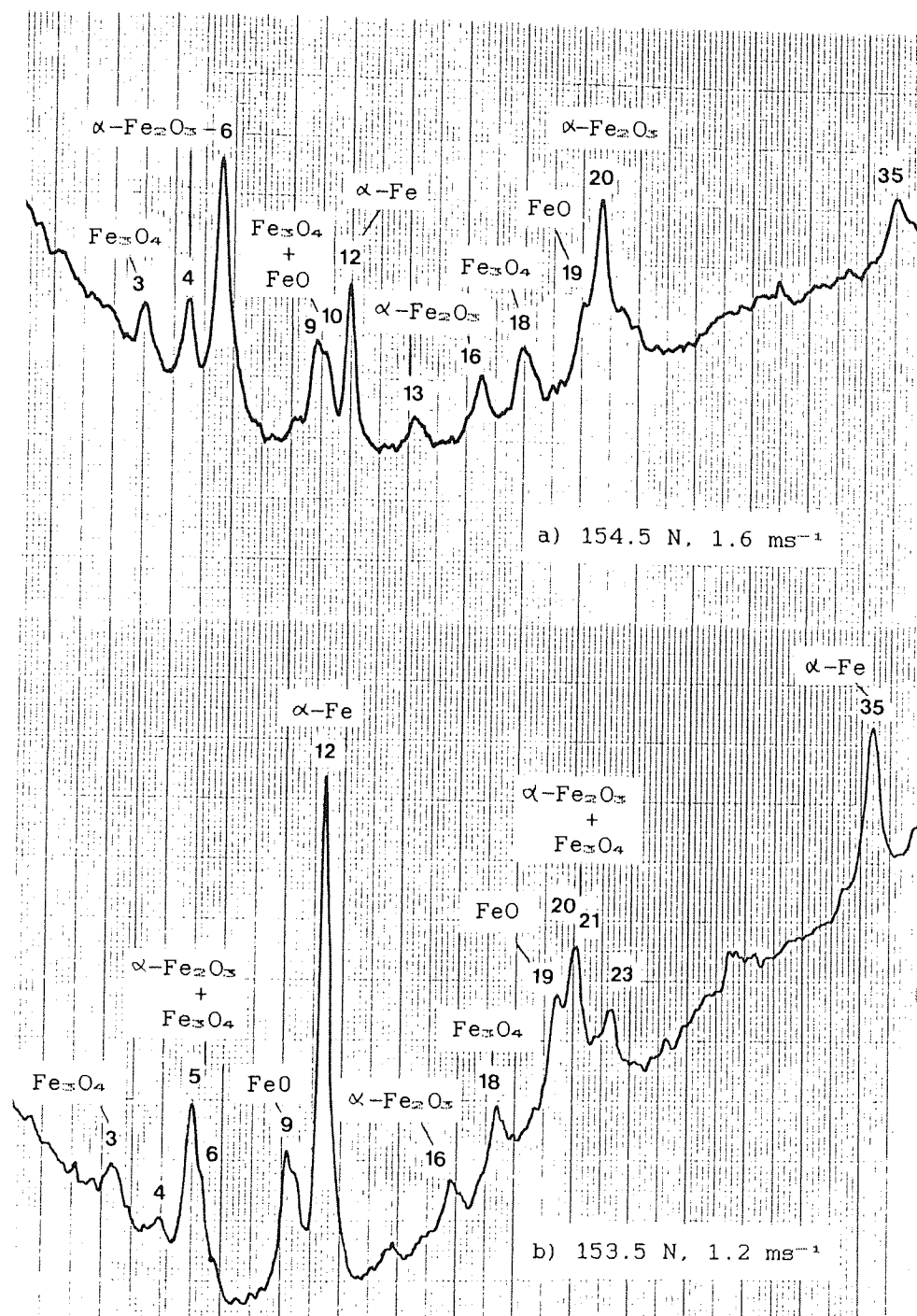
Figure 3.25 Typical microdensitometer traces of the
wear debris in region 4 (long duration).

I D E N T I T Y

Speed (ms^{-1})	Region 1	Region 2	Region 3	Region 4
0.6	Fe_3O_4, $\alpha-Fe_2O_3$, $\alpha-Fe$, FeO	Fe_3O_4, FeO $\alpha-Fe$	FeO, Fe_3O_4, $\alpha-Fe$, $\alpha-Fe_2O_3$	
0.8	Fe_3O_4, $\alpha-Fe_2O_3$, $\alpha-Fe$	Fe_3O_4, $\alpha-Fe$ FeO (L,S)	FeO, Fe_3O_4, $\alpha-Fe$, $\alpha-Fe_2O_3$	
1.0	$\alpha-Fe_2O_3$, Fe_3O_4, $\alpha-Fe$	Fe_3O_4, FeO (S), $\alpha-Fe$	FeO, Fe_3O_4, $\alpha-Fe$	
1.2	$\alpha-Fe_2O_3$, Fe_3O_4, $\alpha-Fe$	Fe_3O_4, FeO (S), $\alpha-Fe$	FeO, Fe_3O_4, $\alpha-Fe$	Fe_3O_4, $\alpha-Fe_2O_3$, FeO, $\alpha-Fe$
1.6	$\alpha-Fe_2O_3$, $\alpha-Fe$	Fe_3O_4, FeO (L,S), $\alpha-Fe$	FeO, Fe_3O_4, $\alpha-Fe$	Fe_3O_4, FeO, $\alpha-Fe_2O_3$ $\alpha-Fe$

Table 3.14 Compounds identified (in order of concentration) in the debris from wear pattern experiments (S and L indicate the short and long duration tests respectively).

3.5.3 Analysis of debris from wear transition experiments

The wear debris collected during the running-in severe wear (from T_2 transition tests) was totally metallic; x-ray analysis, therefore, gave strong ferrite lines on the microdensitometer traces. It was very difficult to detect the small amounts of oxide present in the debris collected at the critical point of transition from severe to mild wear.

3.5.4 Analysis of wear debris from running-in mild wear experiments

Analyses were made to investigate the constituents formed in the wear debris prior to the establishment of equilibrium mild wear. For this purpose samples were taken from different running durations on the four load tests (13.8 N, 40.5 N, 68.1 N and 131.5 N), each of which represented the four mild wear regions illustrated in figure 3.4 at 1.2 ms^{-1} speed. The sequences of change in the contents of wear debris are shown in figure 3.26 to figure 3.29. The various peaks of the x-ray diffraction lines were compared to the ASTM index, given in appendix I, and the results are summarized in table 3.15.

a) **Wear debris with 13.8 N load** (figure 3.26)

After the first 5 minutes of the test run (not shown) wear debris was totally metallic and the trace consisted of

Figure 3.26   Microdensitometer traces of the wear debris
after a) 20, b) 60, c) 120 and d) 240 mins.
of running at 1.2 ms^{-1} and 13.8 N.
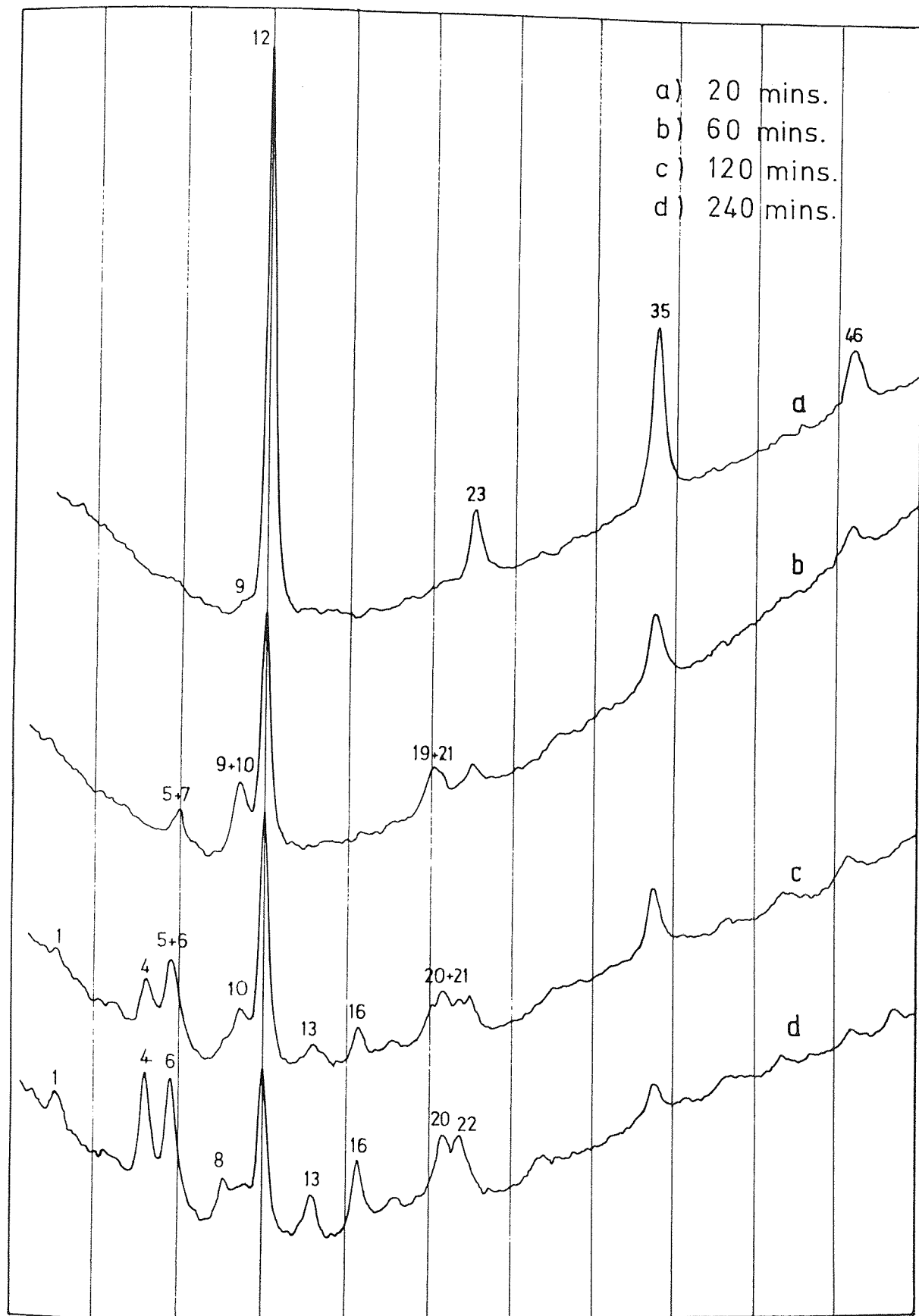
Figure 3.26

strong ferrite lines. As the test progressed to 20 minutes, running duration which was just above the time for transition from severe to mild wear of 18 minutes, a very small amount of FeO was detected at the strongest line peak (no. 9). No other oxide types was detected at this early stage of running. After 60 minutes of running, both Fe_3O_4 and FeO were present in the debris, and at the same time the amount of ferrite was reduced.

Between 60 and 120 minutes run there was a considerable reduction in the amount of Fe_3O_4 and FeO, but little change in the amount of ferrite. $\alpha-Fe_2O_3$ was first detected at the 100 minutes run, and the amount increased after a duration of 120 minutes (see figure 3.26(c)); some Fe_3O_4 was still present while FeO had dissapeared from the debris. During the course of the final run the wear debris appeared dark brown, and the x-ray analysis revealed a large proportion of $\alpha-Fe_2O_3$. An example of 240 minutes run, shown in figure 3.26(d), illustrates this result.

b) Wear debris with 40.5 N load (figure 3.27)

After 5 minutes run the wear debris consisted almost entirely of ferrite. At the end of 20 minutes run, however, small amounts of Fe_3O_4 and FeO were detected in the debris, along with the ferrite. There was little further change found in wear debris in the 60 and 120 minutes running times

Figure 3.27   Microdensitometer traces of the wear debris

after a) 20, b) 60, c) 120 and d) 360 mins.

of running at 1.2 ms^{-1} and 40.5 N.
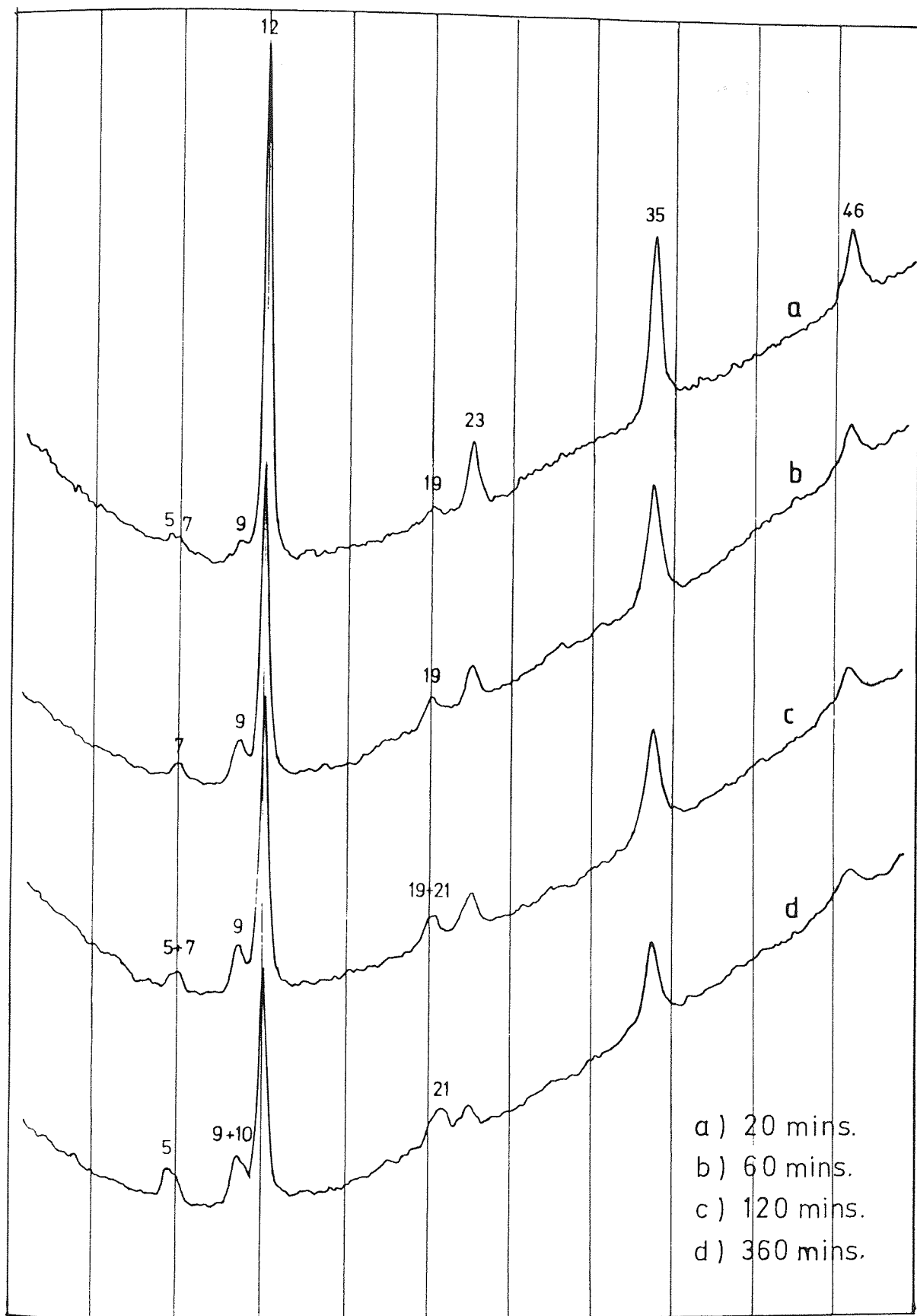
Figure 3.27

where FeO and ferrite were identified, with some Fe_3O_4 present in the case of 120 minutes. The appearance of wear debris during this stage of running was dark and bright metallic. For wear debris collected at 360 minutes run the major constituents were Fe_3O_4 and ferrite although some FeO was still present.

c) Wear debris at 68.1 N load (figure 3.28)

wear debris analysis under these conditions showed the presence of FeO (line 9 and 19) along with ferrite after 5 minutes running time. The composition of wear debris at a running duration of 20 minutes was Fe_3O_4, FeO and ferrite, and this remained unchange after 60 minutes and 120 minutes. However, the amount of ferrite during such three successive running times was much reduced. After 300 minutes the debris was dark grey in appearance and was identified as FeO, ferrite and small amount of Fe_3O_4.

d) Wear debris with 131.5 N load (figure 3.29)

For wear debris at this load the constituents detected after 5 minutes run were ferrite, present in high proportions, and austenite (line 11) with some FeO at very low levels. Similar constituents were observed after 20 minutes but with the amount of FeO increased to a greater proportion than either ferrite or austenite. These are two examples of wear debris analysis found in the first stage of

Figure 3.28   Microdensitometer traces of the wear debris
              after a) 5, b) 20, c) 60, d) 120 and e) 300
              mins. of running at 1.2 ms^{-1} and 68.1 N.

Figure 3.29   Microdensitometer traces of the wear debris
              after a) 5, b) 20, c) 60, d) 120 and e) 240
              mins. of running at 1.2 ms^{-1} and 131.5 N.

a) 5, b) 20, c) 60, d) 120 and e) 300 mins.

Figure 3.28

a) 5, b) 20, c) 60, d) 120 and e) 240 mins.
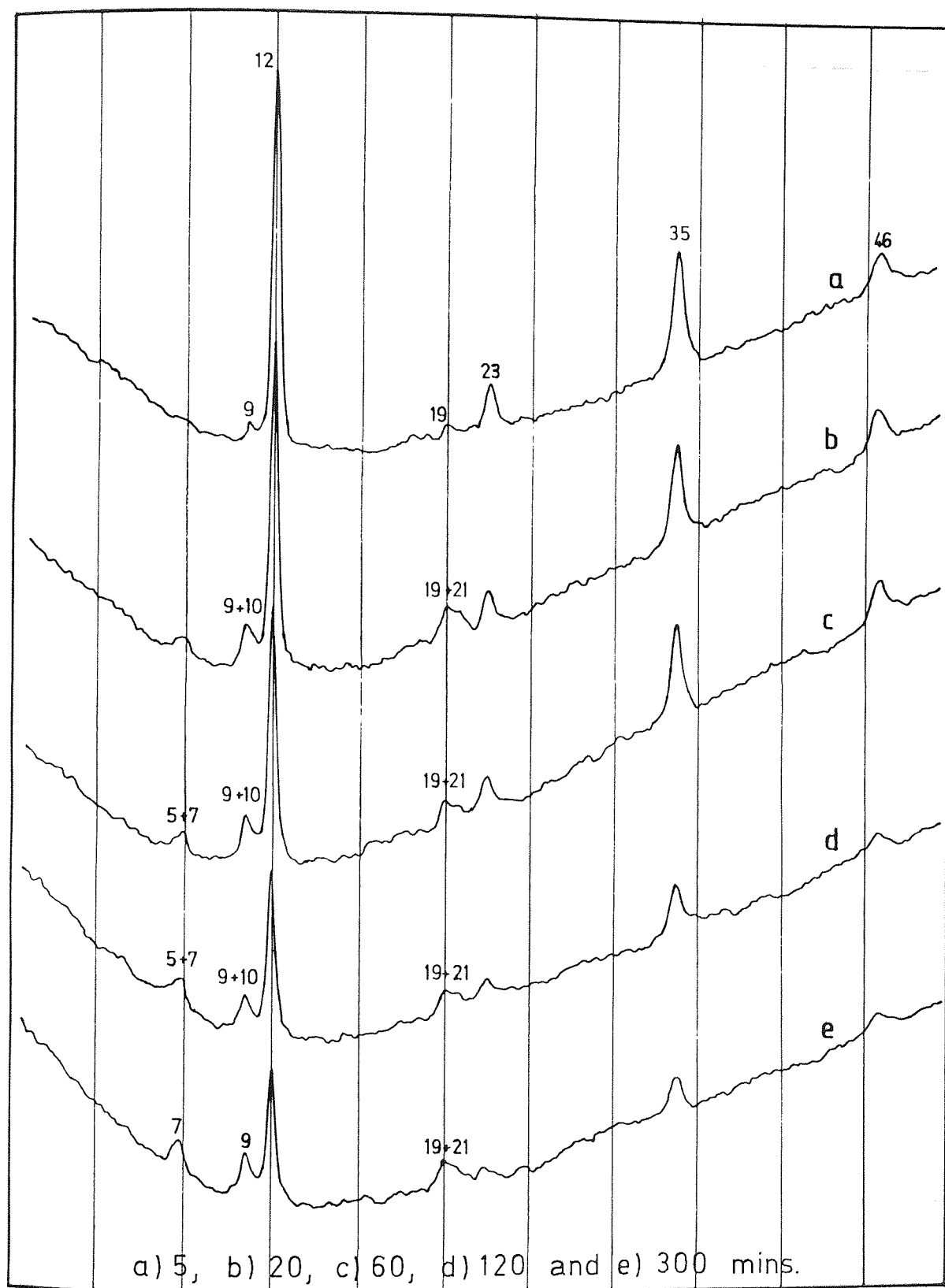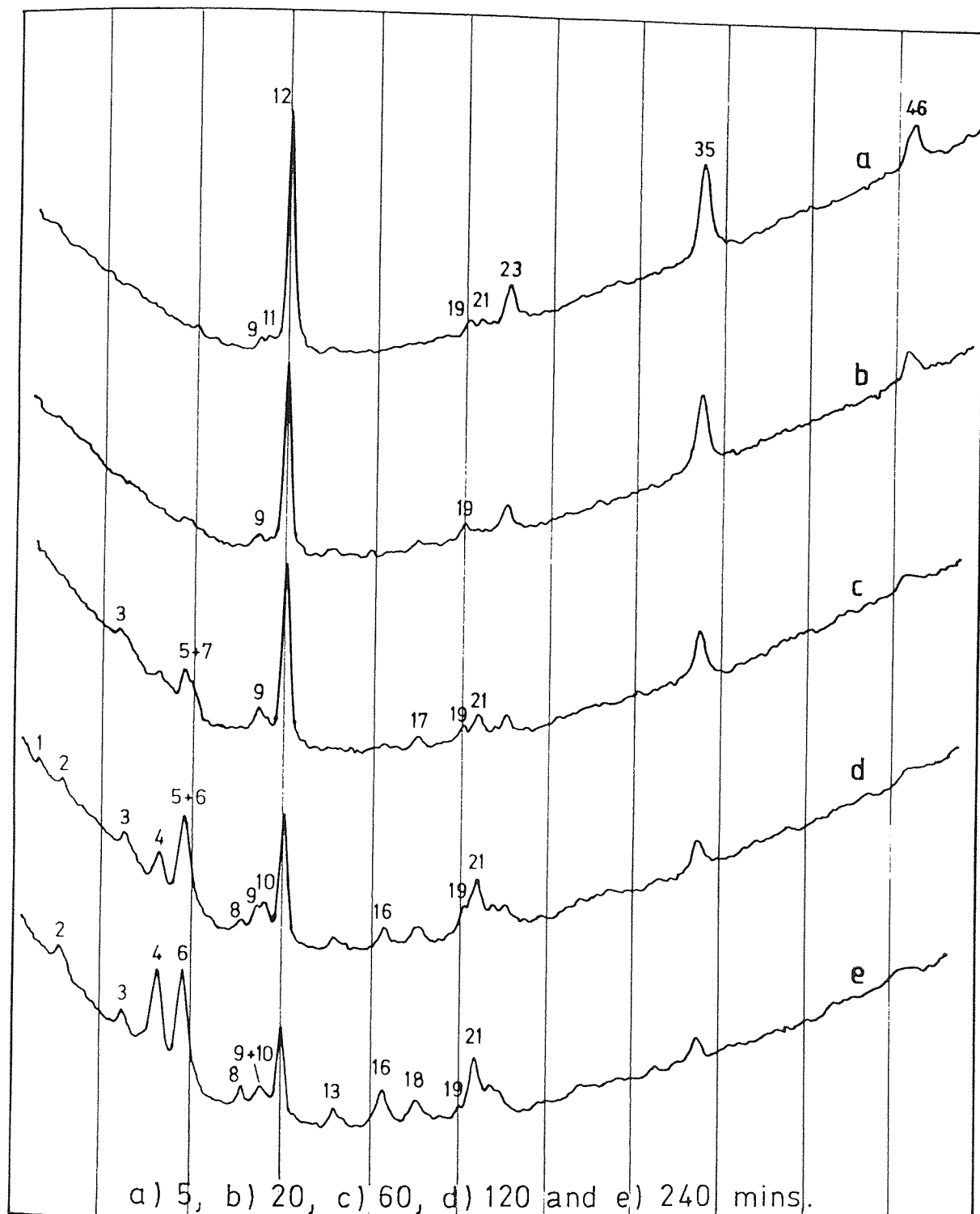
Figure 3.29

Running time (mins.)	Identity			
	13.8 N	40.5 N	68.1 N	131.5 N
5	α-Fe	α-Fe	α-Fe (M) FeO	α-Fe (M) FeO Austenite (P,D)*
20	α-Fe Fe_3O_4 FeO	α-Fe Fe_3O_4 FeO	α-Fe Fe_3O_4 FeO	α-Fe FeO
60	α-Fe Fe_3O_4 FeO	α-Fe FeO		α-Fe Fe_3O_4 FeO
120	α-Fe α-Fe_2O_3 Fe_3O_4 FeO	α-Fe Fe_3O_4 FeO	α-Fe Fe_3O_4 FeO	α-Fe α-Fe_2O_3 Fe_3O_4 FeO Austenite (P,D)*
240	α-Fe α-Fe_2O_3 (M) Fe_3O_4			α-Fe α-Fe_2O_3 (M) Fe_3O_4 (M) FeO
300			α-Fe (M) Fe_3O_4 FeO(M)	
360		α-Fe Fe_3O_4 (M) FeO		

Table 3.15 Compounds identified in the debris and on specimen surface by x-ray diffraction and by glancing angle x-ray diffraction* (M = majority P = pin, D = disc).

mild wear described in section 3.4.3. Analysis for the second stage of mild wear is as follows: After 60 minutes, Fe_xO_4 (line peak 5), FeO and ferrite were detected. At 120 minutes and even longer running periods of 240 minutes a mixture of three iron oxides and ferrite were identified, with the amounts of Fe_xO_4 and $\alpha-Fe_xO_x$ slightly increased. These were shown by the increased number of low intensities line peaks with running durations, such as lines 1, 2, and 3, shown in figure 3.29(c),(d) and (e).

3.5.5 Glancing angle x-ray diffraction

A glancing angle x-ray diffraction technique was used to study the surface films formed on worn pins and discs. The results showed that constituents detected on specimen surfaces corresponded closely to those found in the wear debris. A typical microdensitometer trace is shown in figure 3.30, and shows oxide traces very similar to figure 3.29(d), with large peaks of ferrite, due to the deep penetration of x-ray beam into the bulk of the specimen surface. The lines of the relevent oxides, shown by series of numbers, were compared to the ASTM index (appendix I) to give their oxide identification. An interesting feature of the trace was the existence of austenite at a certain load, this was observed on the 131.5 N pins after 5 minutes (see figure 3.29(a)) and 20 minutes (figure 3.30). Austenite was also
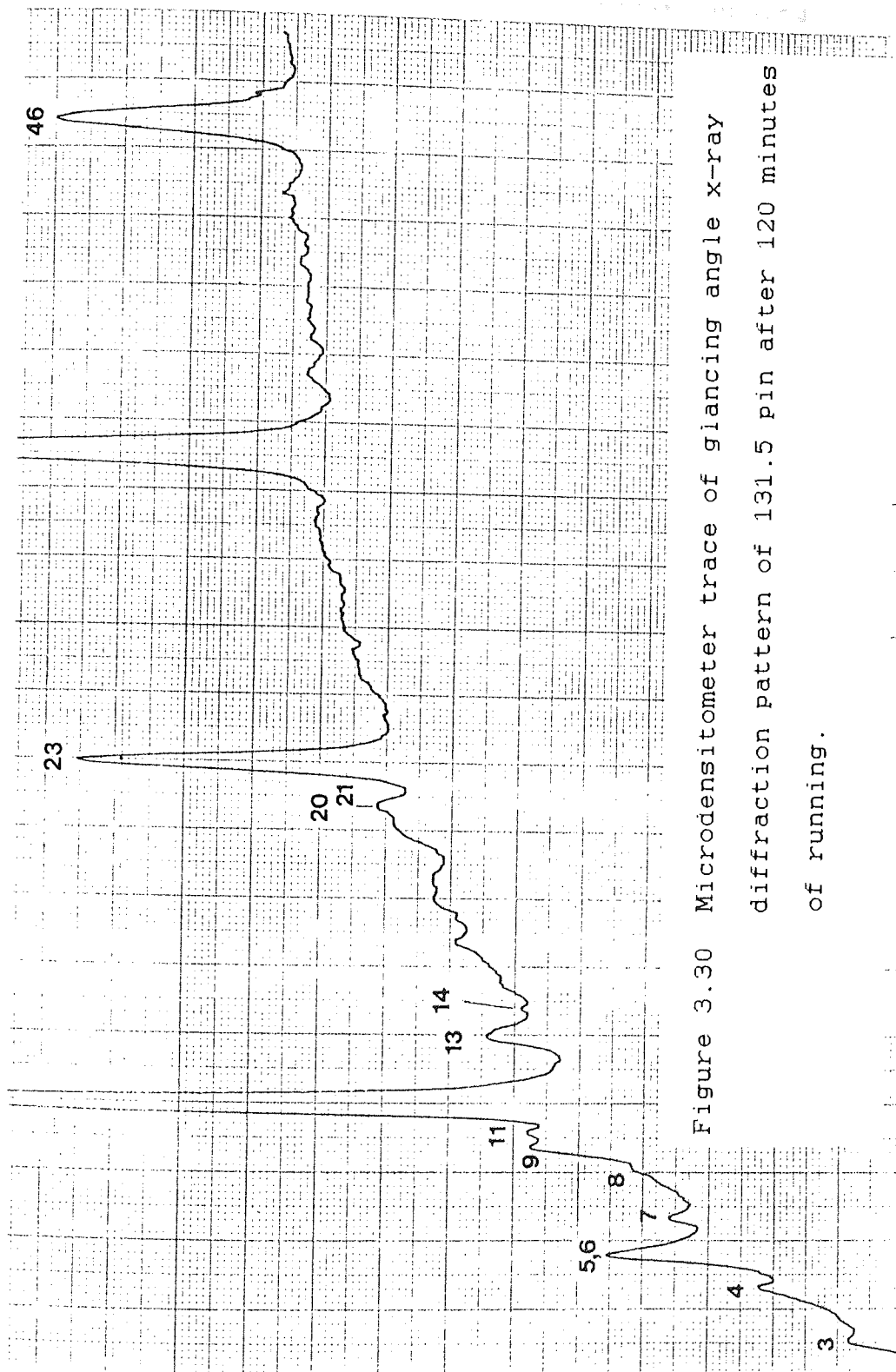
Figure 3.30 Microdensitometer trace of glancing angle x-ray diffraction pattern of 131.5 pin after 120 minutes of running.

observed on the specimen discs under similar running durations.

3.6 Proportional analysis of wear debris

This method of analysis was used to obtain an approximate percentage volume composition of oxides and iron in the debris. The method was originally developed by Averbach and Cohen (99), and used later by Quinn (100) to analyse specimens of low alloy steels. A summary of the theory, given in reference (95), is as follows:

From the basic x-ray diffraction theory it was shown that the intensity of x-rays diffracted, I_x, into a maximum at $2\theta_{hkl}$ to the undeviated direction is given by

$$I_x \propto \frac{F_x^2 \; m \; L_p \; \exp \; (-2M)}{V_x^2} \; (V_x \; A_\theta) \; \ldots\ldots\ldots(3.4)$$

where

F_x = the structure factor of the component x.

m = the multiplicity of the diffracting plane (hkl).

L_p = the Lorentz polarization factor.

$\exp(-2M)$ = the Debye-Waller temperature factor.

V_x = the volume of the unit cell of substrate x irradiated.

A_θ = The sample absorption factor.

More simply the factor of proportionality was taken to be unity when dealing with relative intensities. Thus, equation

3.4 can be rewritten as

$$I_x = R_x \, V_x \, A_\theta \qquad \cdots\cdots\cdots\cdots(3.5)$$

where

$$R_x = \frac{F_x^2 \, m \, L_p \, \exp\,(-2M)}{V_x^2} \qquad \cdots\cdots\cdots\cdots(3.6)$$

All the parameters involved in equation (3.6) can be obtained from x-ray diffraction data as, for example, in reference (95). The relative integrated intensity was assumed to be approximately equal to the product of peak-height density times the `half-width'. Summary of these are given in appendix I. Quinn has indicated that if for a given specimen the adsorption factor has the same dependence upon θ (the Bragg angle), irrespective of the component giving rise to the diffraction maxima, then the graph of I_x/R_x plotted against θ for two components, should lie on the same curve. The difference was the ordinate representing the ratio of their volumes.

By plotting log I_x/R_x against θ for component 1 and 2 the ordinates where two straight lines intercept with the y axis are equal to log V_1 and log V_2 respectively. This gives log (V_1/V_2) = difference in ordinate, and the ratio can thus be calculated. For best results the corrected values of R (given in appendix I) were used throughout the calculations.

This technique was purposely used for the analysis of wear debris obtained from the running-in mild wear tests, so that the percentage of the constituents produced can be estimated. Practically, it was successfully applied for tests with 13.8 N load, but failed to apply for tests with other loads due to difficulties in sorting out the line peaks of adjacent oxides in which the resolution was very low.

Figure 3.31 shows a typical plot of log I_x/R_x versus θ for wear debris collected after 180 minutes run. By using α-Fe_2O_3 as the internal standard the ratio of the volumes and their percentages are as follows:

$$\frac{V(Fe)}{V(Fe_2O_3)} = \frac{0.53}{2.7} = 0.1963$$

$$\frac{V(Fe_3O_4)}{V(Fe_2O_3)} = \frac{0.7}{2.7} = 0.2592$$

$$V(Fe_2O_3) = 100 / (1 + 0.1963 + 0.2592) = 68.7 \%$$

$$V(Fe) = 68.7 \times 0.1963 = 13.5 \%$$

$$V(Fe_3O_4) = 68.7 \times 0.2592 = 17.8 \%$$

Using a similar method of calculation, the volume percentage from different test durations were obtained, and the results are shown in figure 3.32. This figure shows the volume composition of the wear debris (percentage) as a function of running duration.

At the beginning of mild wear (i.e. after 20 minutes
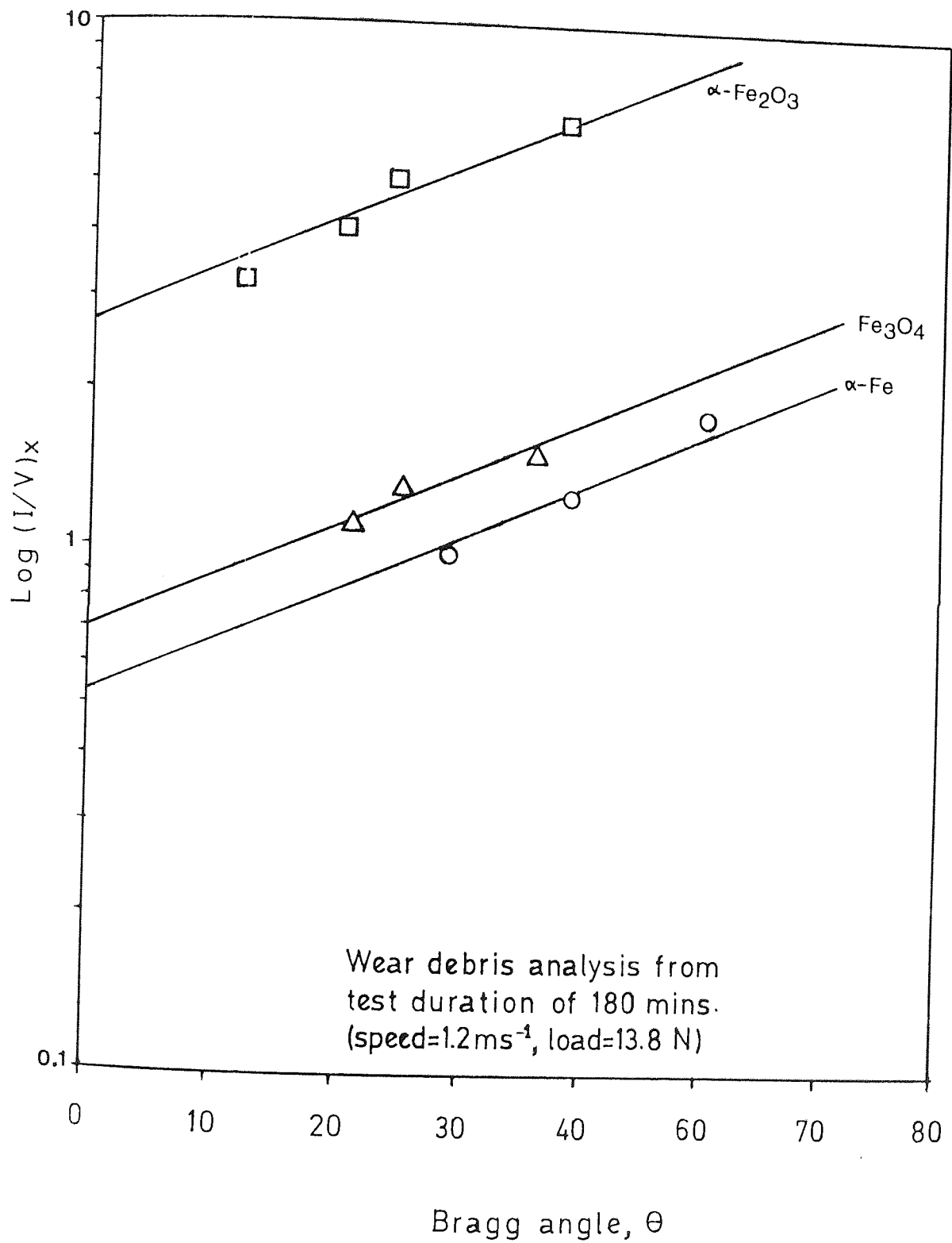
Figure 4.31 Typical graph of log (I/V)ₓ versus Θ.
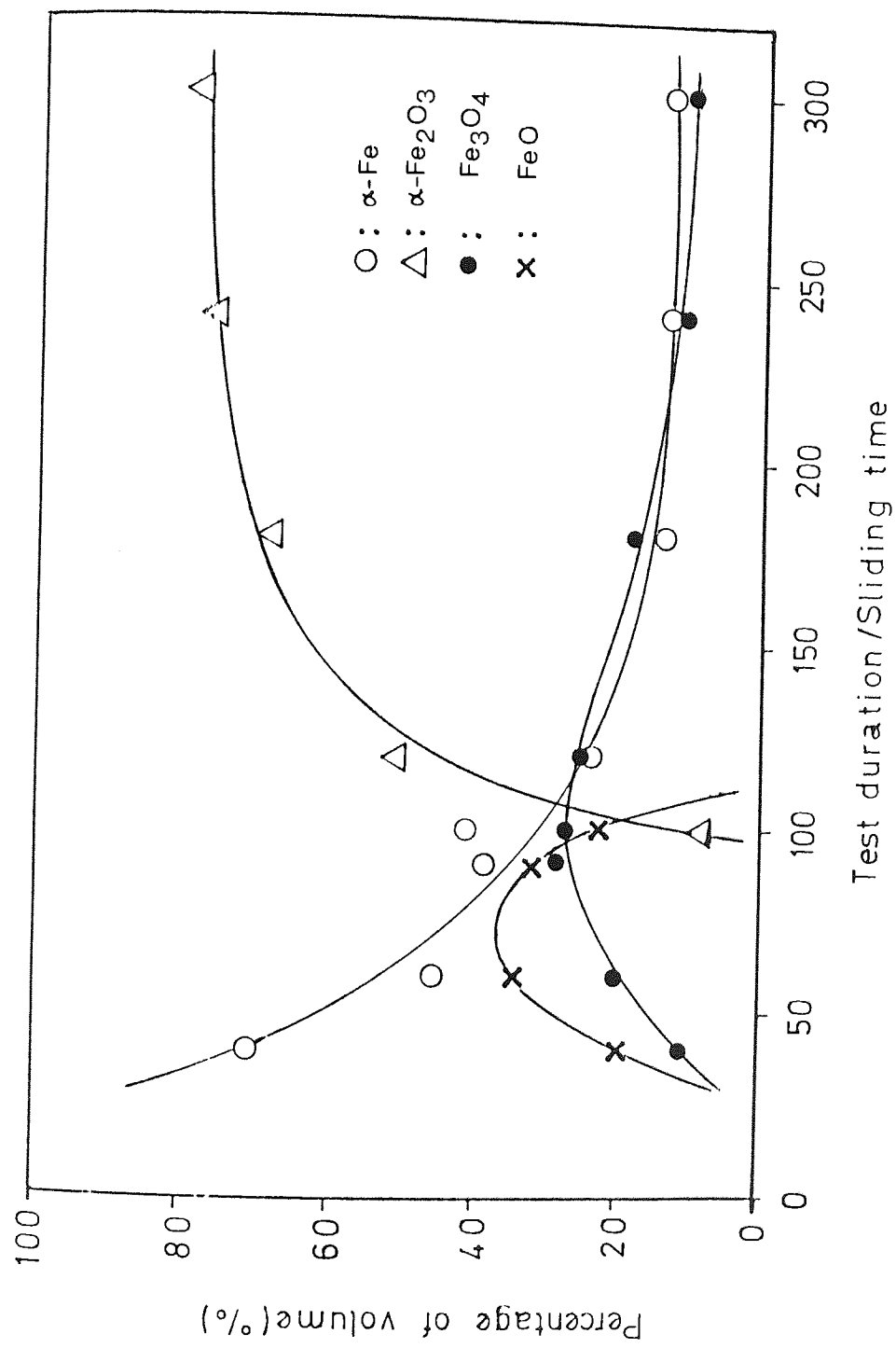
Figure 3.32   Percentage of debris constituents versus
sliding time for running-in mild wear
experiments at 1.2 ms^{-1} and 13.8 N.

run) Fe_3O_4 and FeO were found to increase in volume, while at the same time the amount of metallic iron was reduced from above 90%. The maximum volume reached by FeO was about 37% after 70 minutes run; there was a further rapid decreased and eventually the oxide disappeared from the wear debris after just above the 100 minutes run. By comparison the volume of Fe_3O_4 increased up to 29% at the 100 minutes run followed by a gradual decrease to 10% at the end of the run. On the other hand, the volume of iron continuously reduced and eventually reached a constant value of about 13%. The increase in volume percentage of $\alpha-Fe_2O_3$ took place just before 100 minutes run, and further increased to about 77% at the end of 240 minutes run.

3.7 Microhardness measurements

3.7.1 Surface measurement

(i) Unworn specimen

Microhardness measurements were made on selected specimens. The hardness of the unworn pin and unworn disc were 285 ± 10 VPN and 205 ± 12 VPN respectively. These were based upon twenty five readings made on five random specimens.

(ii) Worn specimen

In the wear transition test at 1.2 ms^{-1}, the hardness of a surface during the running-in periods of severe wear was measured. The readings on three chosen discs (see test number 12, 13 and 14 of table 3.8), each with different running durations did not show any significant variation, and were found to be 653 ± 81 VPN. However, the overall mean hardness for various speed tests described in section 3.3 was

H A R D N E S S (VPN)

Load(N)	Duration of run (minutes)						
	5	20	60	120	240	300	360
13.8	626 ± 121	703 ± 112	737 ± 82		589 ± 60		
40.5	777 ± 69	854 ± 110	764 ± 104		836 ± 85		795 ± 68
68.1	788 ± 126	900 ± 115	924 ± 52	906 ± 95		931 ± 100	
131.5	582 ± 71	621 ± 88	617 ± 105	571 ± 78	580 ± 82		

Table 3.16 Hardnesses of disc surface at 1.2 ms^{-1} and various running durations.

604 ± 110. Difficulties arose because the worn surface was so rough and this caused large errors in the measurements. The hardness of a disc surface at its T_x transition time (see test number 11 of table 3.8) found to be 846 ± 101 VPN (average of more than ten readings).

The disc surfaces obtained from the running-in mild wear tests were also measured. This was aimed at measuring the surface hardness after varying running durations. The results given in table 3.16 were based on at least ten readings made on two discs

3.7.2 Microhardness variation with depth

Subsurface microhardness measurements of the worn pin were made on both wear transition tests and running-in mild wear tests. There were problems encountered in producing diamond indentations very close to the surface, the minimum measurable depth was between 5 and 9 μm depending on the hardness of the surface. Obviously the higher the hardness the lower the depth which can be measured from the top of the surface

Microhardness depth profiles for various durations of mild wear are shown in figure 3.33 to figure 3.36. The curves showed that pronounced hardening occurred below the surface for all the test durations, particularly during the early stage of the running. These occurred on the worn pin
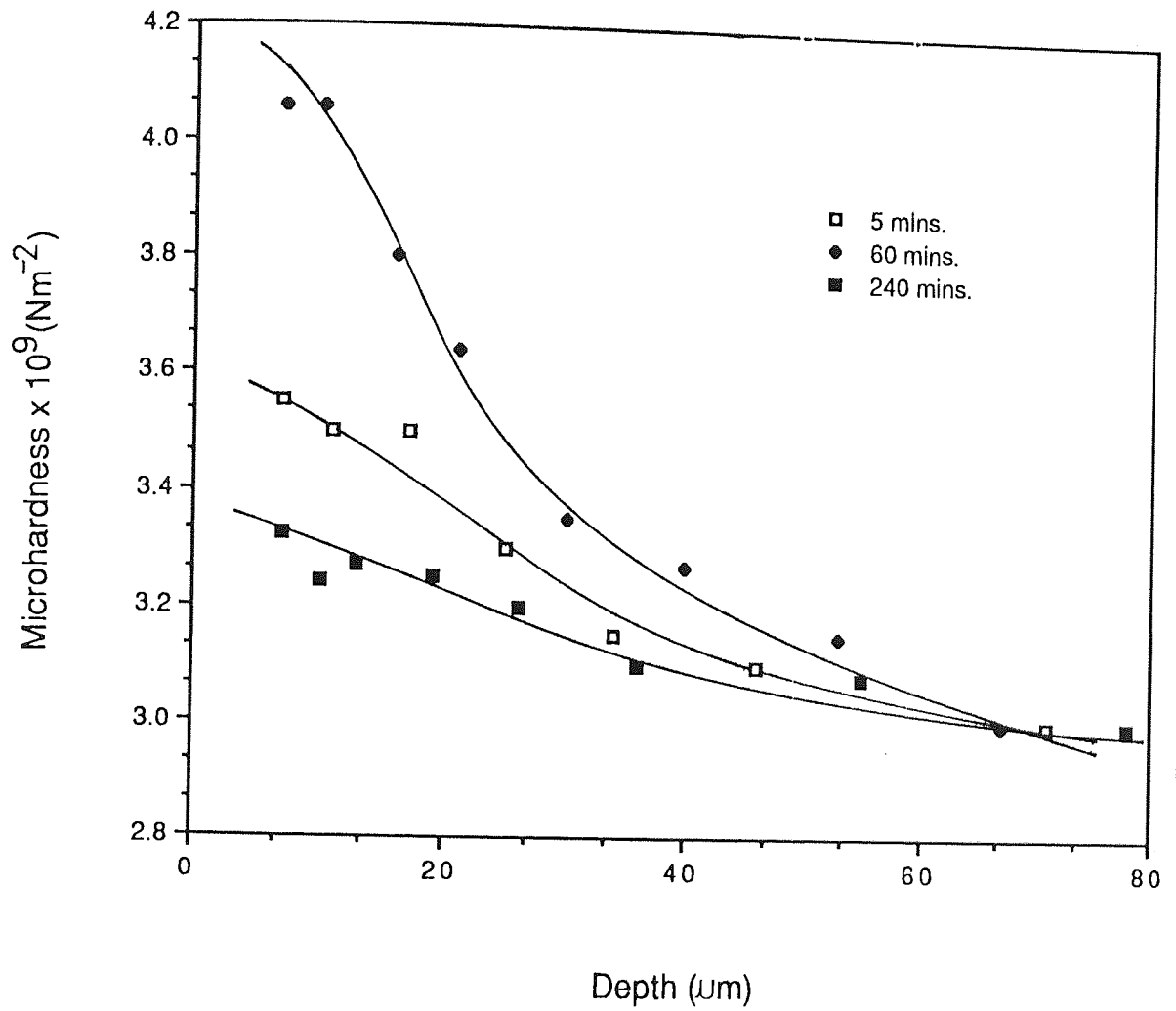
Figure 3.33   Microhardness versus depth curves for

13.8 N experiments at 1.2 ms^{-1}.
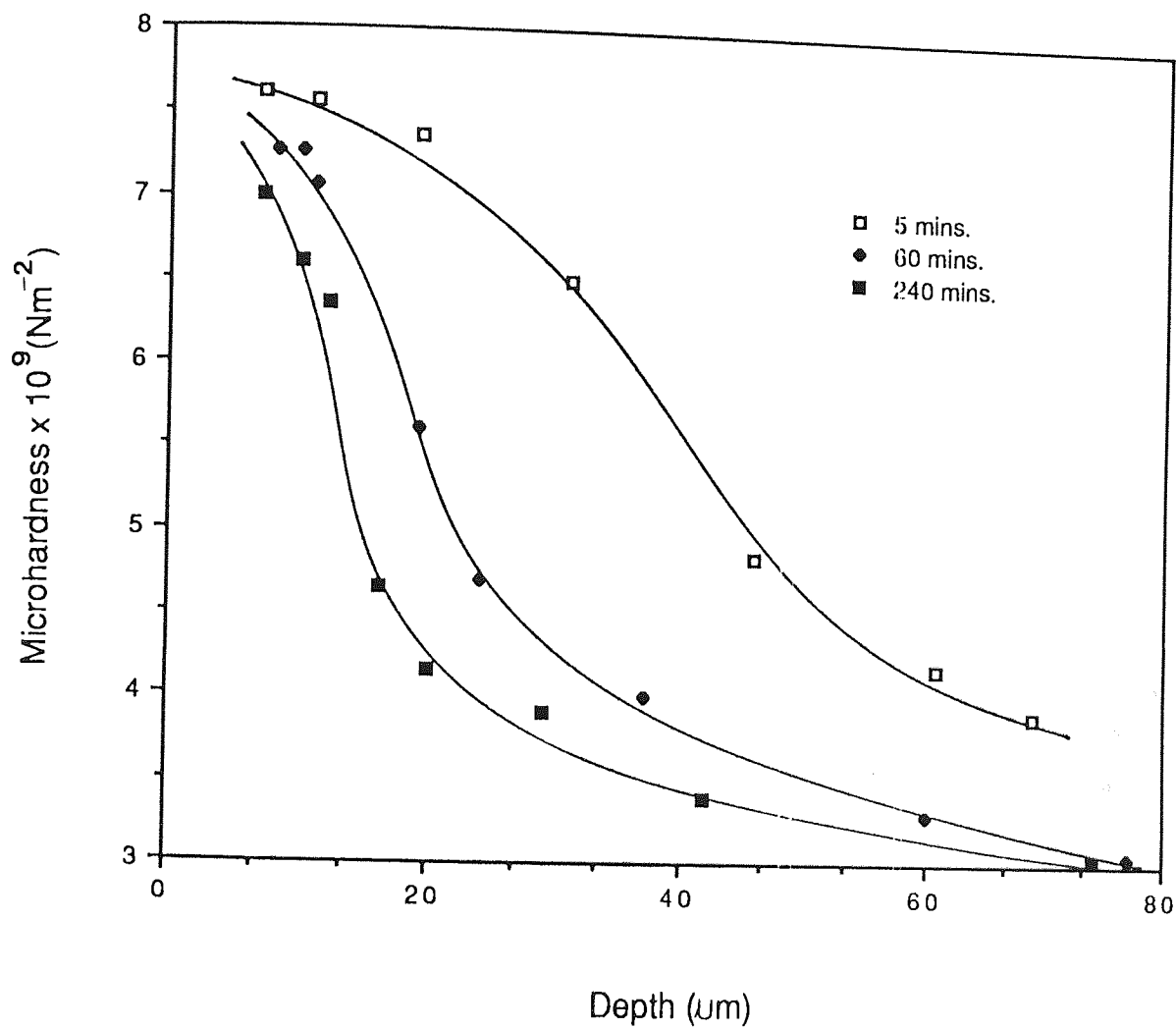
Figure 3.34   Microhardness versus depth curves for

40.5 N experiments at 1.2 ms^{-1}.
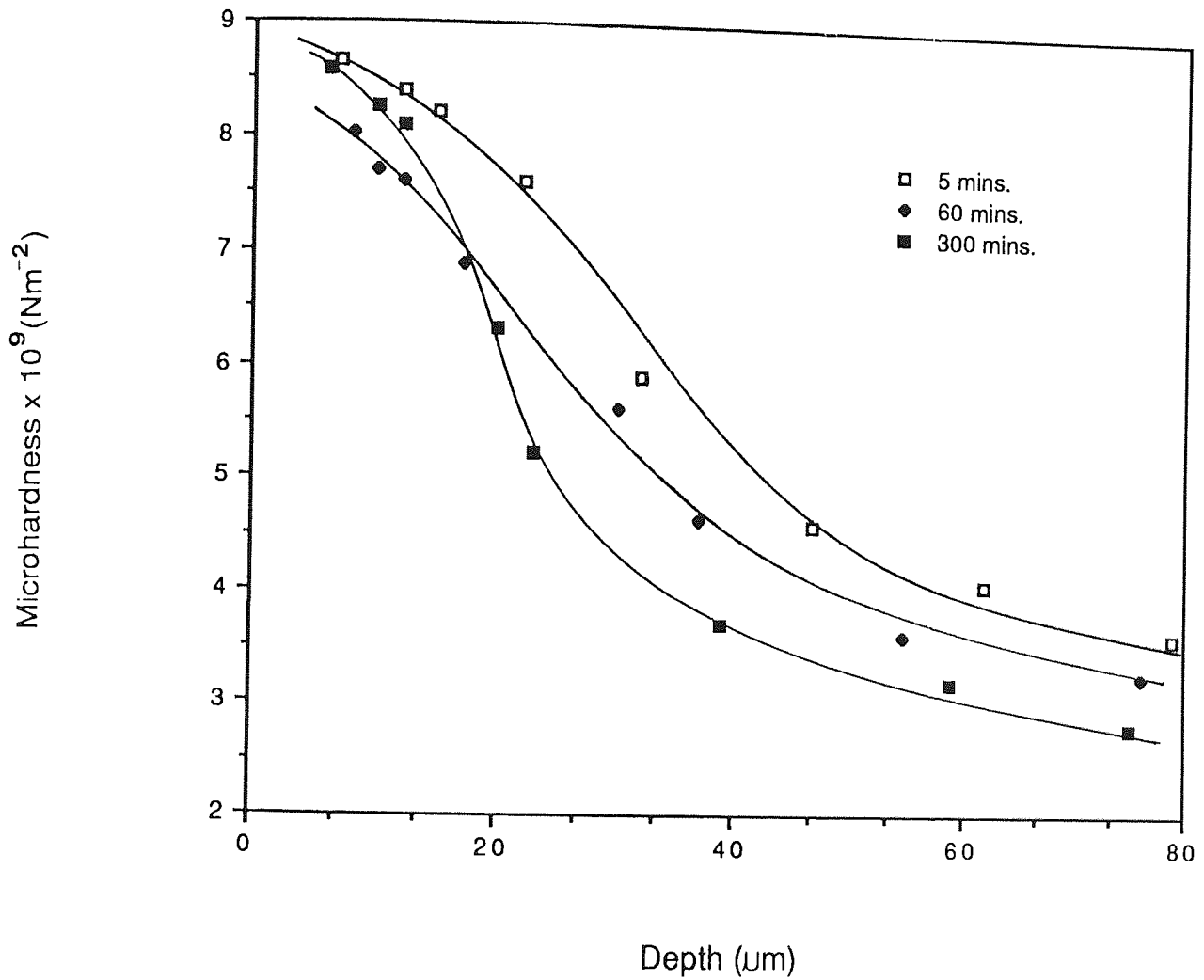
Figure 3.35   Microhardness versus depth curves for

68.1 N experiments at 1.2 ms⁻¹.
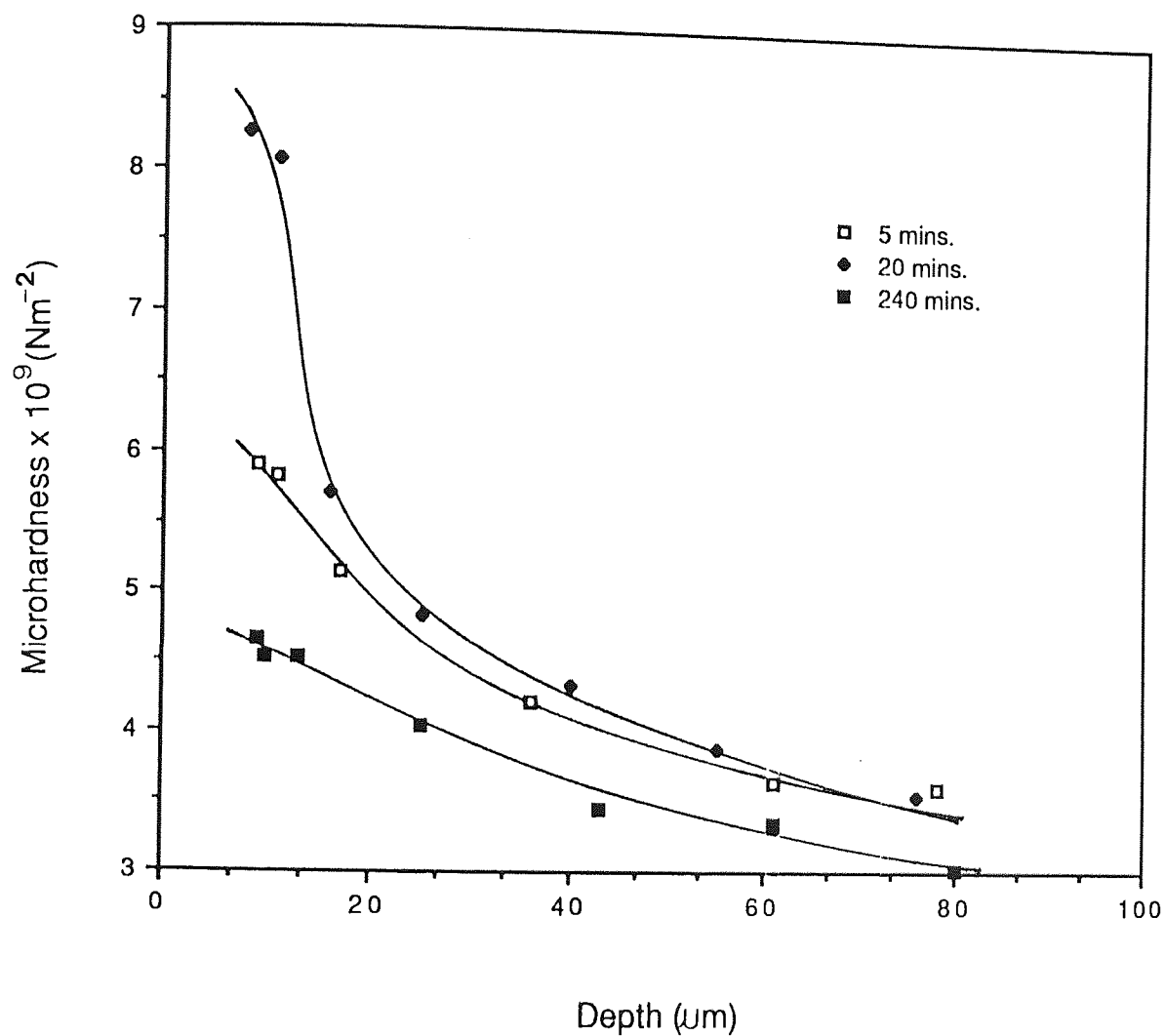
Figure 3.36   Microhardness versus depth curves for
131.5 N experiments at 1.2 ms⁻¹.

surface under 40.5 N, 68.1 N and 131.5 N. The overall
hardness of the surface under 13.8 N load was low and varied
only slightly with the depth.

3.8 Scanning electron microscopy

A selection of scanning electron micrographs of worn
specimens is presented in this section. The various
micographs produced can be divided into three categories; i)
general features of the surface, ii) Oxide plateaux and edges
and iii) subsurface observation.

3.8.1 General features of the surface

General features of the surfaces taken from T_2 wear
transition experiments at 1.2 ms^{-1} speed are shown in figure
3.37. Figure 3.37(a) represents micrograph of the pin after
60 minutes (see test 14 of table 3.8) of the running-in
severe wear periods; it had a metallic surface without any
oxide plateaux. On the transition specimens, particles of
oxide were scattered all over the pin surface (see figure
3.37(b)), while increased amounts of this oxide were observed
on the disc surface (see figure 3.37(c)), and in some area a
pile of oxide particles was found parallel to the direction
of sliding. There is also evidence of oxide plateaux in
these micrographs.

The micrographs shown in figure 3.38 were taken from

worn pin surfaces from the 1.2 ms^{-1} running-in mild wear experiments. In this figure different running durations were selected to indicate the distribution of oxide on the surfaces. Figure 3.38(a) shows the topography of pin surface at a load of 13.8 N after being run for 60 minutes; the surface consisted of oxide patches and tiny wear scars. Some fraction of oxide plateaux was clearly observed after a duration of 120 minutes, as revealed in a micrograph shown in figure 3.39(a); at longer durations of 240 minutes, the surface appeared rough and covered with thin oxide plateaux.

The surface from 40.5 N load and 20 minutes run (see figure 3.38(b)) was observed to consist of small particles of oxide, scattered over a smooth surface, probably an oxide layer. When sliding time increased to 120 and 240 minutes oxide plateaux appeared (see figure 3.39(b)), and the surface became smooth. The situation was rather different in the case of 68.1 N load where the oxide existed sparsely on the surface for the 60 minutes (figure 3.38(c)) and 300 minutes (figure 3.39(a)) durations. Shown in figure 3.38(d) is a micrograph taken from worn surface from a 131.5 load of 60 minutes run. As can be seen the surface was smooth and covered fully with thick oxide plateaux, which had started to become detached from the surface.

Figure 3.37 Topography of the worn specimens during severe

to mild wear transition at T_2.

Experimental conditions: sliding speed 1.2 ms^{-1},
transition load 11.8 N on (a) PIN after 60 mins.
of running and (b) PIN and (c) DISC, both after
90 mins. of running at the onset of mild wear.

Figure 3.38 Topography of the worn pins during running-in

mild wear.

Experimental conditions: sliding speed 1.2 ms^{-1},
loads and running durations of a) 13.8 N, 60
mins.; b) 40.5 N, 20 mins.; c) 68.1 N, 60 mins.
and d) 131.5 N, 60 mins.
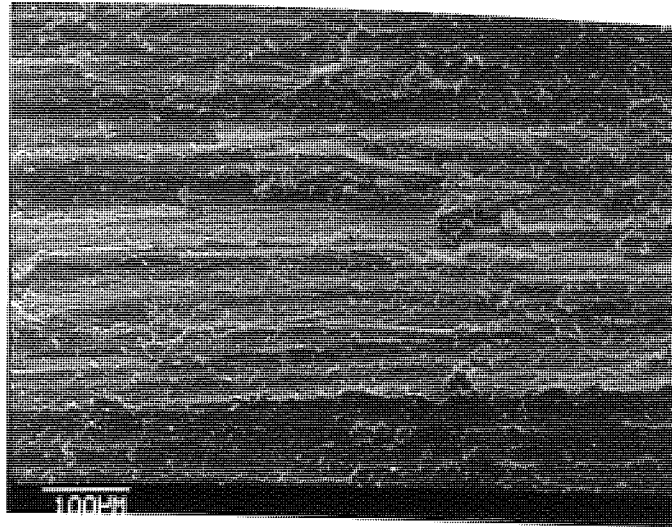
a
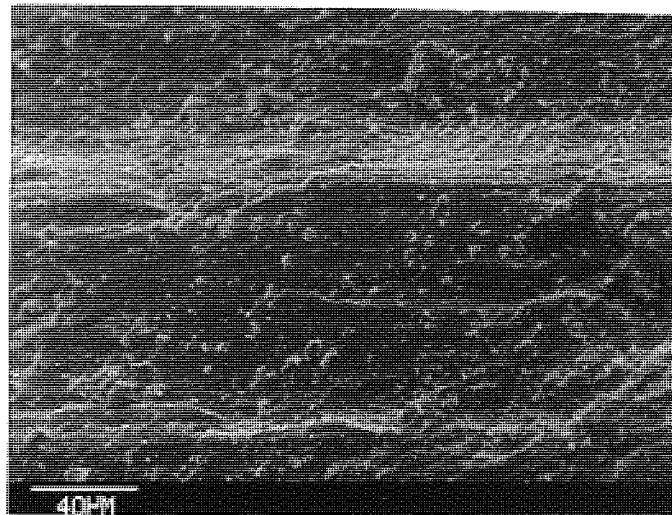
b
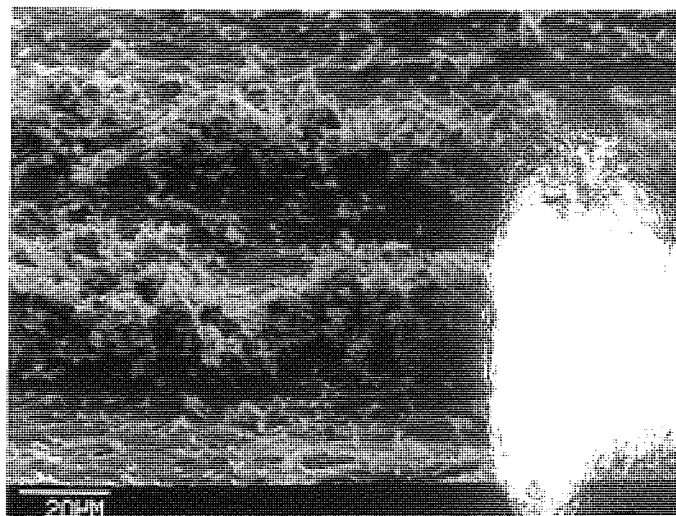
c

Figure 3.37
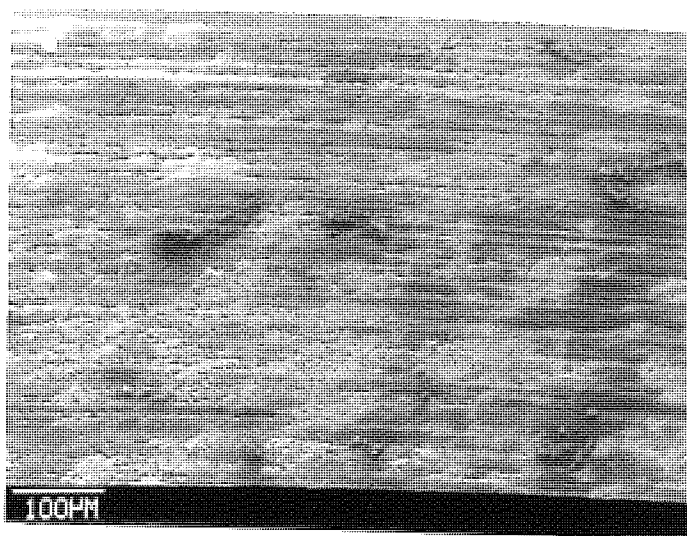
a
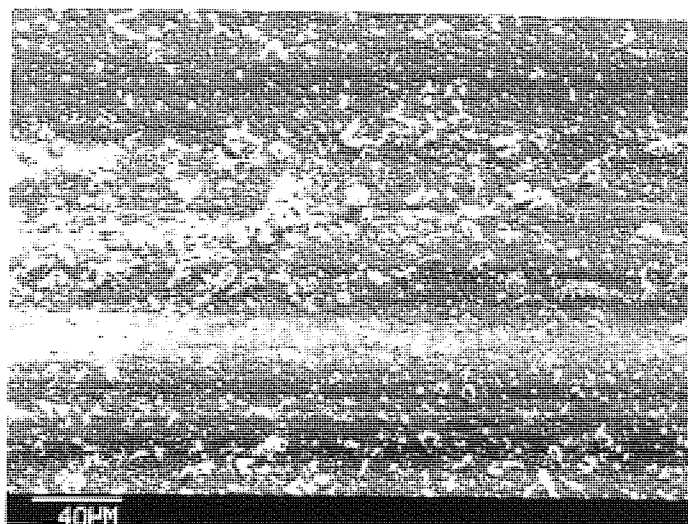
b
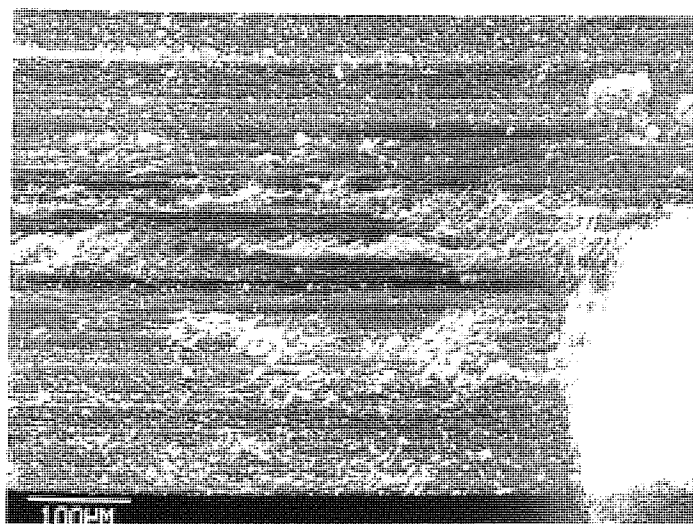
c
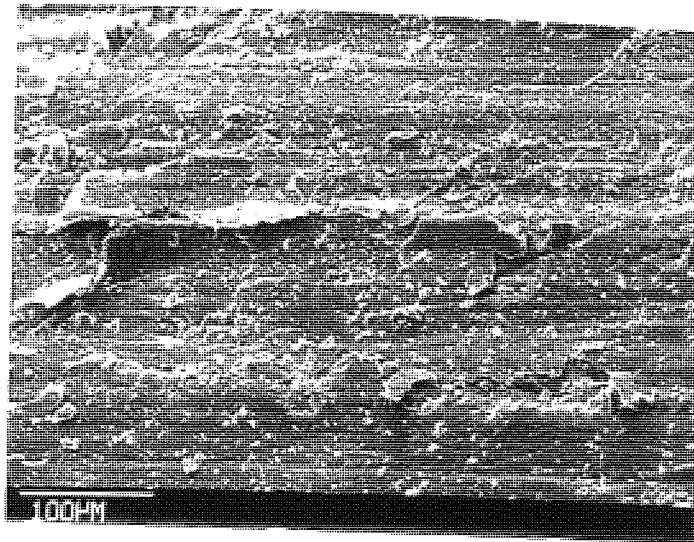
d

Figure 3.38

3.8.2 Oxide film thickness

Oxide edges were examined to give a measure of oxide film thicknesses. This was achieved at a specimen tilt angle of between 50 to 60° towards the electron beam. A selection of some typical oxide edges found on worn specimen surfaces from the Welsh wear pattern experiments and running-in mild wear experiments are given in figure 3.39.

Most micrographs were obtained from long duration experiments specimens above 200 minutes. It was very difficult to obtain oxide edges for shorter test runs because the oxide was present on the surface as loose particles and no substantial plateaux had developed. For tests with a 131.5 N load, oxide plateaux (5 - 6 μm) were observed on the pin surface after just 60 minutes (see figure 3.39(c)), while for test with a 40.5 N load this observation was made after 120 minutes (see figure 3.39(b)). Table 3.17 lists results of the average film thickness based upon eight different measurements from two pins and one disc specimens.

3.8.3 Subsurface observation

Micrographs of taper section of the worn pins are shown in figure 3.40 to figure 3.43. These show the variation of subsurface microstructure in the severe and mild wear regions with running duration and load. Three distinct layers can be observed in the micrographs; firstly, dark unetched regions

Figure 3.39(a) Typical oxide edges in region 1 and 3 of mild wear.

Experimental conditions: sliding speed 1.2 ms^{-1}, loads and running durations of i) 13.8 N, 120 mins. – region 1 and ii) 68.1 N, 300 mins. – region 3.

Figure 3.39(b) Typical oxide edges in region 2 of mild wear.

Experimental conditions: sliding speed 1.2 ms^{-1}, load 40.5 N and running durations of i) 360 mins. on DISC, ii) 120 mins. and iii) 360 mins. both on PIN surfaces.

Figure 3.39(c) Typical oxide edges in region 4 of mild wear.

Experimental conditions: sliding speed 1.2 ms^{-1}, load 131.5 N and running durations of i) 240 mins. on DISC, ii) 60 mins. and iii) 240 mins. both on PIN surfaces.

i

ii
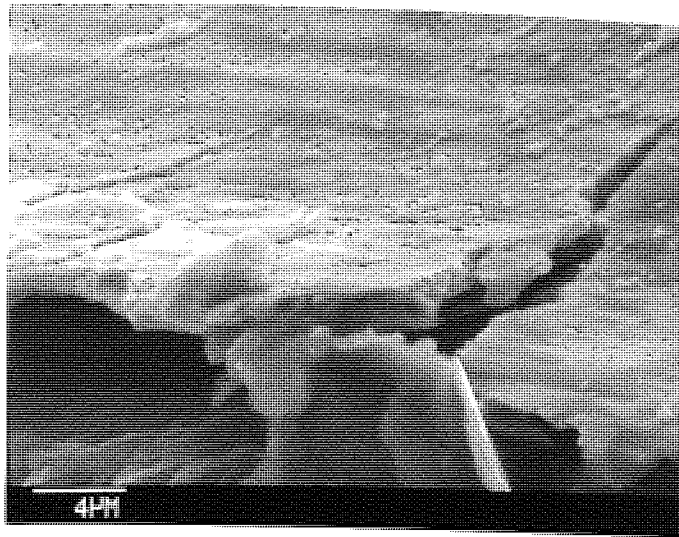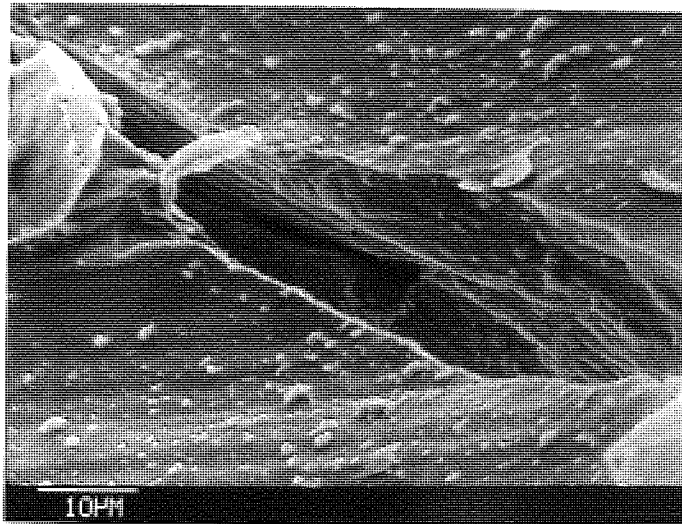
Figure 3.39
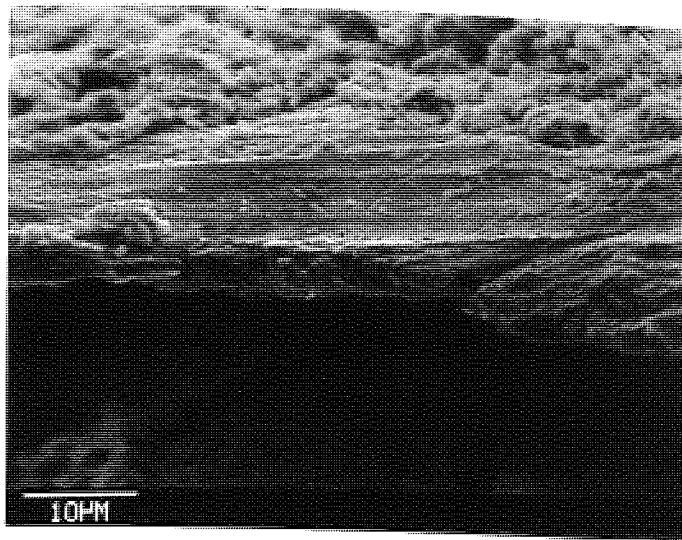
i
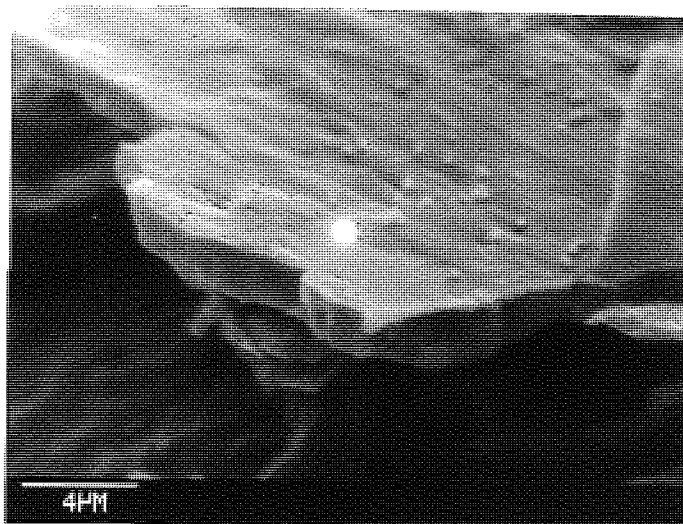
ii
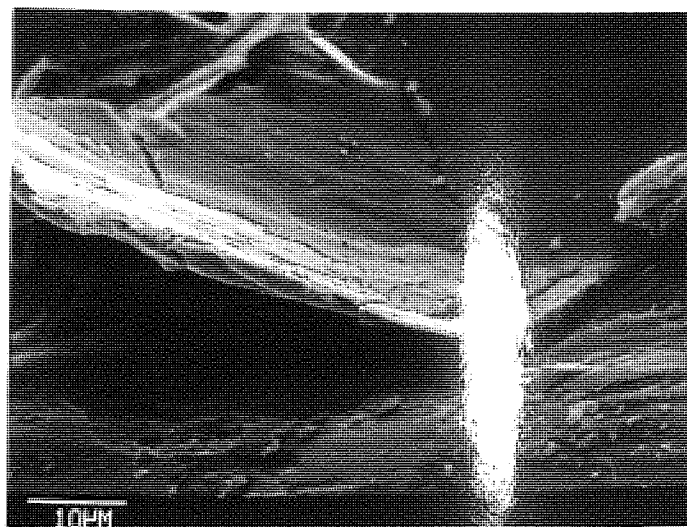
iii

Figure **3.39**b
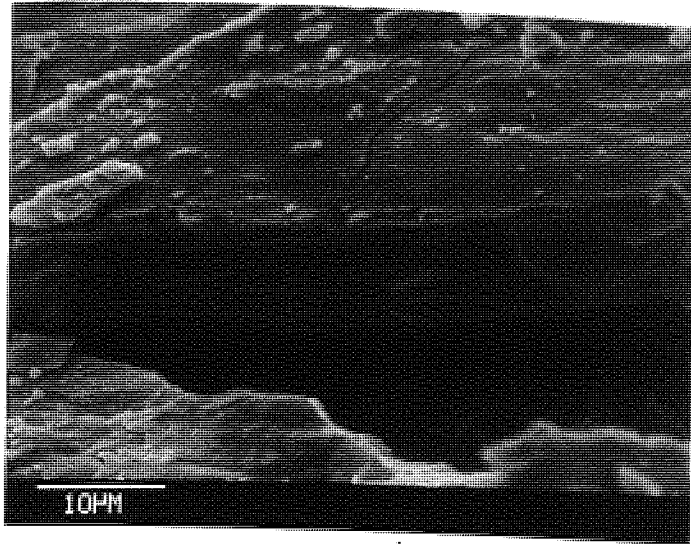
i
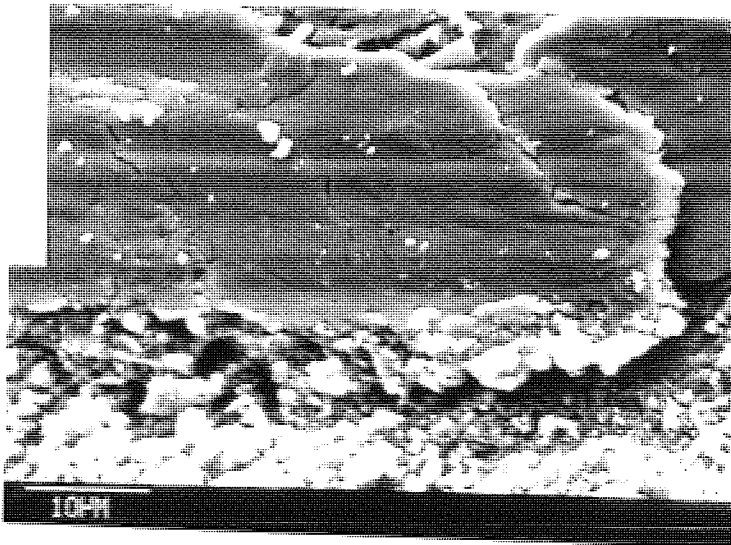
ii
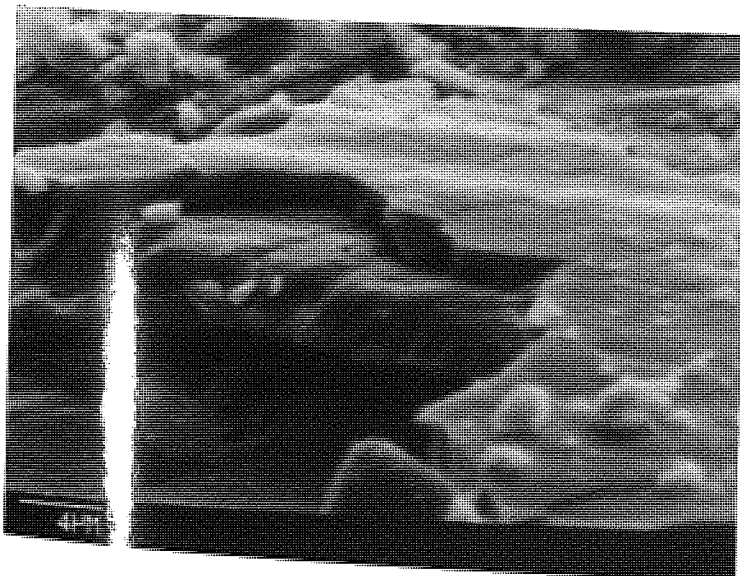
iii

Figure 3.39c

Load (N)	Sliding time (mins.)	Oxide thickness (μm)	
		PIN	DISC
13.8	20	No plateau	
	60	No plateau	
	120	1.0 ± 0.5	
	240	1.2 ± 0.6	1.5 ± 0.8
40.5	20	No plateau	
	60	No plateau	
	120	1.5 ± 0.7	
	360	1.9 ± 0.6	2.4 ± 0.7
68.1	5		
	20		
	120	Scattered oxide particles	
	300		
131.5	20	No plateau	
	60	5.0 ± 0.8	
	120	4.5 ± 0.6	
	240	4.2 ± 0.9	6 ± 2

Table 3.17   Oxide film thicknesses from various running-
in mild wear tests at 1.2 ms^{-1}.

lying topmost on the surface is thought to be oxide films formed during wear, secondly, white hardening layers formed with or without the presence of dark oxide layers and finally, the etched regions of specimens material of white spotted appearance.

Figure 3.40 shows three taper sections of the 13.8 N worn pins in which the irregular hardened layers observed in the severe wear region (see figure 3.40(a)) are distinguished from the uniform layers found in two successive periods of mild wear region (figure 3.40(b) and (c)). Such hardened layers were measured to be between 3 to 5 μm in thickness. For comparison the micrographs of the runing-in severe wear (T_2 transition test) were very similar to those shown in figure 3.40(a). The surface layers in figure 3.41 consisted of thick white hardening layer (10 - 15 μm), with evidence of intense plastic flow of the subsurface material in the rubbing direction, and in one condition (60 minutes run) a thin oxide layer was found on the surface. These were probably caused by the wear under increased load of 40.5 N. A more serious case of hardening was observed on the pin surface with 68.1 N load (see figure 3.42) where a white layer of 40 μm thick was observed in a typical 20 minutes run (figure 3.40(b)). This was, however reduced with further running duration. The dark layer, probably oxide, as observed in the micrographs, increased in thickness with running duration. Its presence seemed to contradict the

Figure 3.40   Micrographs of 13.8 N pin taper section.

Experimental conditions: sliding speed 1.2 ms^{-1} and running durations of a) 5 mins., b) 20 mins. and c) 240 mins.

Figure 3.41   Micrographs of 40.5 N pin taper section.

Experimental conditions: sliding speed 1.2 ms^{-1} and running durations of a) 20 mins., b) 120 mins. and c) 360 mins.

Figure 3.42   Micrographs of 68.1 N pin taper section.

Experimental conditions: sliding speed 1.2 ms^{-1} and running durations of a) 20 mins., b) 120 mins. and c) 240 mins.

Figure 3.43   Micrographs of 131.5 N pin taper section.

Experimental conditions: sliding speed 1.2 ms^{-1} and running durations of a) 5 mins., b) 20 mins. and c) 240 mins.
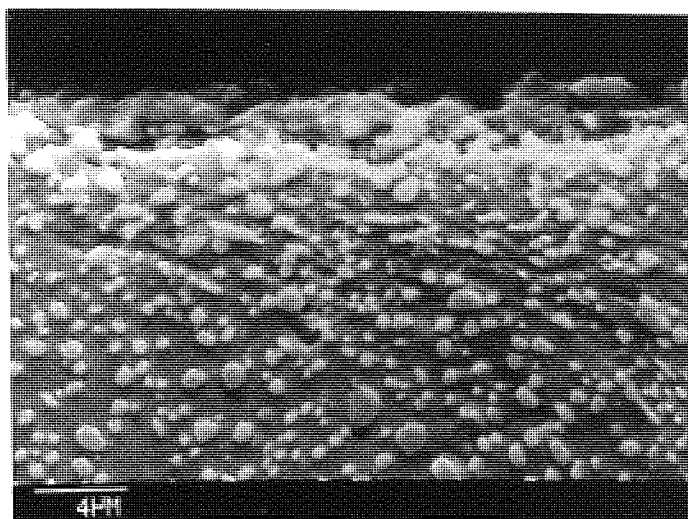
a
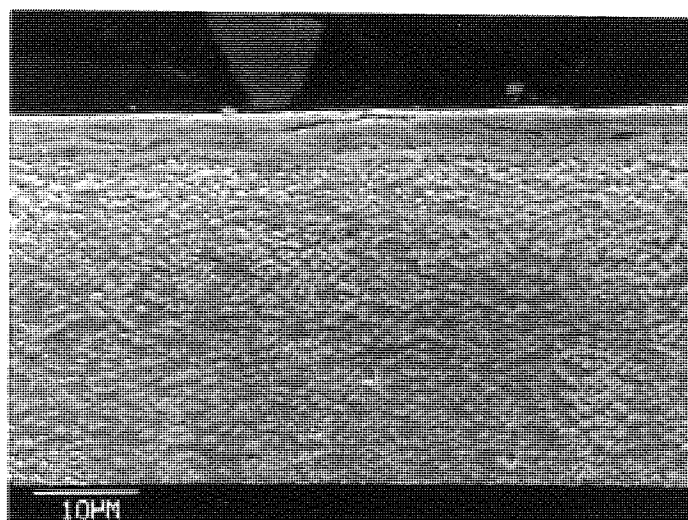
b
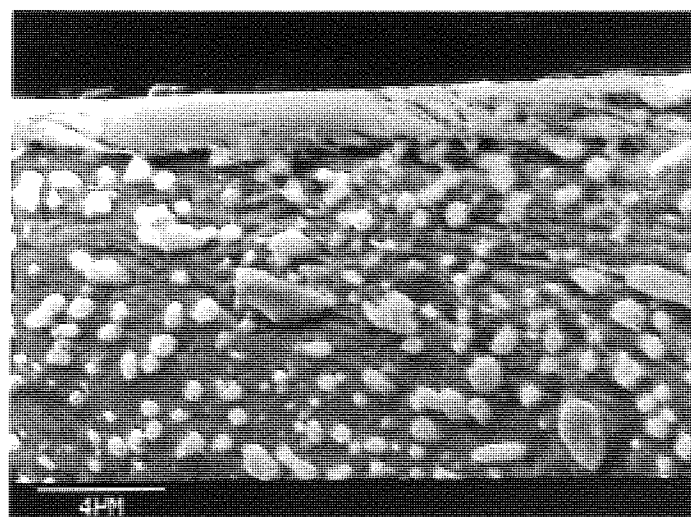
c

Figure **3.40**

a

b

c

Figure **3.41**

a

b
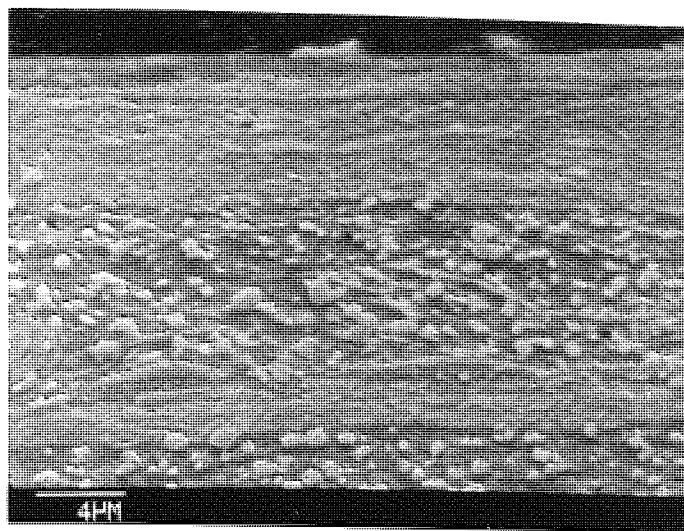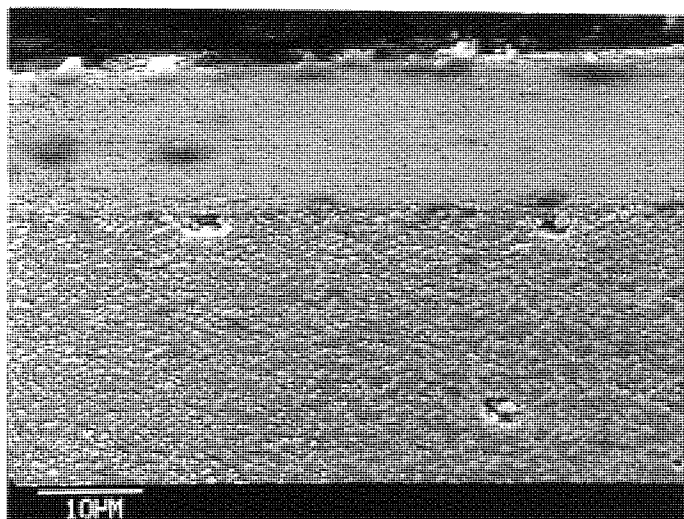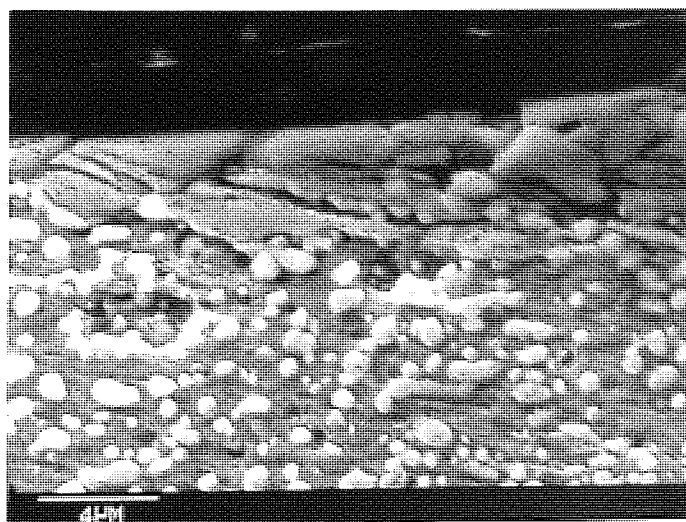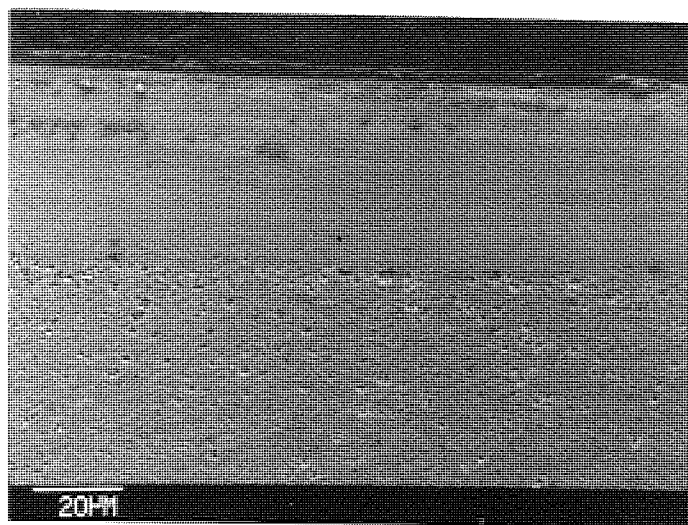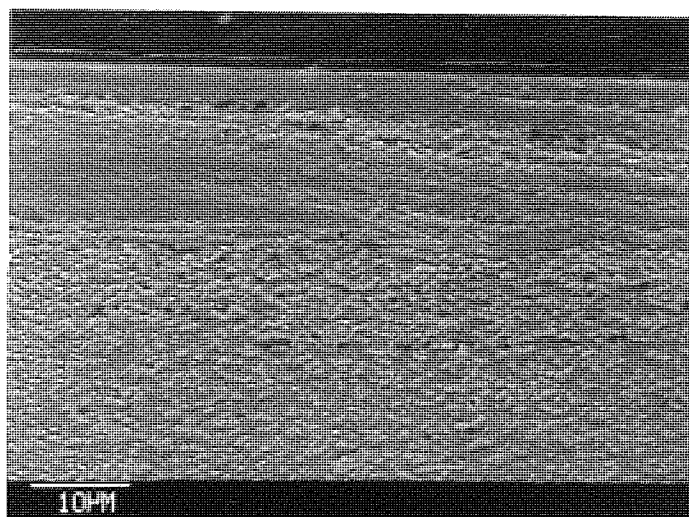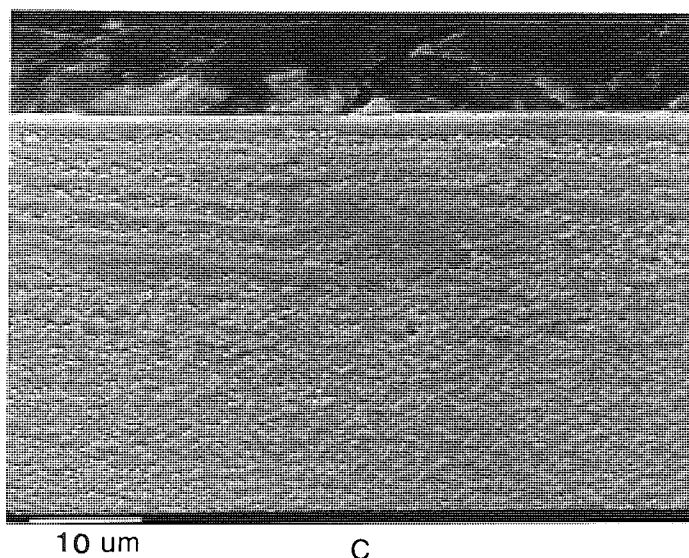
10 um   c
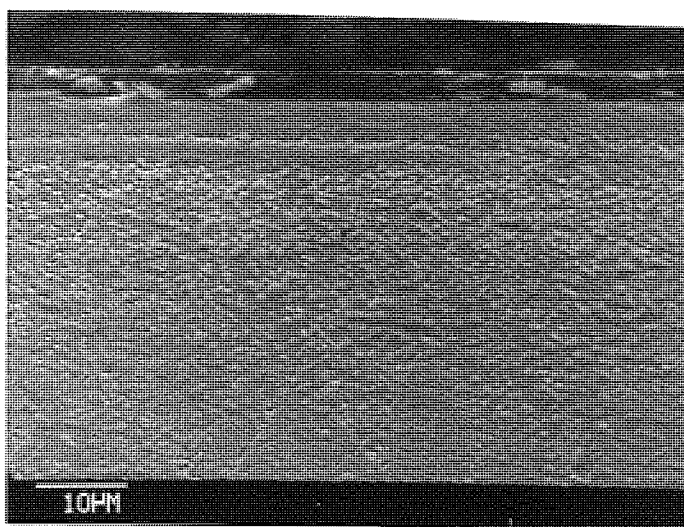
Figure **3.42**

a

b

c

Figure **3.43**

observation shown in figure 3.38(d). The micrograph for 131.5 N pins, shown in figure 3.40, consisted of thin dark layer and white hardening layer of about 10 µm thick for all the runs.

The different ways in which the hardening layer can vary during the course of mild wear are shown in figure 3.44.

3.9 Auger spectroscopy

In Auger analysis, Auger spectra were recorded between successive periods of argon ion bombardment and the resulting calculated composition profiles were used to determine the relative concentration (percentage) of oxygen and iron present with depth into the surface layer. The Auger analyses were repeated every 50 minutes to 100 minutes, and the results are given in graphical form in figure 3.45, 3.46 and figure 3.47. These show that the time required to remove oxide film present on a pin surface was dependent both on the duration of running and load.

For 13.8 N pins from the 20 and 60 minutes runs (see figure 3.45) oxygen concentration falls very rapidly within 50 minutes etching, while for the pin from 240 minutes run similar reduction occurred only after 300 minutes etching. Similar variations are shown in figure 3.46 for the 40.5 N pins, that is a rapid fall for the short duration pin (20 minutes) and steady decrease in oxygen concentration for the
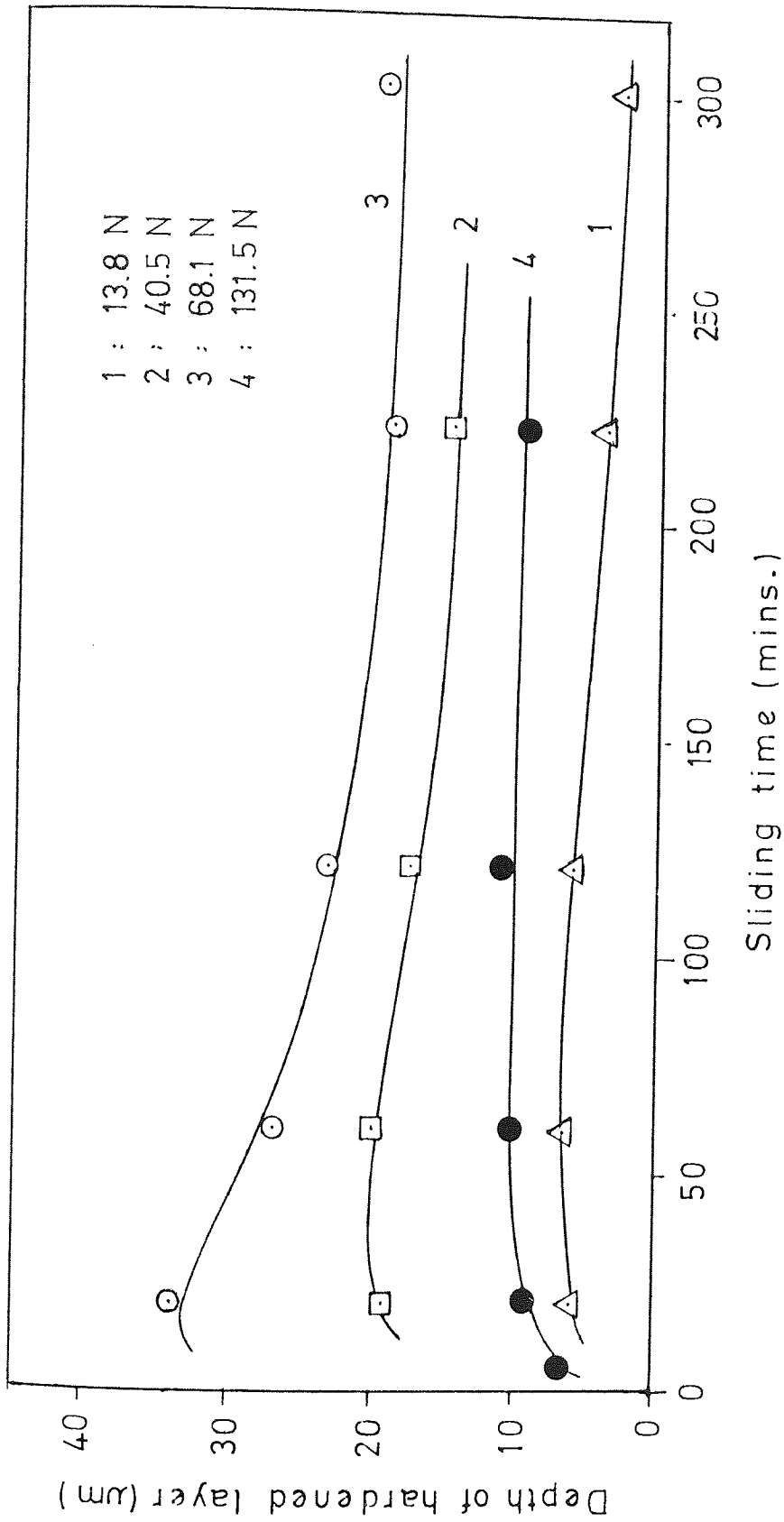
Figure 3.44 Depth of hardened layer versus sliding time
on the worn pins for running-in mild wear
experiments at 1.2 ms^{-1}.

long duration pins (120 and 240 minutes). In the latter case
the etching times were about 170 minutes and 800 minutes
respectively. All the above mentioned features showed that
oxide plateaux were absent during the initial period of mild
wear and only present after sufficient long durations of
running or perhaps that plateaux thickness increases with
running time.

For 68.1 N load the test carried out on three pins of
different running durations gave identical results, typically
shown in figure 3.47(a). These show that there is very
little oxide on these surfaces. On the other hand, the
result for the 131.5 N load, based on long duration pin,
showed that 1600 minutes etching was needed to remove
oxide layer from the pin surface (see figure 3.47(b)),
indicating a thick well established oxide.
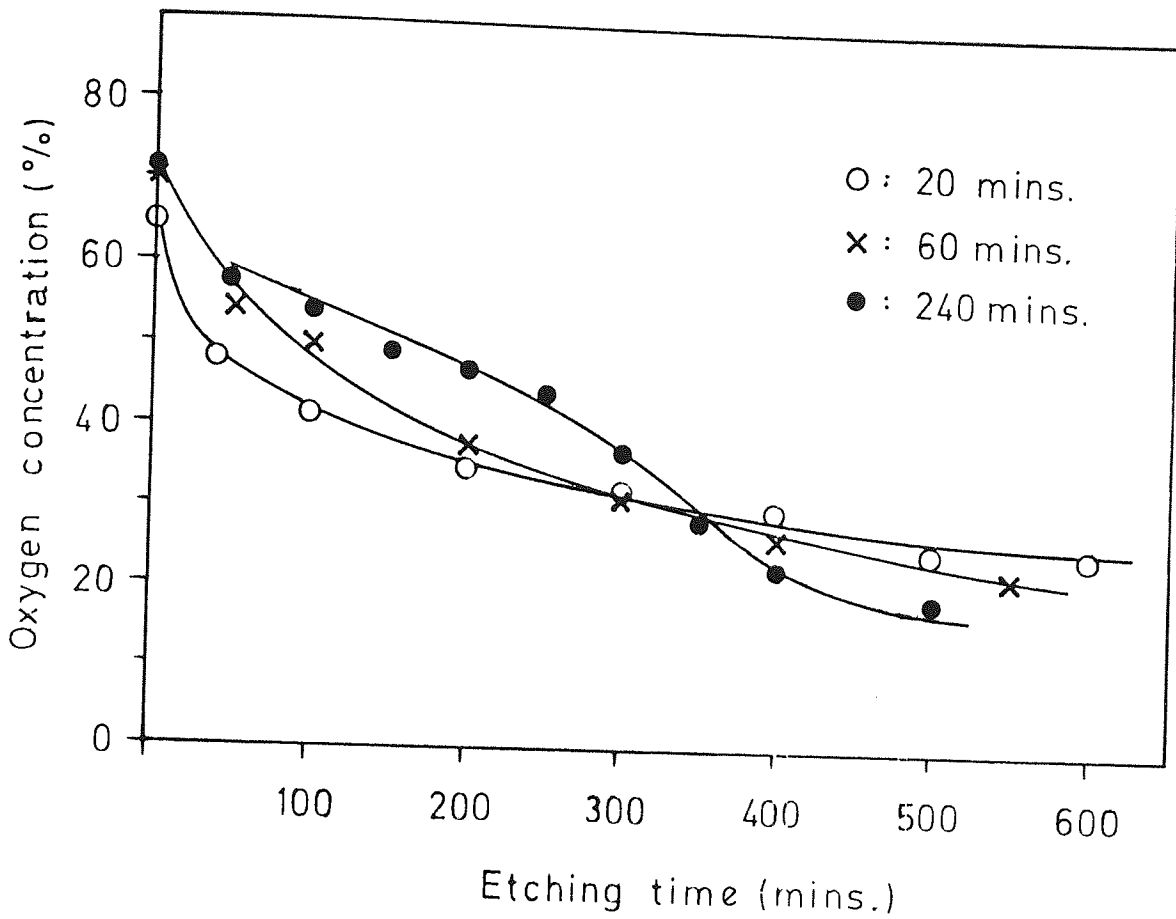
Figure 3.45 Variation of oxygen concentration with
etching time on the pin surfaces (speed
= 1.2 ms⁻¹, load = 13.8 N).
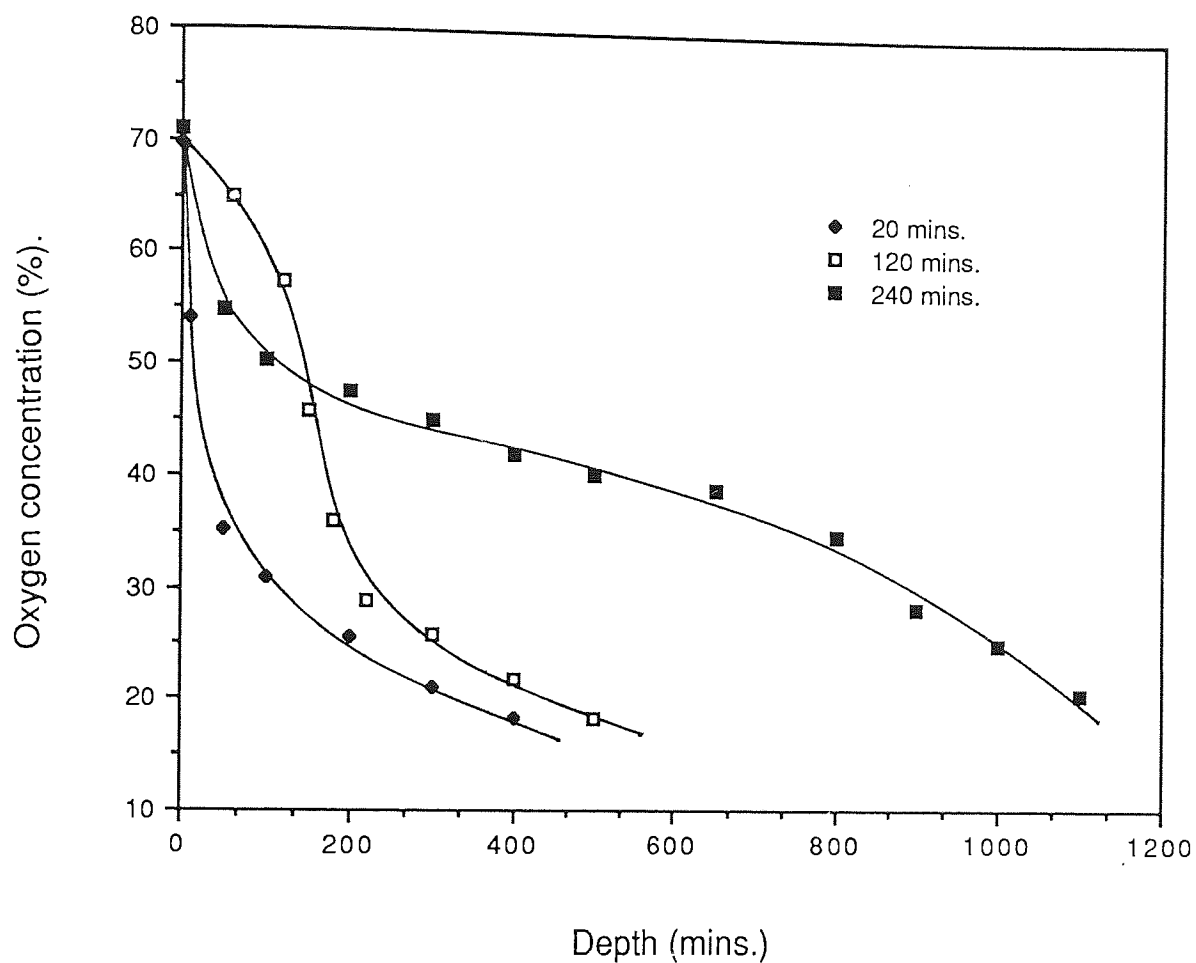
Figure 3.46   Variation of oxygen concentration with etching time on the pin surfaces (speed = 1.2 ms^{-1}, load = 40.5 N).
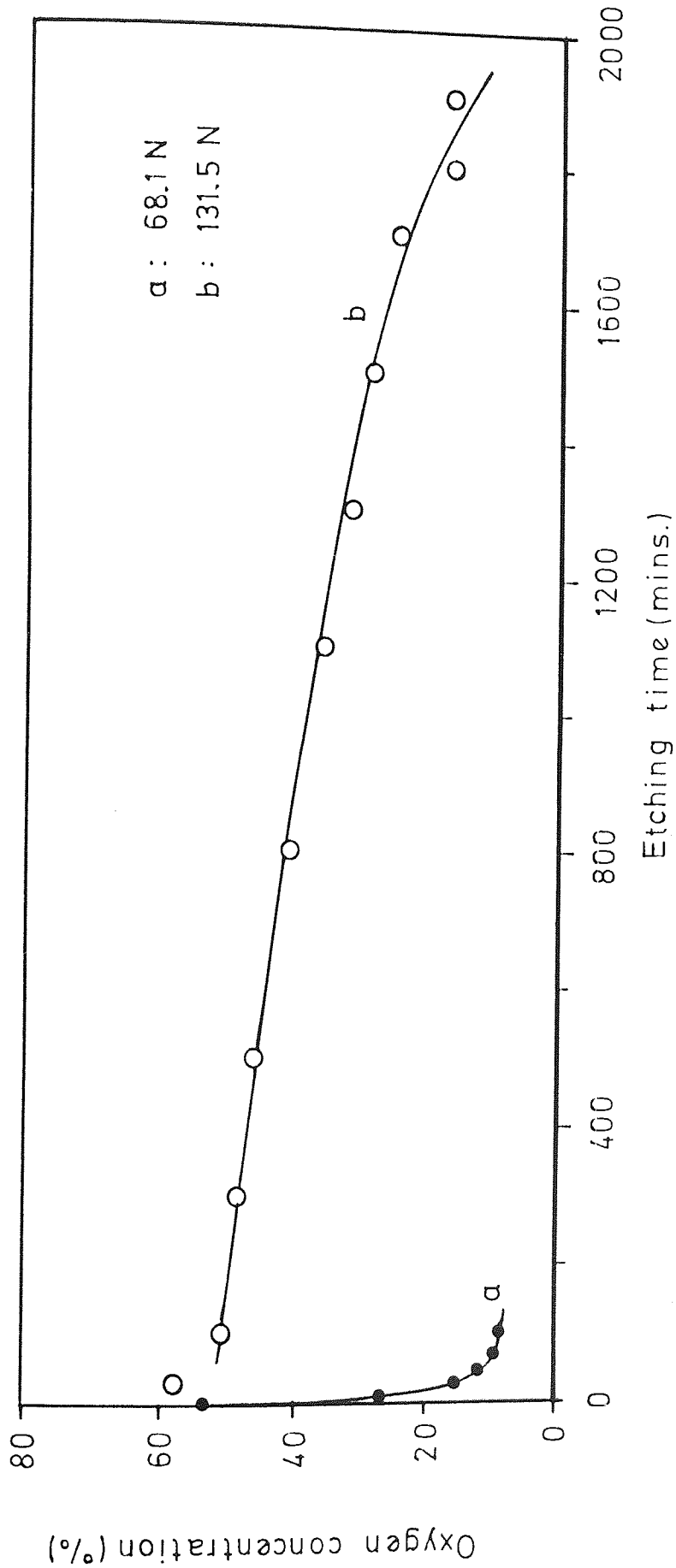
Figure 3.47 Variation of oxygen concentration with etching time on the pin surfaces (speed =1.2 ms⁻¹, loads = 68.1 N and 131.5 N).

CHAPTER 4

THEORETICAL CONSIDERATIONS

4.1 Introduction

In this chapter a theoretical analysis is presented in section 4.2 in order to deduce values of surface parameters under the condition of equilibrium mild wear. The model, therefore, is most relevant to the wear pattern results where different trends of mild wear were shown to exist in the previous chapter; this can give possible clues for the mechanisms responsible for wear.

Section 4.3 will deal with a theoretical prediction of the wear volume of the running-in severe wear prior to mild wear transition. A modification to the theory is made to take account of oxidation by unidirectional sliding of a horizontal pin on vertical disc system.

4.2 Surface model

The energy required to overcome the friction of a sliding contact between two surfaces is released in the form of heat which results in an increase in temperature. Deformation at the tip of asperity contacts leads to a sudden rise in temperature at a localized contact region. This is known as *flash temperature*. The heat generated is then

dissipated into the bulk of the substrate to produce a rise in general surface temperature. Flash temperatures occur only over a small region for a very short duration, and therefore, direct measurement is impossible. A surface model is needed to determine the magnitude of such temperature, since it has a significant role in controlling the oxidation of sliding surfaces.

Block (101,102) may have been the first to realize the importance of temperature in sliding situations when he estimated the *scoring* temperature of a designed gear testing machine under lubricated conditions. He postulated that the maximum conjunction temperature is a summation of the maximum possible temperature and the bulk temperature. Although the treatment involves relatively complicated mathematics, it formed the basis of treatments by Jaeger (103), who carried out lengthy theoretical calculations and Holm (104), who generalized the theory and formulated a simple expression for flash temperature. Archard (9), following this work, distinguished slow moving heat sources from a stationary heat sources, and incoporate several sliding variables to form a theory which predicted temperature rise in the wear of steels, generally of high values up to 1200°C. Quinn (95) used a method originally developed by Grosberg and Molgaard (106) which deduced surface temperature from measurements of heat flow along the sliding specimen away from the interface. The flash temperature was modified from an approach by

Archard, and this was combined with surface temperature in order to obtain an expression for contact temperature. The theoretical analysis below is based on Quinn's surface model.

Consider a pin-on-disc geometry in which the pin surface is supposed to consist of N asperities in contact with a uniform oxide film thickness, ζ_p. The total real area of contact, i.e. $N\pi a^2$ is equal to the expression given in equation (1.1). Hence, the number of asperities can be written as

$$N = \frac{W}{\pi a^2 \, P_m} \qquad \dotfill (4.1)$$

where W is the applied load and P_m is the hardness of the underlying surface (disc). As for the pin, the temperature rise is deduced from the assumption that, all the heat evolved, H_1 (Js^{-1}), goes into the pin and oxide film; this gives the expression of the average contact temperature above the surface temperature, T_s (18,19,20) as

$$T_c \ (pin) \ = \ T_s \ + \ \frac{H_1}{4\pi a \, N \, K_s} \ + \ \frac{H_1 \, \zeta_p}{\pi a^2 \, N \, K_o} \qquad \dotfill (4.2)$$

where K_s and K_o are the thermal conductivities of the steel material and oxide respectively.

For the disc it has been shown that (107), oxide plateaux of uniform thickness ζ_d, are formed on the disc

surface, and this is confirmed by the micrographs shown in figures 3.39(a) and 3.39(b). If the total heat generated at the interface is H_T and assuming the heat flow rate, $H_T - H_1$ (Js^{-1}), goes into the disc, then the average contact temperature above the disc bulk temperature, T_d is

$$T_c \text{ (disc)} = T_d + \frac{\gamma(H_T - H_1)}{4 \pi a N K_s} + \frac{\gamma(H_T - H_1) \zeta_d}{\pi a^2 N K_D} \quad \dots (4.3)$$

where H_T is the product between speed and frictional force, γ is the sliding constant which varies with a dimensionless parameter, L, i.e.

$$L = \frac{Ua}{2 X_s} = \frac{Ua \rho_s C_s}{2 K_s} \quad \dots (4.4)$$

X_s is the thermal diffusivity of steel, comprising of the density, ρ_s, the specific heat, C_s and thermal conductivity, K_s. was assumed to take either of the following values.

a) $\gamma = 1$ if $L < 0.1$ (for low speeds).

b) $\gamma = 0.8605 - 0.1021L$ if $0.1 < L < 5$ (for medium and high speeds).

c) $\gamma = 0.85L^{-1/2}$ if $L > 5$ (for very high speeds).

For the range of speeds between 0.6 to 1.6 ms^{-1} used in the experiments, the calculated values of L varies from

2.18 x 10^4 a   to   5.82 x 10^4 a

If a is assumed to be greater than 5 μm the dimensionless

parameter, L, was between 0.1 and 5, and therefore the value

of V chosen for the calculation was

$$V = 0.8605 - 0.1021 \frac{Ua}{2 X_o} \qquad \dots\dots\dots\dots (4.5)$$

The thermal diffusivity of the oxide, X_o included in equation

(4.5) in place of X_s, since oxide films was found to be

present on the disc surface.   Hence

$$X_o = \frac{K_o}{\rho_o C_o} \qquad \dots\dots\dots\dots (4.6)$$

where K_o, ρ_o and C_o are the relevant parameters associated

with the oxide, and which represents thermal conductivity,

density and specific heat, respectively.

By substituting equations (4.1) and (4.5) into equations

(4.2) and (4.3), and equating both contact temperatures for

the pin and the disc, then a quadratic equation of the form

$Aa^2 + Ba + C = 0$ is obtained by collecting variables in the

asperity radius, a.   The solution can be written as

$$a = \frac{-B \pm (B^2 - 4AC)^{1/2}}{2A} \qquad \dots\dots\dots\dots (4.7a)$$

where

$$A = \frac{0.1021U \, \pi P_m \, (H_T - H_1)}{8 \, W \, K_s \, X_o} \qquad \cdots\cdots\cdots (4.7b)$$

$$B = \frac{\pi P_m \, H_1}{4 \, W \, K_s} - \frac{0.8605 \, \pi P_m \, (H_T - H_1)}{4 \, W \, K_s}$$

$$+ \frac{0.1021U \, P_m \, \zeta_{cl} \, (H_T - H_1)}{4 \, W \, K_s} \qquad \cdots\cdots\cdots (4.7c)$$

$$C = \frac{H_1 \, P_m \, \zeta_F}{W \, K_o} - \frac{0.8605 \, P_m \, \zeta_{cl} \, (H_T - H_1)}{W \, K_o}$$

$$+ \, (T_s - T_{cl}) \qquad \cdots\cdots\cdots (4.7d)$$

Equation (4.7a) gives two solutions of asperity radius if the
inserted parameters result in values where $B^2 - 4AC > 0$.
Each of the K_s, K_o and P_m are dependent on the surface
temperature, and X_o on the contact temperature.

Athwal (50) has measured the hardneness, P_m (for both EN
31 and EN 8 steels) and the conductivity, K_s (for EN 8 steel)
as a function of temperatures. Molgaard and Sweltzer (108)
have shown that the conductivity of the spinel, $\alpha\text{-}Fe_2O_3$ and
wùstite, Fe_3O_4 are given by the following relationship

$$K_o \, (Fe_2O_3) = 0.0839 - 6.63 \times 10^{-3} \, T \quad \cdots\cdots (4.8a)$$

$$K_o \ (Fe_3O_4) = 0.0423 - 1.37 \times 10^{-5} \ T \quad \dots\dots\dots(4.8b)$$

where T is the contact temperature in degrees Kelvin (K) and K_o is expressed in $Wm^{-1} \ K^{-1}$. In the calculation an average value of K_o for the two oxides was used, calculated from equation 4.8a 4.8b. Mean values of $\rho_o = 5210 \ Kg \ m^{-3}$ and $C_o = 756 \ Jkg^{-1}K^{-1}$ were used (106) for the calculation of χ_o in equation (4.6) and these were assumed to be independent of temperature. To a good approximation it is further assumed that the oxide film thickness, ζ_p equals to ζ_d, and the thermal conductivities of the pin and disc materials can be considered to be the same.

The theoretical value δ_{th} of the division of heat along the pin is given by

$$\delta_{th} = \frac{\theta_d}{\theta_d + \theta_p} \quad \dots\dots\dots\dots(4.9)$$

where θ_p and θ_d are the fictitious temperature excess above the general surface temperature for the pin and disc respectively. These are expressed by the following relationship

$$\theta_p = \frac{H_T}{4 \pi a \ N \ K_s} + \frac{H_T \ \zeta_p}{\pi a^2 \ N \ K_o} \quad \dots\dots\dots\dots(4.10)$$

$$\theta_{cl} = \frac{\nu H_T}{4 \pi a \ N \ K_s} + \frac{\nu H_T \ \zeta_{cl}}{\pi a^2 \ N \ K_D} \qquad \ldots\ldots\ldots\ldots(4.11)$$

4.2.1 Determination of T_c, N, a and δ_{th}

A computer program (see appendix II) was used to compute all the parameters concerned. The first part of the program deals with the heat flow analysis using the data from chart pen recorder deflections, together with their callibration factors, in order to obtain the average values of T_A, T_B, T_D, H_1, H_T, T_s and friction coefficient μ. Most of the results are given in tables 3.2, 3.3 and 3.4.

The second part of the program (from line number 3600) was concerned with an analysis for determination of a, N, T_c and δ_{th} using an iterative technique. The initial step involves calculations of X_D (equation 4.6) and K_D (equations 4.8) at the general surface temperature, T_s. These together with estimated ζ and data from heat flow results are substituted into equation (4.7a) to obtain a value for contact radius, a, and this is inserted into equations (4.1) and (4.2) to calculate the number of asperity contacts, N and contact temperature T_c respectively. In the next step of iteration new values for X_D and K_D are recalculated at this new contact temperature and the above procedure repeated to produce new sets of N and T_c, and so on. The iteration process continues in this way until T_c is comparable,

obviously less than or equal to 0.1% with each other. Both δ_{th} (equation (3.1)) and δ_{exp} (equation (4.9)) are then compared before the whole iteration procedure is repeated for a different value of oxide thickness, ξ. The best T_c (also a and N) was that obtained from the oxide film thickness, ξ which gave close agreement between the theoretical and experimental division of heat. Tables 4.1, 4.2 and 4.3 show the results of such surface parameters at the speeds of 0.8, 1.2 and 1.6 ms^{-1}.

The variation of contact temperatures with load at speeds of 0.8, 1.2 and 1.6 ms^{-1} are shown in figures 4.1(a), 4.1(b) and 4.1(c) respectively. Variation of surface temperatures with load are also shown in these figures for comparison. Contact temperatures appear to be proportional to the load in any given region but the gradients vary from one region to another.

The number of asperities, shown in figure 4.2, increases with the load and again these appear to be transition with a sharp fall at T_s transition load (for 1.2 and 1.6 ms^{-1}). For 0.8 ms^{-1} without T_s the trend is a rapid increase with load. The behaviour of asperity radius is opposite to that of the asperity number; this is shown in figure 4.3 as the reduction with load up to T_s where a sharp increase is followed by constant reduction in asperity radius (1.2 and 1.6 ms^{-1}). There is, however, a small increase between T3/T4 transitions with a 0.8 ms^{-1} speed. The calculated oxide film

Load (N)	a (µm)	N	ζ (µm)	T_c (°C)	δ_{th} (%)	δ_{exp} (%)
40.0	14.6	11	2.3	466	14.3	14.8
49.0	13.8	13	2.0	505	14.9	15.4
54.9	11.4	22	1.5	547	23.1	20.4
62.7	11.1	22	1.8	588	20.3	18.1
70.2	11.7	23	1.8	588	17.4	15.7
76.9	11.8	35	3.9	590	16.7	17.4
85.1	12.5	33	4.5	595	13.6	13.6
94.1	12.6	29	4.6	601	12.7	12.9
102.5	5.8	100	1.7	753	30.3	29.6
110.0	5.9	108	1.6	779	29.4	27.5
121.2	6.9	100	2.1	742	27.1	25.0

Table 4.1   Sets of values of a, N, ζ, T_c and δ_{th} from equilibrium mild wear experiments at 0.8 ms^{-1}.

Load (N)	a (μm)	N	ζ (μm)	T_c (°C)	δ_{th} (%)	δ_{exp} (%)
11.8	11.5	7	1.4	302	14.9	14.8
13.8	10.9	10	1.3	331	14.9	15.0
21.6	10.2	14	1.4	400	15.0	15.7
30.8	8.6	22	1.3	470	17.3	19.2
33.3	9.7	20	1.6	515	11.0	11.2
37.2	8.9	21	1.5	543	13.5	14.1
40.5	8.6	23	1.6	559	14.1	14.7
45.1	8.6	26	1.6	560	13.9	14.8
48.5	6.1	52	0.8	624	23.2	24.4
54.9	6.2	54	0.7	636	22.8	23.4
68.1	5.3	83	0.8	700	24.0	25.3
80.4	5.2	98	1.1	768	19.4	21.8
97.0	4.3	192	1.4	801	22.1	25.8
108.0	9.1	72	3.5	594	8.4	8.4
114.7	9.3	75	4.2	588	8.0	7.9
131.5	8.7	100	4.0	624	8.8	8.4
153.5	8.8	133	4.3	646	9.4	9.9

Table 4.2   Sets of values of a, N, ζ, T_c and δ_{th} from

equilibrium mild wear experiments at 1.2 ms^{-1}.

Load (N)	a (µm)	N	ζ (µm)	T_c (°C)	δ_{th} (%)	δ_{exp} (%)
2.6	10.7	3	0.8	200	7.6	8.3
9.8	9.0	10	0.8	293	13.3	13.4
16.2	8.2	16	1.2	370	12.5	13.6
20.6	6.6	30	1.4	506	16.0	16.5
25.0	6.0	38	1.0	575	17.7	16.8
35.1	4.7	69	0.8	626	21.2	23.8
44.8	2.9	192	0.8	726	27.4	31.3
50.1	3.8	126	0.9	763	22.4	23.4
56.1	5.0	131	2.1	686	17.2	17.8
80.4	6.3	113	2.6	623	10.5	11.0
127.9	6.5	146	2.4	625	9.2	8.9
154.4	6.6	164	3.3	639	6.6	6.6

Table 4.3   Sets of values of a, N, ζ, T_c and δ_{th} from equilibrium mild wear experiments at 1.6 ms^{-1}.
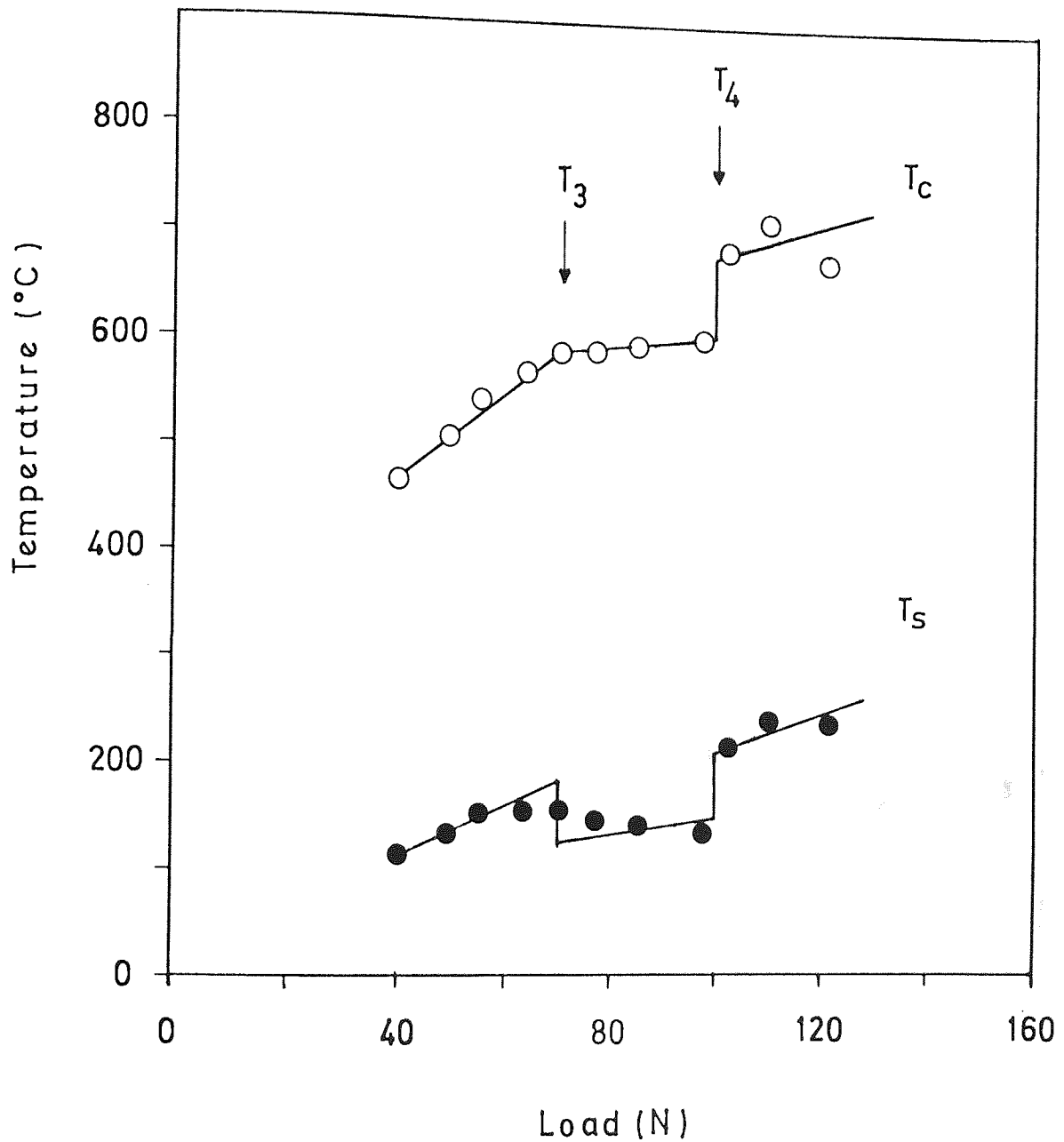
Figure 4.1(a)   Variation of contact temperature, T_c

and surface temperature, T_s with load

at 0.8 ms^{-1}.
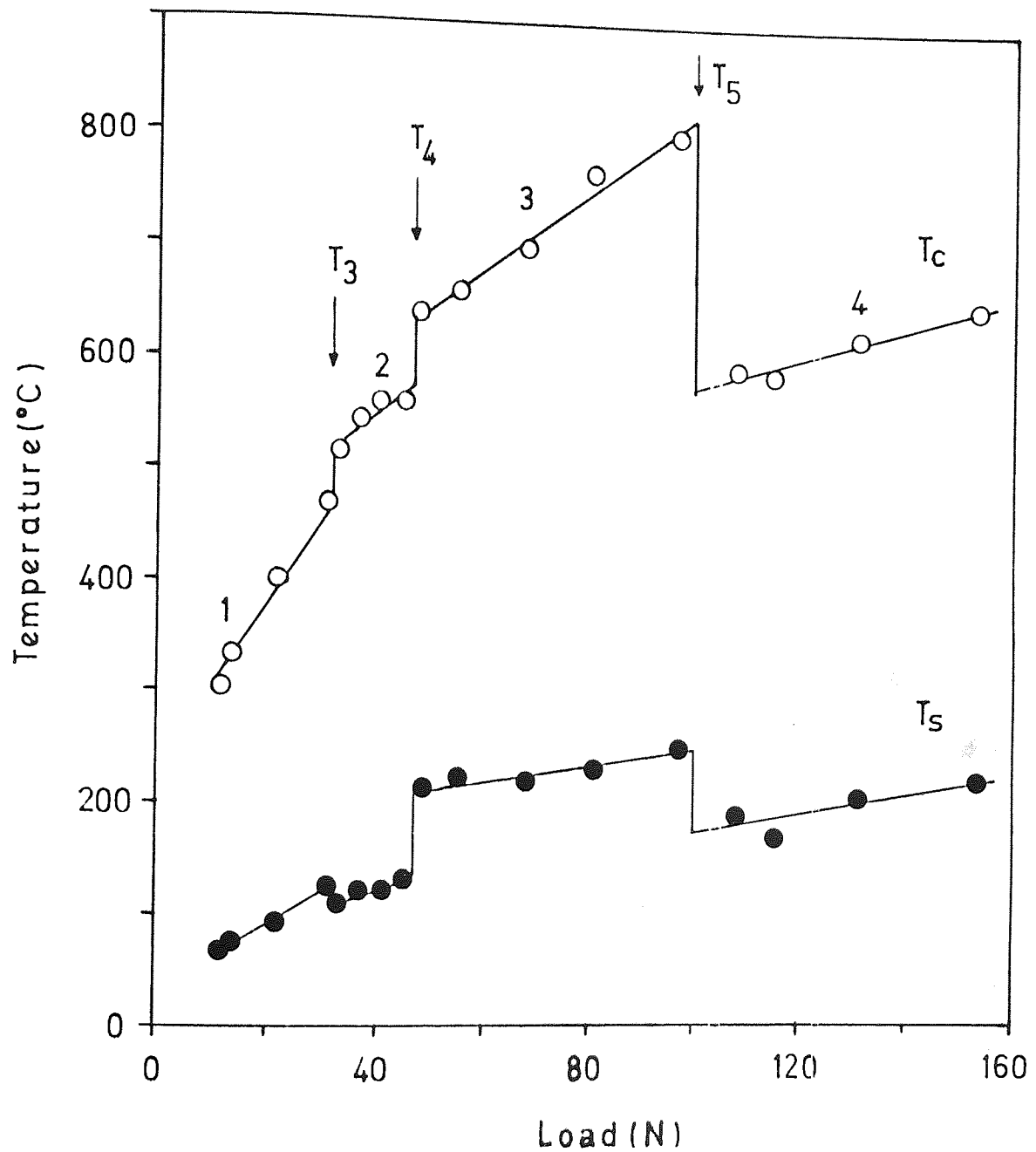
Figure 4.1(b)   Variation of contact temperature, T_c
and surface temperature, T_s with load
at 1.2 ms^{-1}.
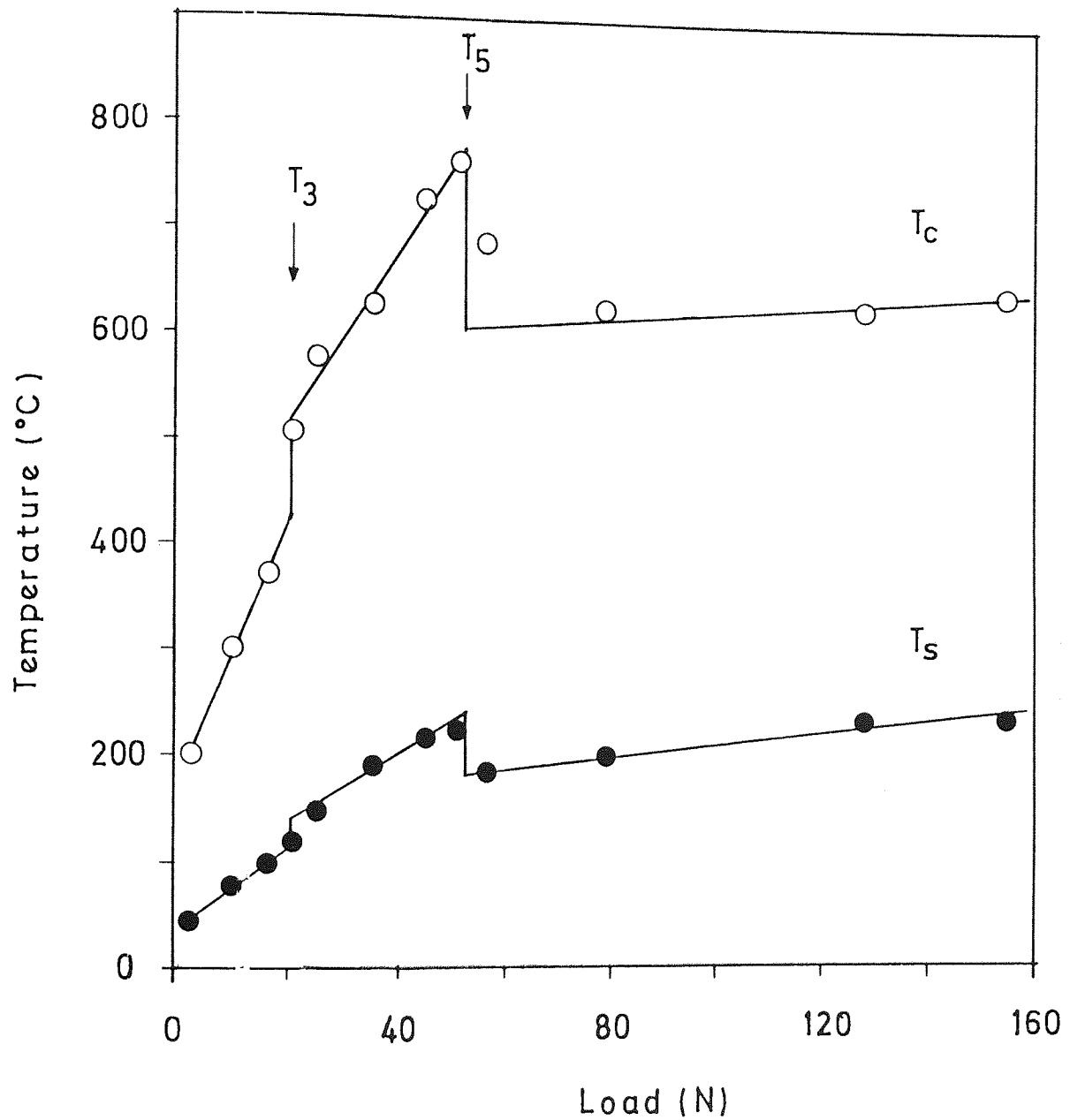
Figure 4.1(c)   Variation of contact temperature, T_c

and surface temperature, T_s with load

at 1.6 ms^{-1}.
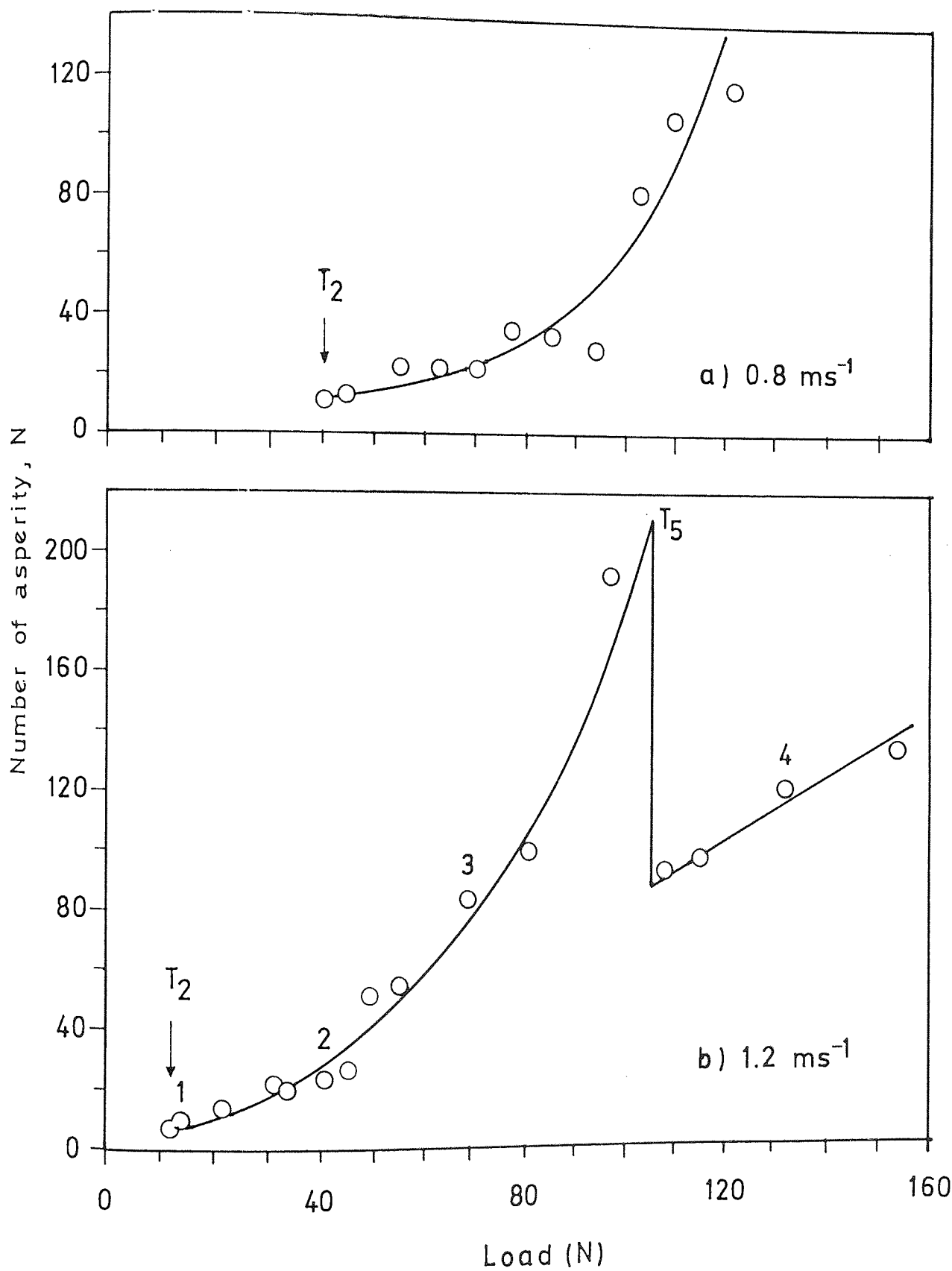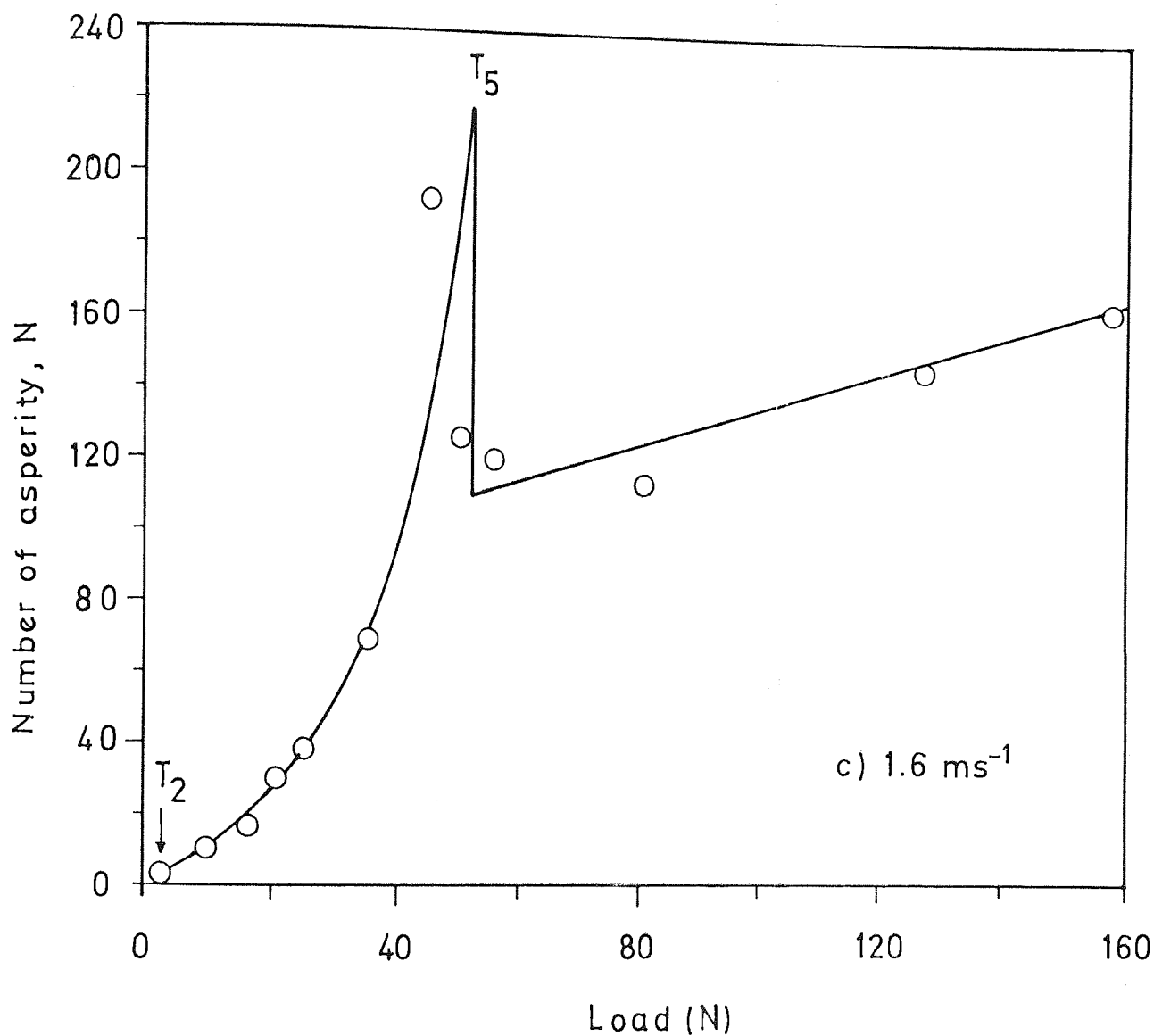
a) 0.8 ms^{-1}

b) 1.2 ms^{-1}

Figure 4.2   Number of asperities versus load at 0.8,

1.2 and 1.6 ms⁻¹.
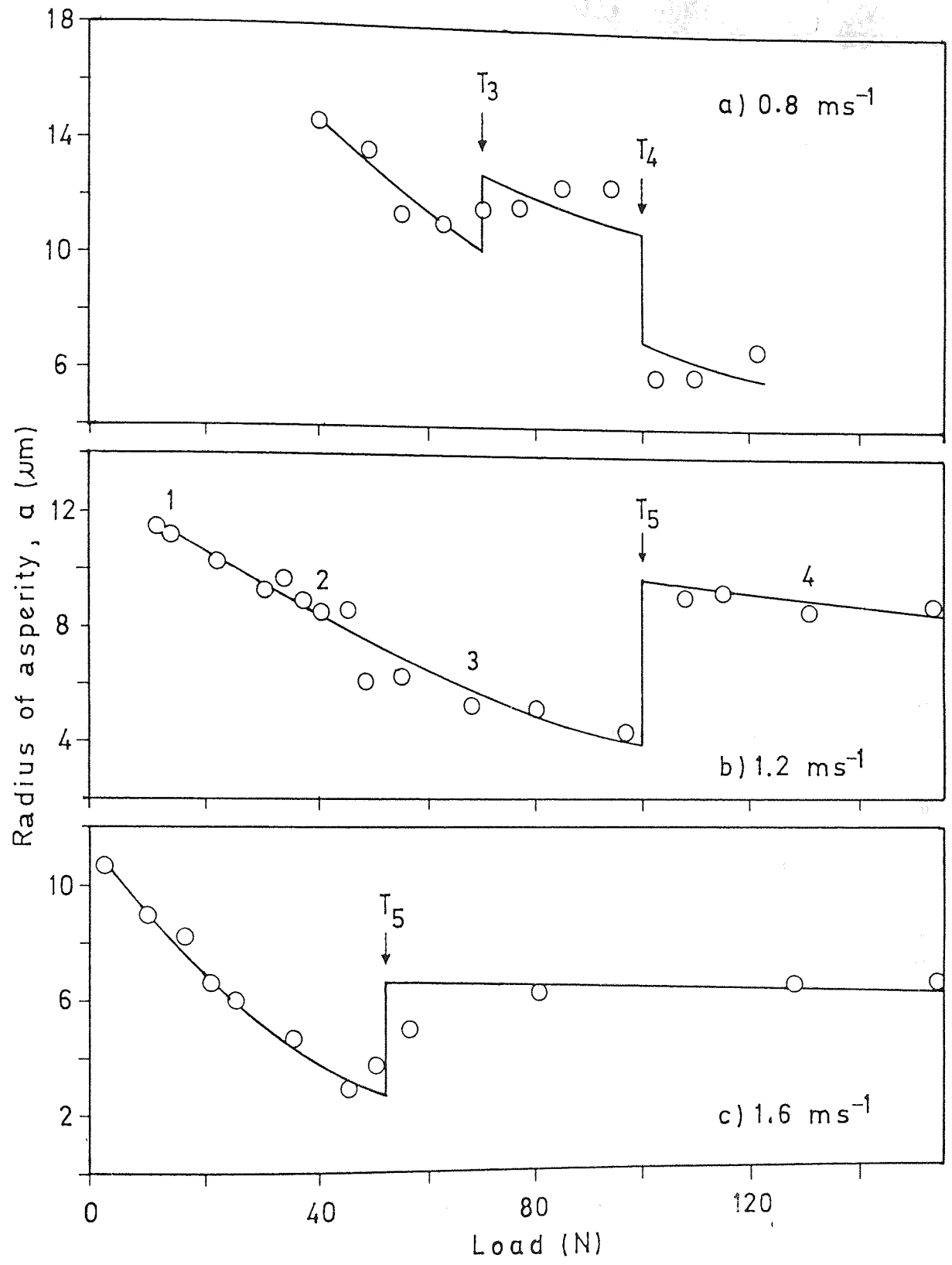
Figure 4.3   Radius of asperity versus load at 0.8, 1.2

and 1.6 ms⁻¹.
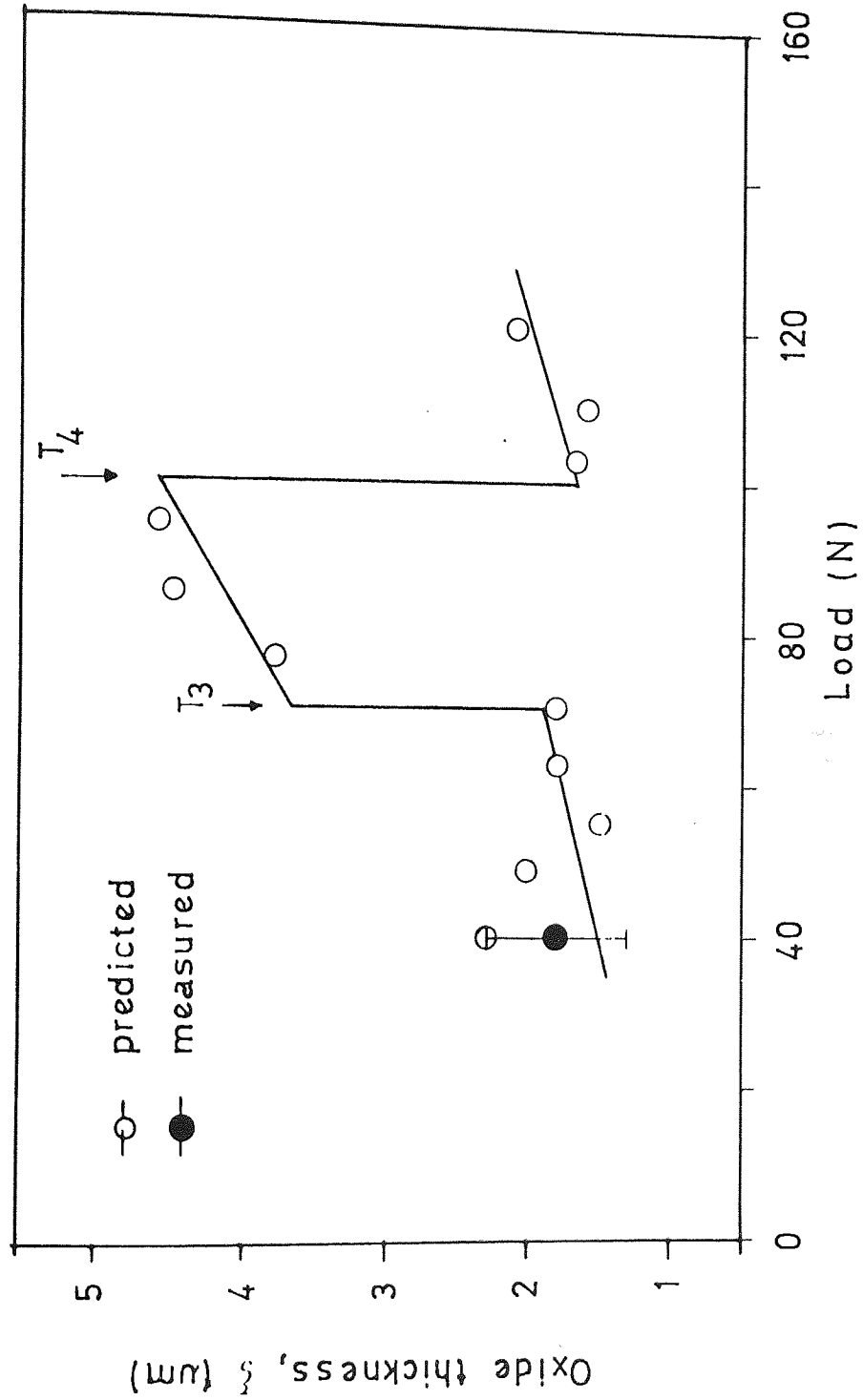
Figure 4.4(a) Oxide film thickness versus load at 0.8 ms⁻¹.
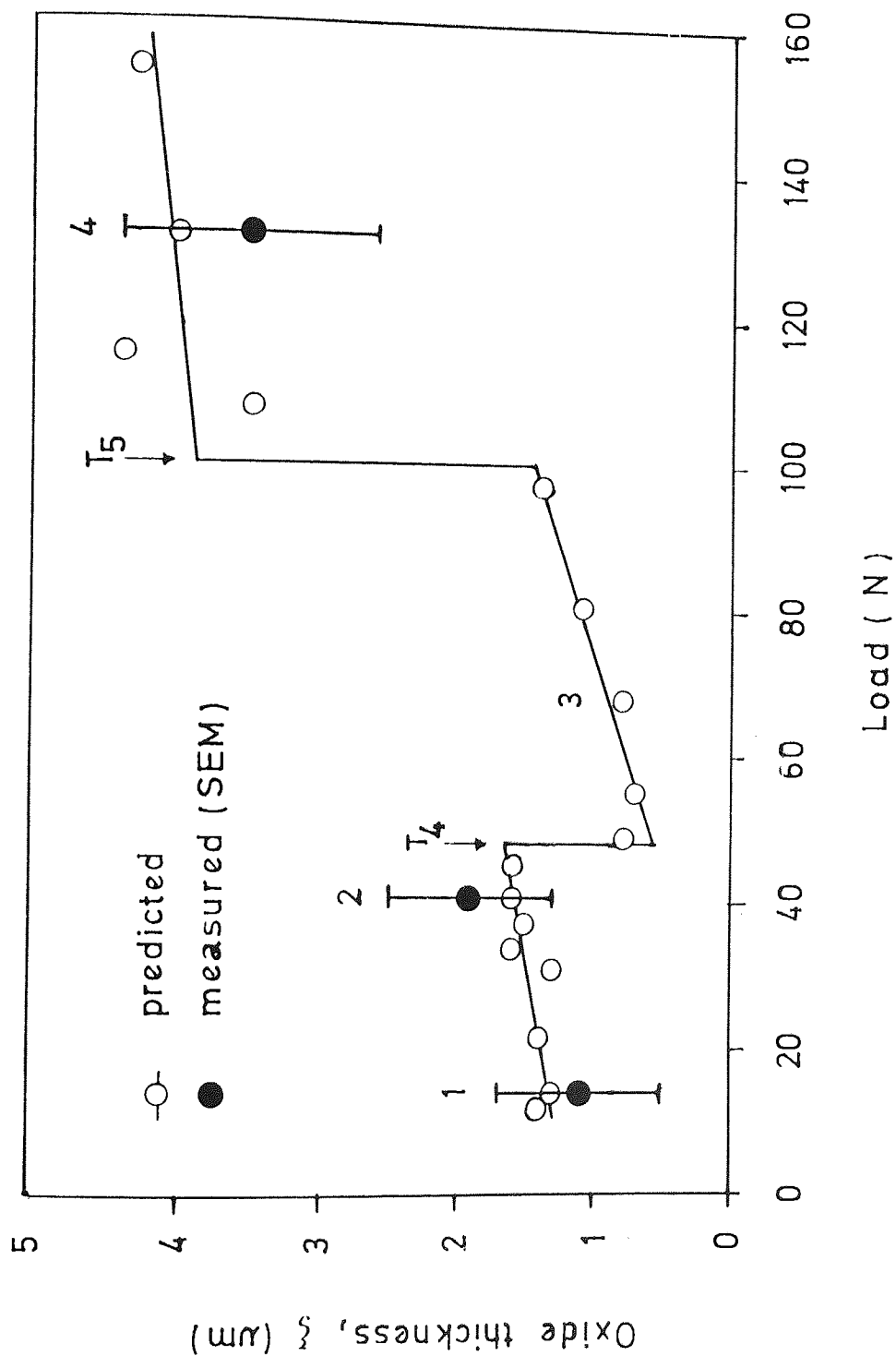
Figure 4.4 (b)   Oxide film thickness versus load at 1.2 ms^{-1}.
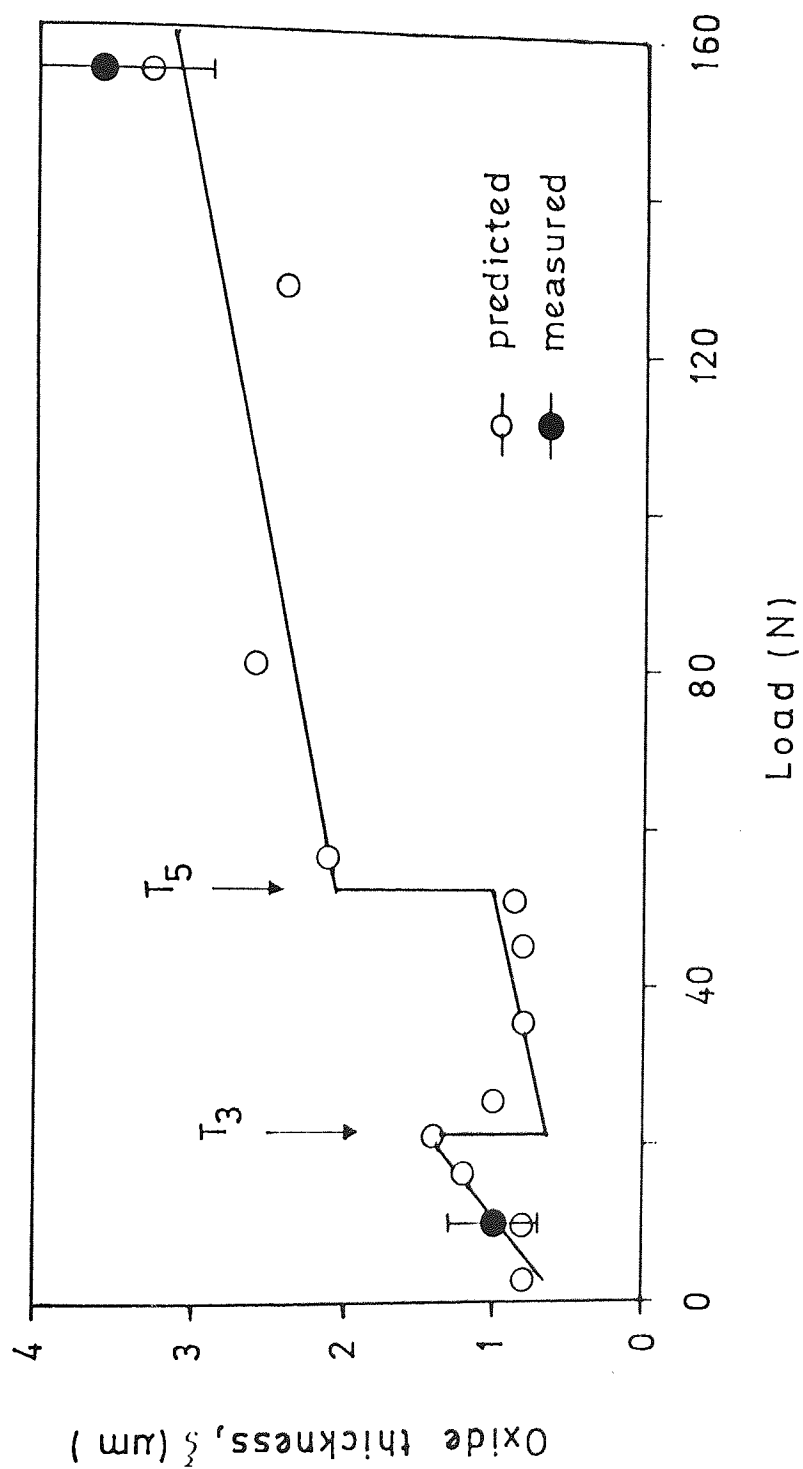
Figure 4.4(c) Oxide film thickness versus load at 1.6 ms⁻¹.

thickness varies as shown in figure 4.4. Some measured
values are also shown in this figure.

Shown on the 1.2 ms⁻¹ graphs mentioned above are the
points at which the four load tests (13.8 N, 40.5 N, 68.1 N
and 131.5 N) were carried out. The contact and surface
temperatures (figure 4.1(b)), asperity numbers (figure
4.2(b)) and asperity radii (figure 4.3(b)) and oxide
thicknesses (figure 4.4(b)) of those loads are marked with 1,
2, 3 and 4 in sequence order.

4.3 Severe to mild wear transition

A model is proposed to account for the change in wear
volume with sliding time preceding the transition to mild
wear. It is expected that, under constant sliding speed, a
load (i.e transition load) is responsible for the generation
of temperatures sufficient to produce oxidation of the
surfaces during the running-in severe wear period. The
possible ways in which the process can take place are
described in the following.

Oxidation may occur over the whole surface at the
ambient temperature but particularly initially around
nucleation sites, probably at the contact temperature T_c.
Most of this oxide removed on a pin on a vertical disk system
will probably fall from the contact areas and therefore not
contribute to any great degree to an agglomerate transfer

film. Thus oxide grows around the nucleation sites (mainly by a diffusion controlled process) both laterally and in thickness until equilibrium thickness is attained and sufficient coverage of the wearing surfaces has occurred to produce mainly oxide-oxide asperity interactions. At this point, the transition from severe to mild wear is complete.

Following the treatment of Sullivan and Granville (57) for transfer wear, consider a pin-on-disc system sometime t after the initiation of an experiment. Let ΔV be the volume of material removed from a surface in time t to t + Δt, then

$$\Delta V = \Delta V_{m-m} + \Delta V_{m-o} + \Delta V_{o-o} - \frac{1}{2} \Delta V_{ox} \quad \ldots\ldots\ldots (4.12)$$

where

ΔV_{m-m} = volume removed due to metal-metal contact in time Δt

ΔV_{m-o} = volume removed due to metal-oxide contact in time Δt

ΔV_{o-o} = volume removed due to oxide-oxide contact in time Δt

$1/2(\Delta V_{ox})$ = volume of oxide produced in time Δt

Since the Pilling Bedworth ratio (84) is approximately 2 for both $\alpha-Fe_2O_3$ and Fe_3O_4, a factor 1/2 is included in the last term of equation (4.12). If α is the fraction of the apparent contact area covered by oxide at time t, the probability, P, of each contact is given by (22)

$$P_{m-m} = (1-\alpha)^2, \quad \text{for metal-metal} \quad \ldots\ldots\ldots\ldots (4.13)$$

$$P_{m-o} = 2\,\alpha(1-\alpha) \qquad \text{for metal-oxide} \quad \dots\dots\dots(4.14)$$

$$P_{o-o} = \alpha^2 \qquad\qquad \text{for oxide-oxide} \quad \dots\dots\dots(4.15)$$

From Archard's wear law given in equation (1.11) the volume removed is a function of sliding distance and real area of contact. Hence, for metal-metal contact in time Δt,

$$\Delta V_{m-m} = K_{m-m} P_{m-m} A_r\; \Delta d \qquad\qquad \dots\dots\dots(4.16)$$

Using A_r from equation (1.1) and P_{m-m} from equation (4.16), then

$$\Delta V_{m-m} = K_{m-m}\; (1-\alpha)^2\,(W/P_m)\,U\;\Delta t \qquad \dots\dots\dots(4.17)$$

where

$K_{m-m} =$ Archard wear constant for metal-metal contact

$A_r =$ real area of contact

$W =$ applied load

$P_m =$ hardness of the worn disk surface

$U =$ sliding speed

$\Delta d\;(= U\Delta t) =$ total sliding distance in time Δt.

Similarly, the volume removed for metal-oxide and oxide-oxide contacts are

$$\Delta V_{m-o} = K_{m-o}\; 2\,\alpha\,(1-\alpha)\,(W/P_m)\,U\;\Delta t \qquad \dots\dots\dots(4.18)$$

$$\Delta V_{o-o} = K_{o-o}\; \alpha^2\;(W/P_m)\,U\;\Delta t \qquad\qquad \dots\dots\dots(4.19)$$

Assuming parabolic oxidation in which the mass uptake of oxygen per unit area, Δm, varies with time according to (61)

$$\Delta m^2 = kt \qquad \qquad \cdots \cdots \cdots (4.20)$$

For a surface covered with an oxide film of area A_r, this mass is given by

$$\Delta m = \frac{Mf}{A_r} = \frac{V_{ox} \, \rho f}{A_r} \qquad \cdots \cdots \cdots (4.21)$$

where

M $(= \Delta V_{ox})$ = mass of oxide film

f = fraction of oxide

V_{ox} = volume of oxide film

ρ = density of oxide

By equating (4.21) which is squared and equation (4.20), then

$$V_{ox} = \frac{A_r}{\rho f} (Kt)^{-1/2} \qquad \cdots \cdots \cdots (4.22)$$

Using equation (4.22) the volume of oxide produced in time t to $t + \Delta t$, ΔV_{ox} is obtained by the following derivation

$$(V_{ox} + \Delta V_{ox})^2 - V_{ox}^2 = (\frac{A_r}{\rho f})^2 \, k(t + \Delta t - t)$$

$$V_{ox}^2 + 2V_{ox}\,\Delta V_{ox} - \Delta V_{ox}^2 - V_{ox}^2 = \left(\frac{A_r}{\rho_f}\right)^2 k\,\Delta t$$

since ΔV_{ox}^2 is negligible compared with V_{ox}, then

$$\Delta V_{ox} = \frac{1}{2V_{ox}}\left(\frac{A_r}{\rho_f}\right)^2 k\,\Delta t \qquad \ldots\ldots\ldots\ldots(4.23)$$

In general, oxide growth is due to out of contact static oxidation at the general surface temperature and in-contact tribo-oxidation at or near to the contact temperature, T_c. Hence equation (4.23) must be written as two components,

$$\Delta V_{ox}(static) = \frac{1}{2V_{ox}}\left(\frac{A_r}{\rho_f}\right)^2 k_s\,\Delta t \qquad \ldots\ldots\ldots\ldots(4.24a)$$

$$\Delta V_{ox}(tribo) = \frac{1}{2V_{ox}}\left(\frac{A_r}{\rho_f}\right)^2 k_T\,\Delta t \qquad \ldots\ldots\ldots\ldots(4.24b)$$

where k_s is the parabolic growth constant for static oxidation and k_P is the parabolic growth constant for in-contact oxidation.

In order to simplify the treatment at room temperature it is assumed that $V_{ox}(static)$ is negligable since out-of-contact oxidation is relatively small if compared to in-contact oxidation. Using V_{ox} from equation (4.22), the volume of oxide produced under tribo-oxidation may be written as

$$\Delta V_{ox} = \frac{W}{2P_m \, \rho f} \, k_T^{1/2} \, t^{-1/2} \, \Delta t \qquad \dots\dots\dots (4.25)$$

Hence if all the expressions given in equations (4.17), (4.18), (4.19) and (4.26) are substituted into equation (4.12) this gives

$$\Delta V = K_{m-m} \, (1-\alpha)^2 \, (W/P_m) \, U \, \Delta t$$
$$+ \, K_{m-o} \, 2 \, \alpha(1-\alpha) \, (W/P_m) \, U \, \Delta t$$
$$+ \, K_{o-o} \, \alpha^2 \, (W/P_m) \, U \, \Delta t$$
$$- \, \frac{W}{4 \, P_m \, \rho f} \, k_T^{1/2} \, t^{-1/2} \, \Delta t$$

and after rearrangement, gives

$$\Delta V = (P \, \alpha^2 - Q \, \alpha + R - St^{-1/2}) \, \Delta t \qquad \dots\dots\dots (4.26a)$$

where

$$P = (K_{m-m} + K_{o-o} - 2K_{o-o}) \, (W/P_m) \, U \qquad \dots\dots\dots (4.26b)$$

$$Q = 2(K_{m-m} - K_{m-o}) \, (W/P_m) \, U \qquad \dots\dots\dots (4.26c)$$

$$R = K_{m-m} \, (W/P_m) \, U \qquad \dots\dots\dots (4.26d)$$

$$S = \frac{W}{4 \, P_m \, \rho f} \, k_T^{1/2} \qquad \dots\dots\dots (4.26e)$$

Growth of oxide

Assuming a diffusion controlled mechanism of oxide growth, and further assuming that oxide growth occurs initially around nucleation sites which eventually will grow and form oxide plateaux. The majority of oxide formed in regions other than these sites will either be removed in the form of fine wear debris, or not contribute to the plateaux formation mechanism. Following an argument similar, but inverse to that of Stott et al. (23) it is assumed that the volume rate of oxide production will be proportional to the area of oxide coverage, α. This may be true in the case of unidirectional sliding wear of horizontal pin on vertical disc system, since experimental evidence from the friction, wear and temperature results (see figures 3.13, 3.14 and 3.15) show considerable changes immediately before the onset of mild wear. For reciprocating sliding at high temperatures, the experimental conditions used by Stott et al., oxidation was assumed to occur mostly from metallic wear debris particles which have been broken up and reduced in size by the sliding process, followed by compaction of the oxide produced. Thus the area growth rate of this oxide, then followed an exponential decay law.

If, from the argument relating oxidation on a pin-on-disc system, the oxide film attains critical thickness one may approximate that the area growth rate is proportional to α. Hence

$$\frac{d\alpha}{dt} \propto \alpha$$

and

$$\frac{d\alpha}{dt} = C\alpha \qquad \cdots\cdots\cdots(4.27)$$

where C is a constant. Assuming pre-oxidation coverage of α_o, initially formed prior to sliding wear. The area of coverage after time t, α, is obtained by integration of equation (4.27).

$$\int_{\alpha_o}^{\alpha} \frac{d\alpha}{\alpha} = \int_{0}^{t} C \, dt$$

or

$$\alpha = \alpha_o \, e^{ct} \qquad \cdots\cdots\cdots(4.28)$$

When t = 0, $\alpha = \alpha_o$ and when t = t_T (transition time), α = fraction corresponding to surface coverage α_T (say). Therefore, C can be written as

$$C = \frac{1}{t_T} \ln\left(\frac{\alpha}{\alpha_o}\right) \qquad \cdots\cdots\cdots(4.29)$$

Equation (4.26a), including the growth rate term then becomes

$$\Delta V = \{P \, \alpha_o^2 e^{2ct} - Q \, \alpha_o e^{ct} + R - St^{-1/2}\} \, \Delta t \quad \ldots \ldots (4.30)$$

In the limit as $\Delta t \to 0$, the total volume removed in time t, V, is given by

$$V = \int_0^t \{P \, \alpha_o^2 e^{2ct} + Q \, \alpha_o e^{ct} + R - St^{-1/2}\} \, dt$$

or

$$V = \frac{P \, \alpha_o^2 e^{2ct}}{2c} - \frac{Q \, \alpha_o e^{ct}}{c} + Rt - 2St^{1/2} \quad \ldots \ldots (4.31)$$

where the constant, C, is given by equation (4.29)

4.3.1. Calculation of wear volume

As an example, a prediction of wear volume from this theory is calculated here from tests carried out at 1.2 ms-1 and 11.8 N transition load. Some of the data is shown in table 3.8. The following steps involve calculations of various constants and variables described in equation (4.31).

1. Pre-oxidation coverage, α_o

From equation (4.28), α_o is the pre-oxidation coverage defined as the ratio between real contact area and apparent contact area. Real areas of contact are highly stress areas with very high energy inputs, hence it is reasonable to assume that these will act as oxide initiation sites. The expression is

$$\alpha_o = \frac{W}{\pi R_p^2 P_o} \qquad \qquad \ldots\ldots\ldots\ldots(4.32)$$

where W (load) = 11.8 N, R_p (radius of the pin) = 3.15 x 10^{-3} m and P_o (disc bulk hardness) = 2.03 x 10^{9} Nm^{-2}. This gives

$$\alpha_o = 1.86 \times 10^{-4}$$

2. The constant, C

Using t_T = 5400 seconds and a value of α_T, based on the micrographs in figure 3.34 of 1/5, then from equation (4.29)

$$C = 1.3 \times 10^{-3} \quad (sec^{-1})$$

3. Tribo-oxidation constant, k_T

The oxidational growth rate constant was used to calculate K_T; this is given by (109)

$$k_T = A_P \exp \{-Q/(RT)\} \qquad \ldots\ldots\ldots\ldots(4.33)$$

where A_P is the Arrhenius constant, Q is the activation

energy, R is the molar gas constant and T is the oxidation

temperature. Since $\alpha-Fe_2O_3$ was the predominant oxide during

the equilibrium mild wear (see the 13.8 N results in figure

3.22(d) and table 3.15), the constants; $A_P = 1.1 \times 10^{16}$

$Kg^2m^{-4}s^{-1}$, Q = 208 KJs^{-1} are readily obtainable from

reference (65). This, together with R = 8.31 J mol^{-1} K^{-1} and

computed T = 302°C = 575 K (see table 3.3), result in a value

of k_T given by

$$k_T = 1.3686 \times 10^{-3} \quad (Kg^2m^{-4}s^{-1})$$

and hence

$$k_T^{1/2} = 3.7 \times 10^{-2}$$

4. Oxide-oxide wear constant, K_{o-o}

Archard's wear constant (37) can be written as

$$K_{o-o} = \frac{w_o P_m}{W} \qquad \ldots\ldots\ldots\ldots(4.34)$$

which for the measured equilibrium wear rate of $w_o = 5.60 \times$

10^{-13} m^3 m^{-1} (see table 3.8 test 6) and $P_m = 8.3 \times 10^9$ Nm^{-2}

gives the following values

$K_{o-o} = 3.94 \times 10^{-4}$

5. Metal-metal wear constant, K_{m-m}

Similarly, for K_{m-m} where

$$K_{m-m} = \frac{W_m P_m}{W} \qquad \dots\dots\dots\dots(4.35)$$

is calculated from the running-in severe wear; $W_m = 1.7 \times 10^{-11}$ m^3 m^{-1} (see table 3.8 for test 6), $P_m = 6.4 \times 10^9$ Nm^{-2}, i.e.

$$K_{m-m} = 9.22 \times 10^{-3}$$

6. Metal-oxide wear constant, K_{m-o}

Assuming that $K_{m-o} \sim K_{o-o} = 3.94 \times 10^{-4}$

7. Variables; P, Q, R and S

Using the above values obtained from 1 to 7 and substituting into equations (4.26b), (4.26c), (4.26d) with the necessary data for equation (4.26e); Pm = 6.4×10^9 Nm^{-2}, f = 0.3006 and $\rho_o = 5.24 \times 10^3$ Kgm^{-3}, then

$$P = 1.87 \times 10^{-11}$$

$$Q = 3.91 \times 10^{-11}$$

$$R = 2.04 \times 10^{-11}$$

$$S = 1.09 \times 10^{-14}$$

The wear volume is then given by

$$V = 2.49 \times 10^{-16} \exp(0.0026 \ t)$$
$$-5.59 \times 10^{-12} \exp(0.0013 \ t)$$
$$+2.04 \times 10^{-11} \ t \ - \ 2.17 \times 10^{-14} \ t^{1/2} \quad (m^3)..(4.36)$$

where $0 < t < 5400$ (t in second)

From equation (4.36) this theoretical wear volume is plotted as a function of time and shown in figure 4.5. Experimental result is shown as a dotted line on the same graph. It can be seen that there is a remarkable agreement between the theory and experiment; the difference being less than 5%.

The theory is capable of predicting the wear volumes from different tests at 1.2 ms^{-1} and from experiments with various speeds. This can be made simple by inserting correct values of the variables; P, Q, R, S, K_{m-m}, C and α_o, which are expressed in term of the speed, U. Using W_r in place of W (where W_r is given by equation (3.2)) for equations (4.26b), (4.26c), (4.26d), (4.26e), and assuming $K_{m-m} \gg K_{m-o}$ and K_{o-o}, the variables can be simplified to

$$P \sim R \sim K_{m-m} \ \frac{1111 \ \exp(-3.9U) \ U}{P_m} \qquad \ldots\ldots\ldots\ldots(4.37)$$

Figure 4.5 Theoretical increase in wear volume with sliding time as an experiment at T_2 transition progressed.
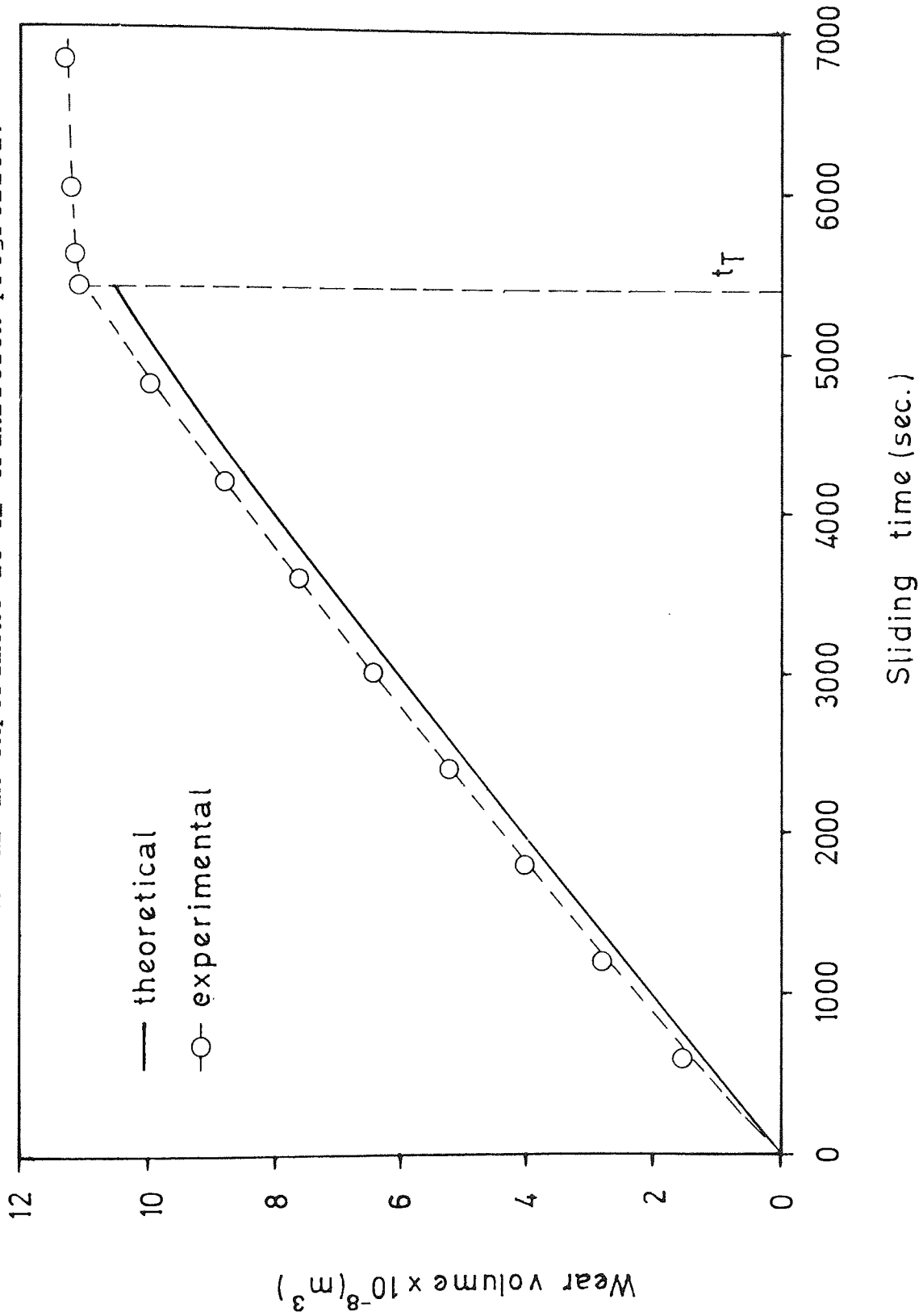
$$Q \sim 2K_{m-m} \frac{1111 \exp(-3.9U) U}{P_m} \qquad \dots \dots \dots (4.38)$$

where the mean value of $P_m = 5.92 \times 10^9$ Nm^{-2}. Similarly, α_o (equation (4.32)) and C (equation (4.29)) are rearranged to include U. The mean wear constant, K_{m-m}, calculated from various speeds, is shown in figure 4.6 and may be expressed by the following relationship

$$K_{m-m} = 8.61 \times 10^{-3} \ln(2.63U) \qquad \dots \dots \dots (4.39)$$

If it is assumed that the fractional oxide coverage at the transition, $\alpha_T = 1/5$ holds for all condition of speed and load, and k_T, f and ρ_o are the average for $\alpha-Fe_2O_3$ and Fe_3O_4. The general wear volume to the transition may be calculated when $t = t_T$. Equation (4.31), therefore, simplifies to

$$V = 2.49 \times 10^{-13} \, Ut_T \ln(2.63U) \frac{\exp(4.86 - 3.9U)}{2.43 + 3.9U}$$

$$-5.68 \times 10^{-11} \, Ut_T \ln(2.63U) \frac{\exp(2.43 - 3.9U)}{2.43 + 3.9U}$$

$$+1.61 \times 10^{-9} \, Ut_T \ln(2.63U) \exp(-3.9U)$$

$$-2.16 \times 10^{-12} \exp(-3.9U) t_T^{1/2} \qquad (m^3) \quad \dots \dots (4.40)$$
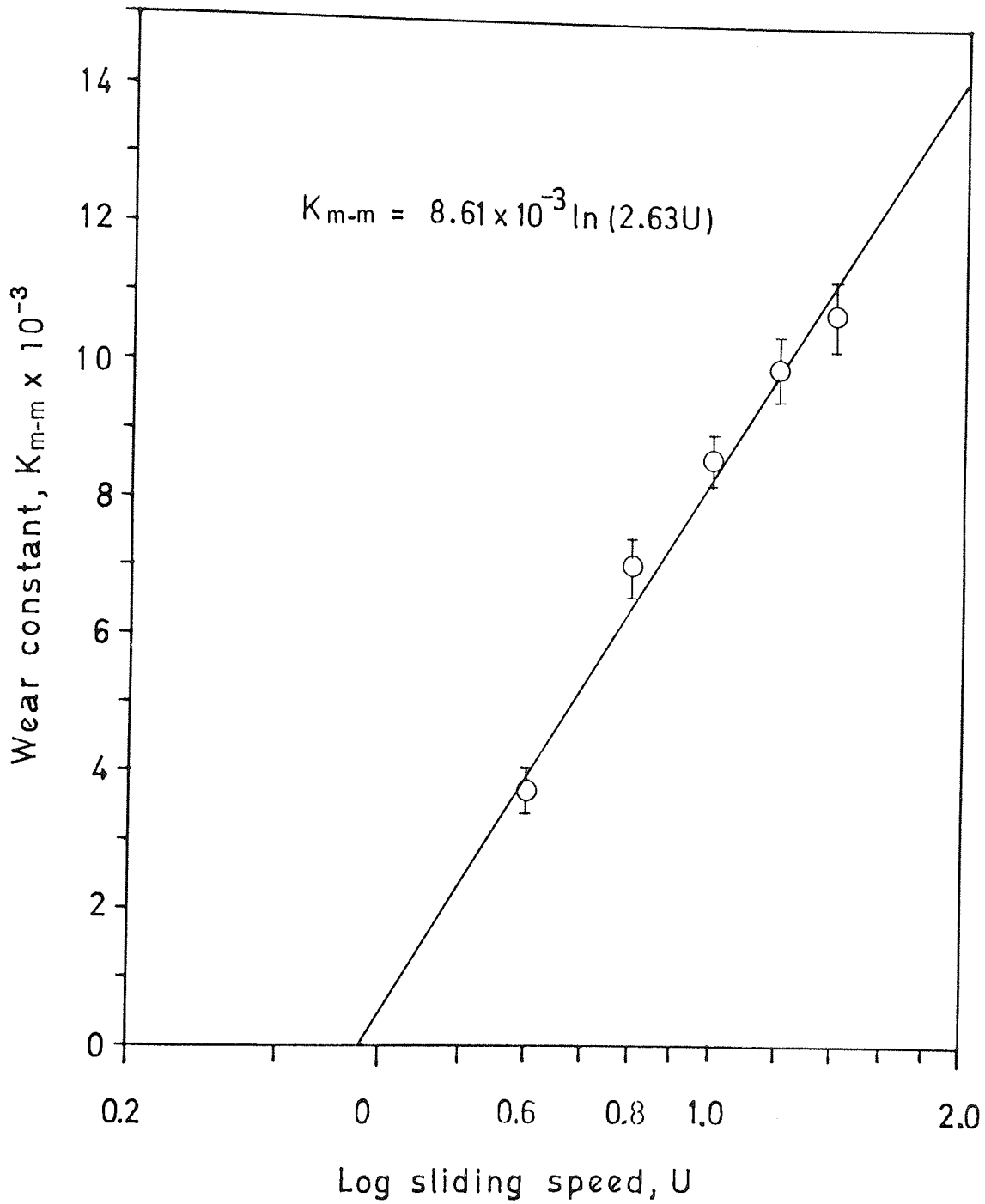
Figure 4.6   Wear constant (metal—metal) versus log
sliding speed.

where U is sliding speed in ms^{-1} and t_{τ} is the transition time in seconds.

Table (4.2) presents the comparison between the measured wear volume and the theoretical values predicted from equation (4.40). A total of thirty six measurements give errors in the range between -25% to +23%, of which twenty six tests had errors under 10%. Despite a -11% mean error there is generally a good agreement between the theory and experiment, as can be seen by smaller errors of 2% found on each set of the speeds.

Sliding speed (ms^{-1})	Transition load, W_T (N)	Volume to transition measured	$\times 10^{-8}$ (m^3) theory	errors %
0.6	126.6	5.47	5.39	+1
	110.4	7.96	7.97	-.1
	107.6	8.77	7.97	+10
	110.4	8.48	9.37	-9
	113.8	6.85	6.56	+4
	108.3	6.21	5.86	+6
0.8	33.5	19.59	15.13	+23
	49.1	13.90	12.77	+8
	48.1	9.98	9.46	+5
	45.1	20.97	19.86	+5
	40.2	15.34	16.08	-5
	57.4	6.78	7.09	-5
	49.1	11.76	11.59	+2
1.0	22.3	8.57	9.06	+6
	27.3	8.91	8.00	+10
	15.2	11.10	13.15	-18
	21.8	9.92	10.13	+2
	26.1	8.63	10.13	-17
	21.1	6.26	7.64	-22
1.2	10.8	9.21	8.19	+11
	9.6	4.74	5.55	-17
	10.3	8.73	8.89	-2
	10.8	9.18	8.42	+8
	11.4	7.49	7.60	-2
	11.8	11.02	10.53	+4
	10.0	5.75	6.67	-16
	10.8	9.79	9.94	-2
	11.3	7.00	8.07	-15
	11.8	8.68	7.84	+10
	11.8	10.63	9.59	+10
1.4	5.5	13.27	10.70	+19
	4.6	4.13	3.85	+7
	4.9	4.33	4.28	+1
	4.4	6.73	7.21	-7
	4.6	5.45	5.35	-6
	5.1	6.22	7.78	-25

Table 4.4   Comparison between the measured and
theoretical wear volume for wear
transition experiments.

CHAPTER 5

DISCUSSION

5.1 General wear behaviour

At least five introductory series of experiments were carried out at sliding speeds of 0.6, 0.8, 1.0, 1.2 and 1.6 ms^{-1} in order to determine the general behaviour of the EN 31/EN 8 steel couples. The resultant wear rate versus load curves form part of the so-called Welsh curves, showing the portion of severe wear, T_2 type transition and broad trends in mild wear above T_2. The lower and upper limits of the speed were restricted to 0.6 and 1.6 ms^{-1} respectively. Any experiment carried out beyond these limits would eliminate T_2, and wear behaviour is then either characterized by solely mild wear for speeds greater than 1.6 ms^{-1} or severe wear with a T_1 transition for speeds less than 0.6 ms^{-1}. Both T_2 transitions and the various mild wear regimes are discussed in this chapter.

In this investigation, severe wear was indicated by high wear rates, of the order 10^{-12} to 10^{-11} m^3m^{-1}, and appeared below the T_2 transition and mild wear by low wear rate, approximately two orders of magnitude less above T_2. Further changes were found in the mild wear regimes, the extent of which can be influenced by test duration. For short duration tests of two hours or less, mild wear

increased with load, followed by a transition to lower wear rates and then a further increase, all within the mild wear regime. For example see figure 3.4 shown in broken line. Quinn, Sullivan and Rowson (19,20) and Sullivan and Athwal (81) considered that such mild wear variations were due to three stages of oxide formation, i.e., whether $\alpha-Fe_2O_3$, Fe_3O_4 or FeO was the predominant oxide.

For long duration tests, up to seven hours, mild wear was characterized by, instead of the existing three, four distinct regions, and each region was separated by a relatively sharp transition. Region 1 lay between the T_2 and T_3 transitions. Region 2 was confined between T_3 and T_4 transition loads; the magnitude of wear rate in this latter region being 100 time less than that between T_2 and T_3. Mild wear in region 3 (between T_4 and T_5) was indicated by an increased wear rate versus load gradient. All tests carried out at low speeds (0.6 to 1.0 ms^{-1}) terminated in this region, since their transition loads were displaced to the higher load ranges of the Welsh curve. For higher speeds (1.2 and 1.6 ms^{-1}), however, another mild wear region was observed above the T_5 transition; this newly-formed region 4, had wear rates of approximately an order of magnitude less than region 1.

The effect of extending test duration in the mild wear region is clearly to alter the wear rate. If both short and long duration curves are shown on one graph, such as that in

figures 3.2 to 3.4, it can be seen that under long duration

of running, the overall wear rates are, in comparison to

short duration, slightly lower in region 1, substantially

lower in region 2, slightly higher in region 3 with a further

sharp decrease in region 4. The coefficient of friction

associated with various wear rates, and thus oxide types,

decreased from region 1 to region 3, but increased slightly

in region 4.

The broad patterns of mild wear are discussed in section

5.2 with reference to the results of the Welsh curves, wear

debris identification and their relation to the surface

parameters predicted from the surface model described in

chapter 4. Discussion of the transition from severe to mild

wear and the running-in periods prior to the establishment of

equilibrium wear are given in section 5.3 and section 5.4

respectively using various experimental results reported in

chapter 4. The theoretical view is also included in the

former case. Section 5.5 attempts to develop an hypothesis

on the mechanism of wear.

5.2 Equilibrium mild wear

Experiments on equilibrium mild wear were carried out

for loads greater than the T_2 transition load, where the

changes in wear rate for various speeds are shown in figures

3.1 to 3.5. At 0.6 ms^{-1} mild wear varied in three different

ranges of load; the first, region 1, occurring between 102

and 108 N where the wear debris consisted of Fe_3O_4 and $\alpha-Fe_2O_3$, with the presence of metallic iron and small amounts of FeO. Region 2 occurred between 108 and 120 N and region 3 above 120 N. X-ray data revealed that Fe_3O_4 and FeO were present in both regions; region 2 had a higher concentration of Fe_3O_4 than FeO and region 3 had the converse, but with some $\alpha-Fe_2O_3$ present in the debris.

The corresponding three mild wear regimes at 0.8 ms^{-1} speed were between 40 and 70 N, 70 and 100 N and above 100 N loads, while at 1.0 ms^{-1} the loads were reduced still further to between 15.2 and 48.0 N, 48.0 and 72.0 N, and above 72.0 N respectively. The constituents of the wear debris for both speeds were similar to that for 0.6 ms^{-1}, but in different proportions. Metallic iron was found in all regions. For 0.8 ms^{-1} in region 1 Fe_3O_4 and $\alpha-Fe_2O_3$ were of approximately equal concentration, while the concentration of the latter oxide was less than the former for 1.0 ms^{-1}. Further, x-ray results revealed that for 0.8 ms^{-1}, Fe_3O_4 and FeO were the major constituents of the wear debris for both short and long duration tests in region 2, and for 1.0 ms^{-1} Fe_3O_4 was the only oxide detected under long duration tests on the same region. In region 3 the identified oxides were FeO which appeared to be of higher concentration than Fe_3O_4; for 0.8 ms^{-1} speed this produced an additional oxide, typically $\alpha-Fe_2O_3$, was also formed.

Mild wear at 1.2 and 1.6 ms^{-1} could be represented by

four regions separated by transition loads. For 1.2 ms^{-1} these were between 11.8 and 32.0 N (region 1), 32 and 47 N (region 2), 47 and 105 N (region 3) and above 105 N (region 4) respectively. Similarly for the case of 1.6 ms^{-1} the regions lay between 2.4 and 21.0 N (region 1), 21 and 52 N (regions 2 and 3) and above 52 N (region 4). In region 1 the predominant oxide was $\alpha-Fe_2O_3$ with a small quantity of Fe_3O_4 for both speeds. The position changed in region 2, where an Fe_3O_4 and FeO mixture appeared in the debris under conditions of short running duration at 1.2 ms^{-1} and both short and long running durations at 1.6 ms^{-1}. However, the concentration of Fe_3O_4 in the debris at the former speed increased with longer test durations of more than four hours. The contents of wear debris for the latter speed remained unchanged, even with an extention of test for up to seven hours. Region 3 maintained its identity with the presence of mainly FeO, while the new region 4 consisted of a mixture of FeO, Fe_3O_4 and $\alpha-Fe_2O_3$. Metallic iron was detected in the debris from all regions.

Lists of the compounds identified in mild wear regions and their limiting transition loads are presented in tables 3.14 and 3.15 respectively. The results show how the speed and load effect the types of oxide produced which in turn determine the form of mild wear in different regions. All the transition loads increase as the speed decreases from 1.6 to 0.6 ms^{-1}, and because the displacement of T_2 is greater than the rest of the transition loads the curve appears

compressed when plotted on a log scale.

The beginning of mild wear in region 1 occurs at the T_2 transition load when the surface, initially in the running-in severe wear mode, becomes oxidized and produces a wear-resistant film. Under equilibrium condition the oxide formed at low load and high speed is predominantly the rhombohedral oxide, $\alpha-Fe_2O_3$ at oxidation temperature above 200°C; this is based on analytical results at 1.6 ms^{-1} presented in table 4.3. The amount of $\alpha-Fe_2O_3$ in this region decreased, either with decreasing speed due to large increase in transition load, or with increasing load at constant speed, and this decrease coincided with increasing amounts of Fe_3O_4 in the debris.

Experiments carried out at T_3 transition load have shown that the wear rate fell slightly when the test duration was relatively short due to the formation of a Fe_3O_4 and FeO mixture at contact temperatures around 570°C. The proportion of FeO in this region was less than that of Fe_3O_4. The wear rate was, however, further substantially reduced after long periods of running, when FeO was eliminated from the debris and Fe_3O_4 produced at temperatures below 570°C predominated. The amount of this oxide increased with loads approaching the T_4 transition. Typical microdensitometer traces of wear debris obtained from 1.0 ms^{-1} tests (figure 3.23) distinguish the oxide formed during the long running periods (Fe_3O_4) from that in the short running durations (Fe_3O_4 and FeO). It has

been shown that (82,83) Fe_3O_4 is the most wear resistant of the oxides of iron, hence the greater proportion of Fe_3O_4 reduces wear rate considerably.

As load increased in region 2, a point is reached where the oxidation temperature ensures that the predominant oxide changes from Fe_3O_4 to FeO. It has been shown that FeO is less wear resistant than Fe_3O_4, hence, this change results in a transition to higher wear at the T_4 transition. Oxidation temperatures greater than 600°C were expected for mild wear at this stage, and this further increased up to the austenisation temperature (750°C) for loads above T_4, with larger concentration of FeO detected in wear debris. Initially, it was expected that mild wear in this region 3 would become severe as the load was increased beyond a certain level, as this behaviour has been reported extensively in previous publication. However, for long durations of running a further transition, T_5 was observed when a substantial decrease in wear rate occurred. It must be assumed that other workers have not noted this transition due to the relatively short periods over which their data has been collected. This T_5 transition extended mild wear into region 4, which exhibited low wear rate and the wear debris comprised of a $\alpha-Fe_2O_3$, Fe_3O_4 and FeO mixture with metallic iron.

The calculated surface parameters appear to be consistent with most of this former experimental evidence.

This is particularly true of contact temperature, T_c, which shows some correlation with the oxide phases present on the surface and in the debris. Contact temperatures of about $200^\circ C$ is predicted when α-Fe_2O_3 is the sole oxide in the debris, as in the case of 2.6 N load and 1.6 ms^{-1} speed in region 1. When the temperature rises to about $500^\circ C$ a mixture of Fe_3O_4 and α-Fe_2O_3 is observed, for example in region 1 at high speeds. For contact temperatures between $500^\circ C$ and $570^\circ C$ Fe_3O_4 was found in the wear debris of region 2 at 1.0 and 1.2 ms^{-1} speeds; the presence of FeO in this region, however, suggests contact temperature not less than $570^\circ C$. In region 3 calculated values up to $800^\circ C$ were obtained for FeO found in this region close to T_3 transition. The associated oxide mixtures in region 4 suggested contact temperatures around $600^\circ C$. The Fe_3O_4 or α-Fe_2O_3 found in the debris from region where contact temperatures are high could be the result of oxidation of the wustite, FeO, during relatively slow cooling.

Figure 4.1 shows three series of contact temperature variation with load at 0.8, 1.2 and 1.6 ms^{-1}. The trends show linear variations in contact temperature with load for all the mild wear regions with sharp changes at the transitions.

Other results from the prediction of the surface parameters are the number of asperities, N, radius of asperity, a, and oxide film thickness, ζ (figures 4.2 to

4.4). In the former, N increased with the load (all speeds), then dropped at T_m transition with a further linear increase with load (for 1.2 and 1.6 ms^{-1}). The rapid increase of N at higher load is caused by reduction in substrate hardness, in particular at temperature greater than 300°C (50). Thus, the lower values of N in region 4 suggest that the surface increases in hardness during asperity contact. The radius of asperities varies in the opposite way to that of the number of asperities, since it is inversely dependent on N. This is indicated by the slight decrease in a with load below and above the T_m transition (figure 4.3). Finally, the predicted oxide film thicknesses show an increase in thickness with load with obvious transitions where there has been a change in oxide type (figure 4.4). These values, especially for the 1.2 ms^{-1} experiments, are in very good agreement with the measured values using scanning electron microscopy. There is an exception for region 3 where no oxide plateaux were observed from the micrographs.

Most of the results predicted from the surface model are in good agreement with those reported by Quinn, Sullivan and Rowson (19,20) who used 2.0 ms^{-1} throughout their experiments. The obvious difference with the current investigation is the presence of the T_m transition which extended mild wear into a new fourth region and has greater effects on the surface parameters. The lowest wear rates in region 2 (between T_m and T_4) seems to result in no change in

the asperity number and asperity radius which appear
independent of the oxide types produced.

5.3 Severe to mild wear transition, the Welsh T₂ transition

Under relatively constant ambient temperature and
sliding speed the transition from severe to mild wear takes
place at a well-defined load or T_2 transition load, below
which severe wear occurs and above which mild wear is
encountered. It was very difficult to specify T_2 as a single
transition point; experimental results showed a slight
variation in this value with different tests, probably due to
change in the bulk properties of the specimen materials
during regrinding and vapour bath cleaning. Microhardness
measurements for various untreated specimens showed a mean
variation of ± 12 VPN.

The transition time recorded for each set of transition
load also had considerable scatter due to the same hardness
variation and environmental conditions. Relative humidity
changes of between ± 3% and ± 5% were recorded for some
experiments. It is expected that adhesion of air moisture
could effect oxidation of the surface at asperity contacts,
and therefore change the duration of the running-in severe
wear. Whitehead (109) has shown that, adhesion of small
particles to surfaces increased with increasing relative
humidity, in particular for values greater than 50%.

At least six tests were carried out to obtain the mean

values of transition parameters. For example, the tests at 0.6 ms^{-1} resulted in transition loads between 108.3 and 126.6 N and transition times between 1500 and 2400 seconds, giving mean values of 113 N (±6%) and 1800 seconds (± 20%) respectively. The corresponding results for tests with speeds up to 1.6 ms^{-1} were as follows: 46 N (±15%) and 3283 seconds (±30%) for 0.8 ms^{-1}, 22 N (±17%) and 3040 seconds (± 25%) for 1.0 ms^{-1}, 10.9 N (±6%) and 4255 seconds (±17%) for 1.2 ms^{-1}, 4.9 N (±8%) and 5490 seconds (±36%) for 1.4 ms^{-1} and 2.3 N (±9%) and 3040 seconds (±18%) for 1.6 ms^{-1}.

The results for transition load, T_2, indicate that an increase of this parameter was associated with a decrease in sliding speed similar to that found by Welsh (14). A close examination of the variation revealed the mean transition load decreased exponentially with the speed according to an empirical relationship given by equation (3.2). This was valid for sliding wear between EN 31/EN 8 steels; no tests have been made to prove the applicability with other materials. Another interesting result was the variation of mean transition time which increased exponentially with the speed according to an empirical relationship given by equation (3.3). Granville (110) has indicated an empirical relationship of transition speed times (load)^2 = 28.8 for 9% chromium steel, based on two series of load and speed experiments using a reciprocating sliding system, but this was found to be inapplicable to the current investigation

(unidirection sliding system). He also found that the distance for the onset of mild wear, and hence the running-in time increased with the speeds from 110 to 140 mms^{-1}. Stott et al. (23) in their work on reciprocating mild wear transitions, did not show any quantitative evidence of the decrease in transition time with ambient temperature. The results obtained by Farrel and Eyre (56) were rather different in the sense that the transition from severe to mild wear was studied using the loads above the T_2 transition. In other word, they maintained, an exponential increase in load above the T_2 can result in a linear decrease in sliding distance (or transition time) for the onset of mild wear.

It has been shown that (19,20) the product between frictional force, F exerted at the sliding interface and sliding speed, U gives the total heat flow per second, which can be related to the rate of energy input (in Js^{-1}) dissipated at the surface. Under condition of Welsh T_2 transition, the total energy required for the transition from severe to mild wear, after running-in time t_T, is $E_{tot} = \mu W_T U t_T$ where μ is the friction coefficient and W_T is the transition load. By substituting $\mu = 0.76U$ (figure 3.10) and two empirically-determined parameters, W_T and t_T, then an expression is obtained as follows:

$$E_{tot} = AU^2 \exp(-BU) \qquad\qquad \dots\dots\dots\dots(5.1)$$

where A and B are constants. Equation (5.1) shows that the total energy dissipation at the surface decreases with the speed. This is true because a small increase in speed causes a large reduction in transition load and hence lower energy. In fact, the lower the energy input the lesser disturbance occurs at the surface with decreased rate of tribo-oxidation, thus the duration preceding the transition to mild wear is lengthened. For example, the eleven tests carried out at 1.2 ms^{-1} speed resulted mean energy input of 13.1 Js^{-1} which was low enough to produce a surface temperature of about 65°C and rate of meterial removal of 1.7 x 10^{-11} m^{3}m^{-1}. This extended transition time to 4255 seconds.

In contrast, the high energy input at low speed increases the number of metallic contact by means of expansion and deformation of the contacting asperities. The resulting high local temperature increases oxidation process at a faster rate, and therefore requires a relatively shorter periods of sliding for the onset of mild wear. An example of low sliding speed at 0.8 ms^{-1} showed that an energy of 36.4 Js^{-1} produced an increase in surface temperature up to 144°C (figure 3.15) and material removal at the rate of 5.0 x 10^{-4} m^{3}m^{-1}. This shortened the transition time to 3283 seconds. According to equation (5.1) the total energy input reaches maximum at a speed between 0.6 to 0.7 ms^{-1} below which energy reduces to zero at zero sliding speed. One possible reason

is that the transition time is reduced as the speed approaches zero despite an increase in transition load.

There is an exception for the 1.6 ms^{-1} speed experiments, particularly in the result of transition time which deviates from equation (3.3). At low transition load measured in these experiments (2.3 N ± 9%), it was very difficult to accurately determine the limit where transition to mild wear occurred due to disturbance on the chart recorder deflection, exerted by the spring force (0.5 to 1.5 N) of the wear transducer device. This result must therefore be regarded as unreliable.

The mean coefficient of friction obtained from the equilibrium mild wear was approximately within the range of those values found in the running-in severe wear, and the increase with speed showed a direct proportionality (figure 3.10). Bowden and Tabor (38) and Moore (45) suggested that the friction coefficient was high at low sliding speeds due mainly to local adhesion and shearing at the regions of contact, whereas, low friction values at high sliding speed were affected by the frictional heating which changed the physical and mechanical properties of the materials.

So far the discussion has concentrated mainly on the variation of transition load, transition time and other parameters with sliding speed. The progressive subsurface and surface changes leading to the transition to mild wear will now be considered in more detail.

The progressive wear test run carried out after 10, 40 and 60 minutes at 1.2 ms^{-1} and 11.8 N revealed no change in the constituents of the wear debris; all ferrite lines on microdensitometer traces showed a slight reduction in concentration with sliding time. There was also no sign of oxide on the pin and disc micrographs. Figure 3.13 shows a gradual decrease in coefficient of friction and reduction in the noise of vibration preceding to transition to mild wear, while figure 3.15 shows a very slight increase in surface temperature, followed by slow reduction in temperature up to the transition point. More pronounced changes in surface temperature were observed on the 0.8 ms^{-1} runs shown on the same graph. This suggests that changes were continually occurring on the surface during the running-in periods, probably due to the oxidation process prior to the mild wear transition.

The virtually zero contact resistance and smooth trace during the first 20 minutes of a run (figure 3.16) was due to metal-metal contact during surface conformity in which the production of metallic wear particles began. A work-hardened subsurface layer was formed as a result. Surface hardnesses of greater than 488 VPN were measured on the disc surface after 10 minutes of running, suggesting that this work-hardened metallic layer was formed almost immediately upon commencement of sliding. Further hardening continued throughout the runs, however, since a value up to 772 VPN was

measured after 60 minutes of running with a final value of 846 VPN at the transition to mild wear. The large fluctuations of contact resistance during the course of the run revealed the discontinous nature of metal-metal contacts. The noise decreased at the transition, indicating the formation of a stable oxide film.

Judging from the surface temperature and contact resistance variations it is likely that, diffusion-controlled oxidation takes place at nucleation sites where contact temperature greater than $300^{\circ}C$ were attained (based on data in table 3.2 for equilibrium wear). This thin film is unstable and easily swept away during each asperity contact, however, some film survives and continues to grow very slowly with duration of running. The rate of growth is governed by the rate of energy input which at the same time induces mating surface to work hardened. There was no evidence on the extent and depth of the hardened layer described in experimental results (chapter 3), since the layer was very thin (less than 5 μm) and it was therefore impossible to measure the hardness across the layer using miniload microhardness tester. Figure 3.37 showed evidence of the oxide formed on the disc surface once transition to mild wear took place, indicating the presence of oxide particles from the very thin plateaux. The unstable nature of the oxide suggested that FeO or a mixture with Fe_3O_4 was formed at this stage of transition; the result from mild wear tests at 13.8

N load, which will be discussed later in the next section, supports this argument.

Details of the oxidation process were described in chapter 4 in conjunction with the establishment of a surface model for predicting wear volume to the transition. Basically, the model comprised of a description of the stages of change from primarily metal-metal contact in the early stage of wear to primarily oxide-oxide contact during equilibrium wear. In addition, the assumption of a 20% oxide coverage at the transition in the proposed model seems to agree both experimentally and theoretically (figure 4.5). This small proportion of oxide suggests an immediate growth of oxide film according to equation (4.28). These arguments are supported by the low noise trace, increased contact resistance and drop in both the friction coefficient and surface temperature at the transition. Stott et al. (23) have noticed similar effects on high chromium steels at temperatures between 100 and 400°C, and attributed the drop in friction coefficient to the formation of a compact oxide with 50% coverage at the transition. The variation of the area growth rate of oxide with the progression of sliding is shown in figure 5.1.

From equation (4.45) and equation (4.47), it is clear that the expression for wear volume is dominated essentially by the linear term combined with two exponential terms and a square root term to form a non-linear curve when plotted

Growth rate area
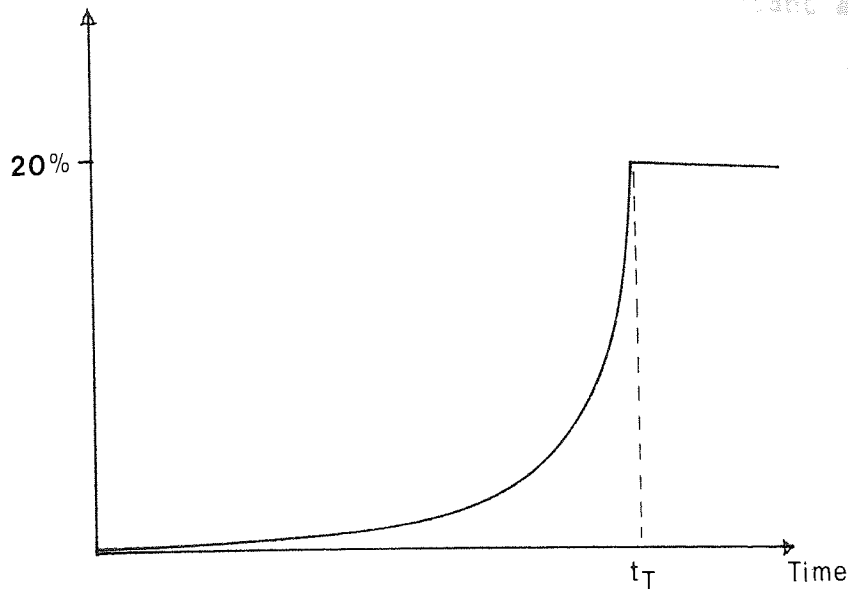
Figure 5.1 Oxide growth rate area versus sliding time.

against sliding time; this is a characteristic form of wear

volume encountered up to T_2 transition load. The expression

is found to be generally valid for the range of speeds

between 0.6 to 1.6 ms^{-1} and loads up to 155 N. This gives

some confidence in the correctness of the model in these

circumstances.

5.4 Running-in mild wear

Two aspects of sliding wear were discussed in the

previous sections, namely equilibrium mild wear and the

initiation of transition to mild wear. Another important

aspect lies in the periods between them or running-in mild

wear. The following discussions will concentrate on this area, based on four series of tests carried out at 13.8 N, 40.5 N, 68.1 N and 131.5 N loads under constant sliding speed of 1.2 ms^{-1}. The loads were chosen to represent each of the mild wear regions described in the previous chapter.

a) 13.8 N (region 1)

Initially, wear under this condition of load exhibited a 20 minutes running-in severe wear period, shown by a rapid increase in the coefficient of friction, μ (figure 3.17) and surface temperature, T_s (figure 3.20). The metallic nature of the sliding contact was indicated by the presence of ferrite from x-ray analysis of the wear debris. At the onset of mild wear, small amounts of FeO were detected (figure 3.26(a)) and both μ and T_s fell to their minimum values. This was followed by a rapid increased up to $\mu = 0.9$ and $T_s = 82°C$ as sliding proceeded to 70 minutes of running. The x-ray analysis of wear debris carried out after 60 and 120 minutes revealed a mixture of FeO and Fe_3O_4 and a mixture of Fe_3O_4 and $\alpha-Fe_2O_3$ respectively (figures 3.26 (b) and (c)), with the addition of ferrite in both cases. Above the 120 minutes run, the friction coefficient and surface temperature further decreased gradually over 200 minutes duration, and then steadied at $\mu = 0.87$ and $T_s = 80°C$. The wear debris identification after 240 minutes run gave $\alpha-Fe_2O_3$, Fe_3O_4 and $\alpha-Fe$.

A 13.8 N load chosen in this investigation was slightly above the mean transition load (10.9 N) in order to ensure that mild wear persisted for all the tests carried out. At loads less than this, it is possible that either severe or mild wear might be encountered. There was evidence of some work hardening occurring below the surface (figure 3.33). Microhardness measurements (table 3.16) showed a variation from 626 VPN at 5 minutes running up to 703 VPN at the onset of mild wear and a further decrease to 589 VPN after long running duration. This small decrease was associated with reduction in contact temperature down to $300^{\circ}C$ where $\alpha-Fe_2O_3$ predominated. All the figures show hardnesses which are higher than those suggested by Welsh (50) for the establishment of mild wear conditions.

The presence of a low intensity line, peak 9, on microdensitomer traces (figure 3.26 (a)) at the end of 20 minutes of running showed that a very small amount of FeO was present in the debris. It is likely that the oxide was formed during the running-in severe wear at contact temperature above $570^{\circ}C$. When a substantial degree of oxide coverage is developed, the associated temperature fall resulted in the formation of Fe_3O_4 and eventually $\alpha-Fe_2O_3$ after 100 minutes of running. The percentages volume of different oxides are shown in figure (3.32) as a function of sliding time. The fact that FeO was always the primary oxide formed at the oxygen/metal boundary illustrates the

hyphothesis that the oxides grow at contact temperature and not at the general surface temperature since FeO is formed only at temperatures greater than 570°C.

Scanning electron micrographs of the pin surface, taken from 60 minutes run, revealed the existence of oxide patches on the bare metallic surface. The appearance of wear scars may explain why the coefficient of friction during this stage of running was high (about 0.9). Figure 3.39 (a) showed a typical oxide plateaux (1.3 μm in thickness) after 120 minutes run being supported by about 5 μm of hardened layer (figure 3.40 (b)). Auger depth profiles (figure 3.45) revealed the presence of oxide plateaux at 240 minutes run.

b) 40.5 N (region 2)

In this particular region the initial rise in friction coefficient and surface temperature (150°C) was due to the removal of the original `ambient oxide' to give essentially metallic contact. It took sometime (about 70 minutes) for the friction and temperature to increase rapidly with time, then further gradually decreased due to the growth of stable oxide plateaux. All these points are illustrated by the virtually zero contact resistance in the first 5 minutes, with rapid rise to an average of 5×10^{3} Ω after the 150 minutes and 10^{5} Ω after the total 360 minutes (figure 3.21) of the run.

Microhardness across the surface (figure 3.34) and

micrographs of the taper section (figure 3.41) showed that intense hardening had occurred in the very early periods of mild wear; this extended to about 10 μm below the surface in the first 5 minutes of running and doubled in depth after just 20 minutes. The corresponding surface hardness (table 3.16) were 777 and 854 VPN respectively with a reduction to 795 VPN after 360 minutes of running. This shows that subsurface work hardening takes place in a very short time after the start of a run and that the values attained are much greater than those quoted by Welsh (15) as necessary to support an oxide film. The contents of the wear debris, as revealed by x-ray analysis, consisted of FeO after 60 minutes run and a mixture of FeO and Fe_3O_4 over the 120 minutes, with the concentration of iron reducing with sliding time. FeO, however, was eliminated from the debris after long duration of running, leaving Fe_3O_4 as the majority component. Micrographs taken after 60 minutes running showed no sign of oxide plateaux, but there were small oxide particles scattered over the surface. Figure 3.39(b) showed the existence of thin oxide plateaux after 120 minutes running, and this was confirmed by Auger depth profile analysis (figure 3.46) in which 300 minutes etching time was required to remove the oxide layer from the surface. The stable nature of Fe_3O_4 was indicated by the presence of thick (1.9 μ m), smooth plateaux on both pin and disc surfaces (figure 3.39 (b) and figure 3.46), resting on 15 μm depth of hardened

layer (figure 3.41 (c)). Sullivan and Athwal (81) found
thicker oxide plateaux of about 3.0 µm in the same region,
produced at higher oxidation temperatures.

c) 68.1 N (region 3)

Observation on the wear with 68.1 N load showed a great
deal of change over the 150 minutes run prior to the
establishment of steady state conditions. The initial value
of coefficient of friction was 0.33. This increased rapidly
and then gradually to a constant value of 0.4. The surface
temperature (figure 3.20), on the other hand, showed a
drastic rise to 230°C within minutes of the start of sliding,
then rapidly increased and gradually fell to constant value
at 225°C. The increase in contact resistance, following
oxide build up in the early mild wear, rose to 35 Ω and
further increased to a mean value of 95 Ω. These were very
low contact resistance values compared to the values of the
previous regions.

It can be seen that the surface underwent similar effect
of work hardening to that of 40.5 N load, but to a greater
extent. The sequence of microhadness across the surface
(figure 3.35) and the depth of hardened layer formed below
the surface (figure 3.42), all showed how the deformation
varied during the course of sliding. For example, a 40 µm
depth hardened layer was observed after 20 minutes running
and this gradually reduced to 20 µm after long running

durations. In the mean time, the surface hardness measured over different periods of sliding reached a value between 850 and 1100 VPN. Under these conditions of hardness, one would not expect an oxide to be necessary for the establishment of relatively low wear rates (15).

X-ray data revealed that FeO was detected after 5 minutes of running, but with ferrite as the major constituents in the debris. The run over 120 minutes further showed the presence of Fe_3O_4 in small proportions and the ferrite line decreased with sliding time. Long durations of running (300 minutes), however, confirmed the presence of FeO as the majority oxide. As the load increased throughout region 3, little FeO was produced and the amount of ferrite detected in the debris increased. One interesting feature which made the mild wear with 68.1 N load different from the other loads was the absence of oxide plateaux, observed using scanning electron microscopy. Figure 3.38(c) taken from 60 minutes run and figure 3.39 (a) from 300 minutes showed the presence of oxide particles, and even when the surface was deformed, as shown in the latter figure, there was still no sign of oxide plateaux. Auger analysis (figure 3.47 (a)) also indicated that no oxide layer was present on these surfaces. Hence it is likely that the very hard surfaces gave rise to relatively low wear rates and what oxide which was observed was due to the oxidation of metallic particles after removal from surface. The presence of sparse covering

oxide of 1.4 μm thickness by Sullivan and Athwal (81) on the same region may suggest the presence of Fe_3O_4 under the short running durations which contributed to the adherence of FeO/Fe_3O_4 mixture on the surface.

d) 131.5 N (region 4)

The wear at greater loads is not only characterized by the high `wear-in' rate but also an initial substantial loss of material. In the case of 131.5 N, it was observed that more than three quarters of the exposed pin length (about 12 mm) was removed by the very severe wear at a mean rate of 5.8 x 10^{-10} m^3m^{-1} (table 3.13) in a period lasting about 3 minutes. The onset of mild wear occurred in two stages, one in which the wear rate was 7.3 x 10^{-11} m^3m^{-1} and the other which was milder at a rate of 1.2 x 10^{-12} m^3m^{-1} after 40 minutes running time. The resulting coefficient of friction increased and gradual fell to a constant value of 0.46; the surface temperature increased and fell sharply after a peak of 400°C, with a further small rise and fall characteristic around 300°C before reaching a constant value of about 220°C (figure 3.20).

X-ray analysis of wear debris and glancing angle x-ray diffraction of the surface made early in the run (5 minutes) indicated the presence of austenite and small amount of FeO (figure 3.29 and table 3.14), suggesting that contact temperature greater than 750°C had been reached. The oxides

detected in the first stage of mild wear (20 minutes) was FeO in majority, while in the second stage an FeO and Fe_3O_4 mixture after 60 minutes and FeO, Fe_3O_4 and $\alpha-Fe_2O_3$ mixture after 120 and 240 minutes run respectively.

Evidence from microhardness depth profiles (figure 3.36) and subsurface taper sections (figure 3.43) did not show any significant changes below the surface if compared to those of 40.5 N and 68.1 N load. Here the depth of the hardened layer was around 10 μm for all the run and a surface hardness of around 600 VPN (table 3.18). Shown in scanning electron micographs of the pin taper section is a dark oxide layer resting on the subsurface hardened layer which was grey (or white) in appearance.

Figures 3.38 (d) and 3.39 (c) showed micrographs of the oxide plateaux taken after 60 minutes run; apparently this thick layer was formed very rapidly after the initial three minutes running-in metallic wear, the oxide reached critical thickness and is about to break up from the surface. The presence of thick oxide plateaux after long duration of running was confirmed by Auger analysis which showed that over 1600 minutes etching time was required to remove the layer.

5.5 General discussion

In this work on the transition at T_2, it was shown

experimentally that, there exists a relationship between the
sliding parameters (transition load, transition time and
speed) and the predicted volume of oxide produced during the
course of running-in periods. Under these circumstances it
may be postulated that diffusion-controlled oxidation is
initiated at nucleation sites at the contact temperature.
The very thin oxide formed around this area may then grow
both laterally and in thickness and at the same time surface
hardness increases to support the oxide film and prevents it
from being disrupted by wear. It is postulated that the rate
of area growth increases with sliding time according to
equation (4.25). No transition can be expected if the rate
of growth is less than the rate of material removal or wear
rate; this normally occurs at the beginning of the run where
thin oxide film is easily removed on subsequent asperity
contacts. As contact temperature increases slightly with
time and sufficient hardness is established, the films grow
at a slow rate until at a point close to the mild wear
transition then the growth rate becomes rapid and exceeds the
rate of removal. This is a reason why the onset to mild wear
takes place fairly abruptly. The establishment of surface
hardness greater than 400 VPN during the initial run is
adequate to support the growing film of oxide and any further
increase in this value, caused by the deformation and work
hardening processes, is not necessary for the formation of
oxide plateaux.

The presence of Wùstite, FeO in the debris at this stage of mild wear transition confirmed that oxidation must occur at high contact temperatures, i.e. over 570°C, but this result was taken from experiments carried out at 13.8 N, just above 11.8 N (transition load). This is not the oxide expected from the dynamics of oxide production which exist on the surface prior to sliding.

The wear above the T_2 transition load is dominated mainly by mild wear due to a greater rate of energy input. Under equilibrium condition the transition from one wear region to another was found to be associated with change in the types of oxide formed on the surface. Experimental evidence has shown that FeO was the oxide originally formed at the onset of mild wear and this was gradually replaced by the lower forms of oxide. At load just above the T_2 transition (13.8 N) three stages of oxide formation occurred during the course of running-in mild wear. Fe_3O_4 and FeO present in the first 100 minutes of running were eliminated from the surface and rapidly replaced by $\alpha-Fe_2O_3$. This was probably due to the reduction in contact temperature from about 570°C down to a steady value of 300°C as oxide plateaux grew and offered increasing protection to surface. At this load subsurface hardening is due to plastic deformation and not temperature phase hardening effects.

The same process is expected to occur in region 2 (40.5 N) where the high contact temperatures induce intense

hardening below the surface just after the start of sliding in order to suport the presence of FeO, probably at temperatures above 570°C. The high energy input and hardness limit the contact temperature fall to just below 570°C where Fe_3O_4 growth predominates, enabling better protection against wear. The high contact temperature occurring in region 3 profoundly intensifies plastic flow below the surface to produce a thick hardened layer (850 to 1100 VPN) in which oxide film is not necessary to produce a low wear rate. This is the reason why contact temperatures above 570°C are maintained throughout running. In region 4 (131.5 N) the very high `metallic cutting' occurring in the early run enable austenisation temperature (750°C) to be exceeded, and the subsurface layer changes its state. Bowden and Tabor (38) pointed out this process would occur with high sliding speed. The resulting process is quenching in air, followed by martensitic phase transformation at temperature down to about 600°C. Due to high surface and bulk temperature, a further slow cooling causes FeO to degenerate to lower forms of oxide, i.e. Fe_3O_4 and $\alpha-Fe_2O_3$.

The above discussion explains why a dominant single oxide is formed in the first three mild regions when the sliding time is extended above a normal two hours of running, rather than a mixture of oxide formed during the short duration which can result in a higher wear rate. The results of surface hardness and contact temperature reject the idea

of phase transformation at T_2 transition load and permanent phase hardening at T_3 transition originally proposed by Welsh (15). In fact, these processes take place beyond region 3 of mild wear and the change in the former is represented by the T_3 transition. It is therefore postulated that the same mechanisms are responsible for the transition to mild wear under equilibrium conditions. Growth of oxide is due to homogenous diffusion-controlled oxide plateaux which increase both in thickness and area during the running-in severe wear period and dependent strongly on contact temperature and substrate hardness supporting the film.

The importance of hardness in maintaining mild wear has been reported elsewhere (15,20,54,55). Eyre and Mynard (54) have shown the existence of white hardening layer and found a range of hardness between 800-1200 VPN during the course of mild wear. Two interesting results from the hardness measurements are (a) the depth of the subsurface hardened layer which increases with the load (except region 4) and decreases slightly with the duration of sliding (figure 3.44) and (b) the estimated ranges of surface hardness with the associated oxides formed in each region, that is between 400 and 600 VPN for $\alpha-Fe_2O_3$ in region 1, between 600 and 850 VPN for Fe_3O_4 in region 2, between 850 and 1100 VPN for FeO and metallic iron in region 3 and between 500 and 600 VPN for oxide mixtures in region 4. These are generally greater than the range between 340 and 425 VPN and maximum range between

553 and 775 VPN quoted by Welsh (15). These diferences are probably due to the fact that Welsh used low carbon steels (0.12-0.78%) with lower bulk hardness. In addition, the oxide types were not specified in his investigation.

CHAPTER 6

CONCLUSIONS

The factors effecting the transition from severe to mild wear and the attainment of equilibrium condition have been investigated using a unidirectional pin-on-disc wear test rig at loads varying from 2 to 155 N and speeds from 0.6 to 1.6 ms^{-1}. All the results can be summarized in the following conclusions:

(1) Based on the wear rate versus load curves the Welsh T_2 transition occurred at a critical load above which mild wear ensued after a period of running-in severe wear and below which the system settled into an equilibrium severe wear mode. Further transition occurred in the mild wear regimes above T_2, at loads designated as T_3, T_4 and T_5, the magnitude of which increased with decreasing speed. All these transitions corresponded to changes in oxide types which were produced after relatively long period of running. α-Fe_2O_3, Fe_3O_4, FeO and oxide mixtures were the predominant oxides in regions 1, 2, 3 and 4 respectively. It was found that the experimentally-measured results were consistent with the theoretically deduced surface parameters.

(2) The transition from equilibrium severe to mild wear occurred at a load corresponding to T_2, the magnitude of which increased exponentially with decreasing speed. The

associated running-in time was found to increase with the speed. It is proposed that in-contact oxidation occurs at nucleation sites by virtue of ionic diffusion at high contact temperature (around $570^\circ C$) and that oxide either grows or is removed by wear on subsequent asperity contact. All the evidence suggests that the oxides grown in this way in these experiments eventually form thick homogenous diffusion controlled oxide plateaux (of thickness greater than 1 μm). Hence a parabolic growth rate law must be responsible for the growth.

(3) A theoretical model was developed to account for the change in relative rates of material removal and oxide formation during the running-in severe wear prior to the onset of mild wear. Remarkable agreement was achieved between the experimentally-measured wear volume and the predicted values.

(4) The results from running-in mild wear experiments have shown that the equilibrium oxide, either α-Fe_2O_3, Fe_3O_4, FeO or oxide mixture all originated from FeO, formed during the initial running-in period. At the beginning of mild wear, this and other oxides begin to protect the surface with consequent reduction in friction coefficient, temperature and wear rate. The predominent oxide then changes to Fe_3O_4 and/or α-Fe_2O_3 depending on the energy input at the surface. α-Fe_2O_3 in region 1 is produced by a contact temperature reduction to about $300^\circ C$, while a corresponding reduction of

about 560°C was apparent in region 2 where Fe_3O_4 was formed on a harder surface. The thick hardened layer in region 3 requires no oxide film for the production of low wear rates and FeO is formed only by oxidation of the material removed at high contact temperature. Oxide mixtures in region 4 were formed by a contact temperature reduction in association with martensitic phase transformation due to very rapid quenching of the asperity contact in air, followed by slow cooling to about 600°C where FeO degenerates to lower oxides. The iron, α-Fe will always be seen in the debris since it only requires one metal-metal contact in 100 oxide-oxide contacts to produce wear debris consisting 50% metal and 50% oxide.

(5) The mechanism of oxide formation in both running-in severe wear and running-in mild wear was associated with the production of hard layer during the initial stages of sliding. This, however, is important only within a short time of commencement of the sliding, when a minimum hardness is exceeded. It has been shown that hardnesses of 400 VPN are more than adequate for the establishment of stable, thick oxide plateaux and the further observed increase in this value is thought to be unnecessary for such oxide plateaux formation.

The current investigation will be more meaningful if a surface model can be developed in order to estimate the contact temperature at metal-metal contacts during the initial running-in severe wear and oxide-oxide contacts

during the course of running-in mild wear prior to the establishment of equilibrium condition. It is desirable that this matter will be considered further with the effect of elevated temperatures so that the realistic depiction of the processes occurring in mild wear transition is obtained.

APPENDIX I

ASTM INDEX VALUES (Cobalt K_α, $\lambda = 1.7902$ °A)

No	IDENTITY	2θ (degree)	hkl	d_{hkl} (°A)	I/I$_o$ (%)	R
1.	Fe_3O_4	21.5	111	4.850	8	4.48
2.	α-Fe_2O_3	28.25	110	3.686	25	10.18
3.	Fe_3O_4	35.25	220	2.967	30	17.96
4.	α-Fe_2O_3	38.75	211	2.703	100	23.11
5.	Fe_3O_4	41.75	311	2.532	100	37.79
6.	α-Fe_2O_3	41.75	$\bar{1}$10	2.519	50	16.85
7.	FeO	42.25	111	2.486	80	24.86
8.	α-Fe_2O_3	48.0	210	2.208	20	6.69
9.	FeO	49.25	200	2.153	100	48.78
10.	Fe_3O_4	50.75	400	2.099	20	10.27
11.	Austenite	50.93		2.080	100	
12.	α-Fe	52.5	110	2.027	100	124.4
13.	α-Fe_2O_3	58.25	220	1.843	40	9.64
14.	Austenite	59.64		1.800	50	
15.	Fe_3O_4	63.25	422	1.715	10	3.94
16.	α-Fe_2O_3	63.75	321	1.696	60	11.72
17.	Fe_3O_4	67.75	511+333	1.616	30	11.5
18.	α-Fe_2O_3	68.0	332+12$\bar{1}$	1.601	16	2.45
19.	FeO	72.0	220	1.523	60	24.42
20.	α-Fe_2O_3	74.0	310	1.487	35	7.3
21.	Fe_3O_4	74.75	440	1.485	40	17.45

No.	Phase					
22.	α-Fe_2O_3	76.0	211	1.454	35	7.28
23.	α-Fe	77.2	200	1.433	19	15.95
24.	α-Fe_2O_3	83.0	224	1.351	4	0.5
25.	Fe_3O_4	85.25	620	1.328	4	0.68
26.	α-Fe_2O_3	86.25	334	1.313	20	2.7
27.	FeO	87.25	311	1.299	25	7.22
28.	Fe_3O_4	89.4	533	1.281	10	2.96
29.	α-Fe_2O_3	90.75	$2\bar{2}0$	1.260	8	1.45
30.	FeO	92.0	222	1.243	15	7.66
31.	α-Fe_2O_3	93.75	303+114	1.229	4	0.40
32.	α-Fe_2O_3	95.0	$31\bar{1}$	1.215	4	0.33
33.	Fe_3O_4	95.75	444	1.212	4	1.51
34.	α-Fe_2O_3	97.5	$134+10\bar{3}$	1.191	8	1.44
35.	α-Fe	99.5	211	1.1702	30	32.98
36.	α-Fe_2O_3	100.75	244	1.165	10	1.28
37.	α-Fe_2O_3	103.25	$23\bar{1}$	1.142	12	11.89
38.	Fe_3O_4	106.5	642	1.122	6	1.10
39.	α-Fe_2O_3	108.5	024	1.104	15	2.51
40.	Fe_3O_4	110.5	731+553	1.093	24	8.73
41.	FeO	112.5	400	1.077	10	4.30
42.	α-Fe_2O_3	112.5	222	1.077	2	0.48
43.	α-Fe_2O_3	116.0	235	1.057	12	2.61
44.	Fe_3O_4	117.5	800	1.050	10	3.27
45.	α-Fe_2O_3	119.0	822+660	0.9896	5	1.43
46.	α-Fe	123.75	220	1.0134	9	15.48

Bragg equation (law) : $n\lambda = 2d_{hkl} \sin\theta$

where

n : an interger or order of reflection,

λ : the wavelength of the x-rays,

d_{hkl} : the interplanar spacing between successive atomic

planes in the crystal, and

θ : the angle between the atomic plane and both the

incident and reflected beams.

I/I_o is the standard relative integrated intensity.

R is a factor relating the structure and temperature of an

atom, volume of unit cell and polarization of diffracted

x-ray beams, given by equation (3.6).

APPENDIX II

```
50 REM PROGRAM SAMSUDI SAKRANI
100 REM HEAT FLOW ANALYSIS
150 REM TO CALCULATE SURFACE PARAMETERS
200 REM H1= HEAT FLOW TO THE PIN
250 REM TS= SURFACE TEMPERATURE
300 REM TD= DISC TEMPERATURE
350 REM FR= FRICTION COEFFICIENT
400 REM U=SPEED, W=LOAD, PM=HARDNESS
450 U=1.2:W=100.16:PM=6.9E9:L3=19E-3:L0=13
500 H1=0:TS=0:TD=0:FR=0
550 INPUT"ENTER NO. OF DATA=";N
600 OPEN1,4
650 PRINT#1,TAB(4);"U=";U;"MS","W=";W;"N"
700 PRINT#1,SPC(3);"================================";PRINT#1,""
750 PRINT#1,SPC(2);"NO.";SPC(7);"H1";SPC(8);"TS";SPC(9);"TD";SPC(10);"FR"
800 PRINT#1,"    ---      ----      ----      ----      ----"
850 PRINT#1,""
900 CLOSE1
950 DIMA(100),B(100),C(100),D(100),E(100),F(100)
1000 FOR L=1 TO N
1050 READ A(L),B(L),C(L),D(L),E(L),F(L)
1100 REM XXXXXXXXXXXXXXXXXXXXXXXXXXXXXXXX
1150 REM A(L)=FRICTION,B(L)=WEAR;C(L),D(L),E(L),F(L)=PIN & DISC TEMPS
1200 REM TEMPERATURES ON CHART RECORDER
1250 REM C=CALLIBRATION FACTOR, J=INITIAL TEMPERATURE
1300 C1=12.69:C3=10.32:C0=12.00:CD=13.1
1350 J1=20.3:J3=20.3:J0=20.3:JD=19.3
1400 T1=C(L)*C1+J1:T3=D(L)*C3+J3
1450 T0=E(L)*C0+J0:PD=F(L)*CD+JD
1500 L9=L0-B(L)*.0616
1550 REM ##############################
1600 REM # RANGE OF F.FORCE IS 1 KG =  #
1650 REM # 4.96 CM (10MV), 5 KG = 2.5  #
1700 REM # CM (1000MV)                 #
1750 REM ##############################
1800 FX=A(L)*9.81*5/2.5 :L1=L9*1E-3
1850 PD=INT(PD*10+.5)/10
1900 REM TO CALCULATE H1,TS,TD & FR
1950 KP=37.2:R1=7.8E-3:R2=3.15E-3:C=1.174E-5:M=24.99:Z=8.28
2000 X=M*L3
2050 A1=(EXP(X)+EXP(-X))/2
2100 A2=(EXP(X)-EXP(-X))/2
2150 H3=KP*3.142*R2^2*M*((T1-T0)*A1-(T3-T0))/A2
2200 H2=H3+C*(T1-T0)/(R1-R2)
2250 Y=L1/(Z*R2)
```

```
2300 B1=(EXP(Y)+EXP(-Y))/2
2350 B2=(EXP(Y)-EXP(-Y))/2
2400 PT=(T1-T0)*B1+Z*H2*B2/(KP*3.142*R2)+T0
2450 PH=KP*3.142*R2*(T1-T0)*B2/Z+H2*B1
2500 PH=INT(PH*100+.5)/100:PT=INT(PT*10+.5)/10
2550 PF=FX/W
2600 PF=INT(PF*100+.5)/100
2650 H1=H1+PH:TS=TS+PT:TD=TD+PD:FR=FR+PF
2700 OPEN1,4
2750 PRINT#1,SPC(1);L;SPC(6);PH;SPC(5);PT;SPC(6);PD;SPC(6);PF
2800 CLOSE1
2850 REM ** PH=H1,PT=TS,PD=TD,PF=FR **
2900 NEXTL
2950 H1=H1/N:TS=TS/N:TD=TD/N:FR=FR/N:HT=FR*U*W
3000 H1=INT(H1*100+.5)/100:TS=INT(TS*10+.5)/10:TD=INT(TD*10+.5)/10
3050 FR=INT(FR*100+.5)/100:HT=INT(HT*100+.5)/100
3100 OPEN1,4
3150 PRINT#1,""
3200 PRINT#1,"AVERAGE HT=";HT;"J/S"
3250 PRINT#1,"AVERAGE H1=";H1;"J/S"
3300 PRINT#1,"AVERAGE TS=";TS;"DEG. C"
3350 PRINT#1,"AVERAGE TD=";TD;"DEG. C"
3400 PRINT#1,"AVERAGE FR=";FR
3450 PRINT#1,"HARDNESS PM=";PM;"N/M^2"
3500 PRINT#1,""
3550 CLOSE1
3600 REM TO CALCULATE R,N,TC,XT
3650 REM R=ASPERITY RADIUS
3700 REM N=ASPERITY NUMBER
3750 REM TC=CONTACT TEMPERATURE
3800 REM XT=OXIDE FILM THICKNESS
3850 C0=756:D0=5210
3900 I=0
3950 HT=U*FR*W
4000 DE=H1/HT
4050 DE=INT(DE*1000+.5)/1000
4100 IFTS>200 THEN 4200
4150 KS=51.83-7.5*TS/365:GOTO 4250
4200 KS=56-22.5*TS/620
4250 HD=HT-H1
4300 FOR X1=.9TO2STEP.05
4350 XT=X1*1E-6
4400 T=TS
4450 K1=8.39-6.63E-3*(T+273)
4500 K2=4.23-1.37E-3*(T+273)
4550 K0=(K1+K2)/2
4600 X0=K0/(D0*C0)
4650 AY=.1021*PM*U*HD*.7854/(2*W*KS*X0)
4700 DY=PM*H1*.7854/(W*KS)
4750 EY=.8605*PM*HD*.7854/(W*KS)
4800 FY=.1021*U*PM*HD*XT/(X0*K0*2*W)
4850 GY=H1*PM*XT/(W*K0)
```

```
4900 HY=.8605*PM*HD*XT/(W*KO)
4950 JY=TS-TD
5000 BY=DY-EY+FY
5050 CY=GY-HY+JY
5100 ZY=BY^2-4*AY*CY
5150 IFZY<=0THEN6200
5200 YY=SQR(ZY)
5250 R=(YY-BY)/(2*AY)
5300 TC=TS+GY+(DY*R)
5350 R=INT(R*1E8+.5)/1E8:TC=INT(TC*10+.5)/10
5400 IF TC<0THEN6200
5450 IFTC>1500THEN6200
5500 IFABS(TC-T)<=(T/1000)THEN5600
5550 T=TC:GOTO4450
5600 MM=.8605-.1021*U*R/(2*XO)
5650 TP=R*PM*HT*.7854/(W*KS)+HT*PM*XT/(W*KO)
5700 TD=HT*PM*R*MM*.7854/(W*KS)+HT*PM*XT*MM/(W*KO)
5750 DT=TD/(TD+TP)
5800 DT=INT(DT*1000+.5)/1000
5850 OPEN1,4
5900 PRINT#1,"XT=";XT:PRINT#1,"------------"
5950 PRINT#1,"R=";R;"T=";TC;"/";"DT=";DT;"DE=";DE
6000 CLOSE1
6050 I=I+1:IF I=1 THEN GOTO 6150
6100 IFABS(DT-DE)>ABS(DX-DE)THEN6200
6150 DX=DT:TX=TC:RX=R:XX=XT
6200 NEXT
6250 IF I=0 THEN GOTO 6950
6300 N=W/(3.142*PM*RX^2)
6350 N=INT(N*10+.5)/10
6400 TX=INT(TX*10+.5)/10
6450 DX=INT(DX*1000+.5)/1000
6500 RX=INT(RX*1E8+.5)/1E8
6550 OPEN1,4:PRINT#1,""
6600 PRINT#1,"EXPT. DIV. OF HEAT=";DE
6650 PRINT#1,"THEO. DIV. OF HEAT=";DX
6700 PRINT#1,"R=";RX;"METER";"/";"N=";N;"/";"TC=";TX;"DEGREE C";"/";"XT=";XX;
6750 PRINT#1,"METER":PRINT#1,""
6800 CLOSE1
6850 GOTO 7050
6900 OPEN1,4
6950 PRINT#1,"NO SOLUTION FOUND"
7000 CLOSE1
7050 GOTO 1050
7100 DATA 1.65,95.2,15.5,7.9,5.35,3.15
7150 DATA 1.6,97.1,15.65,7.98,5.42,3.2
7200 DATA 1.6,98.3,15.7,8,5.45,3.2
7250 DATA 1.7,99.3,15.7,8.03,5.48,3.25
7300 DATA 1.55,100.4,15.75,8.08,5.49,3.3
7350 DATA 1.6,101.3,15.75,8.11,5.5,3.3
7400 DATA 1.7,102.3,15.8,8.12,5.51,3.4
7450 DATA 1.65,103.3,15.82,8.15,5.55,3.4
7500 DATA 1.6,104.2,15.85,8.2,5.55,3.4

READY.
```

REFERENCES

1. Dowson D., *History of Tribology*, Longman, London and N. York (1979).

2. Sheppard J.S. and Standing J.M., Some tribological problems in space mechanisms, *Proc. Seminar Tribology in Aerospace and its Relation to other Industries*, I. Mech. E., London, January 1985.

3. Chivers T.C., Nuclear technology: a personal Perspective, *Tribology International*, **19**, (1986) 225-233.

4. Fink M., Wear oxidation - A new Component of Wear, *Am. Soc. for Steel Treating*, **18**, (1930), 1026-1034.

5. Rosenberg S.J. and Jordan L., The influence of oxide films on the wear of steels, *Trans. Am. Soc. Metals*, **23**, (1935), 577-598.

6. Kehl V.B. and Siebel E., Untersuchungen über des versehleibuerhalten der metalle bei gleitender reibung, *Archiv. Eisenhutt.* **9**, (1935/36), 563-570.

7. Mailander R. and Dies, Contribution to the study of wear phenomena, *Archiv. Eisenhutt.* **16**, (1943), 385-398.

8. Archard J.F. and Hirst W., The wear of metals under unlubricated conditions. *Proc. Roy. Soc.*, **A236** (1956), 397-410.

9. Archard J.F., The temperature of rubbing surfaces, *Wear*, **2**, (1959), 438-455.

10. Archard J.F., Single contact and multiple encounters, *J. Appl. Phys.*, **32**, (1961), 1420-1425.

11. Bowden F.P. and Tabor D., *The Friction and Lubrication of Solids*, Part I, Clarendon Press, Oxford, (1954).

12. Lancaster J.K., The formation of surface films and the transition between mild and severe wear, *Proc. Roy. Soc.*, **A273**, (1963), 466-483.

13. Welsh N.C., Frictional heating and its influence on the wear of steel, *J. Appl. Physics*, **28**, (1957), 960-968.

14. Welsh N.C., The dry wear of steels, Part I – The general pattern of behaviour, Phil. Trans. Roy. Soc., 257A, (1964), 31 -50.

15. Welsh N.C., The dry wear of steels, Part II – Interpretation and special features, Phil. Trans. Roy Roy. Soc., A257, (1964), 51-70.

16. Archard J.F. and Hirst W., An examination of A Mild Wear Process, Proc. Roy. Soc., A238, (1957), 515-528.

17. Sexton M.D., The mild wear of 52100 steel, Wear, 96, (1984), 17-30.

18. Quinn T.F.J., Sullivan J.L. and Rowson D.M., New developments in the oxidational wear theory, Proc. Int. Cong. on Wear of Material, (1979), 1-11.

19. Quinn T.F.J., Sullivan J.L. and Rowson D.M., Developments in the oxidational theory of mild wear, Tribology International, 13, (1980), 153-158.

20. Quinn T.F.J., Sullivan J.L. and Rowson D.M., Application of the oxidational Theory of The Mild Wear of Low Alloy Steel, Wear, 65, (1980), 1-20.

21. Quinn T.F.J., Sullivan J.L. and Rowson D.M., Origin and development of oxidational wear at ambient temperature, Wear, 94, (1984), 175-191.

22. Wilson J.E., Stott F.H. and Wood G.C., The development of wear protective oxides and their influence on sliding friction, Proc. Roy. Soc., A369, (1980), 557-574.

23. Stott F.H., Glacsott J. and Wood G.C., Factors effecting the progressive development of wear-protective oxides on iron-based alloys during sliding at elevated temperatures, Wear, 97, (1984), 93-106.

24. Burwell J.T. and Strang C.D., Metallic wear, Proc. Roy. Soc. (London), 212A, (1953) 470-477.

25. Burwell J.T., Survey of possible wear mechanisms, Wear, 1, (1957/58), 119-141.

26. Quinn T.F.J., The classification, laws, mechanisms and theories of wear, Fundamental of Tribology (1980), MIT press, Cambridge, Massach.

27. Quinn T.F.J., Oxidational wear, Part I, Tribology International, 16, (1983), 257-271.

28. Ko P.L., Metallic wear - A review with special references to vibration-induced wear in power plant components, Tribology International, 20, (1987), 66-78.

29. Peterson M.B., Design considerations for effective wear control, Wear Control Handbook, ASME, (1980), 413-473.

30. Rabinowicz E., Friction and Wear of Materials, John Wiley abd Son Inc., N. York & London (1986).

31. Quinn T.F.J., Oxidational wear, Wear, 18 (1971) 413-419.

32. Halling J., Principles of Tribology, The MacMillan Press Ltd., London (1975).

33. Rabinowicz E., Dunn L.A. and Russel P.G., A study of abrasive wear under 3-body conditions, Wear, 41, (1961), 345-355.

34. Miki H. and Kobayashi S., Pitting failure of annealed steel under rolling contact, Wear, 67, (1981), 1-13.

35. Roberts W.H., Tribology in nuclear power generation, Tribology International, 14, (1981), 17-28.

36. Halliday J.S. and Hirst W., The fretting corossion of mild Steel, Proc. Roy. Soc., A256, (1956), 411-425.

37. Suh N.P. and Saka N., A new interpretation of the mechanism of fretting and fretting corrosion, Fundamental of Tribology, MIT Press, Cambridge, Mass. (1980).

38. Bowden F.P. and Tabor D., The Friction and Lubrication of Solids, Part II, Clarendon Press. Oxford (1964).

39. Timoshenko S., Theory of Elasticity, McGraw-Hill N. York (1934).

40. Archard J.F., Contact and rubbing of flat surfaces, J. Appl. Physics, 24, (1953), 981-988.

41. Archard J.F., Elastic deformation and the laws of friction, Proc. Roy. Soc., A243, (1957), 190-205.

42. Greenwood J.A. and Williamson J.B.P., Contact of nominally flat surfaces, Proc. Roy. Soc., (London), A295, (1966), 300-319.

43. Quinn T.F.J., The application of modern physical techniques to Tribology, Newnes-Butterworth, London, 1971.

44. Kragelskii I.V., Friction and Wear, Butterworth, London (1965).

45. Moore D.F., Principle and Application of Tribology, Pergamon Press, Oxford (1975).

46. Rubenstein C., A general theory of the surface friction of solid, Pro. Phys. Soc., London, B69, (1956), 921-933.

47. Suh N.P. and Sin H.C., The genesis of friction, Wear, 69, (1981), 91-114.

48. Blau P.J., Interpretation of friction and wear break-in behaviour of metals in sliding contact, Wear, 71, (1981), 29-44.

49. Dunckley P.M. and Quinn T.F.J., The effect of elevated temperatures and speed upon the wear of steel, Trans. ASLE, 19(3), (1976), 221-231.

50. Athwal S.S., Ph.D Thesis, University of Aston in Birmingham, U.K., (1983).

51. Glascott J., Stott F.H. and Wood G.C., The transition from severe to mild sliding wear for Fe-12% Cr-base alloys at low temperatures, Wear, 91, (1984), 155-178.

52. Quinn T.F.J., The effect of `Hot Spot' temperatures the unlubricated wear of steels, Trans. ASME, 10, (1967), 158-168.

53. Kerridge M. and Lancaster J.K., The stages in a process of severe metallic wear, Proc. Roy. Soc., London, A236, (1956), 250-264.

54. Eyre T.S. and Mynard D, Surface aspects on unlubricared metal to metal wear, Wear, 18, (1971), 301-310.

55. Eyre T.S. and Baxter A., The formation of white layers at rubbing surfaces, Metal and Materials, 6, (1972), 435-439.

56. Farrel R.M. and Eyre T.S., The relationship between load and sliding distance in the initiation of mild wear in steels, *Wear*, **15**, (1970), 359-372.

57. Sullivan J.L. and Granville N.W., Reciprocating sliding wear of steel in carbon dioxide at elevated temperatures, *Tribology International*, **17**, (1984), 63-71.

58. Eley D.D. and Wilkinson P.R., Adsorption and oxide formation on aluminium films, *Proc. Roy. Soc., London*, **A254**, (1960), 327-342.

59. Smith T. and Crane L.W., Adsorption of oxygen on steel, *Oxidation of Metal*, **10**, (1976), 135-148.

60. Fromhold A.T. Jr., *Theory of metal oxidation, vol. I, Fundementals*, North Holland, Amsterdam (1976).

61. Kubachewski O. and Hopkins B.E., *Oxidation of metals and alloys*, Butterworth, London (1962).

62. Paidassi J., Sur la cinetique de l'oxydation dans l'air dans l'intervalle 700 - 1250°C, *Acta Met.*, **6**, (1958), 184-194.

63. Stanley J.K., Von Hoene J. and Huntoon R.T., The oxidation of pure iron, *Trans. ASM.*, **43**, (1951), 426-453.

64. Davies D.E., Evan U.R. and Agar J.N., The oxidation of iron around 300°C, *Proc. Roy. Soc., London*, **A225**, (1954), 443-462.

65. Caplan D. and Cohen M., The effect of cold work on the oxidation of iron from 100°C to 650°C, *Corrosion Sciences*, **6**, (1966), 321-355.

66. Hauffe K., *Oxidation of Metals*, Plenum press, N. York (1965).

67. *Oxidation of Metals and Alloys*, Paper presented at a seminar of the American Society for Metals, *Am. soc. for Metals* (1971).

68. Cocks M., The role of atmospheric oxidation in high speed sliding phenomena - I, *J. Appl. Phys.*, **28**, (1957), 835-843.

69. Cocks M., The role of atmospheric oxidation in high speed sliding phenomena - II, J. Appl. Phys., 1, (1958), 101-107.

70. Molgaard J.A., A discussion of oxidation, oxide thickness, and oxide transfer in wear, Wear, 40, (1976), 277-291.

71. Sullivan J.L., The role of oxides in the protection of tribological surfaces, Part I, I. Mech. Eng., 1, (1987), 283-291.

72. Sullivan J.L., The role of oxides in the protection of tribological surfaces, Part II, I. Mech. Eng., 1, (1987), 293-301.

73. Quinn T.F.J., The role of oxidation on the mild wear of steel, Brit. J. Appl. Phys., 13, (1962), 33-37.

74. Aronov V., Kinetic characteristics of the transformation and failure of the surface layers of metal under dry friction, Wear, 41, (1977), 205-212.

75. Tao F.F., A study of oxidation phenomena in corrosive wear, Trans. ASLE, 12, (1969), 97-105.

76. Earles S.W.E. and Powell D.G., Stability of self-generated oxide films on unlubricated ENIA steel surface, proc. Inst. Mech. Eng., 182(3N), (1968), 167-179.

77. Molgaard J. and Srivastava V.K., Apparatus for the study of oxidational wear of unlubricated surfaces, Wear, 33, (1975), 179-188.

78. Stott F.H., Lin D.S and Wood G.C., The structure and mechanism of formation of the glaze oxide produced on nickel-based alloys during wear at elevated temperatures, Corrosion Sci., 13, (1973), 449-469.

79. Molgaard J., The activation energy of oxidation in wear, Wear, 41, (1977), 263-270.

80. Carter R.E. and Richardson F.D., An examination of the decrease of surface-activity method of measuring self diffusion coefficients in wüstite, J. Metals, 6, (1954), 1244-1252.

81. Sullivan J.L. and Athwal S.S., Mild wear of a low alloy steel at temperatures up to 500°C, Tribology International, 16, (1983), 123-131.

82. Bisson E.F, Johnson R.L and Swibert M.A., Friction, wear and surface damage of metals as affected by solid surface films, *NASA Tech. note*, **3444**, (1955).

83. Cornelius D.F. and Roberts W.H., Friction and wear of metals in gases up to 600°C, *Trans. ASME*, **4**, (1961), 20–29.

84. Pilling N.B. and Bedworth R.E., The oxidation of metals at high temperatures, *J. Inst. Metals*, **29**, (1923), 529–538.

85. Birk N. and Miler G.H., *Introduction to High Temperature Oxidation of Metals*, Edward Arnold, London (1983).

86. Suh N.P., The delamination theory of wear, *Wear*, **25**, (1973), 111–124.

87. Suh N.P., An overview of the delamination theory of wear, *Wear*, **44**, (1977), 1–16.

88. Engel P.A., *Impact Wear of Materials*, Elsvier, Amsterdam (1978).

89. Yoshimoto G. and Tsukizoe T., On the mechanism of wear between metal surfaces, *Wear*, **1**, (1957), 472–490.

90. Tenwick N. and Earles S.W.E., A simplified theory of oxidative wear, *Wear*, **18**, (1971), 381–391.

91. Stott F.H., Glascott J. and Wood G.C., Models for the generation of oxides during sliding wear, *Proc. Roy. Soc.*, London, **A402**, (1985), 167–186.

92. Dunckley P.M., Ph.D thesis, University of Aston in Birmingham, U.K., (1977).

93. Quinn T.F.J., An experimental study of the thermal aspect of sliding contacts and their relation to the unlubricated wear of steels, *Proc. Inst. Eng.*, **183**, Part III, (1968/69), 131–139.

94. Stott F.C., Glascott J. and Wood G.C., The use of contact resistance measurements to study oxide films developed during high-temperature sliding, *J. Phys. D, Appl. Phys.*, **18**, (1985), 541–556.

95. Klug H.P and Alexander E., *X-ray Diffraction Procedures for Polycrystalline and Amorphous Materials*, John Wiley & Son, N. York (1974).

96. O'Neil H., *Hardness Measurement of metals and Alloys*, Chapman and Hall Ltd., London (1967).

97. Manual of *Miniload Microhardness Tester*.

98. Davies L.E., MacDonald N.C., Palmberg P.W., Riach G.E. Weber R.E., *Handbook of Electron Spectroscopy*, Physical Electronic Ind., Minnesota (1976).

99. Averbach B.L. and Cohen M., X-ray determination of retained austenite by integrated intensities, *Metals Technology*, T.P. 2342 (1948).

100. Quinn T.F.J., *Advances in x-ray analysis*, Plenum press, N. York (1967).

101. Blok H., Surface temperatures under extreme-pressure conditions, *Second world petroleum congress*, Paris, sec. 4, (1937).

102. Blok H., A theoretical study of temperature rise at surfaces of actual contact under oilness lubricating conditions, *Proc. I. Mech. Eng.*, **2**, (1937), 222-243.

103. Jaeger J.C., Moving sources of heat and the temperature at sliding contacts, *Proc. Roy. Soc.*, N.S. W., **56**, (1942), 203-224.

104. Holm R., Calculation of the temperature development in a contact heated in the contact surface, and the application to the problem of the temperature rise in a sliding contact, *J. Appl. Phys.*, **19**, (1948), 361-368.

105. Quinn T.F.J., The division of heat and surface temperature at sliding steel interfaces and their relation to oxidational wear, *Trans. ASLE*, **21**, (1978), 78-86.

106. Grosberg P. and Molgaard J., Aspects of the wear of spinning travellers: The division of heat at rubbing surfaces, *Proc. Inst. Mech. Eng.*, **181(3L)**, (1966/67), 16-24.

107. Allen C.B., Ph.D. Thesis, University of Aston in Birmingham, U.K. (1982).

108. Molgaard J and Sweltzer W.W., Thermal conductivity of magnetite and haemtite, *J. Appl. Phys.*, **42**, (1971), 3644-3647.

109. Dunn J.S., The high temperature oxidation of metals, *Proc. Roy. Soc.*, **A111**, (1926), 203-209.

110. Whitehead W.J., A study of relative humidity on small particle adhesion to surfaces, K.L. Mittel Ed., *Surface contamination*, **7**, (1979), 73-82.

111. Granville N.W., Ph.D. Thesis, University of Aston in Birmingham, U.K., (1984).